A Theoretical Study on VOC Source and Sink Behavior of Porous Building Materials

Chang-Seo Lee

A Thesis

in

The Department

of

Building, Civil & Environmental Engineering

Presented in Partial Fulfilment of the Requirements
for the Degree of Doctor of Philosophy at
Concordia University
Montreal, Quebec, Canada

November 2003

Your file Votre référence
ISBN: 0-612-90391-5
Our file Notre référence
ISBN: 0-612-90391-5

CONCORDIA UNIVERSITY
SCHOOL OF GRADUATE STUDIES

This is to certify that the thesis prepared

By: **Chang-Seo Lee**

Entitled: **A Theoretical Study on VOC Source and Sink Behaviors of Porous Building Materials**

and submitted in partial fulfillment of the requirements for the degree of

DOCTOR OF PHILOSOPHY (Building Engineering)

complies with the regulations of the University and meets the accepted standards with respect to originality and quality.

Signed by the final examining committee:

Dr. A.J. Al-Khalili _____ Chair

Dr. M. Hosni _____ External Examiner

Dr. I. Hassan _____ External to Program

Dr. C. Mulligan _____ Examiner

Dr. R. Zmeureanu _____ Examiner

Dr. W. Ghaly _____ Thesis Co-Supervisor

Dr. F. Haghighat _____ Thesis Co-Supervisor

Approved by _____
Dr. O. Moselhi, Chair, Building, Civil & Environmental Engineering

DEC 11 2003 2003

Dr. N. Esmail, Dean
Faculty of Engineering & Computer Science

Abstract

A Theoretical Study on VOC Source and Sink Behavior of Porous Building Materials

Chang-Seo Lee, Ph.D.

Concordia University, 2003

The indoor air quality (IAQ) of a building can be significantly affected by the building materials. Porous building materials are not only sources of indoor air pollutants such as volatile organic compounds (VOC) but also strong sinks of those pollutants. The knowledge of VOC transfer mechanisms in these materials is an important step for controlling the indoor VOC concentration levels, and for determining the optimum ventilation requirements for acceptable IAQ. This study has investigated theoretically VOC source and sink behavior of porous building materials.

A novel analytical model was developed based on the fundamental theories of mass transfer mechanisms in porous materials. The proposed model considers both primary and secondary source/sink behavior for the first time. The former refers to the transfer of gas-phase and/or physically adsorbed VOC, while the latter is generation or elimination of VOC within the solid due to chemical reactions like oxidation, hydrolysis, chemical adsorption, etc. The proposed model was assessed with experimental data, namely

emission tests of carpets and sorption tests of wood chipboard. It was demonstrated that the proposed analytical model could simultaneously account for the effect of air velocity on both VOC source and sink behavior unlike the existing analytical models.

A parametric study was carried out to investigate the effects of air velocity and material properties including diffusion coefficient, sorption partition coefficient, porosity, thickness and length on the primary VOC source/sink behavior, and these effects were quantified. Due to the lack of knowledge on the secondary source/sink behavior, five hypothetical cases were considered, and the model predictions agree with experimental findings on the secondary emissions available in the literature.

The validity of four main assumptions imposed on the developed analytical model, was investigated through the development of numerical conjugate mass transfer models. The considered assumptions are 1) constant VOC concentration at the solid-fluid interface along the solid plate length; 2) quasi-steady convection mass transfer in fluid; 3) one-dimensional diffusion in solid; and 4) Henry (linear) sorption isotherm. The limits of the proposed analytical model due to each of the mentioned assumptions were clearly defined hence providing a range for the validity of the novel analytical model.

Acknowledgement

I would like to express my gratitude to my supervisors, Dr. Fariborz Haghighat and Dr. Wahid Ghaly, for superb mentorship, encouragement and support throughout my study. Their guidance made me not only a better researcher, but also a better parent.

I would like to thank Dr. Anne-Lise Tiffonnet for the valuable discussions that helped shape up my model, and for providing experimental data. I would also appreciate my colleagues, Ms. Wafa Sakr and Dr. Hongyu Huang for their help and discussions.

I want to acknowledge Natural Sciences and Engineering Research Council (NSERC) of Canada, the EJLB Foundation, and Concordia University for providing financial support for this work.

Finally, I can never thank enough my husband, Kwang-Wook, for his endless love, encouragement and sacrifice. I want to thank my children, Erica and Albert, who always give me true happiness and strength, for their love and suffering – long days in daycare and living in a small apartment. I am deeply indebted to our parents, brothers and sisters for their love and continuous support.

Table of Contents

List of Figures

List of Tables

List of Symbols

English symbols

A area of the solid [m^2]

a coefficient of discretization equation [dimensionless]

A_g constant generation term per unit volume [$mg/m^3/s$]

b thickness of solid [m]

B_g constant generation term per unit area [$mg/m^2/s$]

C gas-phase VOC concentration [mg/m^3] or [mg/g]

$c1$ hyperbolic stretching constant [dimensionless]

C_a VOC concentration of the chamber air [mg/m^3]

C_{ad} adsorbed-phase concentration [mg/m^3]

$C_{ad,s}$ mono-layer surface saturation concentration in Eqs. (2-4) and (2-5) [mg/m^3]

C_b constant concentration at the lower surface of solid [mg/m^3]

C_{in} VOC concentration of the inlet air [mg/m^3]

C_{out} VOC concentration of the exhaust air [mg/m^3]

C_s saturation vapor concentration [mg/m^3]

d pore diameter [Å]

D $D_s/(\varepsilon+K)$ in Eqs. (3-9), (3-11), and (3-12)

D_a molecular diffusion coefficient for binary mixture of air and VOC [m^2/s]

D_{ad} adsorbed-phase or surface diffusion coefficient [m^2/s]

D_e effective diffusion coefficient in a porous material in Eq. (2-6) [m^2/s]

$D_{e,ad}$ effective surface diffusion coefficient of porous material [m^2/s]

$D_{e,g}$ effective gas-phase diffusion coefficient of porous material [m^2/s]

$D_{F,AB}$ molecular or Fick diffusion coefficient of binary gases A and B [m^2/s]

D_g gas-phase diffusion coefficient [m^2/s]

$D_{K,A}$ Knudsen diffusion coefficient of diffusing gas A [m^2/s] or [cm^2/s] in Eq. (2-9)

D_p diffusion coefficient for a straight cylindrical pore [m^2/s]

D_s overall effective diffusion coefficient of the solid [m^2/s]

g VOC generation/elimination due to secondary source/sink behavior [$mg/m^3/s$]

g_c gravitation acceleration [980 g mass·cm/g force/s^2] in Eq. (2-7)

H h_D/D_s in Eqs. (3-9), (3-11), and (3-12)

h_D convection mass transfer coefficient [m/s]

I_D collision integral based on the Lennard-Jones potential in Eq. (2-8)

K Henry adsorption equilibrium constant or partition coefficient [dimensionless]

k thermal conductivity [W/(m·K)]

k_l the first order emission rate decay constant [1/s]

K_{BET} BET equilibrium adsorption constant [dimensionless]

K_F Freundlich's equilibrium adsorption constant [dimensionless]

K_L Langmuir's equilibrium adsorption constant [m^3/mg]

L length of solid [m]

M molecular weight [kg/mol] or [g mass/g mol]

m_{ad} total mass of VOC sorbed by the specimen [mg]

m_{in} total mass of VOC introdued in the chamber [mg]

m_{max} maximum transferable mass of gas-phase VOC per unit area [mg/m^2]

m_{out} total mass of VOC exhausted from the chamber [mg]

N molar flux [mol/m^{2}s]

N_t total number of nodes in Eq. (5-50)

nx last node in x-direction

P pressure [atm] or [g force/cm^2] in Eq. (2-7), i.e., 1 atm=1033.2 g force/cm^2

Q ventilation rate or volume flow rate [m^3/s]

q_w nondimensionalized local mass flux at the interface [dimensionless]

R VOC emission or sorption rate at time t [mg/m^2/s]

r pore radius in Eq. (2-9) [cm]

R_2 maximum secondary emission rate [mg/m^2/s]

$r_{A\text{-}B}$ collision diameter in Eq. (2-8) [Å]

R_c universal gas constant [84780 g force·cm/K/g mol] in Eq. (2-7)

R_o initial VOC emission or sorption rate at t = 0 [mg/m^2/s]

T temperature [K]

t time [s].

t_c convection characteristic time ($t_c = L/u_\infty$) [s]

t_d diffusion characteristic time ($t_d = b^2/D_s$) [s]

t_{end} total time of the sorption period in Eq. (3-27) [s];

numerical computation termination time in Chap. 5 [dimensionless]

t_g generation time [s]

t_{total} total transfer time, i.e., time required to emit/sink 99% of m_{max} [s]

u velocity component in x-direction [m/s]

V chamber volume [m^3]

v velocity component y-direction [m/s]

x coordinate parallel to the wall [m]

x_i x-coordinate at the ith node in Chap. 5 [dimensionless]

xl total length in x-direction in Eq. (5-50) [dimensionless]

y coordinate normal to the wall [m]

y_A mole fraction of gas A [dimensionless]

Greek symbols

α thermal diffusivity [m^2/s]

α_F the order of adsorption in Freundlich isotherm [dimensionless]

β_m eigenvalues for the dimensional analytical solution Eqs. (3-9), (3-11), and (3-12)

B_m eigenvalues for the nondimensionalized analytical solution Eq. (3-20)

γ dimensionless diffusivity, i.e., D_s/D_a for solid and D_a/D_a for air [dimensionless]

$\bar{\gamma}$ solid-air interface diffusivity in Eq. (5-47)

δ momentum boundary layer thickness [m]

ε porosity [dimensionless]

λ mean free path in Eq. (2-7) [cm]

η similarity variable in Blasius' solution, $\eta = y\sqrt{\frac{u_\infty}{2\nu \cdot x}}$ [dimensionless]

μ viscosity [N·s/m^2] or [poise = g mass/cm/s] in Eq. (2-7)

ν kinematic viscosity [m^2/s]

π 3.14159...

ϕ thickness (b) to length (L) ratio of solid [dimensionless]

ψ stream function [m^2/s]

θ nondimensionalized concentration, $\theta = (C-C_\infty)/(C_o-C_\infty)$ [dimensionless]

ρ density [kg/m^3]

τ ratio of diffusion to convection characteristic time, $\tau = t_d/t_c$ [dimensionless]

τ_P tortuosity factor [dimensionless]

Dimensionless groups

Bi mass transfer Biot number ($Bi = h_D \cdot b/D_s$)

Br_L averaged Brun number for heat transfer ($Br_L = \frac{k_f}{k_s} \cdot \frac{b}{L} \cdot \mathrm{Re}_L^{1/2} \cdot \mathrm{Pr}^{1/3}$)

Br_x local Brun number for heat transfer ($Br_x = \frac{k_f}{k_s} \cdot \frac{b}{x} \cdot \mathrm{Re}_x^{1/2} \cdot \mathrm{Pr}^{1/3}$)

Br_L^* averaged Brun number for mass transfer ($Br_L = \frac{D_a}{D_s} \cdot \frac{b}{L} \cdot \mathrm{Re}_L^{1/2} \cdot Sc^{1/3}$)

Br_x^* local Brun number for mass transfer ($Br_x = \frac{D_a}{D_s} \cdot \frac{b}{x} \cdot \mathrm{Re}_x^{1/2} \cdot Sc^{1/3}$)

Fo Fourier number ($Fo = t \cdot D_s / b^2$)

Kn Knudsen number ($Kn = \lambda/d$)

Nu_x local Nusselt number ($Nu_x = h \cdot x/k_f$)

Nu_L average Nusselt number ($Nu_L = h_{ave} \cdot L/k_f$)

Pe mesh Peclet number for mass transfer ($Pe = v_p \cdot \Delta y/D_a$)

Pr Prandtl number ($Pr = \nu/\alpha$)

Re_L Reynolds number based on the plate length ($Re_L = u_\infty \cdot L/\nu$)

Re_x Reynolds number at position x ($Re_L = u_\infty \cdot x/\nu$)

Sc Schmidt number ($Sc = \nu/D_a$),

Sh_L averaged Sherwood number ($Sh_L = (h_D)_{ave} \cdot L/D_a$)

Sh_x local Sherwood number ($Sh_x = h_D \cdot x/D_a$)

Subscripts

∞ far field, i.e., outside the boundary layer

ave average value

cf constant wall mass flux case

cw constant wall concentration case

m material-phase approach

o initial value at $t = 0$

w at the fluid –solid interface

wm wet material

$y=0^-$ at the solid side of the solid-fluid interface

$y=0^+$ at the fluid side of the solid-fluid interface

Superscripts

1 at the time level $t + \Delta t$

0 at the time level t

+ dimensionless variable

Abbreviation

ADI	Alternating Direction Implicit scheme
CFD	Computational Fluid Dynamics
EPA	Environmental Protection Agency in United States
HVAC	Heating, Ventilation, and Air Conditioning system
IAQ	Indoor Air Quality
MTC	Mass Transfer Coefficient
MVOC	Microbial Volatile Organic Compounds
ODE	Ordinary Differential Equation
SBS	Sick Building Syndrome
VOC	Volatile Organic Compounds
WHO	World Health Organization

Chapter 1

Introduction

1.1 BACKGROUND

Since the 1970's energy crisis, the energy conservation has become a global issue. To reduce the energy consumption in buildings, efforts have focused on lowering the ventilation requirements, and increasing insulation and air-tightness of buildings. This, as well as the growing use of synthetic materials, household chemical products and modern office equipment such as photocopiers, printers, computers, etc., have leaded to the deterioration of indoor air quality (IAQ) in non-industrial buildings i.e., residential, commercial, office and institutional buildings.

The indoor air pollution may significantly affect public health and productivity because people spend more than 90% of their lifetime indoors [Godish, 2001]. The United States' Environmental Protection Agency (EPA) mentioned that the health risks associated with breathing indoor air are 2 to 5 times higher than the risks of breathing outdoor air. Also, the EPA places poor IAQ fourth on the list of high cancer risks, with 3500 to 6000 deaths per year attributable to indoor air pollution [EPA, 1991]. The economic effects of IAQ problems are also significant. According to a US Army research, IAQ related health problems cost about $15 billion a year in direct medical costs and about 150 million in lost workdays, which are equivalent to at least $59 billion per year [Hansen and Burroughs, 1999]. Not only these costs but also the costs due to vacant buildings and

facilities, and increased lawsuits [McNeely, 1999] because of IAQ problems are economic burden to our society. This can represent a more serious problem in countries like Canada where people spend more time in climate-controlled buildings due to long cold winters and hot summers.

With the increased environmental awareness, IAQ problems have become a major public concern and demands for healthy indoor environment keep rising. Increased ventilation and fresh air supply rates, and filtration and purification of contaminants will enhance IAQ. However, increased ventilation rate can result in a large increase in global energy consumption considering 40% of the world's energy usage is dedicated to the construction and operation of buildings [Roodman and Lenssen, 1995], and filtration and purification of contaminants are expensive. One of the key strategies in designing and maintaining a healthy indoor environment is to control the source of major indoor air pollutants such as Volatile Organic Compounds (VOC), which are one of the identified causal factors for Sick Building Syndrome* [Maroni et al., 1995].

VOC are chemical agents found in every indoor environment and defined by a boiling point range with a lower limit between 50°C and 100°C, and an upper limit between 240°C and 260°C, where the higher values refer to polar compounds [WHO, 1989]. VOC

* SBS is the representative IAQ problem. In 1982, the World Health Organization, described the SBS as a phenomenon generally associated with the indoor environment of certain non-industrial workplaces that produces a combination of non-specific symptoms related to comfort and health like headache, lethargy, poor concentration, dizziness, nausea, dryness and irritation of eyes, throat, nose and skin, etc. in a significant number of occupants, whose reactions cannot be related to obvious causes such as excessive exposure to a known contaminant or a defective ventilation system [WHO, 1983]. The WHO estimated that 30% of the newly built or renovated buildings have characteristics related to SBS and between 10 and 30% of the occupants are affected [WHO, 1986].

mainly exist in a gas phase under normal indoor environmental conditions and over three hundred VOC have been identified in the indoor air [Berglund et al., 1986]. The VOC concentrations, though low, are significantly higher indoors than the ambient outdoors [WHO, 1989]. The high potential for many VOC's presence in indoor air to cause symptoms is a result of both additive and synergistic effects [Godish, 2001]. The potential harmful health effects of VOC are irritations of upper respiratory system, eye and skin, sinus infection, allergic reaction, asthma, headache, fatigue, poor concentration, nausea, dizziness, and cancer [Maroni, et al., 1995].

VOC are either originated from the outdoor air or generated internally. Since the ambient outdoor air quality is generally controlled under standards or guidelines in many countries, the outdoor air becomes a less significant source. The internally generated VOC are from (1) human metabolism and activities including cleaning, cooking, operating office equipment, etc.; (2) building materials and furnishings including Heating, Ventilating and Air Conditioning (HVAC) system; and (3) metabolic by-products of micro-organisms (MVOC) like molds and bacteria, which are often found in water-damaged building materials and HVAC system.

The major sources of VOC are building materials and furnishings due to their large surface areas and continuous exposure to the indoor air, whilst most human activities and operation of equipment cause short-term intermittent emissions. Building materials and furnishings also act as sinks and later re-emit absorbed chemicals. In addition, some building materials are good sources of microbial growth if wetted, and generate MVOC

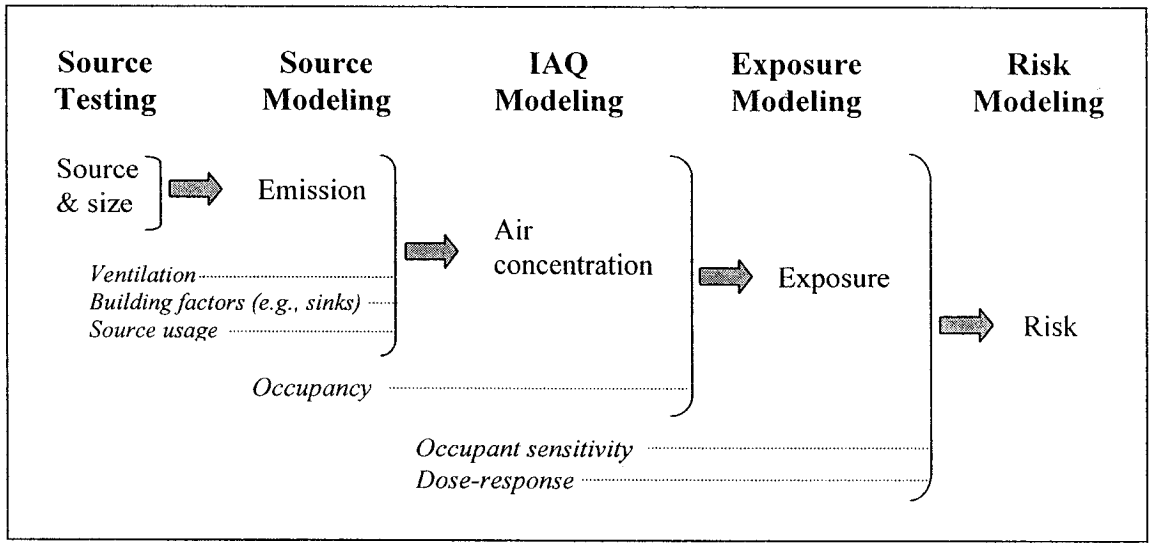

Figure 1-1 Principles of assessing risk due to indoor sources [Sparks et al., 1996a]

[Ström et al., 1994; Salthammer, 1999]. Therefore, a thorough understanding of the emission characteristics of building materials and furnishings, and the interactions with other sources, is essential for controlling the indoor VOC concentration levels, and determining the optimum ventilation requirement for acceptable IAQ. This is also the fundamental step for exposure and risk assessment as shown in Fig. 1-1 [Sparks et al., 1996a].

1.2 BUILDING MATERIALS AS SOURCES AND SINKS OF VOC

The VOC emitted from building materials can be originated from different emission types: primary emissions and secondary emissions [Wolkoff, 1995 and 1999]. The primary emission means the emission of non-bound or free VOC within building materials. These are generally low molecular weight VOC found as accelerators, additives, antioxidants, plasticizers, solvents and unreacted raw materials like monomers. Secondary emission refers to the emission of originally chemically or physically bound

VOC. These VOC are emitted or formed by different mechanisms like decomposition, oxidative degradation, chain scission, sorption processes and microbiological emission, which so called MVOC. Primary emissions decay relatively fast (usually within a year), while secondary emissions for some building products like linoleums may continue for the entire life of the building product [Wolkoff and Nielsen, 1996].

Considerable experimental work has been carried out regarding the VOC source (or emission) and sink (or sorption) behavior of many building materials. Regardless of the types of tests, experimental results are plotted as VOC concentration in the chamber air versus time; however, the results cannot give the origin of the VOC. Hence, the current emission tests cannot distinguish between the primary and the secondary emissions. Most emission test results have been generally regarded as the primary emissions and only a few studies have identified the secondary emissions except the sorption processes. From small-scale chamber tests of PVC flooring and sealants, oxidation processes were observed and air velocity was found to affect the process [Knudsen et al., 1999; Wolkoff, 1998]. From the case studies, it was found that VOC are emitted due to the hydrolysis process from PVC flooring and linoleum applied on wet concrete [Wolkoff *et al.*, 1995; Rothweiler et al., 1993; Gustafsson, 1992]. Even though these studies exhibit the importance of secondary emissions, there is still a lack of experimental and theoretical studies on secondary emissions.

Another limitation of experiments is that the VOC concentration on the surface or within a building material cannot be directly measured; therefore, experimental results

themselves are not sufficient for explaining the mechanisms involved in the source and sink behavior of building materials. Many experimental data have been interpreted using empirical or semi-empirical models [ASTM, 1990; Colombo et al., 1992] like the first order decay model[†] to characterize and classify the source and sink strength of various building materials; however, these models cannot provide any physical insight to the mechanisms involved, and do not allow scaling of the results from chamber to actual building conditions. Therefore, proper physical models are required to provide a better understanding of the mechanism and predictions for real case scenarios.

The physical models, which are the subject of recent research work, are based on the fundamentals of mass transfer processes. The main processes applied to describe source and sink behavior of building materials are (1) internal diffusion of a compound through a material as a result of a concentration gradient, (2) the boundary layer transfer occurring at the material-air interface as a consequence of forced and/or natural convection as well as gas diffusion, and (3) adsorption/desorption, which are physical and/or chemical interactions between VOC and material surfaces including all pore surfaces.

[†] The first order decay model [ASTM, 1990] is the simplest and most commonly used model for finite thin film sources. It assumes that the VOC concentration is uniform in the test chamber. This model calculates the VOC emission rate by

$$R(t) = R_o \cdot e^{-k_1 \cdot t}$$

where, R is VOC emission rate at time t [mg/m^2/s]; R_o is the initial VOC emission rate at t=0 [mg/m^2/s]; k_1 is the first order emission rate decay constant [1/s]; and t is time [s]. R_o and k_1 are unknown and determined by non-linear regression curve fitting of the VOC concentration versus time data from chamber test. This model is often deficient in characterizing the "tail" of the emission curve for rapidly decaying sources.

Several physical models have been proposed considering one or more processes depending on the characteristics of the building material. For wet materials such as paint or wood stain, evaporation is the predominant process early in the drying process and emissions strongly depend on environmental parameters such as air temperature, velocity, relative humidity and turbulent intensity [Haghighat and De Bellis 1998]. In order to predict the early drying-phase emission from wet materials, some physical models have been developed [Tichenor et al. 1993; Sparks et al. 1996b; and Haghighat and Zhang 1999] considering only the boundary layer transfer and assuming negligible internal diffusion and sorption. Tichenor et al. (1993) considered molecular diffusion across a laminar boundary layer, and Sparks et al. (1996) generalized this model further and developed the Sherwood number correlations from experimental data. Haghighat and Zhang's (1999) model considered both mass diffusion and convection processes in the boundary layer between the material surface and the airflow. These models were well validated with short-term experimental data from small-scale chamber. However, the applications of these models are limited to emissions in early drying phase. When wet materials are dried out, internal diffusion and sorption may not be negligible.

For solid materials, internal diffusion and sorption cannot be ignored. Internal diffusion and sorption strongly depend on the solid material structure (e.g., non-porous or porous). Internal diffusion in porous materials is much faster than in non-porous materials, because in porous materials, diffusion takes places as gas-phase and/or adsorbed-phase depending on the size of pore, whilst solid-phase diffusion takes place for nonporous materials [Ruthven, 1984]. Also, adsorption/desorption is more significant in porous

materials than non-porous materials because porous materials have very large surface areas. For example, a non-porous material 1cm^3 in volume will have 6 cm^2 of surface area. The same volume of porous material like gypsum board will have 6000 cm^2 of surface area when the particles are 10 μm diameter; 60 m^2 of surface area with 0.1μm diameter, e.g. cement paste [Sereda, 1969]. Therefore, porous materials can interact more with the surrounding indoor air as sinks and secondary sources as well as primary sources of VOC.

Several physical models have been proposed for source and/or sink behavior of solid materials, and assemblies like wet material applied on solid [Yang et al., 2001a] and two layers of solid materials [Kumar and Little, 2002]. However, as these models focused on the primary emission and/or sorption (sink behavior), no theoretical studies have been carried out on the secondary emissions other than sorption. Many models assume that VOC exist as a homogeneous phase regardless of the material structure [Little et al, 1994; Kumar and Little, 2002; Yang, et al., 1998, 2001b and c; Huang and Haghighat, 2002a]. Some physical models consider only the internal diffusion and/or sorption neglecting the boundary layer transfer [Little et al., 1994; Kumar and Little, 2002; Yang et al., 1998], hence the source and sink behavior are the same regardless of the air velocity. The CFD models have less restriction; however, their usages are generally limited to relatively short-term predictions due to the expensive computational cost [Murakami et al., 1998; Yang et al., 1998, 2001a,c]. A detailed review is presented in Chapter 2.

Even though numerous experiments have been carried out, many aspects of source and sink behavior of building materials, especially solid materials and assembly, have not been investigated due to the limitations of experimental studies. Because of the complexity of the mechanisms involved, the research in this area is still in an early stage. A thorough theoretical study is needed to explain many phenomena observed in the experimental studies and to develop reliable analysis and design tools.

1.3 OBJECTIVES

The objectives of the proposed study are:

- To carry out a critical review of the mass transfer mechanisms in porous materials and the existing physical models for solid building materials and assemblies, and to decide the most appropriate modeling approach of each transfer process involved in source and sink behavior.
- To develop an analytical model that can predict the source (including both primary and secondary emissions) and sink behavior of porous building materials under various air velocities for the entire course of the product service life, and to assess the proposed model predictions with available experimental data.
- Use the proposed model to conduct comprehensive theoretical investigations on the effects of material properties and air velocity on the source and sink behavior of porous building materials.
- Through numerical modeling, assess the validity of assumptions imposed in the proposed analytical model; hence to define the application limits of the proposed analytical model.

Consequently, this study will provide designers and manufacturers with a better understanding of the VOC source and sink behavior of porous building materials and assembly, and a better model to evaluate their designs and products. Hence, ultimately it can contribute to reduce or prevent the IAQ related problems such as SBS.

1.4 THESIS OUTLINE

Chapter 2 contains the literature review on the mass transport mechanisms involved in porous materials and the existing physical models for solid materials and assemblies. Chapter 3 presents the development of an analytical model for source and sink behavior of porous building materials and its assessment through comparisons of its predictions with available emission and sorption test data. The predictions made by the proposed model were compared with those by an existing analytical model. In Chapter 4, the effects of the material properties (diffusion coefficient, sorption property and the thickness of a porous material) and the environmental conditions (air velocity) on long-term primary and secondary emissions as well as the sink effects are presented. In Chapter 5, a numerical simulation of the conjugate mass transfer problem was implemented. Chapter 6 presents the numerical results to assess the limitations in the application of the proposed analytical model due to the assumptions made in the proposed analytical model. Chapter 7 presents the conclusions and the recommendations for future work.

Chapter 2

Literature Review

2.1 INTRODUCTION

Over the last decade, a lot of research has been carried out on material emissions (or source behavior) and sorption (or sink behavior). The objective has been to describe the VOC and their emission/sorption profiles (concentration versus time) through tests from various materials. It has been reported that building materials can be categorized as either solid (dry) or wet materials. For emission, wet materials like surface coating materials are normally applied wet and their emissions are initially relatively high but decay fast; while solid materials are characterized by relatively low emission rates and decay slowly. Since wet materials are generally strong sources in the early wet-phase, they hardly act as VOC sinks during the early evaporation process. However, all solid materials (i.e. dried-out wet materials can be regarded as solid materials) can act as sinks when the concentration in the surrounding air is higher. The sink effects are more significant for porous materials. The presence of porous building materials in indoor environment results in lower peak of VOC concentration in the indoor air but prolonged presence of VOCs in indoor air.

In order to understand the VOC source and sink behavior of porous building materials, fundamentals of mass transport mechanisms in porous solids are reviewed here. The mass transport mechanisms in porous materials are complicated due to the complex nature of

pore structures as well as the physical and/or chemical interactions of transporting gases or vapors with the porous materials. This subject has been investigated for a long time in the areas of chemical engineering and surface science, and the underlying physical and chemical principles are generally well established. The application examples of these principles found in the references are mostly for the industrial processes like adsorption separation, solvent drying, catalytic process, etc, which take place over a wide range of temperature and pressure, and generally high concentration of transporting molecules in porous solids whose pore sizes are generally controlled to achieve the maximum operation efficiency. In the area of building science, this subject has been applied for the moisture transfer through building envelopes. Since moisture can exist in forms of vapor, liquid and ice, wide span of moisture concentration (from dry to saturation vapor pressure) is considered. Also, few studies were carried out on the indoor building materials and furnishings like carpet and ceiling tiles. Therefore, the fundamental theories on mass transport in porous materials reviewed here will be interpreted for the application of the VOC source and sink behavior of porous materials.

Several physical models have been proposed to predict the VOC source and/or sink behavior of solid building materials and assemblies. In that follows these models are reviewed according to the approaches that they used for the mass transfer mechanism(s), e.g. internal diffusion in solid and/or convection over the solid, and their limitations are discussed. Critical review on the existing models combined with the understanding of the fundamentals of mass transfer mechanisms will lead to the development of a suitable model for VOC source and sink behavior in porous building materials.

2.2 MASS TRANSFER MECHANISMS IN POROUS MATERIALS

According to the International Union of Pure and Applied Chemistry (IUPAC) classification, pores are divided into three categories based on their sizes: micropores (pore diameter, $d < 20$ Å), mesopores (20 Å $< d <$ 500 Å), and macropores (500 Å $< d$) [Kärger and Ruthven, 1992]. This classification is based on the forces affecting the mass transfer processes, i.e., diffusion and adsorption. In micropore range, surface forces (van der Waal's force) are dominant and a diffusing molecule never escapes from the force field of surface even when at the center of the pore [Ruthven, 1984]. In the mesopores, capillary forces become important. In macropores, effects of both forces become minor. This classification is appropriate when small molecules are considered but for larger molecules the micropore regime may be shifted to substantially large pore sizes [Kärger and Ruthven, 1992].

Mass transfer in porous materials is a result of diffusion due to concentration gradient, adsorption/desorption due to surface force and/or capillary flow due to suction. Figure 2-1 shows the phases of moisture sorption in pores as the concentration increases. At low concentration, moisture exists as vapor and adsorbed phases, but the transfer takes place by only vapor diffusion (Fig. 2-1(a)). As the concentration increases, the thickness of adsorbed layer increases and both vapor and adsorbed-phase diffusions occur (Fig. 2-1(b)). Then capillary condensation takes place in smaller pores and the adsorbed layer gets thicker, when vapor and adsorbed-phase diffusion, and capillary flow coexist (Fig. 2-1 (c) and (d)). As the pore is filled with condensed water, vapor and adsorbed-phase diffusion no longer takes place (Fig. 1-2 (e) and (f)).

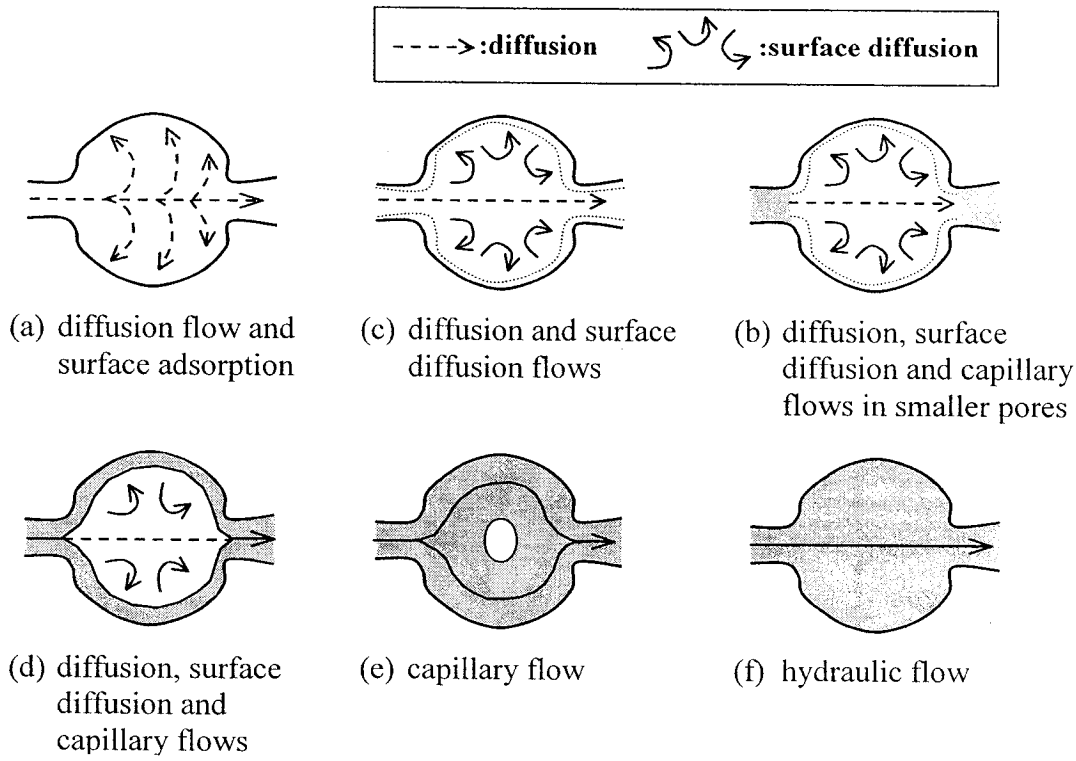

Figure 2-1 Phases of moisture sorption [from Ojanen et al., 1989]

Unlike the moisture transfer problems in building materials, VOC concentrations in indoor air of non-industrial buildings are very low compared with the saturation concentrations. The VOC concentration in various types of non-industrial buildings including dwelling, offices and schools, is generally less than 100 $\mu g/m^3$ for individual compound, 500 $\mu g/m^3$ for total VOC (TVOC) in buildings without IAQ problems, and 2 mg/m^3 up to 18 mg/m^3 for TVOC in low IAQ buildings [Salthammer, 1999]. Considering the fact that the saturation concentration is 97.36 g/m^3 for n-octane and 473.45 g/m^3 for ethyl acetate [Kirchner et al., 1999], VOC concentration levels in indoor air are very low. Hence, this review on the mass transfer in porous materials will be limited to the transport phenomena observed in the low concentration levels: gas or vapor phase and adsorbed phase diffusion, and adsorption/desorption.

2.2-1 Sorption in Porous Materials

Adsorption is the accumulation of gas, vapor or liquid (adsorbate) on a solid or liquid surface (adsorbent). The outermost layer of the solid or liquid molecules on the surface is bound on only one side to the inner layer of molecules by atomic and molecular forces. To compensate for this imbalance of the binding force, an attraction force from the surface captures the surrounding gas, vapor or liquid [Young and Crowell, 1962].

Adsorption can be classified as physical and chemical adsorption depending on the interacting forces between the adsorbate and the adsorbent. Physical adsorption, or van der Waals adsorption, results from a relatively weak interaction. The forces involved in physical adsorption include both van der Waals forces (dispersion-repulsion) and electrostatic interactions [Ruthven, 1984]. The van der Waal's contribution is always present while electrostatic contributions are significant only for adsorbent with ionic structure. Physical adsorption is reversible; hence all the gas adsorbed by physical adsorption can be desorbed by evacuation at the same temperature and the adsorbate layer is always in equilibrium with the molecules of the gas-phase [Attard and Barnes, 1998].

Chemical adsorption is a result of a more energetic interaction than the physical adsorption. The process involves transfer of electrons between the adsorbate and adsorbent. Reversal of chemical adsorption using a vacuum requires elevated temperature and even that may not be sufficient. The general features that distinguish between physical and chemical adsorption are presented in Table 2-1.

Table 2-1 Physical adsorption vs. chemical adsorption [from Ruthven, 1984]

Physical Adsorption (Physisorption)	Chemical Adsorption (Chemisorption)
Low heat of adsorption (less than 2 or 3 times latent heat of evaporation)	High heat of adsorption (more than 2 or3 times latent heat of evaporation)
Non-specific	Highly specific
Monolayer or multilayer	Monolayer only
No dissociation of adsorbed species	May involve dissociation
Only significant at relatively low temperature	Possible over a wide range of temperature
Rapid, non-activated, reversible	Activated, may be slow and irreversible
No electron transfer although polarization of sorbate may occur	Electron transfer leading to bond formation between sorbate and surface

Adsorption isotherm describes the dependence of adsorbed-phase concentration on the gas-phase concentration in equilibrium state at a constant temperature.

$$C_{ad} = f(C,T) \tag{2-1}$$

where, C_{ad} is the adsorbed-phase concentration [$mg/m^3_{material}$]; C is the gas-phase concentration [mg/m^3_{gas}]; and T is the temperature [K].

According to the Brunauer classification of isotherms, there are five basic isotherm shapes for physical adsorption of systems at temperature below the critical temperature of gas, as shown in Fig. 2-2 [Brunauer, 1945]. Type I isotherm is observed for systems where the adsorption is limited for monolayer. For microporous adsorbents, where the pore size is not very much greater than the molecular diameter of the adsorbate, the isotherms are generally of type I, because there is a saturation limit corresponding to complete filling of the micropores [Ruthven, 1984]. Types II to V involve multiplayer

adsorption. Types II and III are generally observed in adsorbents with a wide range of pore sizes, since there is a continuous progression with increasing loading from monolayer to multilayer adsorption and then to capillary condensation occurring in pores of increasing diameters [Ruthven, 1984]. Types IV and V show the flattening of isotherms before the saturation vapor concentration (C_s) due to capillary condensation in porous materials with narrow pores [Adamson, 1990]. If the pores are wider, type II or III behaviour would be observed [Attard and Barnes, 1998]. Type IV suggests the formation of two adsorption layers either on a plane surface or on the wall of pore that are much wider than the molecular diameter of the sorbate [Ruthven, 1984].

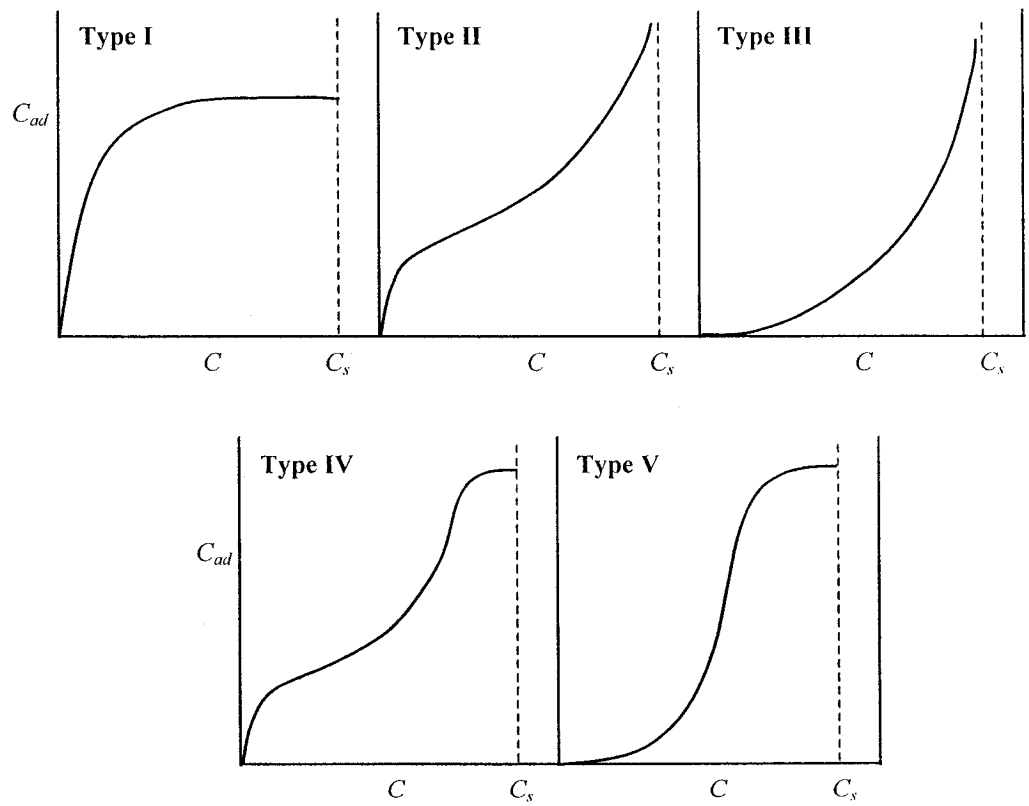

Figure 2-2 Brunauer's classification of adsorption isotherms [from Adamson, 1990]

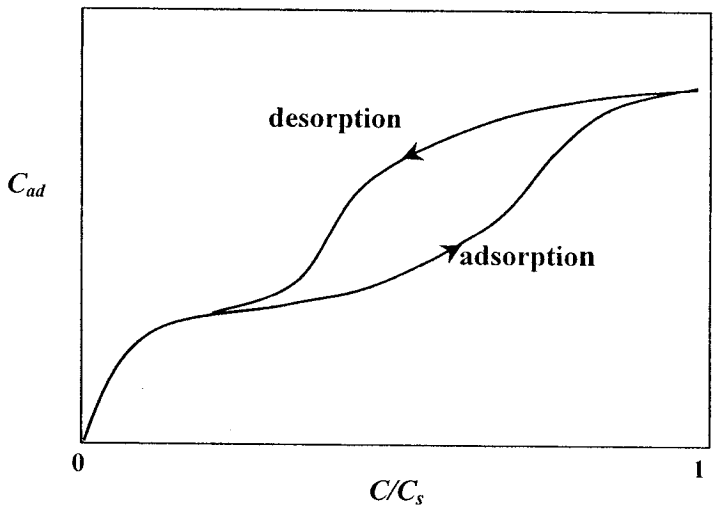

Figure 2-3 Hysteresis loop in sorption isotherm

Continuous progression from multilayer adsorption to capillary condensation can takes place in porous adsorbents, resulting in completely liquid filled smaller pores. Capillary condensation occurs due to the reduced saturation vapor pressure (or concentration) in a small pore by the effect of surface tension, which is described in the Kelvin equation [Hutcheon and Handegord, 1995]. In the case of water at 20°C, the saturation vapor pressure is reduced to 34% in a pore of 20Å in diameter, the lower limit of mesopore according to IUPAC classification. For a pore of 500Å in diameter, the upper limit of mesopore, the saturation vapor pressure is reduced by only less than 5%. Hence, the capillary effect is significant only in quite small pores. In the capillary condensation region the isotherms generally shows hysteresis, where adsorption isotherm and desorption isotherm differ as shown in the Fig. 2-3 [Ruthven, 1984]. The presence of hysteresis in sorption isotherm may indicate the presence of mesopores.

The generally applied models for the adsorption isotherms are as follows [Young and Crowell, 1962; Ruthven, 1984; Axley, 1991]:

- Henry isotherm describes the linear relations. At low concentration levels, all isotherms can be regarded as linear.

$$C_{ad} = K \cdot C \tag{2-2}$$

where, K is Henry adsorption equilibrium constant.

- Freundlich isotherm is an empirical model that can be applied to nonlinear regions of high concentration level.

$$C_{ad} = K_F \cdot C^{\alpha_F} \tag{2-3}$$

where, K_F is Freundlich's equilibrium adsorption constant; and α_F is the order of adsorption.

- Langmuir isotherm is the simplest theoretical model for monolayer adsorption. This represents the Brunauer's type I isotherm (Fig. 2-4).

$$C_{ad} = \frac{K_L \cdot C_{ad,s} \cdot C}{(1 + K_L \cdot C)} \tag{2-4}$$

where, K_L is Langmuir's equilibrium adsorption constant [m^3/mg]; and $C_{ad,s}$ is the mono-layer surface saturation concentration [mg/m^3].

- BET (Brunauer, Emmett, and Teller) isotherm accounts for the multilayer adsorption. This has the general form of the type II or III isotherm in Brunauer's classification (Fig. 2-5).

$$C_{ad} = \frac{K_{BET} \cdot C_{ad,s} \cdot \left(\frac{C}{C_s}\right)}{\left(1 - \frac{C}{C_s}\right) \cdot \left(1 - \frac{C}{C_s} + K_{BET} \frac{C}{C_s}\right)} \tag{2-5}$$

where, K_{BET} is the BET equilibrium adsorption constant.

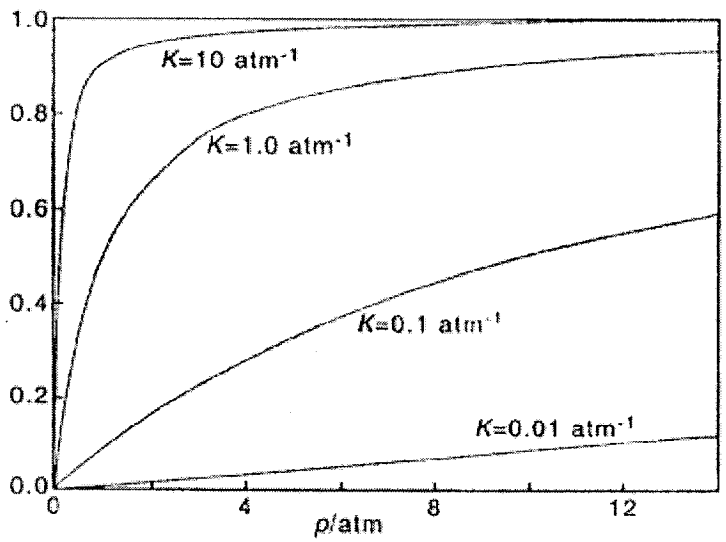

Figure 2-4 Langmuir isotherm [from Attard and Barnes, 1998]

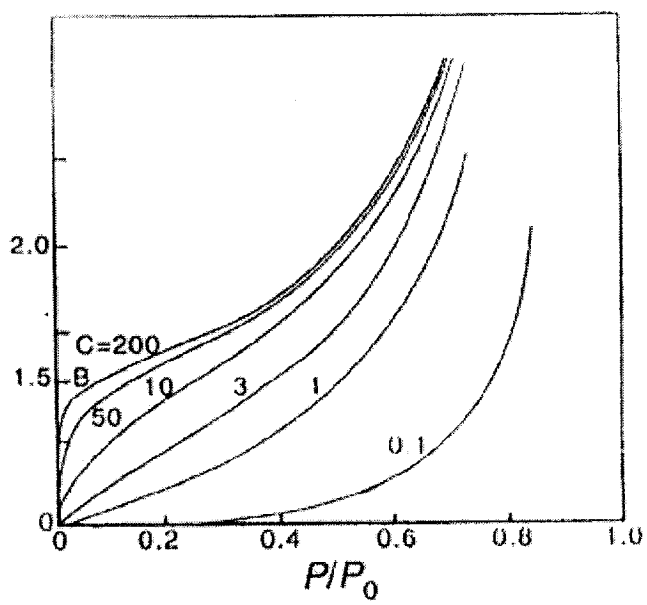

Figure 2-5 BET isotherm [from Adamson, 1990]

Since VOC concentration levels in indoor air are much lower than the saturation concentrations, the Henry isotherm is generally adopted in the modeling of source and sink behavior of building materials. Several studies investigated the effect of gas-phase concentration on the Henry adsorption constant (K) and most studies concluded that little impact of gas-phase concentration. Table 2-2 summarizes these findings from the experimental studies of which data were analyzed using the linear isotherm. Cox et al. (2001b) and Meininghaus et al. (2000b) specifically present the isotherm plots. Due to the sensitivity limitation of microbalance, Meininghaus et al. (2000b) carried out the sorption tests at relatively high concentrations that vary from 40 mg/m^3 to 400~600 mg/m^3. The test results show generally linear isotherms except for the xylene/PVC case, which exhibits Brunauer's type III or type V at low concentration range.

Table 2-2 Effect of concentration on Henry adsorption constant

Reference	Material	VOC	Concentration	Result
Tichenor et al. (1990)	Carpet	Tetrachloro-ethylene	5 – 50 mg/m^3	No effect on K
Popa and Haghighat (2002)	Acrylic paint	Toluene	33 - 164 mg/m^3	No effect on K
Jørgensen et al. (1999)	Wool carpet Nylon carpet	Toluene α-pinene	160~300 μg/m^3 - 5 mg/m^3	No effect on K
Cox et al. (2001b)	Vinyl flooring	Phenol	10-70 mg/m^3	Linear isotherm
Meininghaus et al. (2000b)	Wallpaper Carpet Acrylic paint PVC Aerated concrete gypsum	Xylene n-octane	40 – 400~600 mg/m^3	Nonlinear isotherm for xylene/PVC Others are linear isotherms

Tiffonnet et al. (2002) obtained sorption isotherms for acetone on paint, wood chipboard, and gypsum. A linear isotherm was observed for paint in the range of acetone concentration in the air (C) 0 to 0.7 mg/g_{air}, which is equivalent to 825 mg/m^3_{air}. When wood chipboard was tested for 0-80 mg/g_{air} (≈94 g/m^3_{air}) of C, Brunauer type III or low concentration part of type V were observed, as shown in the Fig. 2-6. The same isotherm shape was observed for the lower concentration region 0-0.3 mg/g_{air} (≈353.4 mg/m^3_{air}). For gypsum, type I or low concentration part of type IV isotherm was obtained for C varying 0 to 3.0mg/g_{air} (≈3.5 g/m^3_{air}) and the hysteresis was observed, as presented in the Fig. 2-7.

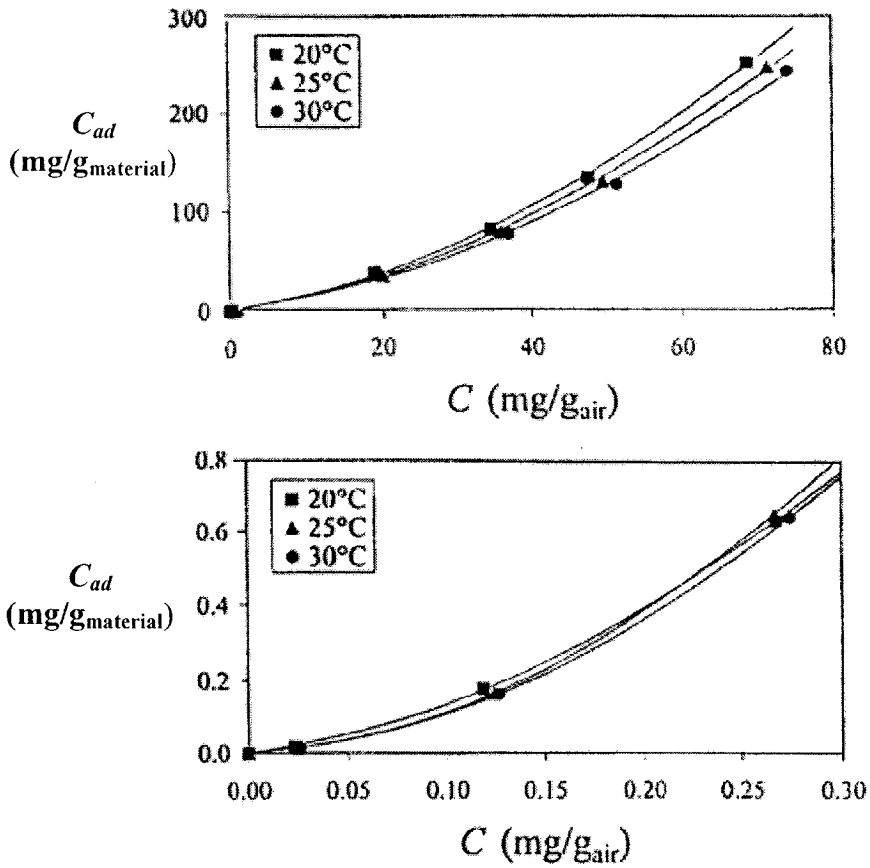

Figure 2-6 Sorption isotherms of acetone/wood chipboard [Tiffonnet et al., 2002]

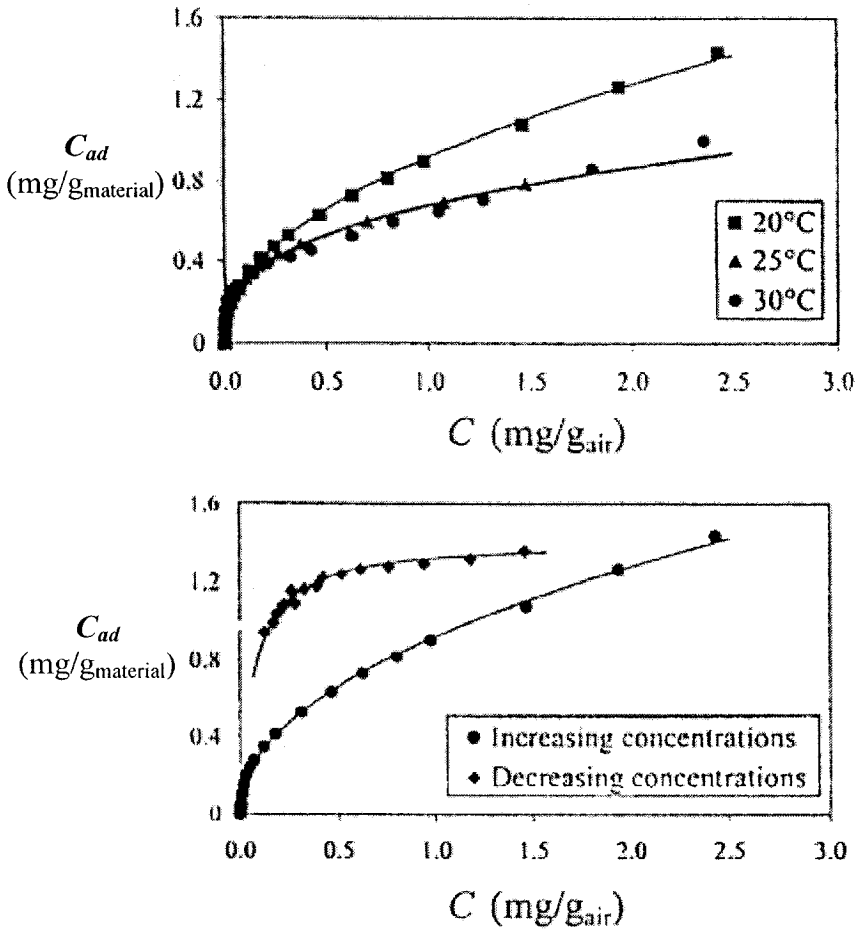

Figure 2-7 Sorption isotherms of acetone/gypsum [Tiffonnet et al., 2002]

In general, the tested acetone concentrations are very high for the application on the VOC source and sink behavior of building materials. Tiffonnet et al. (2002) chose the high acetone concentration levels considering the possible high VOC concentrations in the newly manufactured building materials; however, the selected concentration levels are not associated with the real measurement data of initial VOC concentrations. For a vinyl flooring, which is a strong source of VOCs among solid building materials [Maroni et al., 1995], the measured initial VOC concentrations that are equivalent to the adsorbed-phase concentration (C_{ad}) range from 5.1 μg/g$_{material}$ to 134 μg/g$_{material}$ for 7 VOCs [Cox et al.,

2001a]. For carpets, the initial VOC concentrations obtained as the VOC total mass emitted from one week long emission tests divided by the volume of the carpet, vary from 0.34 $g/m^3_{material}$ to 255 $g/m^3_{material}$ [Little et al., 1994]. When these values are converted to the gas-phase concentration (C) using the given Henry adsorption constants (K), the initial concentrations are within the range from 98 $\mu g/m^3_{air}$ to 4.6 mg/m^3_{air}. These indicate that the tested ranges of VOC concentrations by Tiffonnet et al. (2002) may be much higher even for the initial concentration levels of solid building materials. Solid building materials can sometimes be subjected to high VOC concentrations, e.g. during the application of high VOC contained solvent-based surface coating materials, chemical spill, etc. When source and sink behavior of a single solid building material under typical indoor conditions is considered, the Henry isotherm may be sufficient.

2.2-2 Diffusion in Porous Materials

Porous materials have generally complicate pore structures consisting of random network of interconnecting pores of varying diameter and orientation. Since the diffusion strongly depends on the details of the pore structure, it is hard to predict the effective diffusion coefficient of a porous material. The generally adopted method is to relate the effective diffusion coefficient of a porous solid to the diffusion coefficient in a straight cylindrical pore with the diameter equal to the mean diameter of the porous solid, under comparable physical conditions as follows [Kärger and Ruthven, 1992],

$$D_e = \frac{\varepsilon \cdot D_P}{\tau_P} \tag{2-6}$$

where, D_e is the effective diffusion coefficient in porous material [m^2/s]; ε is the porosity [$m^3_{pore}/m^3_{material}$]; D_P is the diffusion coefficient for a straight cylindrical pore of the same

diameter (taking into account all operative mechanisms of diffusion) [m^2/s]; and τ_P is the tortuosity factor.

The porosity factor, ε, corrects the fact that transport occurs only through the pores and not through the solid matrix, so the diffusion coefficient in the straight cylindrical pore is based on the pore cross sectional area. Due to the introduction of ε, the mass flux given by the effective diffusion coefficient (D_e) is based on the total cross section of the porous solid, not just the pore cross section [Satterfield, 1970]

All the effects arising from pore orientation, connectivity, size variation etc., are lumped together into an empirical factor called the tortuosity factor, τ_P, as shown in Eq. (2-6). Under comparable conditions, diffusion in a random pore network will in general be slower than diffusion in a set of straight cylindrical capillaries. The random orientation will lead to a lengthening of the diffusion path and a corresponding reduction in the concentration gradient while the effects of connectivity and variations in the pore diameter may be expected to lead to further reduction of the flux [Kärger and Ruthven, 1992]. The tortuosity is a characteristic property of the pore structure, independent of the nature of the diffusing molecules [Satterfield, 1970]. The tortuosity factor generally falls within the range of 2 to 6, and tends to vary inversely with the porosity [Ruthven, 1984].

Pore diffusion may occur by one or more of three mechanisms: molecular diffusion, Knudsen diffusion, and surface diffusion. Molecular and Knudsen diffusions are gas-phase diffusions, while surface diffusion is adsorbed-phase diffusion. Poiseuille flow

through a porous material, which is driven by the difference in the total pressure across the porous solid, can affect the diffusion flux. This effect, however, is excluded in this review since it can be generally negligible for building materials in indoor environments.

Depending on the pore size, concentration level, etc., different mechanisms of diffusion control the transport. In micropores, the diffusing molecules never escape from the force field of pore wall and the diffusion takes place by an activated process, proceeding by a sequence of jumps between regions of relatively low potential energy (sites), which is called surface diffusion [Ruthven, 1984]. The diffusion in micropores is generally called "intracrystalline" diffusion, or simply "microporous" diffusion, to tell from the adsorbed-phase diffusion (surface diffusion) in mesopores or macropores. The microporous diffusion coefficients are generally in the order of 10^{-11} to 10^{-16} m^2/s [Ruthven, 1984]. Within the mesopore range, Knudsen diffusion is generally more important but there may also be significant contributions from surface diffusion and capillary effects [Kärger and Ruthven, 1992]. In macropores, the role of the surface is relatively minor and the diffusion occurs mostly by the molecular diffusion.

In gas-phase diffusion, different types of diffusion can occur in the pores depending on the pore size and the mean free path of the diffusing molecule. The mean free path is the average distance a molecule travels before it collides with another molecule, which can be estimated from the following relation [Treybal, 1968],

$$\lambda = \frac{3.2\mu}{P}\sqrt{\frac{R_c T}{2\pi \cdot g_c M}} \qquad (2\text{-}7)$$

where, λ is the mean free path [cm]; μ is the viscosity [poise = g mass/cm/s]; P is the pressure [g force/cm^2, 1 atm=1033.2 g force/cm^2]; T is the temperature [K]; g_c is the gravitation acceleration [980 g mass·cm/g force/s^2]; M is the molecular weight [g mass/g mole]; and R_c is the universal gas law constant [84780 g force·cm/K/g mole]. Figure 2-8 presents the schematics of the three different gas-phase diffusion mechanisms under different combination of pore size and the mean free paths: Knudsen diffusion, molecular diffusion, and transitional diffusion, which is the combination of Knudsen and molecular diffusions. The details of these diffusion mechanisms as well as the surface diffusion are discussed here.

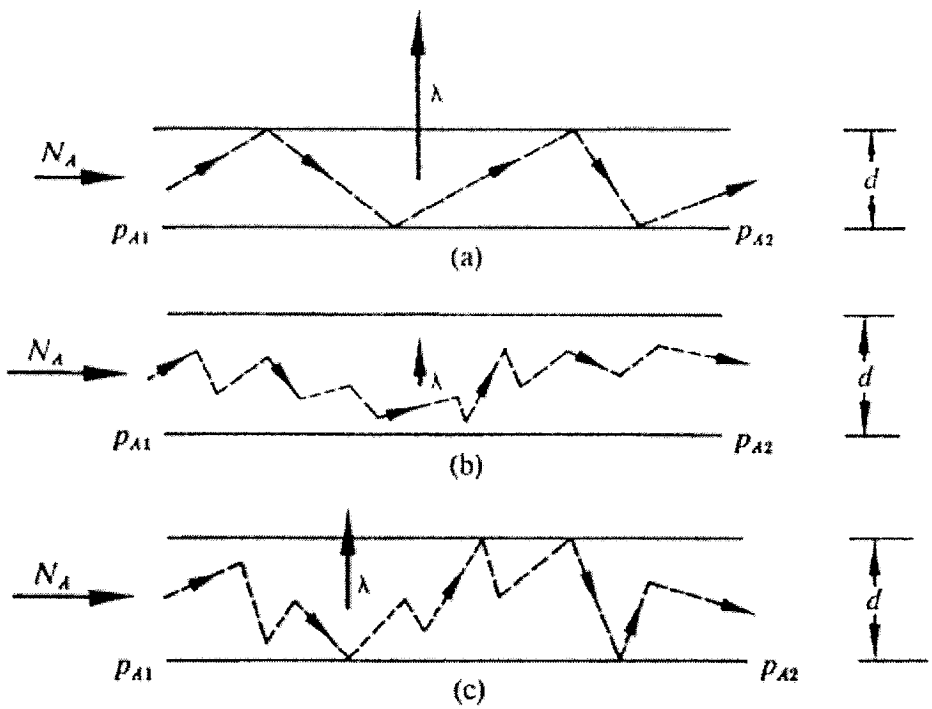

Figure 2-8 Gas-phase diffusion [Geankoplis, 1972]
- (a) Knudsen diffusion, (b) molecular diffusion, (c) transition diffusion

Molecular Diffusion

When pore diameter is large relative to the mean free path as shown in Fig. 2-8 (b) – i.e., when the Knudsen number (*Kn*) defined as the ratio of the mean free path to the pore diameter (λ/d) is less than 0.01, collisions between diffusing molecules will occur far more frequently than collisions between a molecule and the pore wall [Geankoplis, 1972]. Under these conditions, the influence of the pore wall is minor and the diffusion occurs by essentially the same mechanism as in the bulk fluid. The pore diffusivity for a straight cylindrical pore is then identical with the molecular or Fick diffusion coefficient (D_F) [Kärger and Ruthven, 1992].

Molecular diffusion coefficients of binary gas mixtures can be estimated using the Wilke and Lee modification of the Hirschfelder-Bird-Spotz method, which is based on the kinetic theory of gases and the Lennard-Jones expression for intermolecular forces [Treybal, 1968; Perry and Chilton, 1973]. This is recommended for mixtures of nonpolar gases or of a polar with a nonpolar gas. Using this method, Lyman et al. (1990) reported that the absolute average error for about 150 compounds was 4.3% and the average errors for all classes of compounds except acids were less than 8%. The diffusion coeffcient was calculated as follows,

$$D_{F,AB} = \frac{B \cdot T^{3/2} \cdot \sqrt{(1/M_A)+(1/M_B)}}{P \cdot r_{A-B}^2 \cdot I_D} \qquad (2\text{-}8)$$

where, $D_{F,AB}$ is molecular diffusion coefficient of binary gases A and B [m^2/s]; T is the absolute temperature [K]; $B = \left(10.85 - 2.51 \cdot \sqrt{(1/M_A)+(1/M_B)}\right) \times 10^{-8}$; M_A and M_B are the molecular weight of gas A and B, respectively [kg/mol]; P is the absolute pressure [atm];

$r_{A\text{-}B}$ is the collision diameter [Å]; and I_D is the collision integral based on the Lennard-Jones potential. The moelcular diffusion coefficient is inversly proportional to the total pressure. For the temperature, the combined effect of $T^{3/2}$ in the numerator and the temperature dependent function I_D gives an overall temperature dependence of approximately $T^{1.7}$ [Ruthven, 1984]. In general, molecular diffusion coefficients of gases are in the range of 5×10^{-6} to 1×10^{-5} m^2/s [Welty et al., 1976].

Knudsen Diffusion

In small pores and/or at low pressures, the mean free path of a diffusing molecule is greater than the pore diameter- i.e. Knudsen number, $Kn \geq 10$, and collisions between a molecule and the pore wall occur more frequently than intermolecular collisions as shown in Fig. 2-8(a) [Geankoplis, 1972]. This is known as Knudsen flow or Knudsen diffusion. The molecules hitting the wall are momentarily adsorbed and then given off in random direction, which has no relation to its original direction before collision to the wall [Ruthven, 1984]. The gas flux is reduced by the wall resistance that causes a delay because of the randomness in diffuse reflection and the finite time the molecule is adsorbed [Satterfield, 1970]. Knudsen diffusion is not observed in liquids.

Kinetic theory provides the following relations for Knudsen diffusion in gases in a straight cylindrical pore,

$$D_{K,A} = 9700 \cdot r \cdot \sqrt{\frac{T}{M_A}} \qquad (2\text{-}9)$$

where $D_{K,A}$ is the Knudsen diffusion coefficient of diffusing gas A [cm^2/s]; r is the pore radius [cm]; T is the absolute temperature [K]; and M_A is the molecular weight of

diffusing gas A [kg/mol]. When the Knudsen number, $Kn \approx 10$, Eq. (2-9) will predict the diffusion within about 10% of error. As the Kn gets larger, this error decreases since the diffusion approaches more closely to the pure Knudsen type [Geankoplis, 1972]. The Knudsen diffusion coefficient varies only weakly with temperature, i.e., temperature dependence of $T^{0.5}$. It is independent of composition of diffusing gases, pressure, or total gas concentration, since the mechanism does not depend on intermolecular collisions. The inverse square root dependence on molecular weight is the same as for molecular diffusion [Kärger and Ruthven, 1992].

Transition Region

When the mean free path is comparable with the pore diameter, i.e., $0.01 < Kn < 10$, both intermolecular collisions and wall collisions are significant and diffusion occurs by the combined effects of both the molecular and Knudsen diffusion mechanisms as shown in Fig. 2-8 (c) [Geankoplis, 1972]. Due to the dependence of mean free path on the pressure, for a given pore size there will be a transition from the molecular diffusion at high pressure to Knudsen diffusion at low pressure [Ruthven, 1984].

For a binary gas mixture in a porous solid at constant pressure the combined diffusion coefficient in straight cylindrical pore, is given by

$$\frac{1}{D_{p,A}} = \frac{1}{D_{K,A}} + \frac{1}{D_{F,AB}}\left[1 - y_A\left(1 + \frac{N_B}{N_A}\right)\right] \qquad (2\text{-}10)$$

where, $D_{p,A}$ is the diffusion coefficient of diffusing gas A in a straight cylindrical pore [m^2/s]; $D_{F,AB}$ is the molecular diffusion coefficient in binary A-B mixture [m^2/s]; $D_{K,A}$ is

the Knudsen diffusion coefficient of diffusing gas A [m^2/s]; y_A is the mole fraction of gas A [mol/mol]; and N_A, N_B are the fluxes of gas A and B, respectively [$mol/m^2/s$]. For equimolar counter diffusion, $N_A = -N_B$, then Eq. (2-10) is reduced to the simple reciprocal addition rule,

$$\frac{1}{D_{P,A}} = \frac{1}{D_{K,A}} + \frac{1}{D_{F,AB}} \qquad (2\text{-}11)$$

Compared with Eq. (2-10), Eq. (2-11) is always a good approximation when the mole fraction, y_A is small [Kärger and Ruthven, 1992]. In the applications for VOC source and sink behavior of porous building materials, a mole fraction of a VOC in air is generally very small; hence Eq. (2-11) can be used. Since $D_{K,A}$ is proportional to the pore radius and $D_{F,AB}$ varies inversely with the total pressure, Eq. (2-11) clearly predicts the transition from Knudsen diffusion in small pores at low pressure to molecular diffusion in larger pores and at higher pressure [Kärger and Ruthven, 1992].

Figure 2-9 illustrates the effect of pore size on the diffusion flux for the binary system of hydrogen-nitrogen at a fixed 1 atm of total pressure and 298K of temperature. In small pores the Knudsen diffusion dominates. As the pore size increases, both molecular and Knudsen diffusions affect the fluxes until certain limits. At larger pores, only molecular diffusion determines the fluxes. The range of pore sizes for which diffusion will occur in the transition region depends on the relative values of D_K and $D_{F,AB}$, and moves in the direction of smaller pores with increased pressure and/or increased molecular weight [Satterfield, 1970].

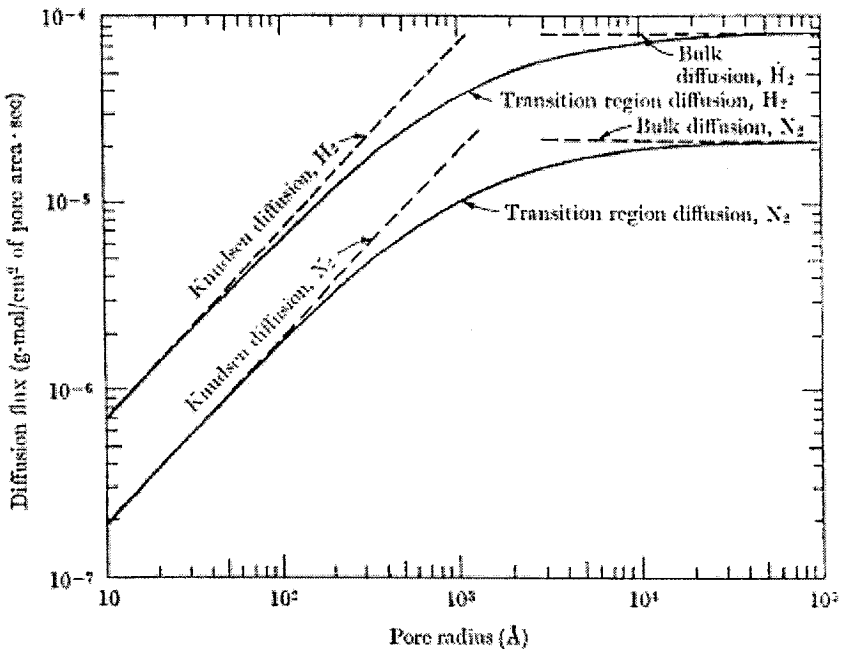

Figure 2-9 Effect of pore sizes on the gas-phase diffusion [Satterfield, 1970]

Surface Diffusion

When there is significant adsorption on the pore wall, there is the possibility of an additional flux due to diffusion through the adsorbed phase diffusion or surface diffusion. Since the mobility of the adsorbed phase is generally much smaller than that of the gas-phase, significant physical adsorption is a prerequisite for the flux from surface diffusion to be noticeable [Ruthven, 1984]. Yet if adsorbed molecules are held so strongly as to be essentially immobile, surface diffusion will be insignificant [Satterfield, 1970].

The fluxes through the gas-phase and the adsorbed phase are parallel and additive so that the overall diffusion coefficient for a straight cylindrical pore can be given by the sum of the gas-phase diffusion coefficient and surface diffusion coefficient considering the adsorption as follows [Ruthven, 1984],

$$D_p = D_g + K \cdot D_{ad} \qquad (2\text{-}12)$$

where, D_p is the overall diffusion coefficient for a straight cylindrical pore [m^2/s]; D_g is the gas-phase diffusion coefficient due to Knudsen and/or molecular diffusion [m^2/s]; D_{ad} is the adsorbed-phase or surface diffusion coefficient [m^2/s]; and K is the dimensionless adsorption equilibrium constant.

The surface diffusion coefficient, D_{ad}, varies from 10^{-7} to 10^{-17} m^2/s depending on the types of adsorbate and adsorbent [Satterfield, 1970]. High D_{ad} values are obtained for weakly adsorbed nonpolar adsorbate on nonpolar surfaces, and small values are obtained for strongly chemisorbed adsorbates [Ruthven, 1984]. For physically adsorbed molecules such as hydrogen, nitrogen, carbon dioxide, methane, ethane, propane, and butane on surfaces like porous glass, carbon, silica gel and typical porous catalysts, D_{ad} are typically in the range of 10^{-7} to 10^{-9} m^2/s at ambient temperature [Satterfield, 1970].

The contribution of the surface diffusion to the overall diffusion coefficient depends on the ratio of the product of $K \cdot D_{ad}$ to D_g, rather than D_{ad} to D_g. With increasing temperature, D_{ad} increase; however, the flux due to surface diffusion always decreases since K- thus the adsorbed concentration, will decrease more rapidly than D_{ad} will increase [Kärger and Ruthven, 1992].

Surface diffusion is generally significant in small diameter pores where the gas-phase flux can generally be attributed entirely to Knudsen diffusion [Ruthven, 1984]. For example, the measured D_{ad} of ethane, propane and butane on silica gel with 22Å of the

average pore diameter, surface diffusion accounted for 64% to 87% of total transfer [Satterfield, 1970]. In larger pores like macropores, molecular diffusion dominates and D_g is generally much larger than D_{ad}. In addition, macropores typically contribute very little to the adsorption capacity [Kärger and Ruthven, 1992]; hence K will be relatively small. Therefore, surface diffusion will be negligible in macroporous materials, unless there is significant adsorption.

Diffusion Coefficient Measurement for Building Materials

Depending on the modes of diffusion mechanisms involved in a porous material, the experimentally measured effective diffusion coefficient can be different. Several experimental methods have been proposed to measure the diffusion coefficients of VOC-air system for various building materials. Table 2-3 summarizes these existing methods including the test procedure, and pros and cons of each type of method. All methods except the porosity test method provide only the effective diffusion coefficients, D_e [Meininghaus et al., 1998 and 2000a; Kirchner, et al., 1999; Hansson and Stymne, 2000; Bodalal et al., 2000]. Other information like tortuosity and porosity factors, and the types of diffusion mechanisms involved, are not available.

Due to the different diffusion mechanisms involved and/or the difference in boundary conditions etc., significant discrepancy in D_e measured by different techniques is often observed. For example, D_e measured by the cup method are often larger than those measured by other methods [Haghighat et al., 2002]. Since the material specimen is subjected to the saturation vapor concentration in the cup method, surface diffusion may

Table 2-3 Summary of the diffusion coefficient measurement methods

Method	Test procedure	Merits	Drawbacks
Cup method Kirchner, et al., 1999; Hansson et al., 2000	• Speciman placed over liquid contained in a cup, and placed in a controlled environment • Periodic measurement of weight loss using microbalance • Calculation of D_e using Fick's 1st law	• Simple experimental procedure • Simple calculation tehnique • No limitation of material type	• Possible overestimation of D_e due to high VOC concentration (wet cup test) • Only one VOC in one test • Long experimental time
Twin chamber method Meininghaus et al., 1998; Hansson and Stymne, 2000; Bodalal et al., 2000	• Speciman placed between two identical chambers • Introduction of VOCs at a constant concentration in one chamber; and clean air in the other chamber • Periodic measurement of VOC concentrations of both chamber air using GC • Calculation of D_e using Fick's 1st or 2nd law	• Controllable VOC concentration • No limitation of materials • VOC mixture can be tested: D_e of various VOCs can be obtained from one test	• Relatively complicated experimental and analysis procedures • Long experimntal time to reach steady state conditions • Possibile multiple existence of best-fits of coefficients (Twin-compartment and Diffusionmetry methods)
Porosity test method Tiffonnet et al., 2000; Blondeau et al., 2000	• Porosity and pore size distribution measurement using Mercury Intrusion Porosimetry (MIP) test • Carniglia's mathematical model	• Short experimental time (up to 2 hours) • D_e of various VOC at various temperature can computed from one test.	• Homogeneous materials only • Relatively complicated analysis procedure • No consideration of the possible interaction between the VOC and the material

significantly contribute to the total flux. This can result in larger D_e in the cup method compared with the twin chamber test data, which are measured at much lower VOC concentration levels relative to the saturation concentration.

In the porosity test method, D_e are obtained using the information on the material structure like the pore size distribution and porosity, which are measured by Mercury Intrusion Porosimetry (MIP) tests [Tiffonnet et al., 2000; Blondeau et al., 2000]. In assessing the diffusion coefficients, the mean diffusion coefficient in the pores of the material and the tortuosity factor of the porous network are computed by applying the

Carniglia's mathematical model, which considers the pore interconnections, the pore constriction, and the pore random orientation. In this method, surface diffusion is not considered.

2.3 PHYSICAL MODELS FOR SOLID MATERIALS AND ASSEMBLY

The physical models for solid materials can be classified by the ways that they treat the internal diffusion, and the surface emission, which describes the transfer between the air-material interface and the bulk air. There are two approaches describing the internal diffusion: material-phase and multiple-phase approaches. The material-phase approach assumes VOC within a solid material as one homogeneous phase, i.e., material-phase, and the phase change of VOC from the material-phase to the gas-phase takes place at the solid-air interface. Generally, the linear partitioning is used to relate the material-phase concentration with the gas-phase one. The mathematical model of the material-phase approach is described as follows,

$$\frac{\partial C_m}{\partial t} = D_m \cdot \nabla^2 C_m \qquad for\ -b \le y \le 0 \qquad (2\text{-}13)$$

$$C_m = K_m \cdot C \qquad at\ y = 0 \qquad (2\text{-}14)$$

where, C_m is the material-phase VOC concentration [mg $_{VOC}/m^3$ $_{material}$]; t is time [s]; D_m is the material-phase VOC-air diffusion coefficient of the solid [m^2/s]; K_m is the partition coefficient [m^3 $_{air}/m^3$ $_{material}$]; and C is the gas-phase VOC concentration [mg $_{VOC}/m^3$ $_{air}$].

This approach is appropriate for nonporous or microporous (i.e., less than 2nm or 20 Å of pore diameter) materials. In nonporous materials, the material surface is limited to the

air-solid interface (y = 0) and solid-phase diffusion of VOC through the solid will occur. For microporous materials, the diffusing VOC cannot escape the Van der Waal's force field within the pores; hence VOC is diffused as adsorbed-phase only [Ruthven, 1984]. Hence, the one-phase approach is correct. However, when it is applied to meso/macroporous building materials, where both gas-phase and adsorbed-phase VOC coexist, "material-phase" term becomes ambiguous and this may cause inconvenience in measuring the diffusion coefficient of a porous material, which is explained later.

The multiple-phase approach describes the VOC diffusion in macroporous building materials. In macroporous materials, it is assumed that the VOC diffusion through solid is negligible compared with that through the pores. Within macropores, VOC exist both in form of gas-phase and adsorbed-phase. Since gas-phase VOC are much mobile than adsorbed-phase, gas-phase diffusion is much faster and significant than adsorbed-phase diffusion (or surface diffusion). Therefore, the surface diffusion, diffusion along pore surfaces as adsorbed-phase is not considered in the modeling. This approach, multiple-phase approach, considers both gas and adsorbed phases of VOC within the material, but assumes that the diffusion occurs only as gas-phase [Murakami et al., 1998 and 1999; Blondeau et al., 2000]. The mathematical model of this approach is expressed using the volume-based concentration as,

$$\varepsilon \frac{\partial C}{\partial t} + \frac{\partial C_{ad}}{\partial t} = D_s \cdot \nabla^2 C \qquad for\ -b \le y \le 0 \qquad (2\text{-}15)$$

where, C is the gas-phase VOC concentration [$mg_{gas\text{-}phase\ VOC}/m^3_{air}$]; ε is the porosity [$m^3_{air}/m^3_{material}$]; C_{ad} is the adsorbed-phase concentration [$mg_{adsorbed\text{-}phase\ VOC}/m^3_{material}$]; and

D_s is the effective diffusion coefficient of the solid [m^2/s]. Generally the sorption model is defined as:

$$C_{ad} = f(C) \tag{2-16}$$

Substituting Eq. (2-16) into Eq. (2-15) gives,

$$\frac{\partial C}{\partial t} = \frac{D_s}{\left(\varepsilon + \frac{\partial f}{\partial C}\right)} \cdot \nabla^2 C \qquad for\ -b \le y \le 0 \tag{2-17}$$

Since this approach describes the internal diffusion as gas-phase, the VOC concentration is continuous at the solid-air interface.

$$C\big|_{y=o-} = C\big|_{y=0+} \qquad at\ y = 0 \tag{2-18}$$

The input parameters for internal diffusion are gas-phase or material-phase diffusion coefficient and sorption property of the solid. Various measurement techniques have been proposed; however, the difference in the measured properties of different techniques is often huge. Review indicates that assumptions made in, and the techniques used to, analyze the data are major reasons of discrepancy [Haghighat et al., 2002]. For example, applying material-phase approach results in material-phase diffusion coefficients (D_m), which are generally several orders of magnitude smaller than gas-phase diffusion coefficient (D_s). While D_s can be obtained independently by analyzing the steady state data, where sorption does not affect the VOC transfer, or by measuring the pore sizes of the solid, D_m is always influenced by the sorption property of the solid. Considering the

possible coupling of D_m and the sorption property, the measurement data have to be analyzed more carefully.

Whilst the internal diffusion described either by material-phase or multiple-phase approach, the surface emission has been described several ways. The most common practice is to treat the surface emission as convection as described in the following two approaches. One approach is the conjugate mass transfer approach using the fourth-kind boundary condition. This approach is the more general but also the more complicated one; therefore, Computational Fluid Dynamics (CFD) methods are often used. Generally, momentum transfer and convective mass transfer equations are solved as a decoupled system since it is assumed that the amounts of emitted VOC are so small that they do not affect the air velocity profile. For all cases presented in this work, this assumption is valid. The air velocity distribution of the intended modeling domain is first obtained by solving the flow governing equations neglecting the VOC transfer into the air. Knowing the air velocity distribution, the mass transfer equations for both VOC convection and internal diffusion are solved with the fourth-kind boundary condition at the solid-air interface as follows,

<u>for multiple-phase approach,</u>

$$-D_s \left.\frac{\partial C}{\partial y}\right|_{y=0-} = -D_a \left.\frac{\partial C}{\partial y}\right|_{y=0+} \qquad at\ y = 0 \qquad (2\text{-}19)$$

<u>for material-phase approach,</u>

$$-D_m \left.\frac{\partial C_m}{\partial y}\right|_{y=0-} = -D_a \left.\frac{\partial C}{\partial y}\right|_{y=0+} \qquad at\ y = 0 \qquad (2\text{-}20)$$

These boundary conditions imply that the flux is continuous at the air-solid interface.

The second approach is the boundary layer approach using the third-kind boundary condition. This approach is much simpler than the conjugate mass transfer approach. In this approach, only the internal diffusion equation with the third-kind boundary condition at the solid-air interface, is required to be solved. The third-kind boundary condition is:

for multiple-phase approach,

$$-D_s \left.\frac{\partial C}{\partial y}\right|_{y=0-} = h_D \cdot (C - C_\infty) \qquad at\ y = 0 \qquad (2\text{-}21)$$

for material-phase approach

$$-D_m \left.\frac{\partial C_m}{\partial y}\right|_{y=0-} = h_D \cdot (C - C_\infty) \qquad at\ y = 0 \qquad (2\text{-}22)$$

where, h_D is the convective mass transfer coefficient (MTC) [m/s], and C_∞ is the ambient VOC concentration outside the boundary layer [mg/m^3].

The key issue in this second approach is how to obtain accurately the convective mass transfer coefficient. The MTC is generally calculated from the heat-mass transfer analogy. If we consider e.g. forced convection over a flat plate, Sherwood number correlations for the material emissions are as follows [Holman, 1990],

- Laminar ($Re_L < 5\times10^5$)

$$Sh_L = 0.664 \cdot \mathrm{Re}_L^{0.5} \cdot Sc^{\frac{1}{3}} \qquad (2\text{-}23)$$

- Turbulent ($Re_L > 5\times10^5$)

$$Sh_L = 0.036 \cdot \mathrm{Re}_L^{0.8} \cdot Sc^{\frac{1}{3}} \qquad (2\text{-}24)$$

where, Sh_L is the averaged Sherwood number ($Sh_L=h_D \cdot L/D_a$); Re_L is the Reynolds number based on the plate length ($Re_L=u_\infty \cdot L/\nu$); Sc is the Schmidt number ($Sc=\nu/D_a$); D_a is the binary molecular diffusion coefficient of air and VOC [m^2/s]; L is the length of the solid [m]; u_∞ is the air velocity outside the boundary layer [m/s]; and ν is the kinematic viscosity [m^2/s]. Sparks et al. (1996b) obtained the Sherwood number relations using pure p-dichlorobenzene emission data from several dynamic small scale and test-house experiments. The correlations were obtained with R^2 of 0.98 as follows,

$$Sh_L = 0.33 \cdot \mathrm{Re}_L^{0.67} \quad \text{or} \quad Sh_L = 0.28 \cdot \mathrm{Re}_L^{0.65} \cdot Sc^{0.333} \qquad (2\text{-}25)$$

There are other ways treating the surface emission apart from convection. One is directly applying the mass balance equation in the chamber air [Little et al., 1994]. This approach assumes that the VOC emitted from the solid is instantaneously fully mixed with the chamber air without considering the boundary layer resistance. Hence, the gas-phase VOC concentration at the surface of the solid is the same as the room air concentration. The internal diffusion equation is solved with the following boundary condition, which is expressed for material-phase approach.

$$V\frac{\partial C_a}{\partial t} = Q \cdot (C_{in} - C_a) + A \cdot \left(- D_m \left. \frac{\partial C_m}{\partial y} \right|_{y=0} \right) \qquad at\ y = 0 \qquad (2\text{-}26)$$

where, C_a is the VOC concentration of the chamber air [mg/m^3]; C_{in} is the VOC concentration of the inlet air [mg/m^3]; V is the chamber volume [m^3]; Q is the ventilation rate [m^3/s]; and A is the area of the solid [m^2]. Considering the linear partitioning between C_a and C_m like Eq. (2-14), Eq. (2-26) becomes,

$$\frac{V}{A \cdot K_m} \cdot \left.\frac{\partial C_m}{\partial t}\right|_{y=0} + D_m \cdot \left.\frac{\partial C_m}{\partial y}\right|_{y=0} - \frac{Q}{A \cdot K_m} \cdot \left(K_m \cdot C_{in} - C_m\big|_{y=0}\right) = 0 \qquad (2\text{-}27)$$

Another approach is to prescribe VOC concentration at the solid-air interface, i.e., the first-kind boundary condition. This approach has many limitations in application, since not only we cannot measure the surface VOC concentrations but also the surface VOC concentration is a function of time. The case of zero surface concentration may be applicable only for the long-term emission.

The previously proposed physical models for single solid materials are summarized according to their approaches of internal diffusion and surface emission in the Table 2-4. Only the models with the material-phase approach were compared with the small-scale emission test data. Since there is still lack of study on the material property measurement, for the validation one or more material properties were determined by the best fitting, which gives the best agreement between the model prediction and the emission test data. If we can assume that the measured VOC emission test data are just primary emissions, fitting one or decoupled two parameters may be acceptable. Unfortunately, not only the emission test cannot tell apart between the primary and the secondary emissions, but also in some cases the secondary emissions may be significant from the beginning [Wolkoff,

1999]. In such cases, fitting the material properties using the primary-emission-only model is not appropriate.

Table 2-4 Physical models for VOC source and sink behavior of solid materials

Models	solution	Internal diffusion	Surface emission	Comment
Little et al. (1994)	analytical	▪ Material-phase ▪ 1-D diffusion ▪ volume-based concentration	▪ Mass balance	▪ Validated with carpet emission test data ▪ D_m was fitted
Yang et al. (1998, 2001c)	CFD	▪ Material-phase ▪ 2 or 3-D diffusion ▪ volume-based concentration	▪ Convection: 4th-kind B.C. ▪ 2 or 3-D laminar momentum and convective mass transfer	▪ validated with carpet and particle board emission test data ▪ C_o, D_m were fitted
	analytical	▪ 1-D diffusion	▪ 1st-kind B.C. ▪ C=0 at solid-air interface	▪ Applicable only for long term emission ▪ Not applicable for sink behavior
Huang & Haghighat (2002a)	numerical	▪ Material-phase ▪ 1-D diffusion ▪ volume-based concentration	▪ Convection: 3rd-kind B.C.	▪ Validated with Yang's particle board emission test data with the same material properties
	analytical	▪ 1-D diffusion	▪ Convection: 3rd-kind B.C. ▪ C_∞ = 0 always	▪ Overestimation of emission rates at early stage ▪ Not applicable for sink behavior
Murakami et al. (1998, 1999)	CFD	▪ Multiple–phase ▪ 2-D diffusion ▪ mass-based concentration	▪ Convection: 4th-kind B.C. ▪ 2-D turbulent momentum and convective mass transfer ▪ mass based concentration	▪ No validation ▪ Simulation using the parameters in literature
Blondeau et al. (2000)	numerical	▪ Multiple-phase ▪ 1-D diffusion ▪ mass-based concentration	▪ Convection: 3rd-kind B.C.	▪ No validation ▪ Simulation using experimentally obtained parameters ▪ Reactions at the material surfaces discussed but not simulated
Yang et al. (2001b)	analytical	▪ Material-phase ▪ 1-D diffusion ▪ volume-based concentration ▪ C(t,y=-b)=0 ▪ Co=0	▪ C(t,y=0) is given or obtained by solving the momentum and convective mass transfer equations numerically	▪ Sink behavior only (not applicable for emission)

These emission models can be generally applied for sink behavior, except some models with zero concentration in the air like the analytical models by Yang et al. (1998) and Huang and Haghighat (2002a). Yang et al. (2001b) developed an analytical model to evaluate the sink rate of single solid material with the known material properties and air-phase concentration. The model only considers the internal diffusion as 1-D unsteady material-phase diffusion. The solid has zero initial VOC concentration. Since the model assumes zero concentration at the bottom of the solid, the model cannot be applicable for thin substrate materials, where VOC can diffuse to the bottom.

Only a few models have been developed for building material assemblies. Yang et al. (2001a) expanded the sorption model mentioned above to investigate the sink effects on the emissions from wet/solid material assembly like paint/gypsum board. For the solid material, the modeling is exactly the same. Other mechanisms that the model considered are convection using 4th-kind boundary condition; linear partitioning between the VOC concentration in the air and that in the wet material film; the three-dimensional unsteady diffusion in the wet material film of which the diffusion coefficient (D_{wm}) of wet material film was described as

$$D_{wm} = D_{wmo} \cdot \left(\frac{C_{wm}}{C_{wmo}} \right)^3 \qquad (2\text{-}28)$$

where, D_{wmo} is the initial diffusion coefficient in wet material film [m^2/s]; C_{wm} is the material-phase VOC concentration of wet material film at time t [mg/m^3]; and C_{wmo} is the initial VOC concentration [mg/m^3]. At the wet material film and the solid interface, the flux and the concentration are continuous as

$$-D_{wm}\frac{\partial C_{wm}}{\partial y} = -D_m\frac{\partial C_m}{\partial y} \tag{2-29}$$

$$C_{wm} = C_m \tag{2-30}$$

where, D_m is the material-phase diffusion coefficient of solid material [m^2/s]; and C_m is the material-phase VOC concentration of solid material [mg/m^3]. Since this model uses the material-phase approach, Eq. (2-30) means that the sorption partition coefficient of solid is the same as the partition coefficient of the wet material film. The assumptions underlying in Eqs. (2-28) and (2-30) need to be validated. Yang et al. (2001a) compared the prediction made by the model with the small-scale emission test data of wood stain/oak assembly; however, both D_{wmo} and D_m were fitted with the emission test data due to the difficulty in measurement especially D_{wmo}.

Haghighat and Huang (2003) developed numerical models for various material assemblies. The model considers the one-dimensional material-phase diffusions in the materials and convection with 3rd-kind boundary condition. For wet material, the same modeling approach with Yang et al. (2001a) was used and Eqs. (2-29) and (2-30) were applied at the wet-solid material interface; hence, the same limitation and difficulty mentioned above can arise. At the solid-solid material interface, the flux and the equivalent gas-phase VOC concentration is continuous assuming perfect contact as follows,

$$-D_{m1}\frac{\partial C_{m1}}{\partial y} = -D_{m2}\frac{\partial C_{m2}}{\partial y} \tag{2-31}$$

$$C_{m1} = \frac{K_{m1}}{K_{m2}}\cdot C_{m2} \tag{2-32}$$

where, D_m is the diffusion coefficient of solid material [m^2/s]; C_m is the material-phase VOC concentration in the solid material[mg/m^3]; K_m is the partition coefficient; and subscripts *1,2* refers to the two solid materials in contact.

Kumar and Little (2002) developed an analytical model for VOC emissions from solid/solid material assembly considering the one-dimensional material-phase internal diffusions in solid materials and mass balance approach as in Eq. (2-15) for surface emission without considering the boundary layer resistance. At the solid-solid interface, Eqs. (2-31) and (2-32) were used.

To predict and investigate the long-term source and sink behavior of building materials covering e.g. the entire product service life, analytical models are desirable. The previously proposed analytical models have many limitations. The models proposed by Little et al. (1994), and Kumar and Little (2002) do not consider the boundary layer resistance and they considered the gas-phase VOC concentration at the surface is the same as the ambient chamber air concentration. In order to investigate the effect of convection on the material emissions, Lee et al. (2000) applied a conjugate mass transfer model with two-dimensional forced convection mass transfer over a flat plate coupled with one-dimensional diffusion within the solid. The airflow is assumed laminar and the solid material is subjected to a constant VOC concentration at the lower surface. The results showed that, for solid and porous materials with high diffusion coefficient (i.e., larger than 10^{-11} m^2/s), convection effects cannot be ignored. Therefore, when Little's model is applied for porous materials, it may overestimate the VOC emission/sorption

rate, especially for the early stage of emission when it is controlled by convection [Zhang et al., 1996, Low et al., 1998].

The analytical model proposed by Yang et al. (1998) assumes zero VOC concentration at the solid surface, which can be applicable to aged materials when the emission rate is very small. The analytical model proposed by Huang and Haghighat (2002a) considered the convection with the third-kind boundary condition with zero VOC concentration for the ambient air outside the boundary layer; hence, the unsteady one dimensional diffusion equation of material-phase approach with the homogeneous boundary condition were solved using the separation of variables method. The assumption of zero ambient VOC concentration causes over estimation of VOC emission rate at the early stage of emission, when the emission rate is high. Both analytical models are applicable only for emission not sorption. The review indicates that more detailed analytical model is needed for the investigation of the VOC emissions from porous materials.

2.4 SUMMARY

Fundamental theories on the mass transfer mechanisms in porous materials were summarized. The review of the various aspects of adsorption/desorption indicates that linear adsorption isotherm may be adequate to model VOC source and sink behavior in building materials. Only in some extreme cases where the building material is subjected to very high VOC concentrations, nonlinear isotherms and/or hysteresis is observed. In a porous material, molecular, Knudsen, and/or surface diffusions can occur depending on the pore size and the concentration levels that the porous material is subjected to. The

types of diffusion mechanisms involved in the mass transfer can affect the measured effective diffusion coefficient, which is an important input parameter in mass transfer models.

The previously proposed models for VOC source and sink behavior of solid building materials and assemblies were reviewed and classified based on the modeling approach of each VOC transfer mechanism considered, and the limitations of these modeling approaches were discussed. For internal diffusion, the material-phase approach is appropriate for microporous materials, and the multiple-phase approach is suitable for macroporous materials since only the gas-phase diffusions are considered. For surface transfer, the 4^{th} or 3^{rd} kind convection approach, which considers the convective boundary layer over the material, is desirable especially for porous materials. Existing models for material assemblies are based on invalidated assumptions and/or require input parameters that are hard to measure. This review showed that there is a need for the development of more comprehensive analytical models that can predict long-term VOC source (including primary and secondary emissions) and sink behavior of porous materials considering both internal diffusion and convection.

Chapter 3

Analytical Model

3.1 INTRODUCTION

This chapter presents an analytical model that was developed to predict VOC source (or emission) and sink (or sorption) behavior of porous building materials. Previous studies have tried to explain the source and the sink behavior as two different phenomena; so that many existing models can be applicable for either emission or sorption. For wet materials, transfer mechanisms involved in source and sink behavior are different: evaporation is the dominant process for the early drying phase, whilst diffusion and adsorption control the sink behavior. However, for dry (solid) materials the transfer mechanisms are the same for both VOC source and sink behavior except for the direction of mass transfer, i.e., from material to air for source and from air to material for sink, analogous to the convective heating and cooling of a plate. The source and sink behavior are treated unitary in the proposed model.

According to the definition by Wolkoff (1995 and 1999), the primary emission is the emission of originally free or non-bound VOC and the secondary emission is the emission of originally bound VOC, whether physically or chemically, through various mechanisms like sorption, decomposition, oxidation, etc. As reviewed in Chapter 2, physically adsorbed VOC always exist in the porous materials due to the van der Waal's forces. Since any VOC can move freely from adsorbed phase to gas phase, or vice versa

to satisfy the equilibrium, it is not possible to separate the free VOC from the physically adsorbed VOC in describing the VOC transfer. To eliminate any confusion that arise from the terminology, the terms used in this work are defined as follows,

- Primary source behavior: emission of VOCs originally in gas and physically adsorbed phases within a porous material
- Secondary source behavior: emission of VOCs from other than the primary source behavior. This includes the emissions of VOCs generated from chemical reaction and the various secondary emissions described by Wolkoff (1995 and 1999), except sorption.
- Primary sink behavior: transfer of VOCs from the surrounding air into the material in the form of gas and physically adsorbed phases
- Secondary sink behavior: sink effects of the material other than the primary sink behavior. This includes chemical adsorption, and chemical reactions that consume the VOC of interest

All four behaviors will be considered in the proposed model.

This chapter also presents an assessment of the proposed analytical model for primary source and sink behavior. The assessment involves a comparison of the predictions made by the proposed model with that of the analytical model by Little et al. (1994), and experimental data of carpet emission test and wood chipboard sorption test. Due to a lack of experimental data, the secondary source/ sink behavior was excluded in the model assessment; however, case studies applying hypothetical functions for the secondary source behavior are presented in Chapter 4.

3.2 ANALYTICAL MODEL DEVELOPMENT

The proposed model is developed for porous materials with mesopores and/or macropores. These materials generally have effective diffusion coefficients larger than nonporous or microporous solids. This makes meso/macroporous materials to interact faster with the surrounding environment and have more impact on the indoor air. Many building materials like various wood products, gypsum, concrete, brick [Blondeau et al., 2000], and carpet [Zhou and Warner, 1999], etc. can be classified as meso/macroporous solids. According to the mercury porosimetry measurement introduced by Blondeau et al. (2000), gypsum, wood chipboard, solid and aerated concretes, and brick have mainly macropores, whilst mortar has mainly mesopores following the IUPAC classification.

The proposed model considers that VOC exist in both gas and physically adsorbed phases within the pores following the multiple-phase approach for internal diffusion. Diffusion can take place in the form of molecular, Knudsen, and/or surface diffusions depending on the pore size and the VOC concentration as reviewed in Chapter 2. The proposed model assumes that VOCs diffusion through the solid is negligible as compared with the one through the pores. The proposed model can be applied for porous materials under isobaric and isothermal conditions. Any difference in total pressure will cause a bulk flow of gas, which will eliminate differences in local concentration in a smaller time than the characteristic time for molecular exchange by diffusion. Similarly, any temperature gradient can promote thermal diffusion. Hence, the proposed model does not include any bulk flow due to total pressure difference like Poiseuille flow, and thermal diffusion.

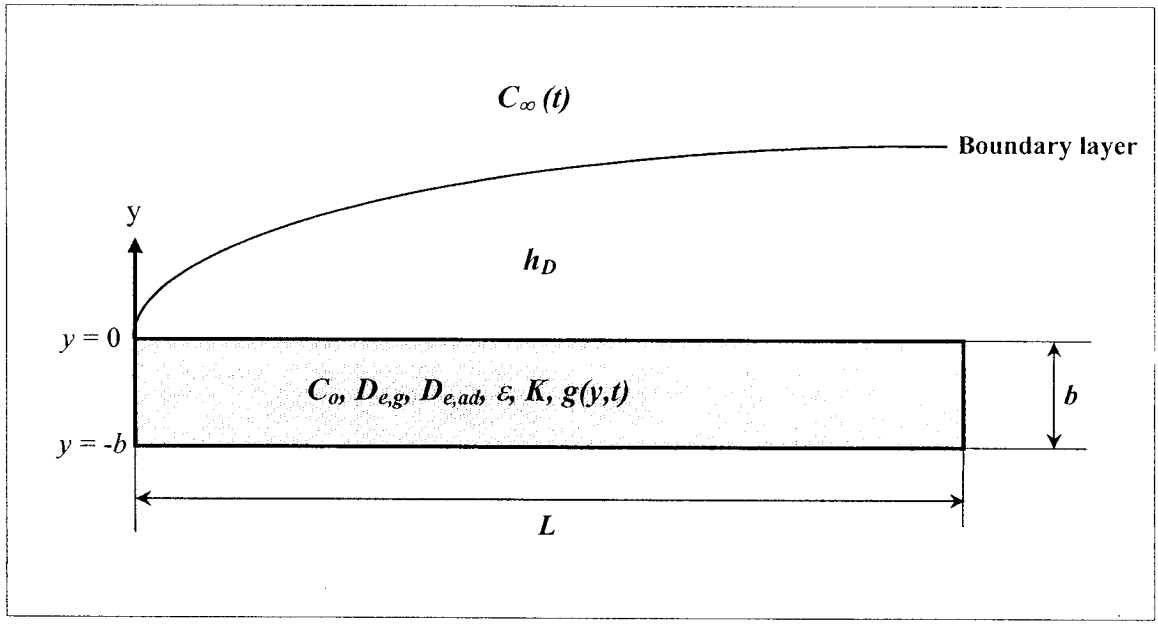

Figure 3-1 Schematic diagram of the model

Figure 3-1 shows the schematic diagram of the VOC source and sink problem considered. A porous solid material of length L, and thickness b, has a constant gas-phase effective diffusion coefficient $D_{e,g}$, effective adsorbed-phase or surface diffusion coefficient $D_{e,ad}$, sorption property K, porosity ε, and initial concentration C_o. VOC can be generated or eliminated by secondary emissions or sink within the solid and this is described by the function $g(y,t)$, which can be a function of time (t) and space (y). There is no mass transfer along the edges of the solid. The boundary layer exists due to laminar or turbulent convection over the solid and the VOC concentration in the ambient air (C_∞) can be a function of time. The convection mass transfer coefficient (h_D) can be obtained from Sherwood number correlations described earlier. The Sherwood number relations are obtained from steady convection problems. Although the VOC source and sink behavior are unsteady, the convection mass transfer problem was assumed quasi-steady since the convection time scale are generally smaller than the diffusion time scale.

The governing equation of one-dimensional gas-phase and surface diffusions within the porous material including physical adsorption/desorption and generation or elimination of VOCs due to secondary source or sink behavior is given by,

$$\varepsilon \frac{\partial C}{\partial t} + \frac{\partial C_{ad}}{\partial t} = D_{e,g} \cdot \frac{\partial^2 C}{\partial y^2} + D_{e,ad} \cdot \frac{\partial^2 C_{ad}}{\partial y^2} \pm g(y,t) \qquad (3\text{-}1)$$

where, ε is the porosity [$m^3_{air}/m^3_{material}$]; C is the gas-phase VOC concentration [mg_{voc}/m^3_{air}]; C_{ad} is the physically adsorbed-phase VOC concentration [$mg_{voc}/m^3_{material}$]; $D_{e,g}$ is the effective diffusion coefficient for gas-phase diffusion [m^2/s]; $D_{e,ad}$ is the effective diffusion coefficient for adsorbed-phase or surface diffusion [m^2/s]; y is the space coordinate [m]; and $g(y,t)$ is time and space dependent VOC generation/elimination due to secondary source/sink behavior [$mg_{voc}/m^3_{material}/s$]. The positive sign (+) for g(y,t) is for the secondary source behavior and the negative (-) is for the secondary sink behavior. The merit of this model is that there are few limitations on the secondary source/sink function, $g(y,t)$.

An adsorption isotherm relates the adsorbed-phase concentration (C_{ad}) with the gas-phase concentration (C). In this model, Henry (linear) isotherm was used considering relatively low VOC concentration levels compared to the saturation VOC concentration,

$$C_{ad} = K \cdot C \qquad (3\text{-}2)$$

Substituting this into Eq. (3-1) gives,

$$(\varepsilon + K)\frac{\partial C}{\partial t} = (D_{e,g} + K \cdot D_{e,ad})\frac{\partial^2 C}{\partial y^2} \pm g(y,t) \qquad (3\text{-}3)$$

Let us define the overall effective diffusion coefficient of the porous material (D_s) as follows,

$$D_s = D_{e,g} + K \cdot D_{e,ad} \tag{3-4}$$

Equation (3-4) is similar to Eq. (2-12). But Eq. (2-12) is for the diffusion coefficient in a straight cylindrical pore, i.e., porosity and tortuosity factors are not included. If ($K \cdot D_{e,ad}$) is very small compared with $D_{e,g}$, the gas-phase diffusion dominates, which is equivalent to the previously proposed models that consider the molecular and/or Knudsen diffusions only for internal diffusion [Murakami et al, 1998, and Blondeau et al., 2000]. Applying Eq. (3-4), Eq. (3-3) becomes,

$$\frac{\partial C}{\partial t} = \frac{D_s}{(\varepsilon + K)} \cdot \frac{\partial^2 C}{\partial y^2} \pm \frac{g(y,t)}{(\varepsilon + K)} \tag{3-5}$$

The third boundary condition was used to describe the convection mass transfer. This is imposed at the upper surface of the solid as follows,

$$-D_s \frac{\partial C}{\partial y} = h_D\left(C_w - C_\infty(t)\right) \qquad \text{at y = 0} \tag{3-6}$$

Since only one solid material is considered, there is no mass flux at the bottom surface of the solid.

$$\frac{\partial C}{\partial y} = 0 \qquad \text{at y = -b} \tag{3-7}$$

Initially (at t=0) the solid material is assumed to have a uniform VOC concentration (C_o).

$$C = C_0 \qquad \text{at t = 0, } -b \le y \le 0 \tag{3-8}$$

The governing equation for $C(y,t)$, Eq. (3-5) together with the boundary conditions given in Eqs. (3-6) and (3-7), and the initial condition given in Eq.(3-8) is of the so-called heat diffusion type (parabolic in time and elliptic in space) and can be solved analytically using the integral transform method (See Appendix A) [Özisik, 1980]. The VOC concentration, $C(y,t)$ in the solid is given as

$$C(y,t) = 2\sum_{m=1}^{\infty}\left[\frac{\beta_m{}^2 + H^2}{b\cdot\left(\beta_m{}^2 + H^2\right)+H}\right]\cdot\cos\{\beta_m\cdot(y+b)\}\cdot e^{-D\cdot\beta_m{}^2\cdot t}$$
$$\times\left[\frac{C_o}{\beta_m}\cdot\sin(\beta_m\cdot b)+\frac{h_D}{(\varepsilon+K)}\cdot\cos(\beta_m\cdot b)\cdot\int_{t'=0}e^{D\cdot\beta_m{}^2\cdot t'}\cdot C_\infty(t')\,dt'\right. \qquad (3\text{-}9)$$
$$\left.\pm\frac{1}{(\varepsilon+K)}\int_{t'=0}\int_{b}^{0}e^{D\cdot\beta_m{}^2\cdot t'}\cdot\cos\{\beta_m\cdot(y+b)\}\cdot g(y,t')\,dy\,dt'\right]$$

where, $H=\dfrac{h_D}{D_s}$; $D=\dfrac{D_s}{(\varepsilon+K)}$; and β_m's are the eigenvalues, which are the positive roots of the following equation,

$$\beta\cdot\tan(\beta\cdot b)=H \qquad (3\text{-}10)$$

When C_∞ is constant, the solution becomes,

$$C(y,t) = 2\sum_{m=1}^{\infty}\left[\frac{\beta_m{}^2 + H^2}{b\cdot\left(\beta_m{}^2 + H^2\right)+H}\right]\cdot\cos\{\beta_m\cdot(y+b)\}\cdot e^{-D\cdot\beta_m{}^2\cdot t}$$
$$\times\left[\frac{C_o}{\beta_m}\cdot\sin(\beta_m\cdot b)+\frac{h_D\cdot C_\infty}{D_s\cdot\beta_m{}^2}\cdot\cos(\beta_m\cdot b)\cdot\left(e^{D\cdot\beta_m{}^2\cdot t}-1\right)\right. \qquad (3\text{-}11)$$
$$\left.\pm\frac{1}{(\varepsilon+K)}\int_{t'=0}\int_{b}^{0}e^{D\cdot\beta_m{}^2\cdot t'}\cdot\cos\{\beta_m\cdot(y+b)\}\cdot g(y,t')\,dy\,dt'\right]$$

When C_∞ is constant and there is no secondary source/sink behavior, then the solution becomes,

$$C(y,t) = 2\sum_{m=1}^{\infty}\left[\frac{{\beta_m}^2 + H^2}{b\cdot\left({\beta_m}^2 + H^2\right)+H}\right]\cdot\cos\{\beta_m\cdot(y+b)\} \times\left[\frac{C_o}{\beta_m}\cdot\sin(\beta_m\cdot b)\cdot e^{-D\cdot{\beta_m}^2\cdot t} + \frac{h_D\cdot C_\infty}{D_s\cdot{\beta_m}^2}\cdot\cos(\beta_m\cdot b)\cdot\left(1-e^{-D\cdot{\beta_m}^2\cdot t}\right)\right] \quad (3\text{-}12)$$

If C_∞ is zero, the solution in Eq. (3-12) reduces to Huang's analytical solution [Huang and Haghighat, 2002a].

The emission rate at the upper surface of the solid can be obtained as,

$$R(y=0,t) = h_D\cdot[C(y=0,t) - C_\infty(t)] \quad (3\text{-}13)$$

Equations (3-9) to (3-13) give $C(y,t)$ and $R(y=0,t)$ once the material properties, convection property, and initial and boundary conditions are given.

Nondimensionalized Model

Since the proposed model considers secondary source/sink behavior as the generation/elimination term, $g(y,t)$, which can be any function, it is not feasible to be nondimensionalized. Assuming that $g(y,t)$ is constant, the proposed model Eq. (3-5) can be nondimensionalized as follows,

$$\frac{\partial\theta}{\partial t^+} = \frac{1}{(\varepsilon+K)}\cdot\frac{\partial^2\theta}{\partial {y^+}^2} \pm \frac{g^+}{(\varepsilon+K)} \quad (3\text{-}14)$$

and the nondimensional variables are taken as

$$\theta = \frac{C-C_\infty}{C_o-C_\infty}; \qquad t^+ = \frac{t}{t_d} = \frac{t}{b^2/D_s} = Fo; \quad (3\text{-}15)$$

$$y^+ = \frac{y}{b}; \qquad g^+ = \frac{g}{(C_o-C_\infty)\cdot D_s/b^2}$$

where, t_d is the diffusion characteristic time; and Fo is the Fourier number. The initial and the boundary conditions in Eqs. (3-6) to (3-8) become,

$$\frac{\partial\theta}{\partial y^+} + Bi\cdot\theta = 0 \qquad \text{at y = 0} \tag{3-16}$$

$$\frac{\partial\theta}{\partial y^+} = 0 \qquad \text{at y = -b} \tag{3-17}$$

$$\theta = 1.0 \qquad \text{at t = 0, } -b \le y \le 0 \tag{3-18}$$

where, Bi is the Biot number.

$$Bi = \frac{h_D\cdot b}{D_s} \tag{3-19}$$

Solving Eq. (3-14) with Eqs. (3-16) to (3-18) using the integral transform technique like the dimensional model, gives the nondimensionalized concentration, θ, as follows

$$\theta(y^+,t^+) = 2\sum_{m=1}^{\infty}\left[\frac{B_m^{\,2}+Bi^2}{B_m^{\,2}+Bi+Bi^2}\right]\cdot\cos\left\{B_m\cdot\left(y^+ +1\right)\right\}\cdot e^{-\frac{B_m^{\,2}}{\varepsilon+K}\cdot t^+} \times\left[\frac{\sin(B_m)}{B_m}\pm\frac{g^+\cdot\sin(B_m)}{B_m^{\,3}}\left(e^{\frac{B_m^{\,2}}{\varepsilon+K}\cdot t^+}-1\right)\right] \tag{3-20}$$

where, B_m's are the eigenvalues, which are the positive roots of the following equation,

$$B\cdot\tan(B) = Bi \tag{3-21}$$

It should be noted that θ can represent the normalized emission/sorption rate (i.e., the ratio of the emission/sorption rate to the initial emission/sorption rate, R/R_o). This nondimensionalized model was used in a parametric study on the primary source and sink behaviors. This will be presented in Chapter 4.

3.3 ANALYTICAL MODEL ASSESSMENT

The proposed model can be applied for both source and sink behavior of porous materials. For the assessments of the proposed model, two sets of dynamic chamber experimental data for emission and sorption were used. Also, the predictions made by the proposed model were compared with the ones made by Little's model, which considers only the internal diffusion.

3.3-1 Primary Source Behavior

The predictions of the proposed model considering only the primary source behavior were compared with those of Little's model as well as carpet emission test data. Little et al. (1994) reported one-week-long VOC emission test results using a $20m^3$ environmental chamber for three types of new carpet denoted as carpet 1, 3 and 4. The experimental conditions were 0.98-1.00 h^{-1} of air exchange rate; 22.8-23.5°C of temperature; 46.5-50.2 % of the relative humidity; 0.065-0.09 m/s of air velocity near floor; and 0.44 m^2/m^3 of loading factor.

Little et al (1994) used the material-phase approach for the internal diffusion and mass balance equation for the surface emission. They obtained material parameters in the following manner.

1. The initial concentration (C_{mo}) was obtained by dividing the total VOC mass emitted during the emission test by the material volume.
2. The partition coefficient (K_m) was obtained by dividing the C_{mo} by the VOC concentration in the air of the carpet storage bag (C_∞).

3. The diffusion coefficient of the carpet (D_m) was determined by an iterative fitting procedure using their model. A value that can give the best agreement between the emission test data and their model prediction was chosen.

For the case of carpet 3, C_∞ could not be measured, so both K_m and D_m were fitted using their model.

Since Little's model uses the material-phase approach for the internal diffusion, the material properties reported in Little et al. (1994) are for the material-phase modeling approach. These properties need to be converted in order to use multiple-phase modeling approach. This conversion is possible assuming that the material-phase VOC are in gas and adsorbed phases only, not the solid phase, because the proposed model considers gas and adsorbed phases for the primary source behavior. Then the (ε+K) term in the proposed model becomes the same as K_m,

$$(\varepsilon + K) = K_m \tag{3-22}$$

Since the concentration is described as gas-phase in the proposed model, the gas-phase initial concentration can be obtained by

$$C_o = \frac{C_{mo}}{K_m} \tag{3-23}$$

The gas-phase diffusion coefficient of the solid (D_s) can be obtained by

$$D_s = D_m \times K_m \tag{3-24}$$

Table 3-1 Material properties of carpets: converted to multiple-phase approach

Carpet	VOC		C_o [ug/m^3]	(ε+K)	$D_s\times10^8$ [m^2/s]
Carpet 1-(a) b= 0.00125 [m]	STY	styrene	428.57	4200	1.722
	C2B	ethyl benzene/ xylene	226.67	1500	1.530
	PCH	4-phenyl cyclohexene	246.91	81,000	4.779
Carpet 1-(b) b= 0.00125 [m]	STY	styrene	430.77	6500	2.340
	VCH	4-ethenyl cyclohexene	478.57	1400	0.728
	C2B	ethyl benzene/ xylene	233.33	2400	1.032
	PCH	4-phenyl cyclohexene	253.73	67,000	3.350
Carpet 3 b= 0.002 [m]	FOR	formaldehyde	409.09	11,000	3.520
	ACE	acetaldehyde	1.30×10^6	1	0.00064
	ISO	2,2,4-trimethyl-pentane	438.98	59,000	0.354
	PRO	1,2-propanediol	1416.67	180,000	1.170
	ETH	2-ethyl-1-hexanol	58.89	450,000	3.960
Carpet 4 b= 0.001 [m]	STY	styrene	4561.4	5700	1.767
	VCH	4-ethenyl cyclohexene	1588.2	1700	0.357
	C2B	ethyl benzene/ xylene	245.28	5300	0.795
	PCH	4-phenyl cyclohexene	98.24	170,000	20.40

The above relations were derived through a critical review of the diffusion coefficient and sorption property measurement and calculation procedure [Haghighat et al., 2002]. Table 3-1 summarizes the material properties applied to the proposed model.

In addition to the material properties, the proposed model requires the convective mass transfer coefficient (h_D); the latter was estimated from the Sherwood number relations for laminar forced convection flow over a flat plate, given in Eq. (2-23). For VOCs with a Schmidt number less than 1.0, the following Sherwood number relation was used [Bejan, 1995].

$$Sh_L = 1.128 \cdot \mathrm{Re}_L^{0.5} \cdot Sc^{0.5} \qquad (3\text{-}25)$$

The air velocity near the floor is 0.065-0.09 m/s; therefore, three levels of air velocity – 0.065, 0.078, and 0.09 m/s – were applied. In order to use the Sherwood number relations, the diffusion coefficient of VOC-air (D_a) is required. When the experimentally determined D_a [Bolz and Tuve, 1973] is not available, D_a was estimated using the Wilke and Lee method using Eq. (2-8). D_a and h_D values of every VOC at various air velocity levels are presented in Table 3-2. C2B refers ethylbenzene and xylenes. The data for both VOCs are reported in Table 3-2, but the ethylbenzene data were used for simulating C2B emissions.

Table 3-2 Convection parameters for carpet emissions

VOC		$D_a\times10^6$ [m²/s]	Sc	u_∞=0.065 Re_L=12519		u_∞=0.0775 Re_L=14926		u_∞=0.09 Re_L=17334	
				Sh_L	$h_D\times10^4$ [m/s]	Sh_L	$h_D\times10^4$ [m/s]	Sh_L	$h_D\times10^4$ [m/s]
styrene	**STY**	7.63	2.02	93.9	2.415	102.5	2.637	110.5	2.842
ethyl benzene	**C2B**	7.70	2.00	93.6	2.430	102.2	2.653	110.1	2.859
xylene	**C2B**	7.10	2.17	96.2	2.302	105.0	2.514	113.2	2.709
4-ethenyl cyclohexene	**VCH**	7.34	2.10	95.1	2.354	103.9	2.570	111.9	2.770
4-phenyl cyclohexene	**PCH**	5.89	2.62	102.4	2.031	111.8	2.218	120.5	2.390
formaldehyde	**FOR**	16.7	0.922	121.2	4.497	132.3	4.911	142.6	5.292
acetaldehyde	**ACE**	13.4	1.15	77.8	3.521	84.9	3.845	91.5	4.143
1,2-propanediol	**PRO**	9.14	1.69	88.4	2.724	96.5	2.974	104.0	3.205
2,2,4-trimethyl-pentane	**ISO**	6.72	2.29	97.9	2.219	107.0	2.423	115.3	2.611
2-ethyl-1-hexanol	**ETH**	6.27	2.46	100.2	2.119	109.5	2.313	118.0	2.493
vinyl acetate	**VA**	9.00	1.71	88.9	2.696	97.0	2.944	104.6	3.173

Little et al. (1994) reported their results in terms of the VOC concentration in the outlet air versus time. The simplest way to obtain the VOC concentration in the chamber air (C_a) is to apply the mass balance equation and assuming that it is fully mixed outside the boundary layer, i.e., $C_a = C_\infty$;

$$V \cdot \frac{dC_\infty}{dt} = Q \cdot (C_{in} - C_\infty) + A \cdot R(y = 0, t) \tag{3-26}$$

where, C_{in} is the VOC concentration of the inlet air [mg/m^3]; V is the chamber volume [m^3]; Q is the ventilation rate [m^3/s]; A is the area of the solid [m^2]; and $R(y=0,t)$ is obtained from Eqs. (3-8) to (3-13). Since $C_\infty(t)$ is coupled, closed form solution for the above first order ordinary differential equation cannot be obtained. The Euler forward method was used to solve Eq. (3-26).

The predictions of the proposed model were compared with those of Little's model and experimental data and they are presented in Figs. 3-2 to 3-5. The mass transfer coefficients (h_D) at the averaged air velocity, i.e., 0.078 m/s were used. Considering the fact that one or more material properties were obtained from the best-fit values for the predictions of Little's model, the simulation results of the proposed model agree rather well with the experimental data. Little's model tends to overestimate the chamber air VOC concentration at the early stage of emission as compared with the proposed model and emission test data. The reason is that Little's model does not consider the boundary layer resistance due to convection. At early stage when the emissive power of a material is strong, both convection and diffusion control the emission but as time progresses the difference due to convection become less and diffusion effect increases significantly.

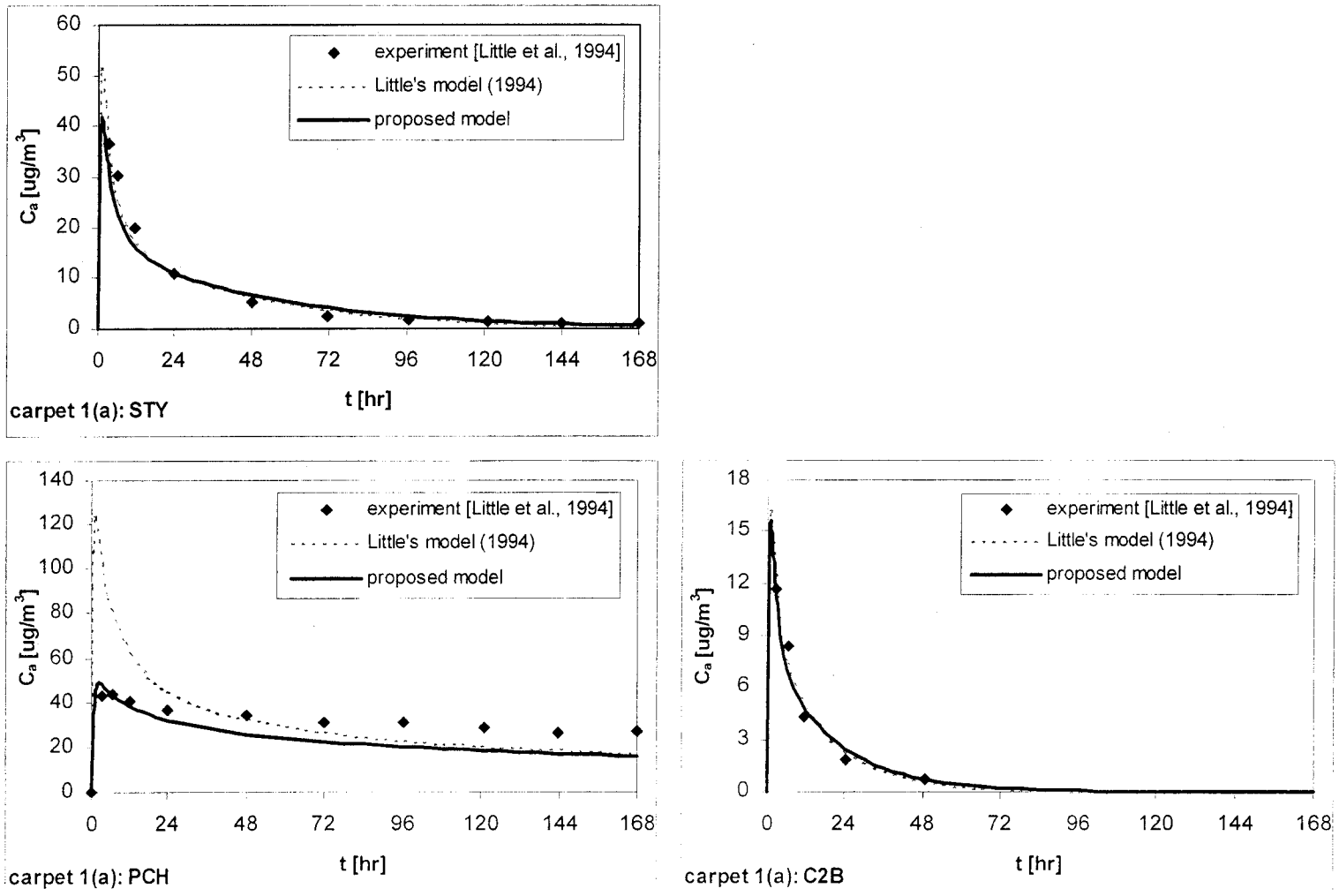

Figure 3-2 Model assessment for primary source behavior: Carpet 1-(a)

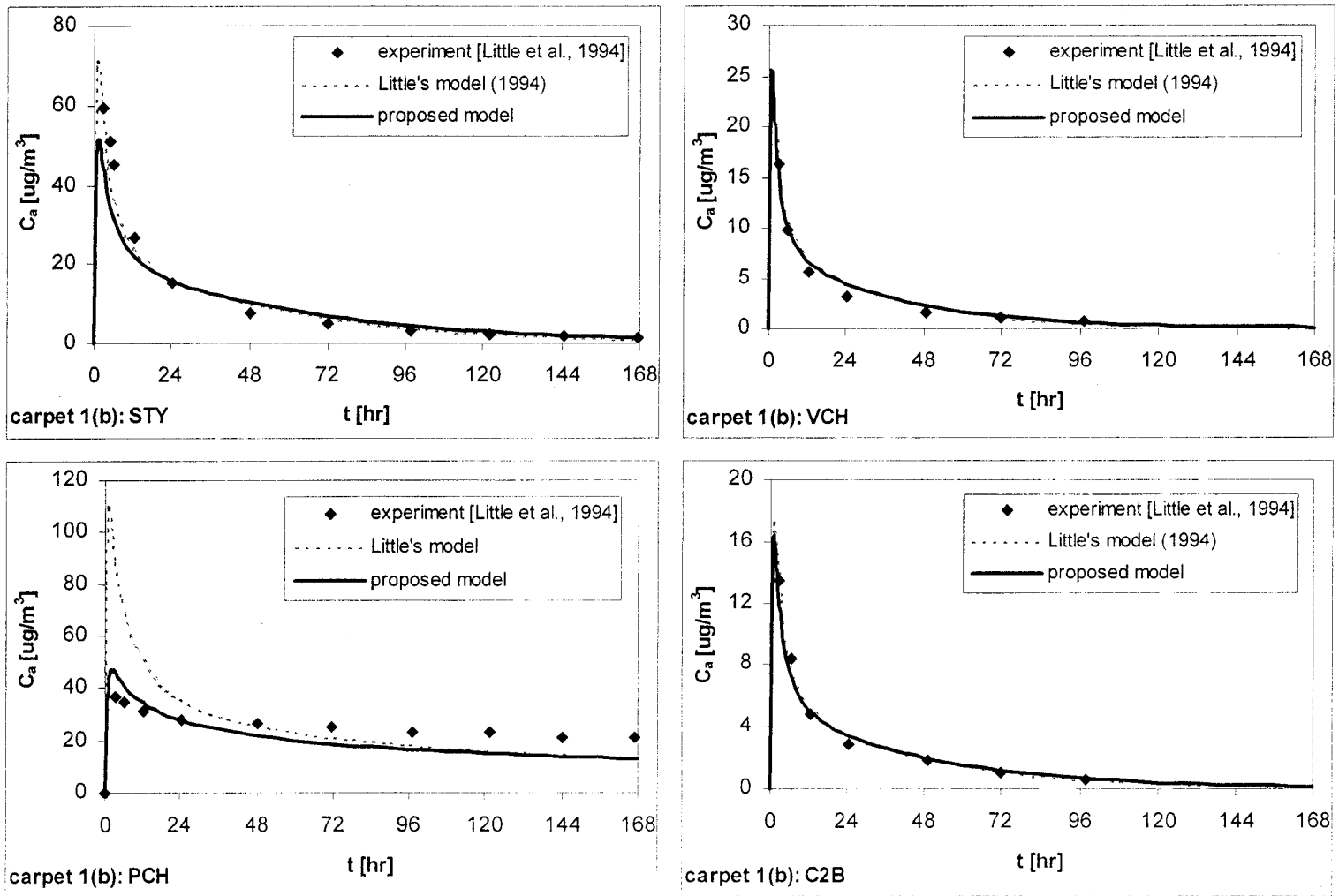

Figure 3-3 Model assessment for primary source behavior: Carpet 1-(b)

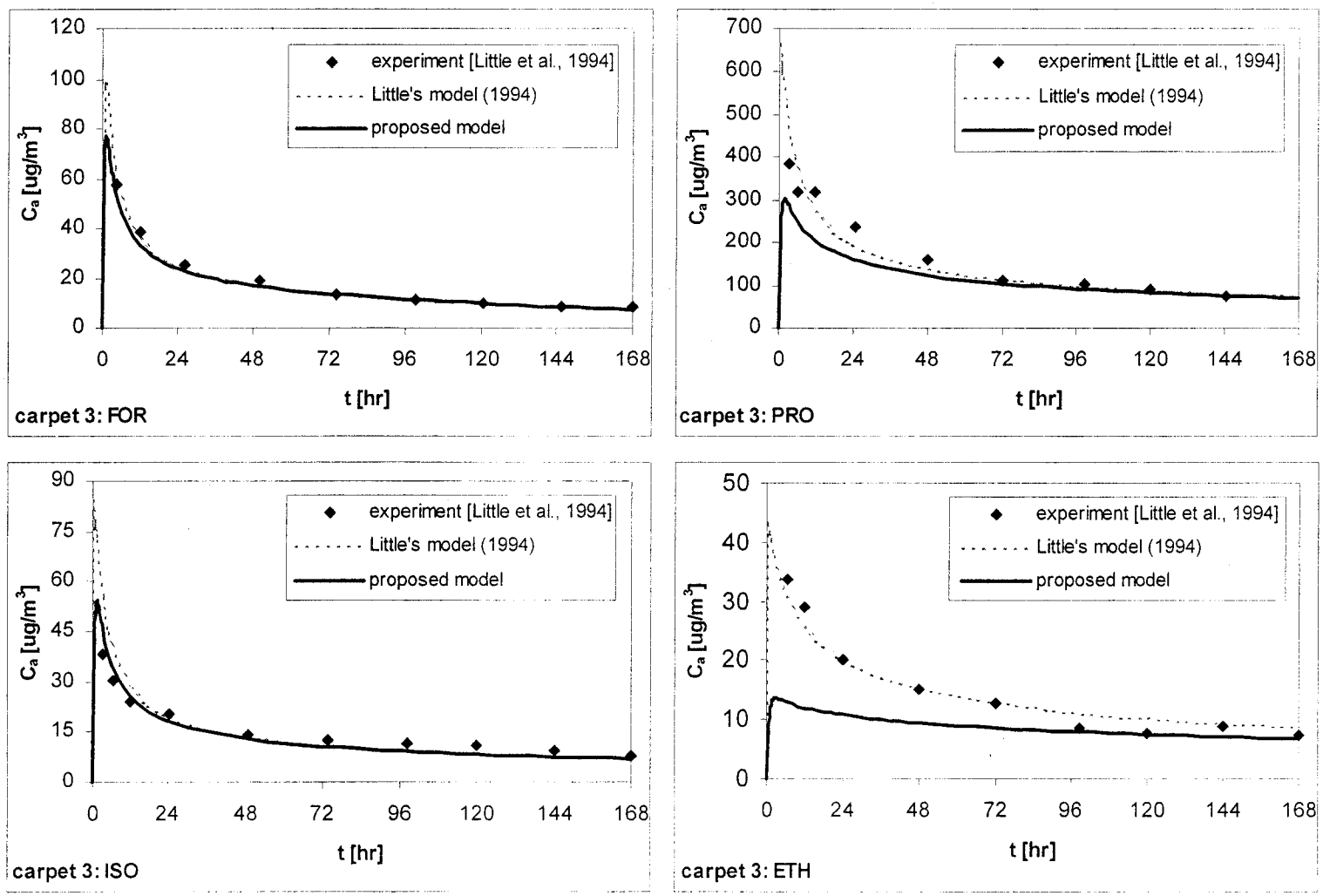

Figure 3-4 Model assessment for primary source behavior: Carpet 3

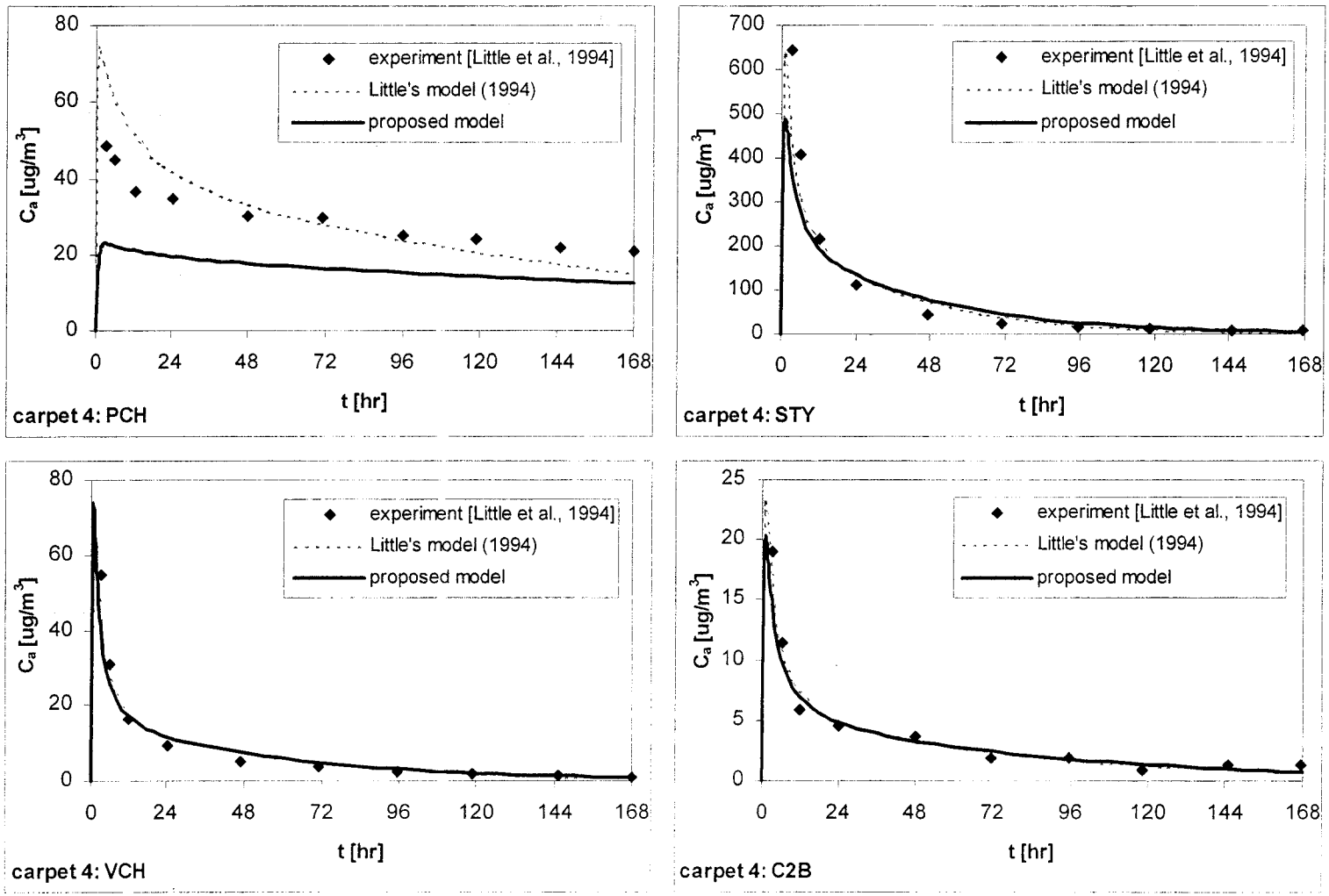

Figure 3-5 Model assessment for primary source behavior: Carpet 4

For the cases of PRO and ETH of carpet 3, and PCH of carpet 4, large differences are observed between the predictions by the proposed model and those by Little's model. This is probably due to large $(\varepsilon+K)$ values. In these three cases, $(\varepsilon+K)$ values are of the order of 10^5. The detailed effects of $(\varepsilon+K)$ will be presented in Chapter 4.

Figure 3-6 shows the effect of air velocity in the range of 0.065 to 0.09 m/s. The peak concentrations at the minimum and maximum air velocities are normalized by the peak concentration at the average air velocity. The higher the air velocity, the higher the peak concentration. The error associated with the given range of air velocity is less than ±5%. At higher air velocity, the analytical results become generally closer to those of Little's model. When the air velocity is higher, the boundary layer thickness becomes smaller hence the boundary layer resistance becomes smaller; therefore, its prediction becomes closer to that of Little's model, which ignores the boundary layer resistance.

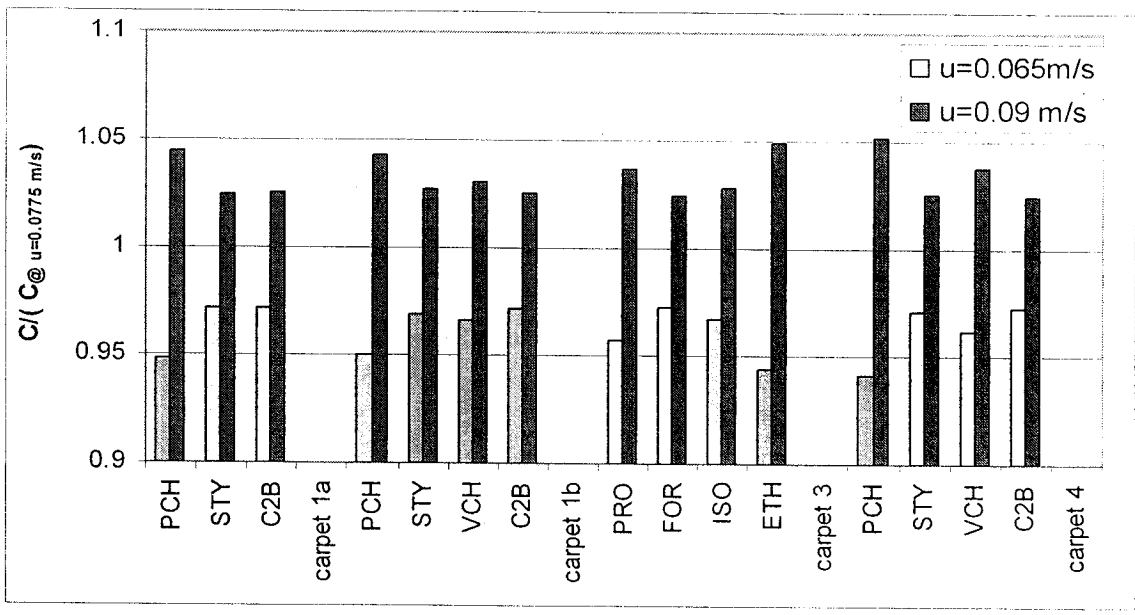

Figure 3-6 Model assessment for primary source behavior: Effect of air velocity

3.3-2 Primary Sink Behavior

For sink behavior, the proposed model was assessed by applying it to the dynamic sorption tests of acetone on wood chipboard conducted by Dr. A.L. Tiffonnet in the Indoor Air Quality Laboratory, Concordia University. Wood chipboards of various thickness (i.e., 0.5/ 1.0/ 1.5/ 2.0 cm), were tested and the effect of the relative humidity (RH) was investigated. In this validation, the test data with varying RH were not included due to the lack of current knowledge on how the moisture affects the VOC emission and sorption in the building materials. All tests were carried out in accordance with the ASTM guideline D-5116-90 using a small-scale environmental chamber with 0.0522 m^3 in volume, made of electropolished stainless steel to minimize the sink effects on the chamber walls [De Bellis, 1995].

Typical sorption tests were carried out for 8 hours: the specimen, which was preconditioned to ensure no VOC emissions, is placed in the chamber, then the air with a constant VOC concentration is introduced in the chamber and the air sample was taken regularly from the exhaust. Two levels of VOC concentrations in the supplied air, namely 75.25 mg/m^3 and 15.05 mg/m^3, were tested. The experimental conditions were 25°C temperature; 0 % of the relative humidity; 0.24 m^2/m^3 of loading factor; and 1.16 h^{-1} of air exchange rate for 75.25 mg/m^3 of inlet air concentration and 1.0 h^{-1} for 15.05 mg/m^3.

To apply the proposed model, the thickness (b), gas-phase diffusion coefficient (D_s), porosity (ε) and sorption equilibrium constant (K) of solid, and the convective mass transfer coefficient (h_D) are required as input. The thickness is given. The other

parameters were obtained as follows. Tiffonnet et al. (2000) reported the measured D_s and ε for wood chipboard through the Mercury Intrusion Porosimetry (MIP) tests. The reported ε value was used in this work, i.e., $\varepsilon = 0.2579$ [$m^3_{air}/m^3_{material}$]. D_s for acetone was not reported; however, in the measurement of D_s using MIP test it assumes that D_s is proportional to the diffusion coefficient in air (D_a) and the ratio D_a/D_s is given as 7.78. Using Eq. (2-8) D_a was estimated at 1 atm and 25°C; hence, D_s was calculated as 1.45×10^{-6} m^2/s. Since the tested wood chipboards are not identical, the adopted values for ε and D_s may introduce some error in the prediction.

The sorption equilibrium constant, K can be calulated from the measured sorption test data. Generally, desorption data are analyzed to calculate K. Since desorption data are not available, adsorption data was used. The sorption tests were carried out for a relatively short period of time (i.e., about 8 hours). Since equilibrium will be reached faster for thinner material, sorption test data for the cases of 0.005 m thickness were analyzed to calulate K. The final reading of the VOC conentration of exhausted chamber air was regarded as the equilibrium VOC concentration in the air. The total mass sorbed to the wood chipboard was then calculated applying the mass balance as

$$m_{ad} = m_{in} - m_{out} = Q \cdot C_{in} \cdot t_{end} - Q \int_0^{t_{end}} C_{out}\, dt \qquad (3\text{-}27)$$

where, m_{ad}, m_{in}, and m_{out} are the total mass of VOC sorbed by the specimen, introduced in the chamber, and exhausted from the chamber, respectively [mg]; C_{in} and C_{out} are the VOC concentration of the inlet air and exhaust air, respectively [mg/m^3]; Q is the volume flow rate of air [m^3/s]; and t_{end} is the total time of the sorption period [s]. C_{ad} is then

calculated dividing m_{ad} by the volume of the material. The sorption isotherm is then plotted at two concentration points as shown in Fig. 3-7. Henry isotherm was applied and the best fit value of K was found to be $K = 3748.8$ [$m^3_{air}/m^3_{material}$] with $R^2 = 0.9873$.

In Eq. (3-27), the mass of VOCs adsorbed to the chamber wall was not included since the sorption measurement results by Popa and Haghighat (2002), who conducted the sorption tests of the empty chamber, paint, and painted gypsum board using the same experimental set-up, indicated that the sink effect of the test chamber was neglible. Popa and Haghighat (2002) used toluene for the sorption test of the empty chamber and the total mass adsorbed to the chamber was 0.174 mg with high inlet VOC concentration, i.e., $C_{in} = 372$ mg/m^3. The sink effects depend on the degree of volatility of the VOC and generally, the higher the boiling point of VOC, the greater will be the sink effect of the test chamber [Salthammer, 1999]. The boiling point of acetone is 56.5°C and that of toluene is 110.8 °C [Perry and Chilton, 1973]; hence the sink effect of acetone may be less than that of toluene, which was measured by Popa and Haghighat (2002).

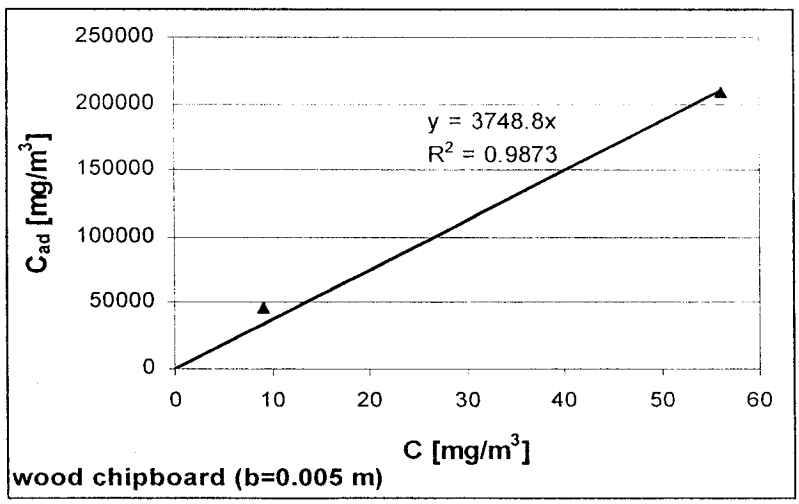

Figure 3-7 Estimation of *K* for wood chipbaord

Table 3-3 Input parameters for sorption

Convection properties (Acetone at 25°C)	Diffusion coefficient in air (D_a)	1.131×10^{-5} [m^2/s]
	Schmidt no. (Sc)	1.36
	Air velocity (u_∞)	0.1 [m/s]
	Mass transfer coefficient (h_D)	1.792×10^{-3} [m/s]
Material properties	Effective diffusion coefficient (D_s)	1.454×10^{-6} [m^2/s]
	Porosity (ε)	0.2579 [$m^3_{air}/m^3_{material}$]
	Sorption partition coefficient (K)	4420 [$m^3_{air}/m^3_{material}$]
	Thickness (b)	0.005/0.01/0.015/0.02 [m]
Chamber test parameters	Loading factor	0.2414 [m^2/m^3]
	Inlet VOC concentration (C_{in})	75.25/ 15.05 [mg/m^3]
	Air exchange rate (ACH)	1.16 [h^{-1}] for C_{in} = 75.25 [mg/m^3]
		1.0 [h^{-1}] for C_{in} = 15.05 [mg/m^3]

The convection mass transfer coefficient (h_D) was calculated using the Sherwood number correlation for larminar forced convection given in Eq. (2-23). Popa (2002) reported that the median air velocity inside the chamber is 0.1 m/s for 1.01 h^{-1} air exchange rate. Applying the reported air velocity as the air velocity outside the boundary layer (u_∞) with the given properties of acetone (Sc = 1.36) and the specimen length (L = 0.14 m), h_D was calculated as 1.792×10^{-3} m/s. The detailed input parameters are presented in Table 3-3.

The predictions made by the proposed model using the above mentioned parameters were compared with the experimental data as well as the predictions made by the Little's model. Figure 3-8 presents these comparisons for the wood chipboard thickness of 0.005,

0.01, 0.015, and 0.02 m. Generally, the prediction made by the proposed model agrees well with the experimental data. The predictions tend to overestimate the VOC concentration in the chamber air or in other words underestimate the sorption rate of the specimen in the early stage of the sorption test. Since the edges of the specimen were not sealed but were directly exposed to the chamber air in the experiments, sorption occurs not only from the face but also from the edges of the wood chipboard specimen, whilst the proposed model considers the sorption only from the exposed face of the specimen to the air, which is equivalent to the edge-sealed specimen. Hence, the measured sorption rate may be greater in the early stage and may get smaller in the later stage than the prediction. In the later stage, the concentration increase is slower in the measured data compared with the prediction. More error is observed in low concetration cases. This may be caused by the fact that the input value for K may underestimate the real K value in low concentration case as shown in Fig. 3-7.

With the given air velocity level, C_a predicted by the proposed model is higher than that estimated by Little's model and the difference gets smaller as time progresses. By the time the sorption tests end (around 8 hours later), the predictions by both models become similar. As mentioned in the model assessment for the primary source behavior, Little's model only considers the internal diffusion while the convective resistance is neglected. Hence, the sorption rates by Little's model are greater in the early stage than those obtained from the proposed model.

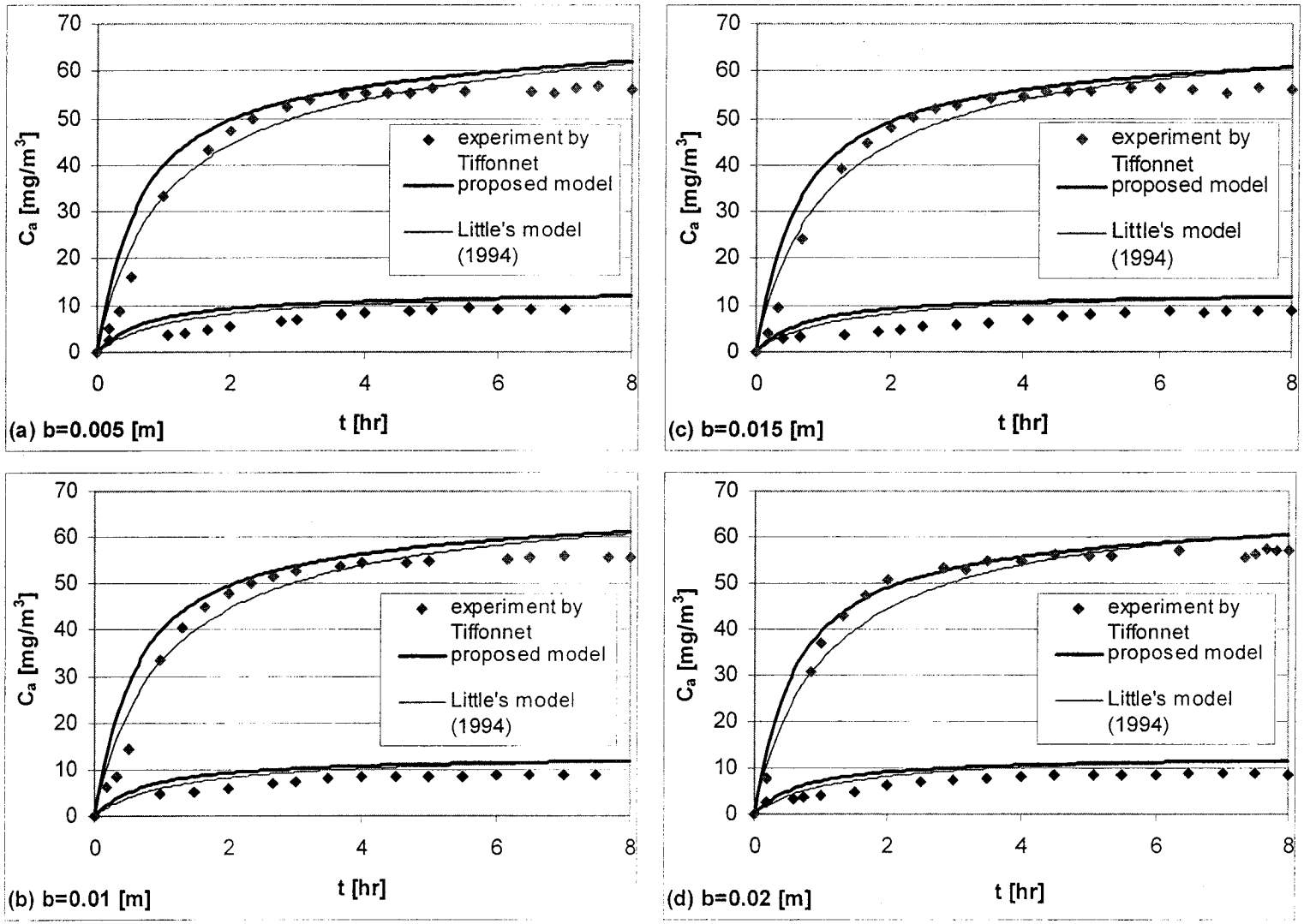

Figure 3-8 Model assessment for primary sink behavior

3.3-3 Comparison with Little's Model at Various Air Velocity Levels

One of the advances in analytical modeling that was brought about by the proposed model is the inclusion of convective resistance in the VOC source and sink behavior of solid materials. Other than the proposed model, the only analytical model that can be applied for both source and sink behavior of solid materials is Little's model (1994). The major limitation of Little's model is that it can be applicable only for diffusion controlled materials. In other words, the diffusion resistance of the solid is much larger than the convection resistance, so the change in air velocity will not affect the source and sink behavior. With the absence of the proper model, Little's model have been applied regardless of the diffusion resistance of the solid [Zhang et al., 2001]. To investigate the applicability of Little's model for solids with low diffusion resistances, the prediction made by Little's model was compared with the proposed model at various air velocity levels, expressed as Reynolds number.

A full scale room (L = 4.5 m) was considered and both source and the sink behavior of the wood chipboards for acetone were investigated. The material properties of the wood chipboard are the same as the ones in Section 3.3-2. The thickness of the wood chipboard is 0.01 m. The loading factor is 0.4 m^2/m^3 and the air exchange rate is 1 h^{-1}. For the primary emission, the initial concentration of the solid is 100 mg/m^3 and the inlet air concentration is 0 mg/m^3, and vice versa for sorption. The Reynolds number (Re_L) was varied from 100 to 5×10^5 and the convective mass transfer coefficient was calculated from the Sherwood number correlation for the laminar forced convection over a flat plate given in Eq. (2-23).

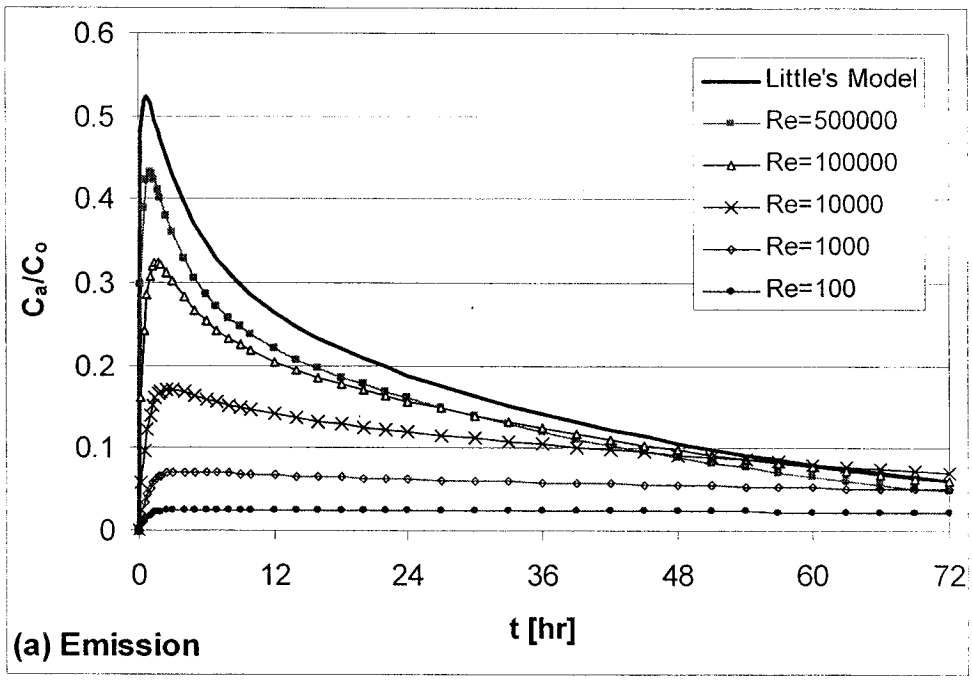

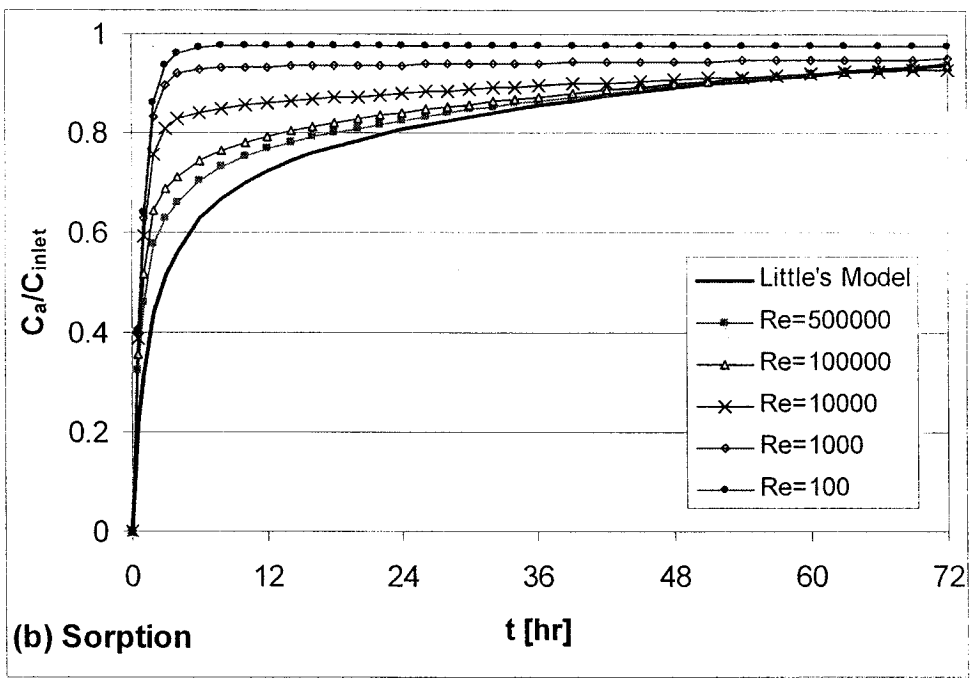

Figure 3-9 Proposed analytical model versus Little's model

Figure 3-9 presents the simulation results by Little's model and the propsed model at various Re_L for 72 hours for the primary source and sink behavior. Since Little's model does not take into consideration of the convection, the prediction is always the same regardless of Re_L. Figure 3-9 shows that as Re_L increases, the emission/sorption profile become closer to that of Little's model. For Re_L greater than 10^4, the VOC concentration in the air becomes similar to that by Little's model after the early phase of emission/sorption (e.g. around 60 hours later in these simulations). When the air veocity is low, Little's model may significantly overestimate the emission or sorption rates especially for the early stage. More detailed study on the effect of Reynolds number on the source and the sink behavior of porous materials is presented in Chapter 4.

3.4 SUMMARY

An analytical model based on the fundamentals of mass transfer was proposed for the VOC source and sink behavior of porous building materials. This model allows distinction between the primary and the secondary source/sink behavior. The primary source/sink behavior are described by the transfer of gas-phase and physically adsorbed-phase. The secondary source or sink behavior was modeled as generation or elimination term, which could be any function of space (y) and/or time (t). The model considers the convective boundary layer resistance applying the third-kind boundary condition. The exact analytical solution was obtained using the integral transformation technique.

The proposed model was assessed for the primary source and sink behavior. The prediction of the proposed model agrees well with the carpet VOC emission test data and

wood chipboard sorption test data. The prediction of the proposed model was compared with the prediction of the existing analytical model proposed by Little et al. (1994). For the given test conditions, both models generally agree well after the early stage of emission/sorption, when the internal diffusion dominates. In the early stage, Little's model tends to overestimate the emission/sorption rates compared with the proposed model, since Little's model does not consider the boundary layer resistance due to convection. Prediction of Little's model was compared further with the proposed model at various air velocity. The simulation results indicate that Little's model can significantly overestimate the emission/sorption rate during the early stage if the air velocity is low, i.e., when the convective boundary layer resistance is large.

Chapter 4

Theoretical Investigation of Source and Sink Behavior in Porous Building Materials

4.1 INTRODUCTION

This chapter reports on the results of the theoretical investigation on the source and sink behavior of porous building materials; these results were obtained by applying the proposed analytical model presented in Chapter 3. This investigation includes a parametric study on the effects of material properties and air velocity on the source rate (emission rate) and/or the sink rate (sorption rate) of building materials.

A few studies presented the effects of material properties like diffusion coefficient and sorption partition coefficient [Little et al., 1994, Yang et al., 2001c] or air velocity [Huang and Haghighat, 2002a] on the emission rates of solid building materials. These, however, can only provide basic trends on the effect of a single parameter on emissions such as, the larger the diffusion coefficient, the higher the chamber concentration. The effects were not quantified and the possible interactions among parameters were not considered. Huang and Haghighat (2002b) carried out a systematic parametric study using statistical analysis of factorial design and concluded that only diffusion coefficient and the thickness of solid have significant effects among the considered parameters:

diffusion coefficient, partition coefficient, and thickness of solid, and the air velocity. However, the considered ranges of parameters are not inclusive and the results suffer from this limitation. For the partition coefficient, three levels (1095/ 3458/ 17651) were considered, whilst an experimental study showed it could vary from 810 to 4.2×10^5 depending on the VOC considered [Cox, et al., 2001b].

To overcome the limitations of previous studies, a parametric study on the primary source and sink behavior was carried out applying the nondimensional system presented in Chapter 3 for inclusive ranges of parameters taken from various experimental data. Nondimensionalization results in a reduced number of variables and a more generalized solution. This is a common and useful practice in engineering science; however, no previous studies applied nondimensional systems for VOC source and sink behavior of building materials.

This chapter also presents case studies on the secondary source behavior. Since there is a lack of studies on real case mechanism of secondary source behavior, five hypothetical cases of VOC generation functions were applied.

4.2 PARAMETRIC STUDY: PRIMARY SOURCE AND SINK BEHAVIOR

The parameters considered in the proposed dimensional model are the dependent variable, C and independent variables like material properties, i.e., diffusion coefficient (D_s), porosity (ε), sorption partition coefficient (K) and the thickness (b); initial and boundary conditions, i.e., the initial concentration (C_o) of the solid and the concentration

outside the boundary layer (C_∞); and flow property like the mass transfer coefficient (h_D), which is a function of air velocity (u_∞), length of solid (L), viscosity (μ), density (ρ) and diffusion coefficient of air (D_a). Through dimensional analysis [Welty et al., 1976], these parameters can be reduced to the dependent variable, θ, and independent variables, Re_L, Sc, D_a/D_s, b/L, ε and K. These six independent parameters can be combined into two nondimensional groups, i.e., (ε+K) and Biot number (Bi), which will be shown later. The parametric study on the primary source and sink behavior was carried out using the nondimensional model.

N-octane at the temperature of 25°C was used as VOCs of interest. Hence, the Schmidt number is set as 2.57. In this study, the effect of Schmidt number was not investigated since the Schmidt number for various VOC varies in a relatively small range, 0.9 – 3.1 [Sparks, et al., 1996b]. To investigate the effects of parameters on primary source and sink behavior only, the generation term for secondary source/sink behavior was set to zero. (ε+K) was varied from 10 to 10^5. The porosity (ε) is within the range of 0 to 1; however, K varies significantly. Cox et al. (2001b) measured the sorption partition coefficients of various VOCs on the vinyl flooring and reported that they may vary from 810 to 4.2×10^5. Biot number (Bi) is defined as $(h_D\times b)/D_s$, which is the ratio of the diffusion to convection resistance of mass transfer. Bi was varied from 9.1×10^{-3} to 2.9×10^5, which were determined from the combination of separate ranges of D_a/D_s, b/L, and Re_L. D_a/D_s was varied in the range of 10 to 10^5. This range was decided based on the previous study, which showed the range of measured D_a/D_s for gas-phase diffusion of various building materials are from 4.42 to 1.55×10^4 [Haghighat et al., 2002]. The

thickness to length ratio (b/L) was varied from 10^{-4} to 10^{-2}. The Reynolds number was varied from 10^2 to 10^5, which is equivalent to the air velocity from almost stagnant to 0.34 m/s when the solid length L = 4.5m. The mass transfer coefficient (h_D) was obtained from the Sherwood number relation for the laminar forced convection over a flat plate, Eq. (2-23). Table 4-1 summarizes the input parameters.

The maximum mass of gas-phase VOC that can be emitted from or be absorbed by a porous material per unit area m_{max} is

$$m_{\max} = |C_o - C_\infty| \times b \qquad (4\text{-}1)$$

where, m_{max} has the unit of [mg/m^2]; C_0 is the initial gas-phase VOC concentration in the material [mg/m^3]; and C_∞ is the VOC concentration outside the boundary layer, i.e., in the bulk air [mg/m^3]. The total transfer time, t_{total} is defined as the time required to emit/sink 99% of m_{max} from/into the material. The effects of considered parameters were quantified using t_{total}. Since the nondimensional model was used, t_{total} is normalized by the diffusion characteristic time, t_d, which is defined as b^2/D_s, and denoted as t_{total}^+.

Table 4-1 Parametric study input

Constant parameter	**n-octane at 25°C**		
	D_a [m^2/s]	ν [m^2/s]	Sc
	6×10^{-6}	1.54×10^{-5}	2.57

Variable parameter	$(\varepsilon+K)$	**Biot : 9.10×10^{-3} – 2.88×10^{5}**		
		D_d/D_s	b/L	Re_L
	10^1	10^1	10^{-4}	10^5
	10^2	10^2	5×10^{-4}	10^4
	10^3	10^3	10^{-3}	10^3
	10^4	10^4	5×10^{-3}	10^2
	10^5	10^5	10^{-2}	-

Figure 4-1 presents the effects of (ε+K) and the Biot number on t_{total}^{+}. Fig. 4-1 (a) shows that as the Biot number increases, t_{total}^{+} decreases. However, when the Biot number is larger than 10, in other words, if the diffusion resistance is 10 times larger than the convection resistance, t_{total}^{+} becomes almost constant. As (ε+K) increases, t_{total}^{+} increases. As shown in Fig. 4-1 (b), (ε+K) has linear impact on t_{total}^{+}. Fig 4-1 also indicates that there is no interaction between (ε+K) and the Biot number.

The Biot number is a nondimensional parameter that gives the ratio of diffusion resistance to convection resistance, it can also be rewritten as follows:

$$Bi = \frac{h_D \cdot b}{D_s} = \frac{h_D \cdot L}{D_a} \cdot \frac{D_a}{D_s} \cdot \frac{b}{L} = Sh_L \cdot (D_a / D_s) \cdot (b/L) \tag{4-2}$$

Substituting the Sherwood number correlation of Eq. (2-23) into Eq. (4-2) gives,

$$Bi = 0.664 \cdot \mathrm{Re}_L^{\frac{1}{2}} \cdot Sc^{\frac{1}{3}} \cdot (D_a / D_s) \cdot (b/L) \tag{4-3}$$

Instead of lump summed effect of the Biot number, the effects of separate parameters, i.e., Re_L, (D_a/D_s) and (b/L), on t_{total}^{+} were investigated.

Applying all combinations of material parameters and Reynolds number presented in Table 4-1, the observed trends on t_{total}^{+} are presented in Fig. 4-2, where, t_{total}^{+} is plotted versus (D_a/D_s)×(b/L) and (ε+K) for various Reynolds numbers, Re_L. For a given set of material properties, t_{total}^{+} increases as Re_L decreases: when (D_a/D_s)×(b/L) is 0.01 and (ε+K) is 100, t_{total}^{+} is 326 for Re_L=10^5, while t_{total}^{+} is 5217 for Re_L=10^2. This figure also shows that as (D_a/D_s)×(b/L) increases the effect of Re_L decreases. When (D_a/D_s)×(b/L) is 0.01, t_{total}^{+} for Re_L=10^2 is 16 times larger than that for Re_L=10^5, while the same ratio

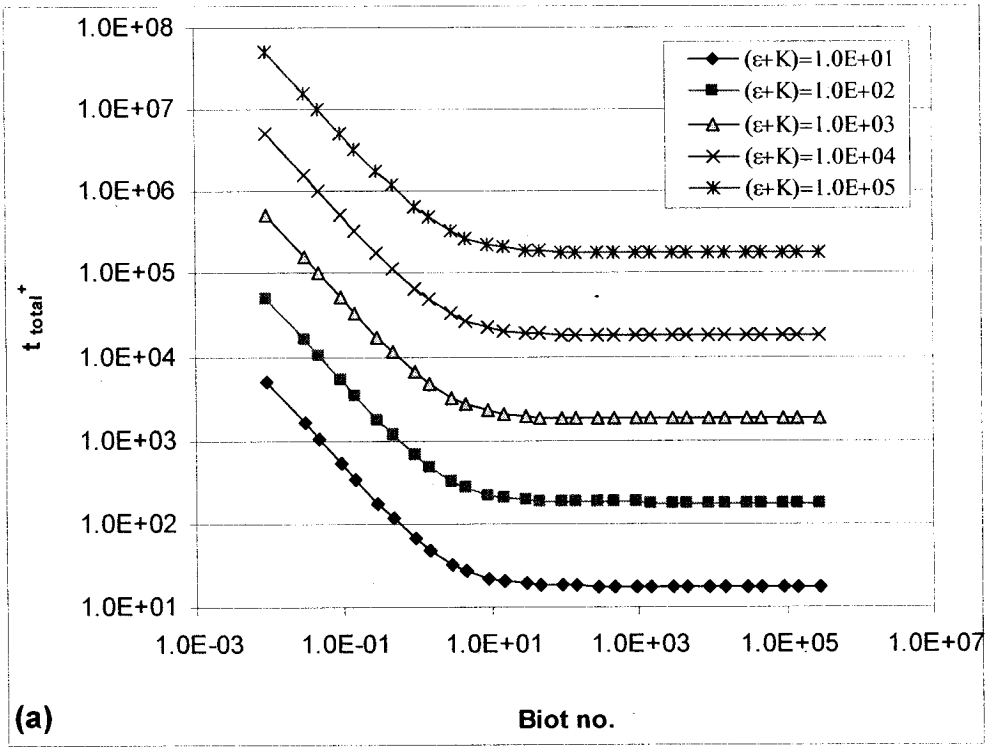

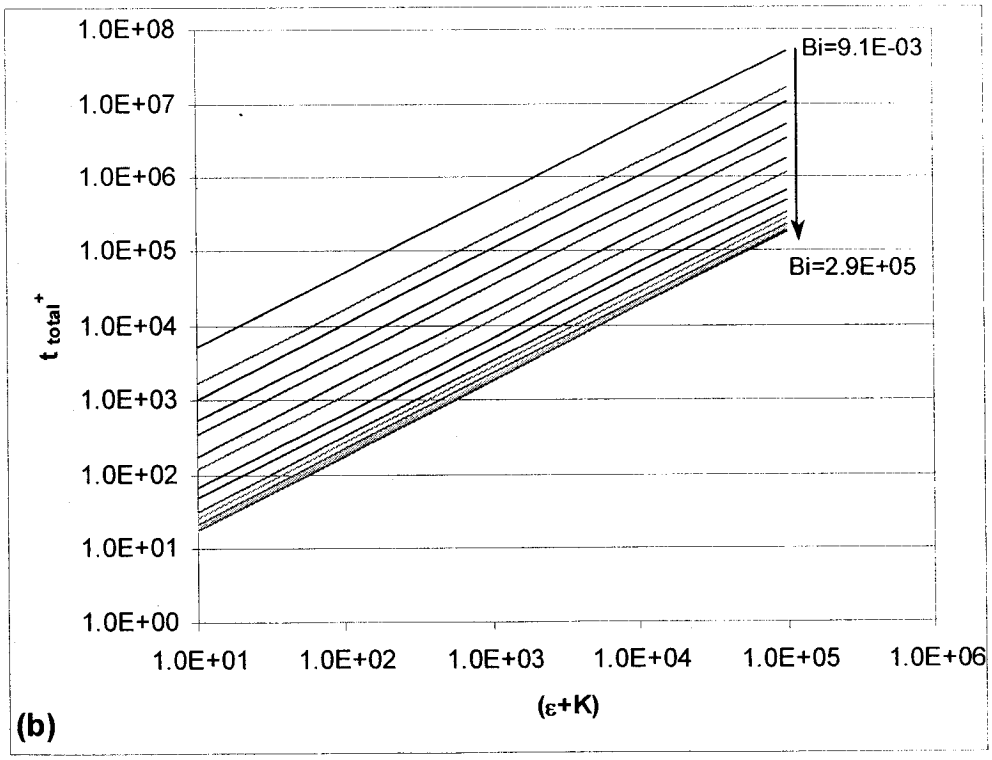

Figure 4-1 Effects of (ε+K) and Biot number on the total transfer time, t_{total}^{+}

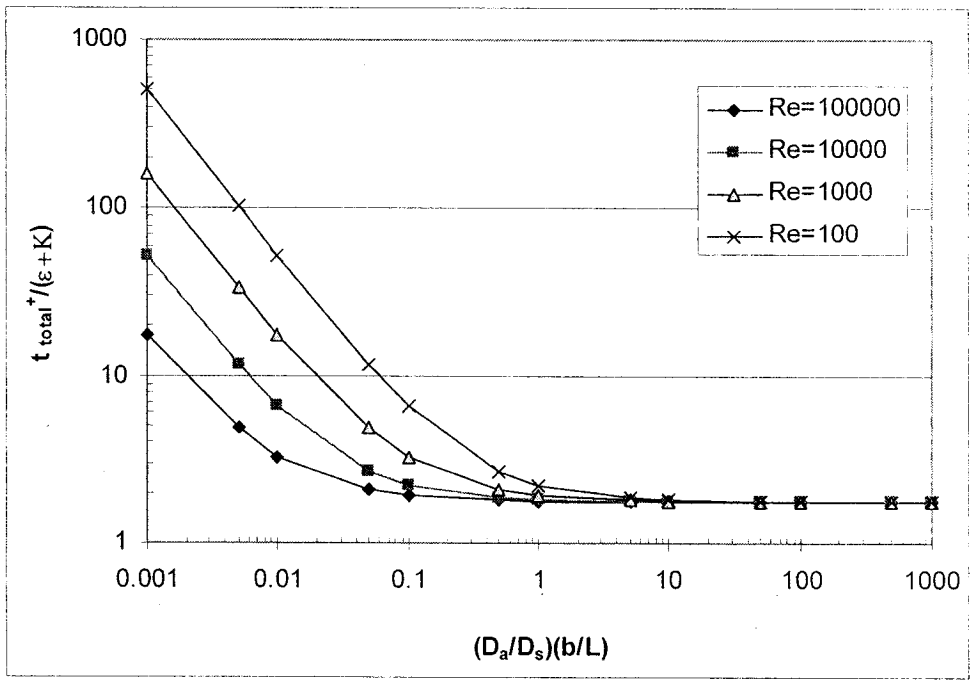

Figure 4-2 Effects of Reynolds number on the total transfer time, t_{total}^{+}

drops to 1.24 when $(D_a/D_s)\times(b/L)$ is 1.0. The influence of Re_L diminishes when $(D_a/D_s)\times(b/L)$ is larger than 1.0. In other words, the assumption of negligible convection, which was adopted in Little's model, is valid for values of $(D_a/D_s)\times(b/L)$ larger than 1.0. In that region, $t_{total}^{+}/(\varepsilon+K)$ is almost constant. Hence, the dimensional total transfer time, t_{total}, becomes,

$$t_{total} \approx A_1 \cdot (\varepsilon + K) \cdot t_d = A_2 \cdot (\varepsilon + K) \cdot (b/L)^2 \cdot (D_a/D_s) \qquad (4\text{-}4)$$

where, A_1, A_2 are constants, i.e., $A_2 = A_1 \cdot L^2/D_a$ [s]. Equation (4-4) indicates that (b/L) can have a more significant impact on t_{total}^{+} than that of $(\varepsilon+K)$ and (D_a/D_s).

Since t_{total}^{+} varies linearly with $(\varepsilon+K)$, more significant effect of Reynolds number can be observed at larger values of $(\varepsilon+K)$. For example for $(D_a/D_s)\times(b/L)$ equals to 0.01, when $(\varepsilon+K)$ is 10, t_{total}^{+} is 32.6 and 521.7 for $Re_L=10^5$ and 10^2; but when $(\varepsilon+K)$ is 1000, t_{total}^{+} is

3261 and 52175 for Re_L=10^5 and 10^2. Even though the relative increase is the same, the absolute magnitude of increase with the decrease of Re_L is much larger for larger values of (ε+K). This explains the larger discrepancy between the proposed model and Little's model predictions observed for the cases of large (ε+K), which was presented in Section 3.3-1. Since Little's model does not consider the convection resistance, it can correspond to the case of very high Re_L, i.e., negligible convection resistance. The Reynolds number of a given system is generally lower; hence, discrepancy exists between Little's model prediction and the proposed model prediction for a given Re_L, and the discrepancy becomes larger for higher (ε+K), which can be clearly shown in dimensional plots like Figs. (3-2) to (3-5).

To evaluate whether t_{total}^{+} can be a good index for this parametric study, the effect of Reynolds number on the emission rate (R) was investigated for cases of D_a/D_s=10 and 1×10^3, (ε+K)=100, and b/L = 1×10^{-3}. Figure 4-3 shows the big difference on the effect of Re_L depending on the D_a/D_s and the results agree well with those presented in Fig. 4-2.

Figure 4-4 presents the effects of Biot number and (ε+K) on θ_w, which is the nondimensionalized concentration at the air-solid interface, i.e., $(C_w-C_\infty)/(C_o-C_\infty)$. Since the proposed model assumes that the convection mass transfer coefficient, h_D is constant, θ_w can be regarded as the ratio of the emission/sorption rate at time t (R) to the initial emission/sorption rate (R_o). To show the variation of θ_w during the entire transfer period of primary source/sink behavior, the time was normalized by t_{total}.

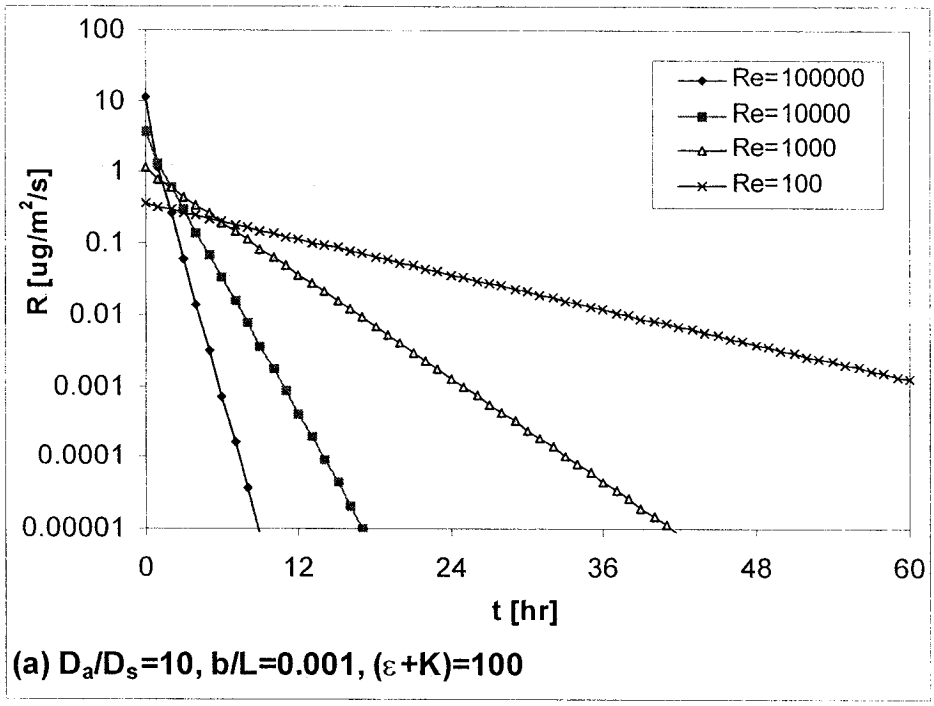

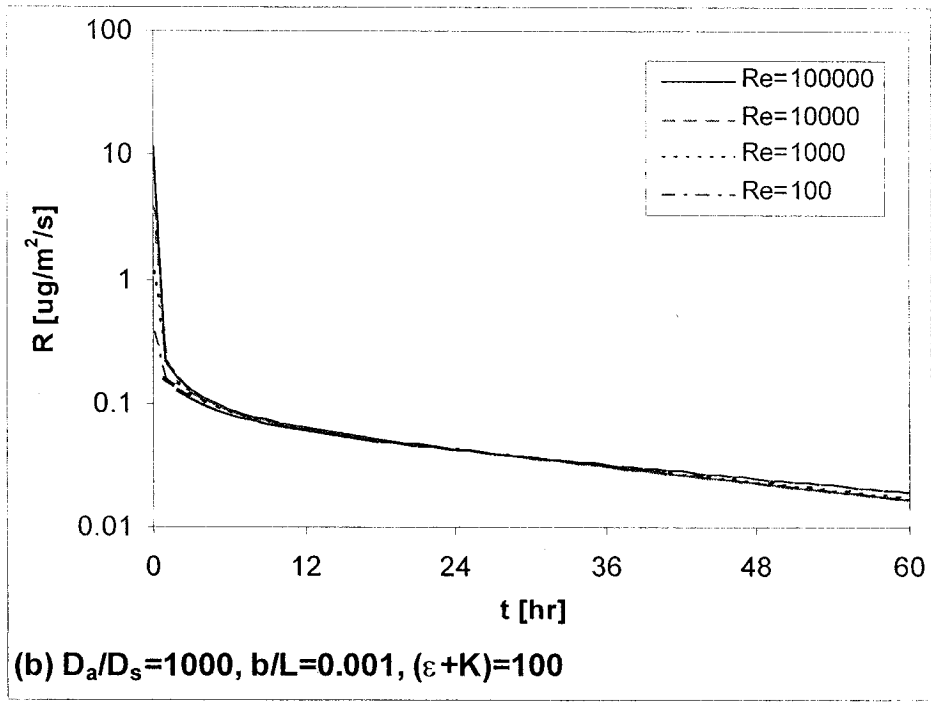

Figure 4-3 Effects of Reynolds number on emission rates

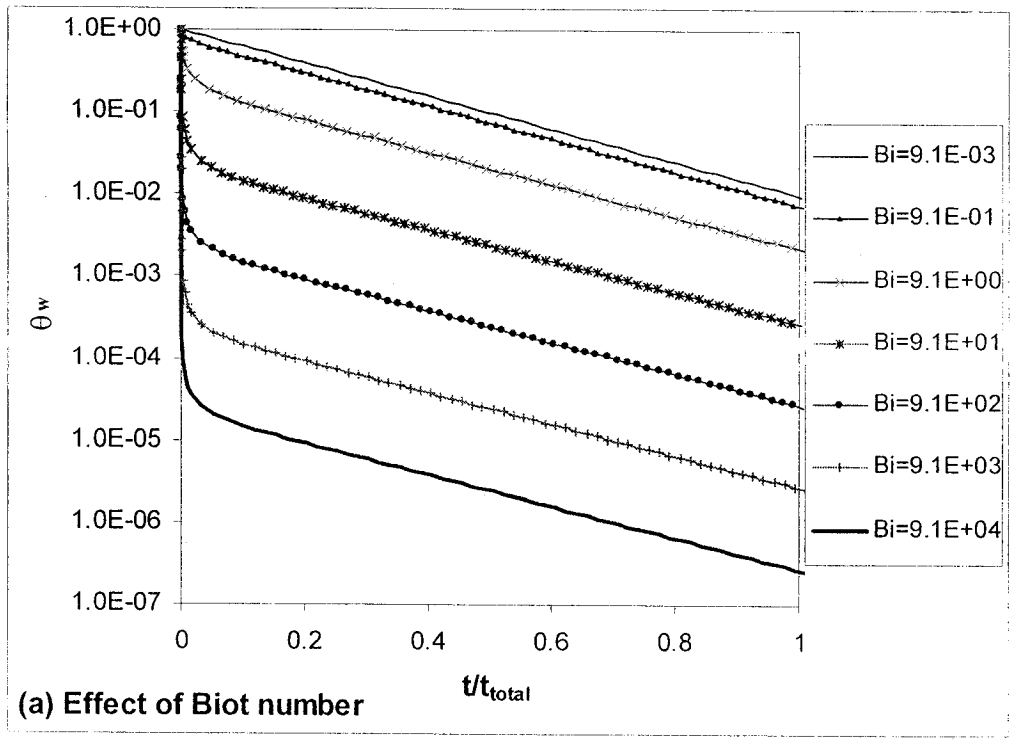

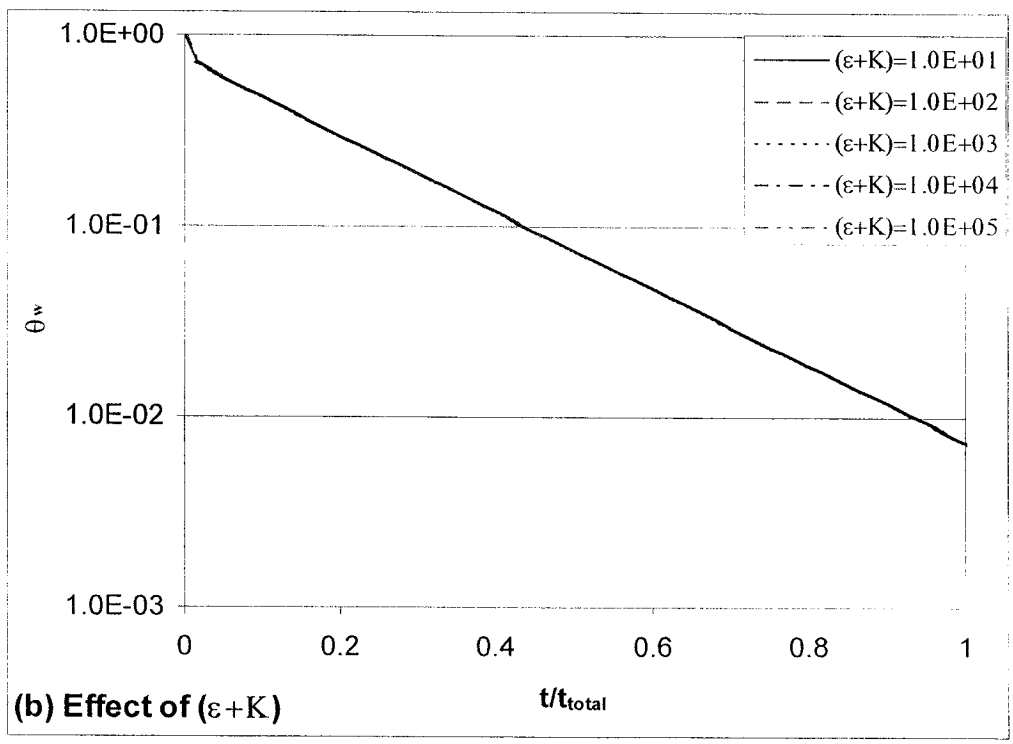

Figure 4-4 Effects of Biot number and (ε+K) on θ_w

Figure 4-4 (a) indicates that θ_w, or R/R_o decreases as Biot number increases, in other words, the ratio of the diffusion resistance to the convection resistance increases. When Biot number is small, θ_w decreases gradually throughout the whole emission time; however, when Biot number is large, θ_w decreases abruptly at the early stage of transfer period, i.e., t/t_{total} is less than 0.1. After this period, θ_w becomes logarithmically linear. Figure 4-4 (b) shows the influence of $(\varepsilon+K)$ on θ_w when it was varied from 10 to 10^5. All cases of $(\varepsilon+K)$ collapse into one θ_w versus t/t_{total} line, which indicates the effect of $(\varepsilon+K)$ on primary source/sink behavior is linear.

The length of a solid (L) affects the Reynolds number (Re_L) and the thickness to length ratio of the solid (b/L). Applying Eq. (4-3), the Biot number has the length dependence of $L^{-0.5}$. When the length of a solid is increased by a factor of 4, Biot number decreases by a factor of 2. Though the dependence on the length is not significant, it can affect t_{total}^{+} and θ_w as shown in Figs. (4-1) and (4-4). If an identical solid material is tested in two different sized chambers under the same test conditions (e.g., air exchange rate, loading factor, air velocity, temperature, and relative humidity), the measured emission or sorption rates can be different due to the difference in the length scale. In order to obtain the identical experimental results, Biot number needs to be matched. This can be achieved by adjusting the air velocity level. Biot number depends on the air velocity and the length as follows.

$$Bi \propto \sqrt{\frac{u_\infty}{L}} \tag{4-5}$$

If the length becomes 4 times larger, then the air velocity needs to be increased at the same rate. The above discussion is limited to the laminar flow cases. If the Sherwood number relation for turbulent flow presented in Eq. (2-24) is applied in Biot number calculation, then the length dependence becomes weaker, i.e., $L^{-0.2}$.

4.3 CASE STUDY: SECONDARY SOURCE BEHAVIOR

Unlike the primary source/sink behavior, there are few experimental data for the secondary source/sink behavior and no model has been proposed, so the following five hypothetical generation functions were considered.

1. Constant generation

   a. Generation throughout the whole thickness

$$g(y,t) = A_g \qquad -b \le y \le 0, \qquad 0 \le t \le \infty \tag{4-6}$$

   where, A_g is the constant generation term [mg/m^3/s]

   b. Generation at the solid-air interface

$$g(y=0,t) = B_g \qquad 0 \le t \le \infty \tag{4-7}$$

   where, B_g is the constant generation term [mg/m^2/s]

   c. Generation at the bottom of the solid

$$g(y=-b,t) = B_g \qquad 0 \le t \le \infty \tag{4-8}$$

2. Constant generation for a limited period of time throughout the whole thickness

$$g(y,t) = A_g \qquad -b \le y \le 0, \qquad 0 \le t \le t_g \tag{4-9}$$

   where, t_g is the generation time [s].

3. Sinusoidal function to represent the seasonal variation throughout the whole thickness

$$g(y,t) = \frac{A_g}{2} + \frac{A_g}{2} \cdot \sin\left(\frac{2\pi \cdot t}{t_g}\right) \qquad -b \le y \le 0 \qquad (4\text{-}10)$$

where, t_g is the period of the sinusoidal function [s].

Constant VOC generation for the entire thickness (Case 1-a) may be applicable for the homogeneous decomposition of an aged building material. A study indicated that degradation takes place in linoleum resulting in a continuous production of VOCs during the lifetime of the material [Jensen et al., 1995]. VOC can be generated by chemical reactions like oxidation of material surface (Case 1-b). Oxidative degradations, which may be caused by ozone (O_3) or nitrogen oxides (NO_x) in the air [Wolkoff et al., 1997], have been reported for building materials like linoleum [Jensen et al., 1996], PVC flooring [Wolkoff, 1998; Knudsen et al., 1999] and carpet [Weschler et al., 1992].

VOCs can also be generated at the bottom surface of a solid material (Case 1-c) when a solid material reacts with the underlying material. Many IAQ complaint cases reported elevated VOC concentration (i.e., 2-ethyl hexanol) in indoor air, which was generated from hydrolysis of the plasticizer in PVC flooring material placed on damp concrete [Gustafsson, 1992; Rothweiler, et al. 1993; and Saarela, 1999]. VOC generation at the bottom surface of a solid may also be applicable for MVOCs generated by microbiological agents growing on the underlying water-damaged building material [Bjurman, 1999].

Cases 2 and 3 represent the time-dependent secondary source behavior, whilst Case 1 describes the geometry-dependant generation functions. Most secondary source behavior is transient in nature. Photocopiers and laser printers have been reported to emit ozone as well as VOCs while they are in use [Wolkoff, 1995]. The intermittent use of the equipment may result in oxidative degradation of building materials for a limited period of time. Different types of MVOC can be produced during different growth phases of microorganisms [Bjurman et al., 1997; Bjurman, 1999], so some MVOC are generated only for a certain period of time. For example, the 16-week-long experimental study on the VOC emission by *Penicillium Brevicompactum* growing on wood, indicated that 3-methyl-1-butanol is detected only during the first 4-week period while 1-octen-3-ol appeared late in growth cycle, i.e., 9-12 week period [Bjurman et al., 1997]. Case 2 shows the secondary source behavior that occurs for a limited time as a step function. Though the simplest step function is presented here, any arbitrary generation term can be described by a series of step functions.

Some secondary source behavior would have periodic nature. The outdoor ozone concentration, which is a major source of indoor ozone by the outdoor-to-indoor transfer, generally varies by hour and by season: maximum ozone level in a day at mid-afternoon hours and minimum at early morning hours; and maximum in a year in summer month and the minimum in winter months [Weschler, 2000]. Case 3 describes the seasonal variation of the secondary source behavior using a sinusoidal function.

The above five functions can be easily implemented in the exact solution of the dimensional proposed model (Eq. (3-9)) and closed form solutions can be obtained (see appendix B). When a generation function is too complicated to obtain a closed form solution, the generation term in the Eq. (3-9) can be easily evaluated by numerical integration procedures.

For each case, the considered parameter ranges are the same as the parametric study on the primary source/sink behavior presented in Section 4.2. To observe the secondary source behavior only, the initial VOC concentration in solid (C_o) and the VOC concentration in the outside boundary layer (C_∞) were set to zero. The emission rate (R) was normalized by dividing it by the maximum secondary emission rate (R_2), which was determined as follows.

$$R_2 = A_g \cdot b \qquad \text{for Cases 1-a, 2, and 3} \qquad (4\text{-}11)$$

$$R_2 = B_g \qquad \text{for Cases 1-b and c} \qquad (4\text{-}12)$$

where, R_2 has the unit of [mg/m^2/s].

The three cases of continuous constant generation (i.e., Cases 1-a, b, and c) were compared for two cases of D_a/D_s (i.e., D_a/D_s = 10 or 1000) with constant other properties: (ε+K) =100, b/L =0.001, and Re_L =1.0×10^4. Fig. 4-5 shows both the R/R_2 versus t/t_{total} curves and R/R_2 versus t for 60 hours. Nondimensionalized time plot can show the overall emission behavior. For all combination of considered parameters, the time (t) to reach 99% of R_2, t_2 was obtained for the Case 1-a. One interesting point is that t_2 of Case 1-a is

the same as t_{total} in the primary source/sink behavior, which was presented in Figs. 4-1 and 4-2. When generation occurs at solid-air interface (at $y = 0$), t_2 is similar or less than that of Case 1-a depending on the parameters. However, sometimes it never reaches 99% of R_2. When the generation takes place at $y = -b$, t_2 is generally longer than that of the Case 1-a. For convenience in the comparison, t_{total} was used for nondimensionalizing the time.

In Figs. 4-5 (a) and (b), the emission profiles (R/R_2 versus t/t_{total}) of Case 1-a for both D_a/D_s cases are similar. Case 1-b (i.e., generation at solid-air interface) gives the highest emission rate. Since the generation occurs at the solid-air interface, more VOCs are emitted to the air than diffused through the material. This becomes more significant when the diffusion resistance of the solid increases. In Case1-c, the VOCs are generated at the bottom of the solid (at $y = -b$) and have to be transferred to the upper surface through diffusion. When the diffusion resistance of the solid is lower, the more VOCs can be transferred. When D_a/D_s is high (i.e., 1000 or more), the early stage emission rate (R/R_2) is almost zero, since the emission rate is obtained at the upper surface and it takes longer time for VOCs to transfer from the bottom surface to the upper surface. The emission rate of Case 1-c is always the lowest among three cases. When the emission profiles are plotted as a function of time up to 60 hours as in Fig 4-5 (a') and (b'), the difference in emission profiles is negligible for the case of D_a/D_s=10; however, the difference become significant for the case of D_a/D_s=1000 (i.e., at higher diffusion resistance).

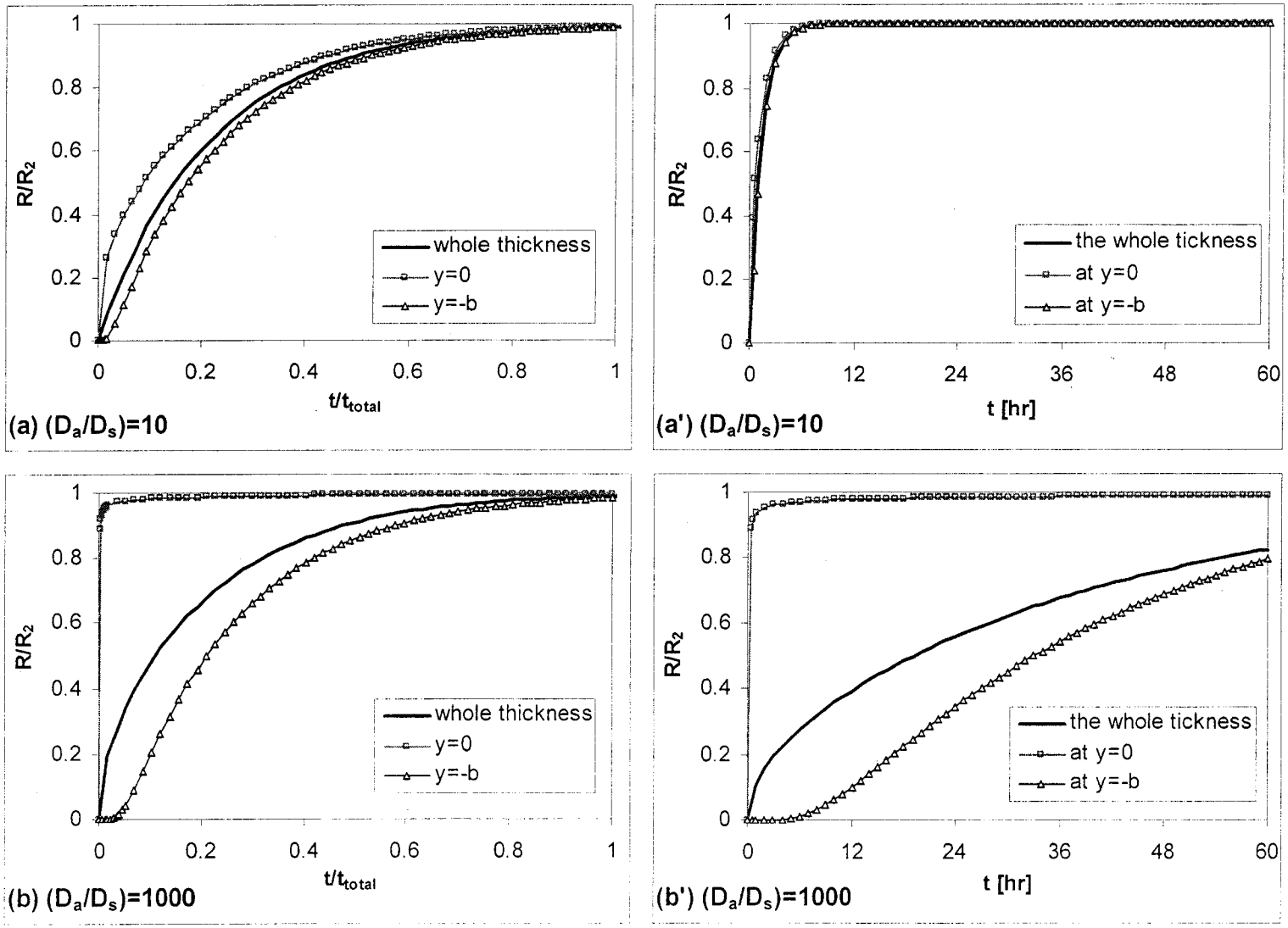

Figure 4-5 Comparison of the secondary source Cases 1-a, b, and c

Figure 4-6 presents the effect of Reynolds number (Re_L) on the secondary emission rate (R/R_2) for Cases 1-a, b, and c, when the material properties are D_a/D_s = 10, (ε+K) =100, and b/L =0.001 (or (D_a/D_s)×(b/L)=0.01), which are the same as the primary source/sink behavior case presented in Fig 4-3 (a). Re_L has significant impact like the primary source/sink behavior, and almost identical effects of Re_L were observed for three cases. The secondary emission rate increases as the Re_L increases (i.e., the air velocity increases).

When the diffusion resistance is larger as presented in Fig. 4-7, which D_a/D_s = 1000, (ε+K) = 100, and b/L = 0.001 (or (D_a/D_s)×(b/L) = 1.0), the effects of Re_L on R/R_2 become smaller in all three cases. Unlike the primary source/sink case with the same material properties (Fig. 4-3 (b)) that shows negligible effect of Re_L, Fig. 4-7 shows mild effects of Re_L. Among three cases, the largest effect of Re_L was observed in Case 1-b, i.e., generation at the solid-air interface (at y = 0). Cases 1-a and c show similar effects of Re_L. For both cases, the VOCs generated have to be transferred through the solid to reach the air overlaying the solid, so the diffusion resistance of the solid plays a decisive role in the effect of Re_L. When the generation takes place at the air-solid interface as in Case 1-b, the effect of the diffusion resistance of solid becomes less significant.

Previous experimental studies on VOC emissions [Knudsen et al., 1999; and Wolkoff, 1998] have concluded that air velocity affects the secondary emission whilst no significant effect was observed for the primary emission. Both studies observed that 2-ethylhexanol and phenol emissions from PVC flooring are promoted at high air velocity.

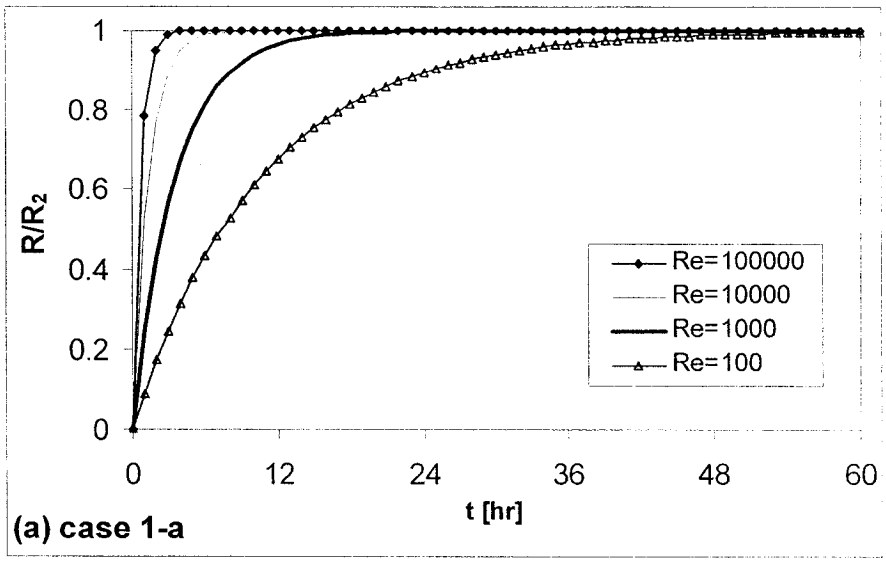

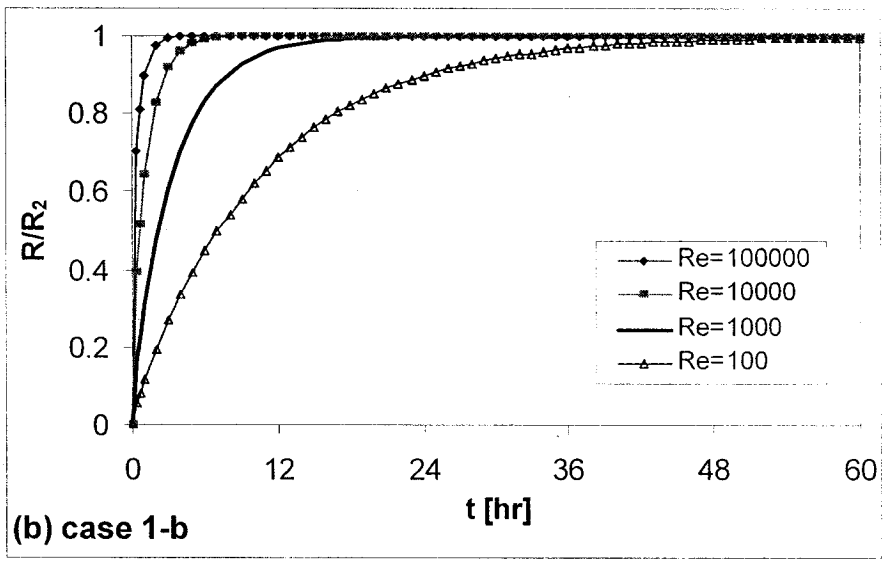

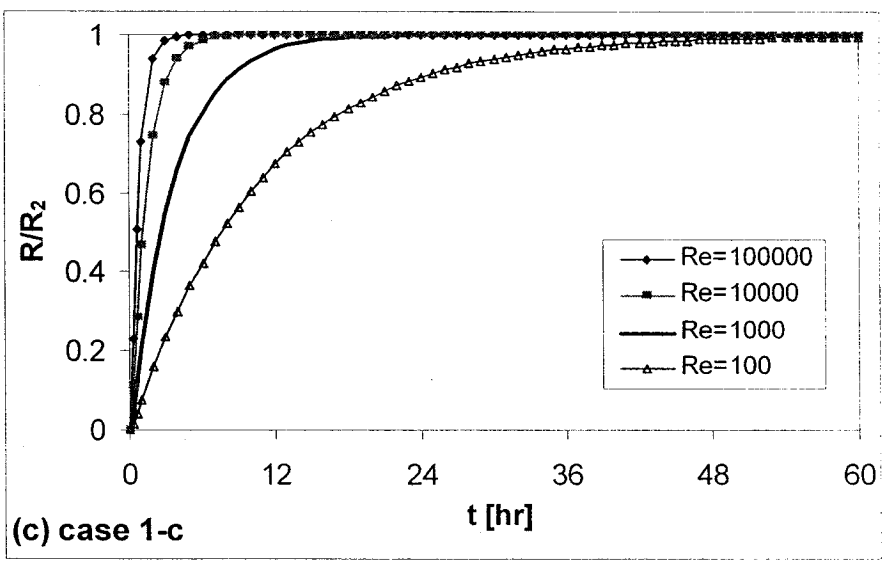

Figure 4-6 Effect of Reynolds number for Cases 1-a, b, c with D_a/D_s=10

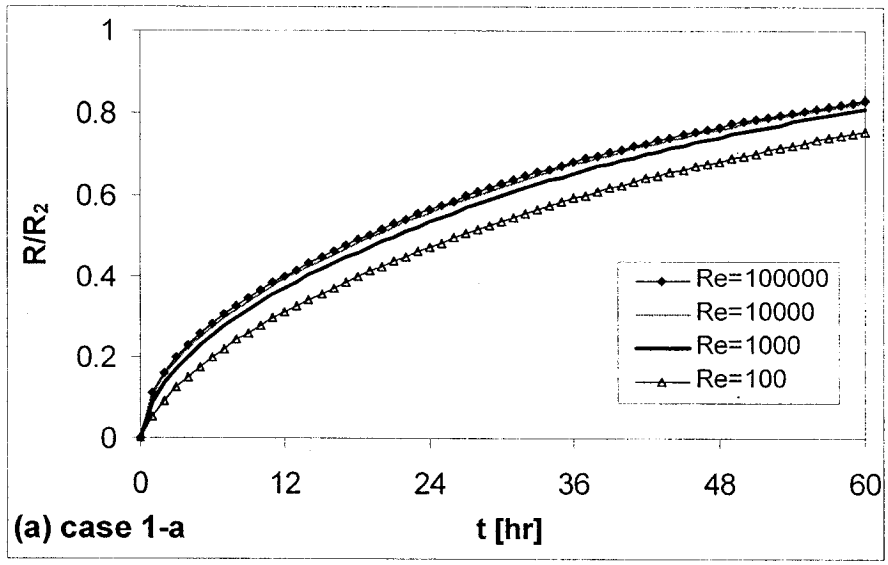

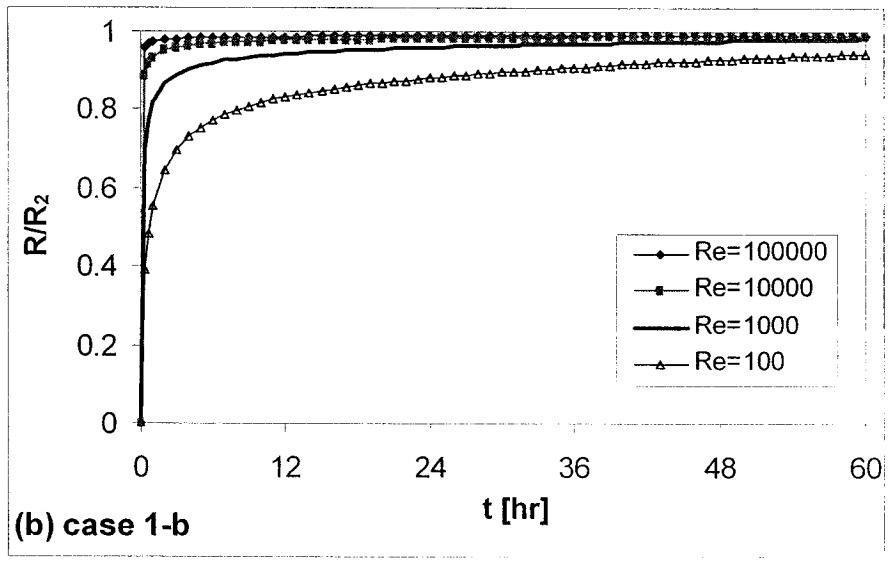

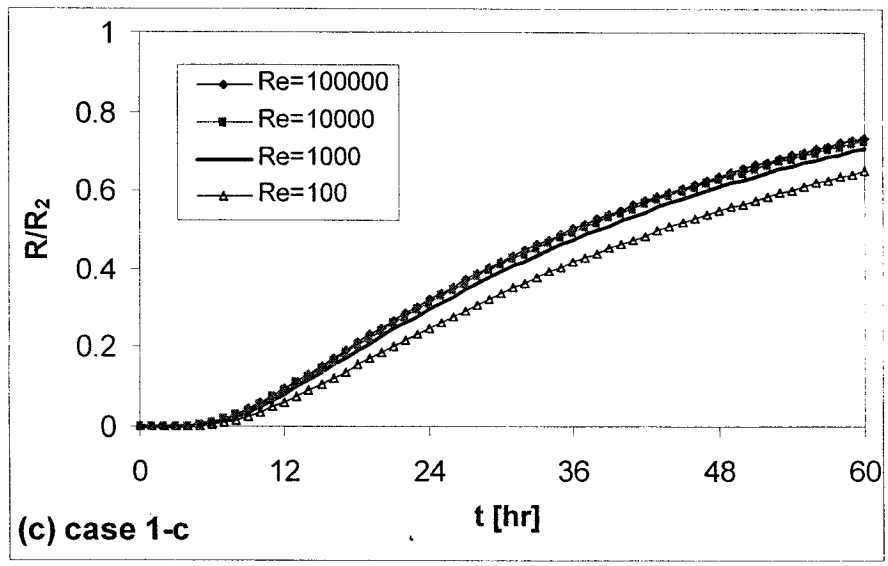

Figure 4-7 Effect of Reynolds number for Cases 1-a, b, c with D_a/D_s=1000

This phenomenon was explained as oxidative degradation: the plasticizer in PVC reacts with the oxygen in the air. When the air velocity increases, the boundary layer thickness decreases, and this can cause the increased effective contact of oxygen with building material surface. Since the oxidation takes place at the solid-air interface, the Case 1-b may describe the ideal case of oxidation process. Generally, the diffusion resistance of PVC flooring material is large; hence, the air velocity does not affect the primary emission as shown in Fig. 4-3 (b), but still can affect the secondary emission like Case 1-b given in Fig. 4-7 (b). This agrees with the experimental findings of an oxidation process.

Figure 4-8 presents the secondary source behavior of Cases 2 and 3 at various b/L. The time was normalized by dividing it with t_g, which is 1 hour of generation time for Case 2, and one period of sinusoidal generation for Case 3. For Case 2 (Fig.4-8 (a)), the emission rate increases during the generation time (t_g). As the generation stops, the emission rate decreases like the primary emission. The peak emission rate at t/t_g =1.0 increases as b/L decreases. For other parameters, the peak emission rate increases as (D_a/D_s) and (ε+K) decrease, and Re_L increases.

In Case 3 (Fig. 4-8 (b)), when b/L is small, the emission profile just follows the generation profile. When b/L is larger than certain limits, the emission profiles show the reduced and delayed peak emission rates and the accumulation in the peak emission rate of the second period (after 1 year) compared with that of the first period. Similar results were observed in other material properties (D_a/D_s and (ε+K)). In Case 3, little effect of

Re_L is observed. When VOCs are generated throughout the whole thickness, the impact of Re_L is clear when the diffusion resistance of the solid is small. Since in this case, the emission profile with low diffusion resistance always follows the generation profile, the effect of Re_L become always negligible.

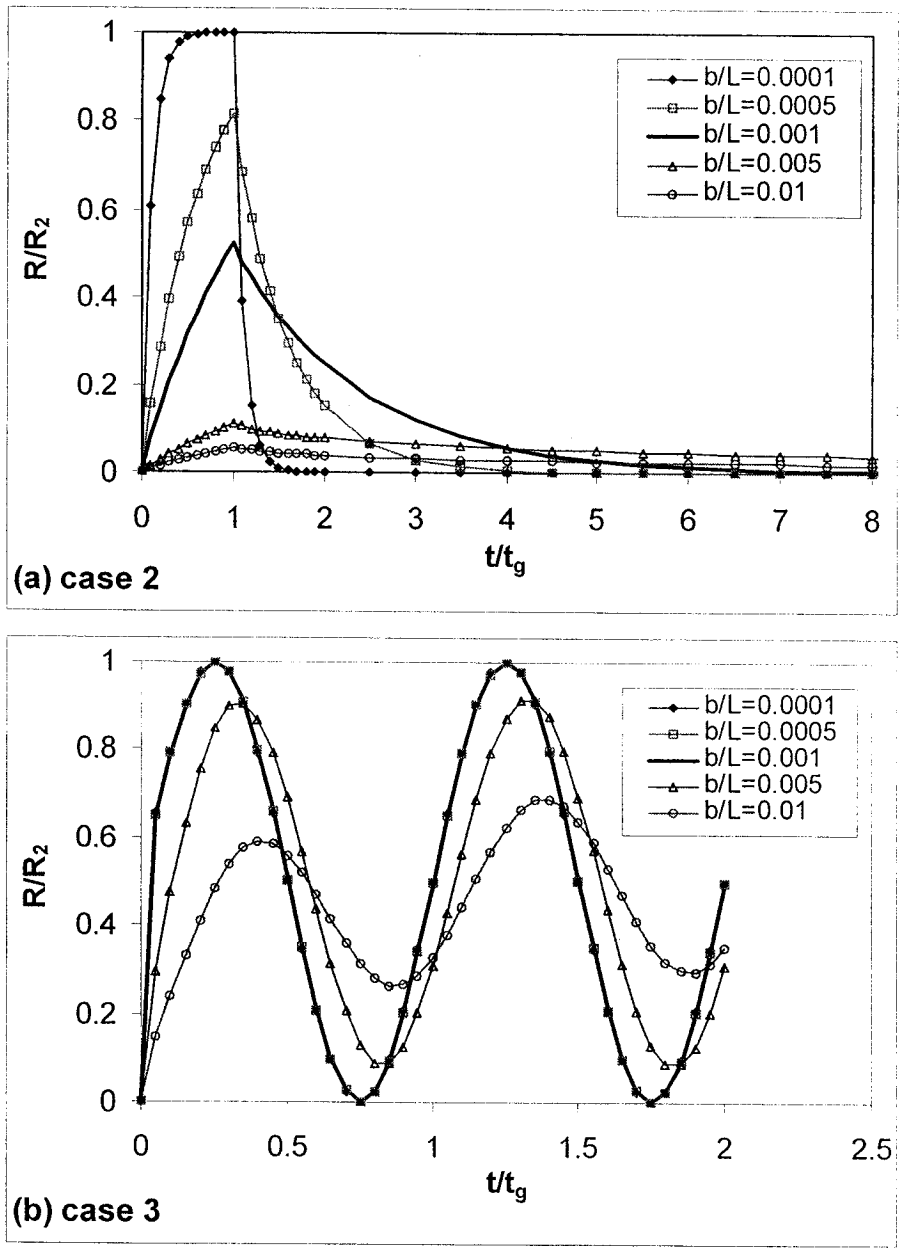

Figure 4-8 Secondary source behavior of Cases 2 and 3

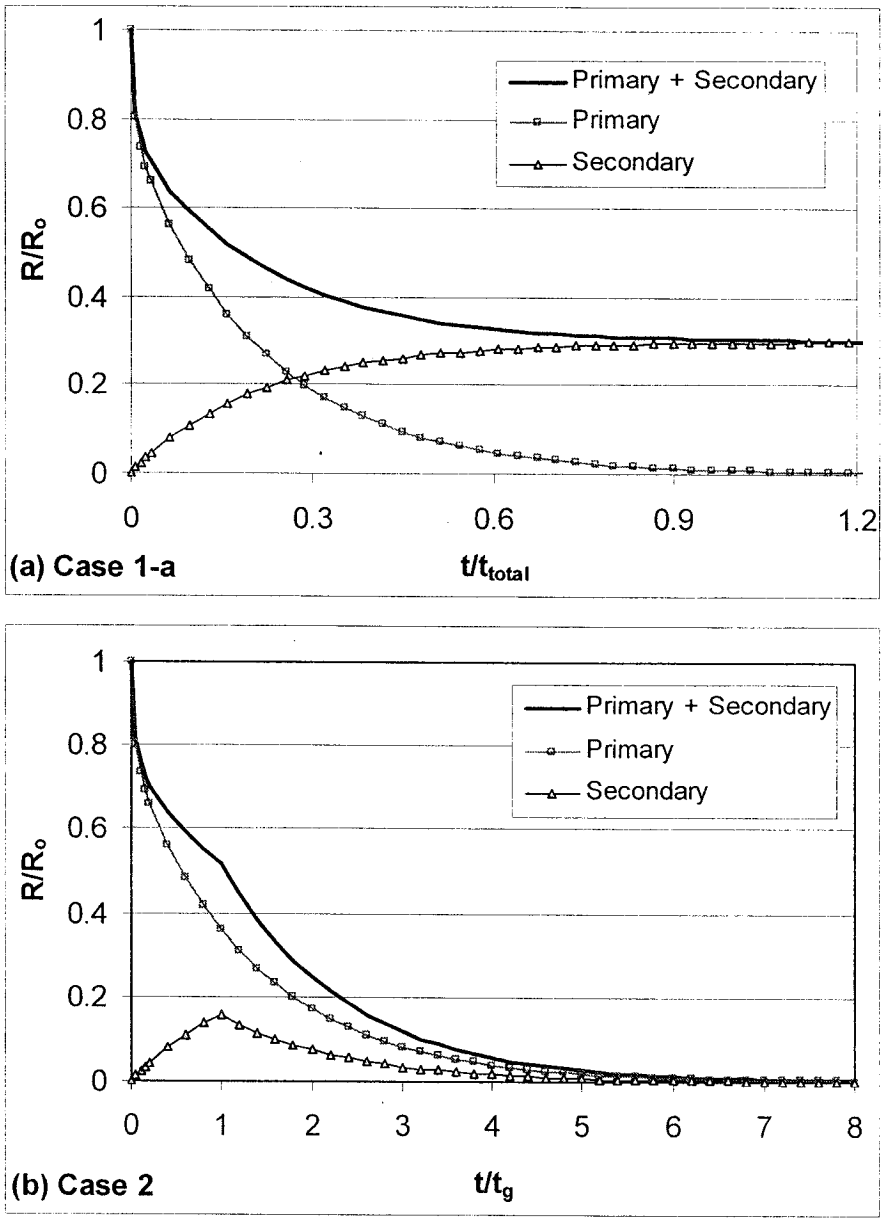

Figure 4-9 Primary and secondary source behavior

Figures 4-9 (a),(b) present the emission profiles when both primary and secondary source behavior is considered. For the secondary emissions, Case 1-(a) and 2 were applied and the maximum secondary emission rate (R_2) was maintained as 30% of the initial primary emission rate (R_o). As we can notice in the analytical solution of the proposed model, as in Eq. (3-9), the emission rate for both primary and secondary emissions is simply the

sum of the two and Fig. 4-9 confirms this. For the secondary emission case of 1-a (Fig. 4-9 (a)), the primary emission dominates at the early stage of emission; however, as time passes by (i.e., t/t_{total} larger than 0.3), secondary emission takes over. The emission profile of both primary and secondary emissions, decay more gradually compared with that of the primary emission only and the difference in emission rates between two profiles becomes constant as the secondary emission dominates. Similar results were observed in the experimental study [Jensen et al., 1996] as shown in Fig. 4-10. Linoleum emission tests were carried out using air or nitrogen. When the air was used, the emission rates of some VOC were larger than those using the nitrogen, which was speculated due to reactions of linoleum with the oxidants in the air.

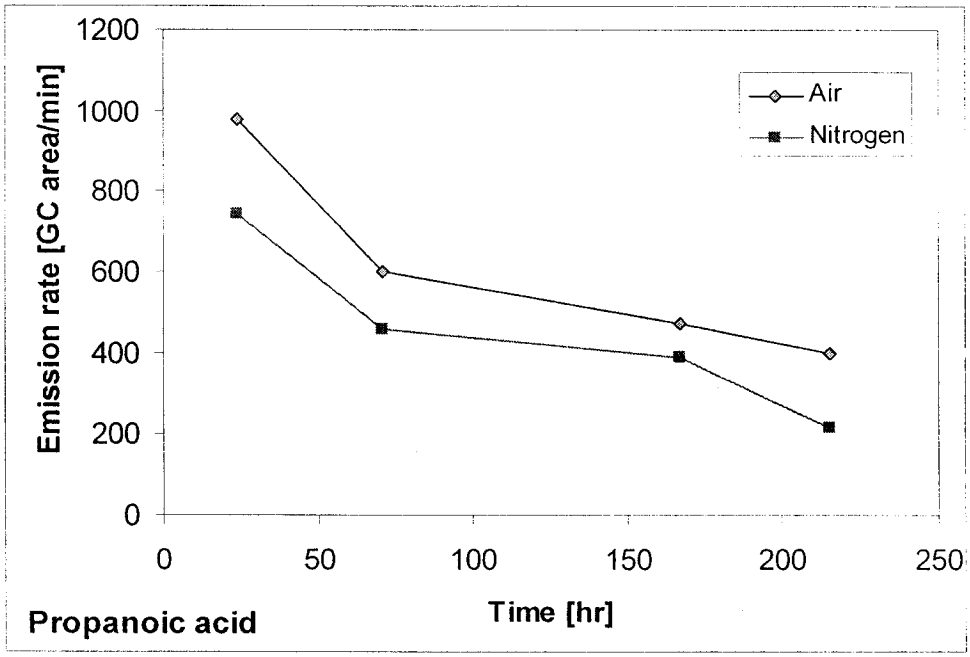

Figure 4-10 Experimental study on a secondary emission [Jensen et al, 1996]

4.4 SUMMARY

Applying the proposed analytical model presented in Chapter 3, a theoretical investigation was carried out on the source and sink behavior of porous building materials. First, the effects of parameter were investigated for the primary source/sink behavior. (ε+K) linearly affects the primary source/sink behavior, which were expressed in terms of the total transfer time t_{total}^{+}, and non-dimensional wall concentration or emission/sorption rate, θ_w. Biot number, which comprised of material properties- (D_a/D_s) and (b/L), and convection parameters- Re_L and Sc, shows nonlinear effects. As Biot number increases, i.e., (D_a/D_s), (b/L), Re_L and/or Sc increases, t_{total}^{+} decreases but after certain limit, i.e., Bi = 10, it becomes constant; and θ_w decreases. Generally, the effects of material properties are more significant than the air velocity, expressed as Re_L on the primary source/sink behavior. The effect of air velocity is conditional. The effect of Re_L is noticeable when the diffusion resistance of the solid material is small, i.e., (D_a/D_s)×(b/L) is less than 1.0. The length scale (L) can also affect the emission rates.

To examine the capacity of the proposed model for secondary behavior, five cases of hypothetical generation functions were implemented and the parametric study of material properties and air velocity was carried out for each case. Some case study results agree well with experimental findings on the secondary emissions available in literature. From the case study for the secondary emission, the following conclusion was made.

- The proposed model can describe various functions of secondary behavior.
- Generally, the material parameters: diffusion coefficient, porosity, sorption parameter and the thickness of the solid, have significant effects on the emission.

- The effect of air velocity expressed as Reynolds number, strongly depends on the material properties of the solid and the generation/elimination function of the secondary behavior considered.
- The location where the secondary behavior occurs can significantly affect the emission/sorption rate.

For the secondary behavior, the merit of the proposed model is that it imposes few limitations on the generation/elimination term of secondary behavior; hence, it is suitable for describing various mechanisms involved in the secondary behavior. As long as the generation function is given from experimental or theoretical studies, this proposed model can be applied to predict the VOC emission/sorption rates, which are affected by the material properties of the solid and the air velocity as shown in the analytical solution.

Chapter 5

Numerical Simulation of the Conjugate Mass Transfer Problem: Method Development and Validation

5.1 INTRODUCTION

In analytical modeling, simplifying assumptions are imposed in order to make the problem mathematically tractable. The major assumptions made in Chapter 3, in developing the exact analytical model for VOC source/sink behavior of porous building materials are:

1. Constant VOC concentration at the wall (C_w) along the length of the porous material. In other words, C_w is not varying along the x-direction.
2. Quasi-steady convective mass transfer
3. One-dimensional diffusion in solid
4. Henry (linear) sorption isotherm

The above mentioned assumptions are commonly used in other previously developed analytical or numerical models reviewed in Chapter 2. The constant C_w assumption is either implicitly or explicitly applied in all models except for the CFD models using the fourth-kind boundary condition at the solid-air interface, i.e. Eq. (2-19) or (2-20). In the proposed analytical model, this assumption is implicitly introduced by employing the

commonly used Sherwood number correlations for material emission, Eq. (2-23). The assumption of quasi-steady convective mass transfer is made in models such as by Huang and Haghighat (2002a), and Blondeau et al. (2000) using the third-kind boundary condition as shown in Eq. (2-21) or (2-22). All analytical models discussed in previous chapters [Little et al., 1994; Yang et al, 1998; Huang and Haghighat, 2002a] and some numerical models [Huang and Haghighat, 2002a; Blondeau et al., 2000] assumed one-dimensional diffusion within the solid. All models with the material-phase approach for diffusion in solid [Little et al., 1994; Yang et al., 1998, 2001b and c; Huang and Haghighat, 2002a] use only the Henry isotherm.

In order to assess the range of validity and the limitations of the analytical solution derived in the previous chapter, a numerical method for simulating the conjugate mass transfer problem was developed and implemented by relaxing the above-mentioned assumptions. This chapter presents the development and the testing of the numerical model. In this investigation, the VOC source/sink behavior of porous materials was treated as conjugate mass transfer problems. This approach is physically more appropriate than the traditional convective mass transfer, where the concentration or the mass flux at the solid-fluid interface is prescribed usually as a constant over the entire interface like the proposed analytical model and other models [Little et al., 1994; Yang et al, 1998; Blondeau et al., 2000; Huang and Haghighat, 2002a]. In a conjugate mass transfer problem the governing equations for fluid flow and mass transfer have to be simultaneously solved, and the mass concentration as well as mass flux have to be continuous at the fluid-solid interface. Therefore, the conjugate mass transfer problem,

which describes rather accurately the VOC transfer in porous media, was solved numerically and the control volume based finite difference method was chosen and was implemented as described later in this chapter.

5.2 DEVELOPMENT OF NUMERICAL MODELS

The conjugate mass transfer problem for VOC source/sink behavior of porous materials consists of laminar forced convection over a flat plate coupled with diffusion and sorption within the solid through the concentration and the flux continuities at the solid-air interface. The geometry and flow characteristics were chosen to be consistent with the commonly used Sherwood number correlation of laminar forced convection over a flat plate, given in Eq. (2-23).

In order to gradually relax the assumptions made in the analytical model, four numerical models were developed, as described in Table 5-1.

Table 5-1 Description of numerical models

Model	Convection	Diffusion	Sorption isotherm	Relaxed assumptions
1	Quasi-steady	Unsteady 1-D	Linear	• Constant C_w
2	Unsteady	Unsteady 1-D	Linear	• Constant C_w • Quasi-steady convection
3	Unsteady	Unsteady 2-D	Linear	• Constant C_w • Quasi-steady convection • 1-D diffusion in solid
4	Unsteady	Unsteady 2-D	Nonlinear	• Constant C_w • Quasi-steady convection • 1-D diffusion in solid • Linear sorption isotherm

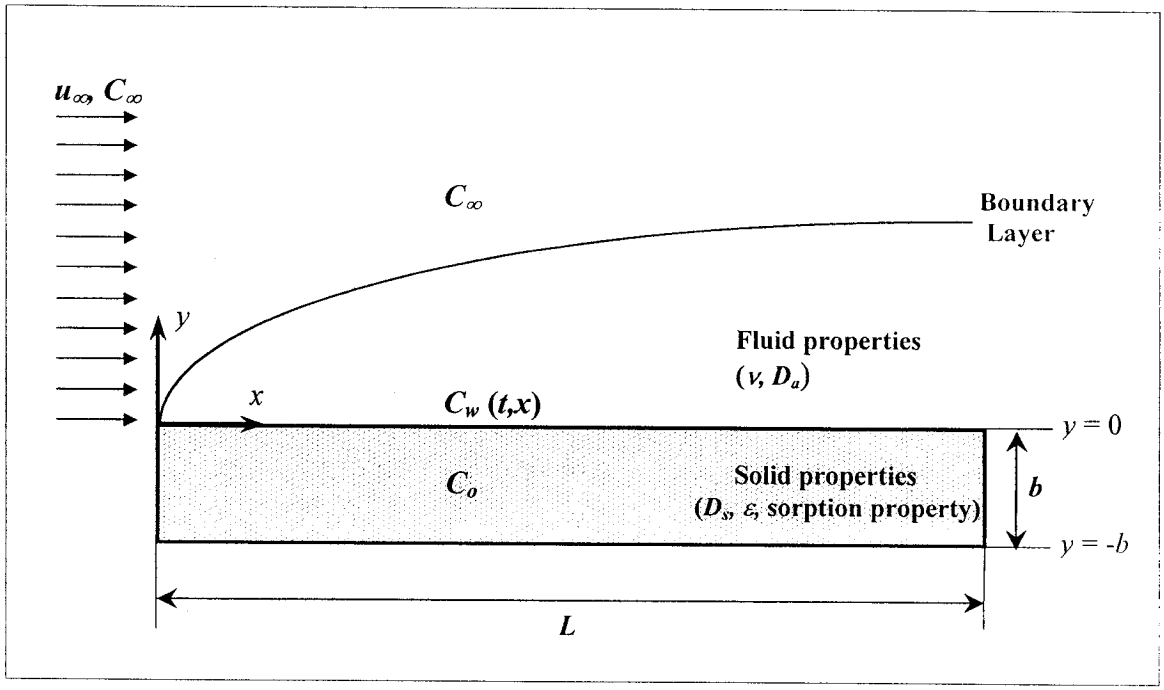

Figure 5-1 Schematic diagram of the conjugate mass transfer problem

By comparing the predictions of the first numerical model (Model 1) with those of the proposed analytical model, the validity of the constant C_w assumption can be examined. The assumption of quasi-steady convection mass transfer can be evaluated by comparing the simulation results between Models 1 and 2, and so forth.

A schematic of the conjugate mass transfer problem considered in this study is shown in Fig. 5-1. Steady, laminar flow of an incompressible fluid (air) is flowing over a flat plate with uniform velocity u_∞ and VOC concentration C_∞. The porous material occupies the region $0 \le x \le L$, $-b \le y \le 0$, while the air fills the region $0 \le x < \infty$, $y \ge 0$. The porous material has a uniform thickness (b), constant mass diffusion coefficient (D_s), sorption property (K), and initial VOC concentration (C_o). There is no mass transfer along the

edges of the material (at $x = 0$ and $x = L$). Note that the secondary source/sink behavior is not considered in the numerical model.

The assumptions and limitations of the proposed model are as follows.

1. Regarding the overall set up,
    - All material properties are assumed constant: diffusion coefficient in the air (D_a), kinematic viscosity (ν), effective diffusion coefficient of solid (D_s), sorption properties (e.g., K)
    - The temperature and the relative humidity are assumed to be constant
2. Regarding VOC transfer in the air,
    - Steady laminar fluid flow with uniform velocity, u_∞ over the material surface
    - Uniform VOC concentration in ambient air, C_∞
    - Low mass transfer rate; hence, fluxes through solid-fluid interface will not disturb the air velocity field.
3. Regarding VOC transfer within the material
    - Only primary source/sink behavior is considered.
    - Adsorption is fully recoverable: the whole amount of VOC adsorbed will be desorbed at the same temperature. Heat of adsorption/desorption is negligible. Also, the adsorption reaches equilibrium quickly in comparison with the rate of diffusion within the pores.
    - There is no mass transfer along the edges of the materials (at $x = 0$ and $x = L$).
    - Diffusion coefficient of the solid material is isotropic.

5.2-1 Governing Equations

Since the mass fraction of VOCs in air is very small and the mass transfer at the fluid-solid is low, the governing equations for fluid flow can be written ignoring the presence of VOCs. For steady two dimensional flow of a constant-property Newtonian fluid, the continuity and the momentum equations, assuming a boundary layer developing in the x-direction, are written as follows:

Continuity equation

$$\frac{\partial u}{\partial x}+\frac{\partial v}{\partial y}=0 \tag{5-1}$$

x-momentum boundary layer equation

$$u\frac{\partial u}{\partial x}+v\frac{\partial u}{\partial y}=\nu\frac{\partial^2 u}{\partial y^2} \tag{5-2}$$

where, u and v are velocity components in x-direction and y-direction, respectively [m/s].

VOC convection in the fluid region is expressed in terms of the concentration boundary layer equation and is written in both quasi-steady and unsteady convection as follows.

Convective mass transfer (fluid)

- Unsteady

$$\frac{\partial C}{\partial t}+u\frac{\partial C}{\partial x}+v\frac{\partial C}{\partial y}=D_a\frac{\partial^2 C}{\partial y^2} \tag{5-3}$$

- Quasi-steady

$$u\frac{\partial C}{\partial x}+v\frac{\partial C}{\partial y}=D_a\frac{\partial^2 C}{\partial y^2} \tag{5-4}$$

The governing equation of unsteady diffusion in the solid material of constant effective diffusivity including physical adsorption/desorption is

$$\varepsilon \frac{\partial C}{\partial t} + \frac{\partial C_{ad}}{\partial t} = D_s \left(\nabla^2 C \right) \tag{5-5}$$

The sorption isotherm that relates C_{ad} in terms of C, can be generally described as:

$$C_{ad} = f(C) \tag{5-6}$$

Substituting Eq. (5-6) into Eq. (5-5) gives

$$\left(\varepsilon + \frac{\partial f}{\partial C} \right) \frac{\partial C}{\partial t} = D_s \left(\nabla^2 C \right) \tag{5-7}$$

In this study, both one-dimensional and two-dimensional mass diffusion in the solid material were considered.

Diffusion mass transfer (solid)

- One-dimensional analysis

$$\left(\varepsilon + \frac{\partial f}{\partial C} \right) \frac{\partial C}{\partial t} = D_s \frac{\partial^2 C}{\partial y^2} \tag{5-8}$$

- Two-dimensional analysis

$$\left(\varepsilon + \frac{\partial f}{\partial C} \right) \frac{\partial C}{\partial t} = D_s \left(\frac{\partial^2 C}{\partial x^2} + \frac{\partial^2 C}{\partial y^2} \right) \tag{5-9}$$

The boundary conditions for momentum transfer are as follows,

$$at\ y = 0, \qquad u = v = 0 \tag{5-10}$$

$$as\ y \rightarrow \infty, \qquad u \rightarrow u_\infty \tag{5-11}$$

The initial conditions for mass transfer are as follows,

$$t = 0 \text{ and } y > 0, \qquad C = C_\infty \tag{5-12}$$

$$t = 0 \text{ and } -b < y < 0, \qquad C = C_o \tag{5-13}$$

The boundary conditions for mass transfer at the fluid-solid interface follow from the fact that both mass concentration and mass flux have to be continuous,

$$t > 0 \text{ and } y = 0, \qquad C_{y=0^-} = C_{y=0^+} \tag{5-14}$$

$$D_s \left.\frac{\partial C}{\partial y}\right)_{y=0^-} = D_a \left.\frac{\partial C}{\partial y}\right)_{y=0^+} \tag{5-15}$$

Outside the concentration boundary layer, the concentration reaches the ambient concentration (C_∞).

$$t > 0 \text{ and } y \to \infty, \qquad C \to C_\infty \tag{5-16}$$

At the bottom of the solid and at the edges, there is no mass transfer

$$t > 0 \text{ and } y = -b \qquad \frac{\partial C}{\partial y} = 0 \tag{5-17}$$

$$t > 0 \text{ and } x = 0 \text{ or } x = L \qquad \frac{\partial C}{\partial x} = 0 \tag{5-18}$$

5.2-2 Nondimensional Governing Equations

The governing equations, and initial and boundary conditions for mass transfer, are non-dimensionalized using the following nondimensional variables.

$$\theta = \frac{C - C_\infty}{C_o - C_\infty} \qquad t_c^+ = \frac{t}{t_c} = \frac{t}{L/u_\infty}$$

$$x^+ = \frac{x}{L} \qquad y^+ = \frac{y}{b} \tag{5-19}$$

$$u^+ = \frac{u}{u_\infty} \qquad v^+ = \frac{v}{u_\infty}$$

where t_c is the convection characteristic time [s], which physically corresponds to the time taken by a particle moving with a velocity of u_∞ to travel along the plate from $x = 0$ to $x = L$.

The nondimensional system of governing equations, and initial and boundary conditions for mass transfer can be expressed as follows:

Nondimensional convection mass transfer (fluid)

- Unsteady

$$\frac{\partial \theta}{\partial t_c^+} + u^+ \frac{\partial \theta}{\partial x^+} + \frac{v^+}{\phi} \frac{\partial \theta}{\partial y^+} = \frac{1}{\phi^2 \,\mathrm{Re}_L \, Sc} \frac{\partial^2 \theta}{\partial y^{+2}} \tag{5-20}$$

- Quasi-steady

$$u^+ \frac{\partial \theta}{\partial x^+} + \frac{v^+}{\phi} \frac{\partial \theta}{\partial y^+} = \frac{1}{\phi^2 \,\mathrm{Re}_L \, Sc} \frac{\partial^2 \theta}{\partial y^{+2}} \tag{5-21}$$

Nondimensional diffusion mass transfer (solid)

- One-dimensional analysis

$$\left(\varepsilon + \frac{1}{(C_o - C_\infty)} \cdot \frac{\partial f}{\partial \theta} \right) \frac{\partial \theta}{\partial t_c^+} = \frac{1}{\phi^2 \,\mathrm{Re}_L \, Sc \cdot \left(\dfrac{D_a}{D_s} \right)} \frac{\partial^2 \theta}{\partial y^{+2}} \tag{5-22}$$

- Two-dimensional analysis

$$\left(\varepsilon + \frac{1}{(C_o - C_\infty)} \cdot \frac{\partial f}{\partial \theta}\right) \frac{\partial \theta}{\partial t_c^+} = \frac{1}{\phi^2 \, \mathrm{Re}_L \, Sc \cdot \left(\frac{D_a}{D_s}\right)} \left(\phi^2 \frac{\partial^2 \theta}{\partial x^{+2}} + \frac{\partial^2 \theta}{\partial y^{+2}}\right) \tag{5-23}$$

Nondimensional initial and boundary conditions for mass transfer

$$t_c^+ = 0 \text{ and } y^+ > 0, \qquad \theta = 0 \tag{5-24}$$

$$t_c^+ = 0 \text{ and } -1 < y^+ < 0, \qquad \theta = 1 \tag{5-25}$$

$$t_c^+ > 0 \text{ and } y^+ = 0, \qquad \theta_{y^+=0^-} = \theta_{y^+=0^+} \tag{5-26}$$

$$\frac{D_s}{D_a} \frac{\partial \theta}{\partial y^+}\bigg)_{y^+=0^-} = \frac{\partial \theta}{\partial y^+}\bigg)_{y^+=0^+} \tag{5-27}$$

$$t_c^+ > 0 \text{ and } y^+ \to \infty, \qquad \theta \to 0 \tag{5-28}$$

$$t_c^+ > 0 \text{ and } y^+ = -1 \qquad \frac{\partial \theta}{\partial y^+} = 0 \tag{5-29}$$

$$t_c^+ > 0 \text{ and } x^+ = 0 \text{ or } x^+ = 1 \qquad \frac{\partial \theta}{\partial x^+} = 0 \tag{5-30}$$

where, ϕ is thickness (b) to length (L) ratio.

The relation between t_c^+ and the Fourier number (or t_d^+) given in Eq. (3-15) is

$$t_c^+ = Fo \cdot \frac{b^2}{D_s} \frac{u_\infty}{L} = Fo \cdot \mathrm{Re}_L \cdot Sc \cdot \frac{D_a}{D_s} \cdot \phi^2 \tag{5-31}$$

For nonlinear sorption isotherm, the Freundlich isotherm presented in Eq. (2-3) was applied. Table 5-2 presents the governing equations for mass transfer of each model.

Table 5-2 Governing equations for mass transfer in numerical models

#	Convection (fluid)	Diffusion (porous solid)
1	- Quasi-steady 2-D $u^+\frac{\partial\theta}{\partial x^+}+\frac{v^+}{\phi}\frac{\partial\theta}{\partial y^+}=\frac{1}{\phi^2\,\mathrm{Re}_L\,Sc}\frac{\partial^2\theta}{\partial y^{+2}}$	- Unsteady 1-D with Henry isotherm $(\varepsilon+K)\frac{\partial\theta}{\partial t_c^+}=\frac{1}{\phi^2\,\mathrm{Re}_L\,Sc\cdot\left(\frac{D_a}{D_s}\right)}\frac{\partial^2\theta}{\partial y^{+2}}$
2	- Unsteady 2-D $\frac{\partial\theta}{\partial t_c^+}+u^+\frac{\partial\theta}{\partial x^+}+\frac{v^+}{\phi}\frac{\partial\theta}{\partial y^+}=\frac{1}{\phi^2\,\mathrm{Re}_L\,Sc}\frac{\partial^2\theta}{\partial y^{+2}}$	- Unsteady 1-D with Henry isotherm $(\varepsilon+K)\frac{\partial\theta}{\partial t_c^+}=\frac{1}{\phi^2\,\mathrm{Re}_L\,Sc\cdot\left(\frac{D_a}{D_s}\right)}\frac{\partial^2\theta}{\partial y^{+2}}$
3	- Unsteady 2-D $\frac{\partial\theta}{\partial t_c^+}+u^+\frac{\partial\theta}{\partial x^+}+\frac{v^+}{\phi}\frac{\partial\theta}{\partial y^+}=\frac{1}{\phi^2\,\mathrm{Re}_L\,Sc}\frac{\partial^2\theta}{\partial y^{+2}}$	- Unsteady 2-D with Henry isotherm $(\varepsilon+K)\frac{\partial\theta}{\partial t_c^+}=\frac{1}{\phi^2\,\mathrm{Re}_L\,Sc\cdot\left(\frac{D_a}{D_s}\right)}\left(\phi^2\frac{\partial^2\theta}{\partial x^{+2}}+\frac{\partial^2\theta}{\partial y^{+2}}\right)$
4	- Unsteady 2-D $\frac{\partial\theta}{\partial t_c^+}+u^+\frac{\partial\theta}{\partial x^+}+\frac{v^+}{\phi}\frac{\partial\theta}{\partial y^+}=\frac{1}{\phi^2\,\mathrm{Re}_L\,Sc}\frac{\partial^2\theta}{\partial y^{+2}}$	- Unsteady 2-D with Freundlich isotherm $\left(\varepsilon+\frac{1}{(C_o-C_\infty)}\cdot\frac{\partial f}{\partial\theta}\right)\frac{\partial\theta}{\partial t_c^+}=\frac{1}{\phi^2\,\mathrm{Re}_L\,Sc\cdot\left(\frac{D_a}{D_s}\right)}\left(\phi^2\frac{\partial^2\theta}{\partial x^{+2}}+\frac{\partial^2\theta}{\partial y^{+2}}\right)$ with $\frac{1}{(C_o-C_\infty)}\cdot\frac{\partial f}{\partial\theta}=\alpha\cdot K_F\{C_\infty+(C_o-C_\infty)\cdot\theta\}^{\alpha-1}$

5.3 NUMERICAL PROCEDURE FOR MOMENTUM TRANSFER

Since the fluid flow equations are decoupled from the mass transfer equation in the proposed numerical model, the continuity and momentum boundary layer equations can be solved first. Then, the resulting flow field information can be used as input in solving the convection mass transfer equation. In this study, the velocity field is calculated from the Blasius similarity solution and the VOC mass concentration field is obtained by

solving numerically the concentration equation using the control volume based finite difference method.

Blasius found a similarity solution for laminar boundary layer flow over a flat plate given in Eqs. (5-1, 2, 10 and 11). The dimensionless similarity variable is

$$\eta = y\sqrt{\frac{u_\infty}{2\nu \cdot x}} \tag{5-32}$$

The stream function of the flow (ψ) has the nondimensional form:

$$\psi = f(\eta)\sqrt{2\nu \cdot u_\infty \cdot x} \tag{5-33}$$

where, f is a function to be determined. From Eq. (5-33), velocity u and v are obtained as,

$$u = \frac{\partial \psi}{\partial y} = u_\infty f'(\eta) \qquad v = -\frac{\partial \psi}{\partial x} = \{\eta \cdot f'(\eta) - f(\eta)\}\sqrt{\frac{\nu \cdot u_\infty}{2x}} \tag{5-34}$$

Substituting u and v from Eq. (5-34) into the boundary layer equation, Eq. (5-2), yields the following ordinary differential equation:

$$f''' + f \cdot f'' = 0 \tag{5-35}$$

The boundary conditions given by Eqs. (5-10) and (5-11) are converted to

$$f'(0) = f(0) = 0 \qquad f'(\infty) = 1 \tag{5-36}$$

Since Eq. (5-35) is nonlinear, an iterative procedure is necessary to obtain the solution. The shooting method was implemented in this study. Since this approach employs Newton's method instead of trial-and-error searching technique in determining the new

values of $f''(0)$, it generally provides quadratic convergence of the iterations and decreases the computation time [Cebeci and Bradshaw, 1977]. For the integration procedure, a fourth-order Runge-Kutta method was applied. The obtained numerical solutions, i.e., $f(\eta), f'(\eta)$ and $f''(\eta)$, were validated by comparing them with the solutions presented in literature [White, 1991]. With the known $f(\eta)$ and $f'(\eta)$, velocity u and v can be calculated using Eq. (5-34).

5.4 FINITE DIFFERENCE EQUATIONS FOR MASS TRANSFER

Once the flow field is obtained, it is introduced into the mass transfer equation, e.g. Eq. (5-23), which is solved for the concentration using the finite volume method. In this method, the governing differential equation is integrated over the control volume and the terms appearing in the integral are evaluated in terms of the values at the nodal values of concentration.

In this study, nodes are at cell-vertices for piecewise linear interpolation structure, and the control volume faces are located midway between the nodes, as shown in Fig. 5-2. The nodes are denoted by the upper case letters like ***P***, ***N***, ***S***, ***E***, ***W*** - point of interest, north standing for the positive y-direction, south for the negative y-direction, east for the positive x-direction, and west for the negative x-direction. The lower case letters ***n***, ***s***, ***e***, ***w*** denote the control volume faces at north, south, east, and west, respectively.

The governing differential equation for the diffusion in porous solid, Eq. (5-22) or (5-23), is parabolic in time (t) and elliptic in space (x and/or y). Time is discretized using Euler

Backward differencing, which is implicit and first order accurate. This method is recommended for general-purpose transient calculations because of its robustness and unconditional stability [Versteeg and Malalasekera, 1995]. This is especially desirable for the application on VOC source and sink behavior of building materials, where the product service time or the total transfer time (t_{total}) as defined in Chapter 4 can last several years. For space discretization, the second-order central difference scheme was applied, and the finite difference stencil for two-dimensional diffusion is shown in Fig. 5-2. Integrating the governing equations over the control volume with the above mentioned discretization schemes in time and space results in the following relations:

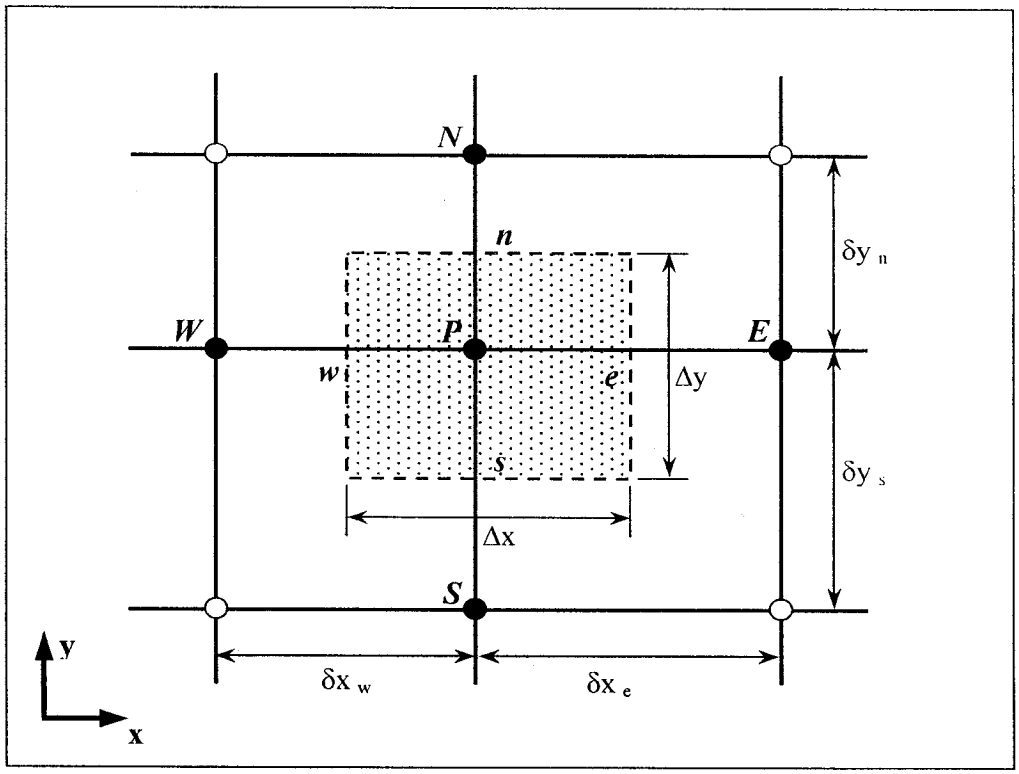

Figure 5-2 Control volume for two-dimensional diffusion

For one-dimensional diffusion in the solid,

$$\left(\varepsilon+\frac{1}{(C_o-C_\infty)}\cdot\frac{\partial f}{\partial\theta}\right)\frac{\theta_P^{\,1}-\theta_P^{\,0}}{\Delta t}\cdot\Delta y=\frac{\gamma}{\phi^2\,\mathrm{Re}_L\,Sc}\left(\frac{\theta_N^{\,1}-\theta_P^{\,1}}{\delta y_n}-\frac{\theta_P^{\,1}-\theta_S^{\,1}}{\delta y_s}\right) \tag{5-37}$$

And for two-dimensional diffusion in the solid,

$$\begin{aligned}&\left(\varepsilon+\frac{1}{(C_o-C_\infty)}\cdot\frac{\partial f}{\partial\theta}\right)\frac{\theta_P^{\,1}-\theta_P^{\,0}}{\Delta t}\Delta x\cdot\Delta y\\&=\frac{\gamma}{\mathrm{Re}_L\,Sc}\left[\Delta y\cdot\left(\frac{\theta_E^{\,1}-\theta_P^{\,1}}{\delta x_e}-\frac{\theta_P^{\,1}-\theta_W^{\,1}}{\delta x_w}\right)+\frac{\Delta x}{\phi^2}\cdot\left(\frac{\theta_N^{\,1}-\theta_P^{\,1}}{\delta y_n}-\frac{\theta_P^{\,1}-\theta_S^{\,1}}{\delta y_s}\right)\right]\end{aligned} \tag{5-38}$$

where, $\gamma = D_s / D_a$ for the diffusion in solid; and the superscripts ^{1} and ^{0} refer to the time levels $t+\Delta t$ and t, respectively.

Equations (5-37) and (5-38) can be expressed in the following standard forms of discretization equations:

- for one-dimensional diffusion in the solid

$$a_P\cdot\theta_P^{\,1}=a_N\cdot\theta_N^{\,1}+a_S\cdot\theta_S^{\,1}+a_P^{\,0}\cdot\theta_P^{\,0} \tag{5-39}$$

where,
$$a_N=\Gamma_n=\frac{\gamma}{\phi^2\,\mathrm{Re}_L\,Sc\cdot\delta y_n};$$

$$a_S=\Gamma_s=\frac{\gamma}{\phi^2\,\mathrm{Re}_L\,Sc\cdot\delta y_s};$$

$$a_P^{\,0}=\left(\varepsilon+\frac{1}{(C_o-C_\infty)}\cdot\frac{\partial f}{\partial\theta}\right)\frac{\Delta y}{\Delta t};$$

$$a_P=a_N+a_S+a_P^{\,0}$$

- for two-dimensional diffusion in the solid

$$a_P \cdot \theta_P{}^1 = a_N \cdot \theta_N{}^1 + a_S \cdot \theta_S{}^1 + a_E \cdot \theta_E{}^1 + a_W \cdot \theta_W{}^1 + a_P{}^0 \cdot \theta_P{}^0 \qquad (5\text{-}40)$$

where, $a_N = \Gamma_n \cdot \Delta x$;

$$a_S = \Gamma_s \cdot \Delta x;$$

$$a_E = \Gamma_e \cdot \Delta y = \frac{\gamma}{\mathrm{Re}_L \, Sc \cdot \delta x_e} \cdot \Delta y;$$

$$a_W = \Gamma_w \cdot \Delta y = \frac{\gamma}{\mathrm{Re}_L \, Sc \cdot \delta x_w} \cdot \Delta y;$$

$$a_P{}^0 = \left(\varepsilon + \frac{1}{(C_o - C_\infty)} \cdot \frac{\partial f}{\partial \theta} \right) \frac{\Delta x \cdot \Delta y}{\Delta t}; \text{ and}$$

$$a_P = a_N + a_S + a_E + a_W + a_P{}^0$$

The governing equations for convective mass transfer presented in Eqs. (5-20) and (5-21) are parabolic in time and along the flow direction (i.e., x-direction), and elliptic in the y-direction. As for time integration, the Euler Backward differencing scheme was used to advance the solution in time while integration in the x-direction is performed using the Crank-Nicolson method, which is implicit and second order accurate, so that all spatial derivatives are second order accurate. Note that physically unrealistic overshooting or oscillatory results can be obtained if the mesh in the x-direction is not sufficiently fine [Anderson et al., 1984, Hoffman, 1992]. As for the y-direction, the central difference scheme was used. Due to the existence of a convection term in the y-direction, numerical instability can occur if the grid spacing in the y-direction permits the convective transport to dominate the diffusive transport, or in other words, diagonal dominance is not

maintained for the tridiagonal algorithm [Anderson et al., 1984]. To ensure the stability of the central difference scheme, the mesh Peclet number (*Pe*), which is defined as ($v_p \cdot \Delta y / D_a$), has to be within the range of –2 and 2 [Patankar, 1980]. Figure 5-3 presents the finite difference stencils for both quasi-steady and unsteady convection.

Applying those schemes to Eqs. (5-20) and (5-21) gives the following algebraic equations:

- for the quasi-steady convective mass transfer

$$\frac{1}{2}\cdot(u_W + u_P)\cdot\frac{(\theta_P - \theta_W)}{\delta x_w}\cdot\Delta y + \frac{1}{2}\cdot\left[\frac{v_P}{\phi}\frac{(\theta_N - \theta_S)}{2} + \frac{v_W}{\phi}\frac{(\theta_{WN} - \theta_{WS})}{2}\right] = \frac{1}{2}\cdot\frac{\gamma}{\phi^2\,\mathrm{Re}_L\,Sc}\cdot\left[\left(\frac{\theta_N - \theta_P}{\delta y_n} - \frac{\theta_P - \theta_S}{\delta y_s}\right) + \left(\frac{\theta_{WN} - \theta_W}{\delta y_n} - \frac{\theta_W - \theta_{WS}}{\delta y_s}\right)\right] \tag{5-41}$$

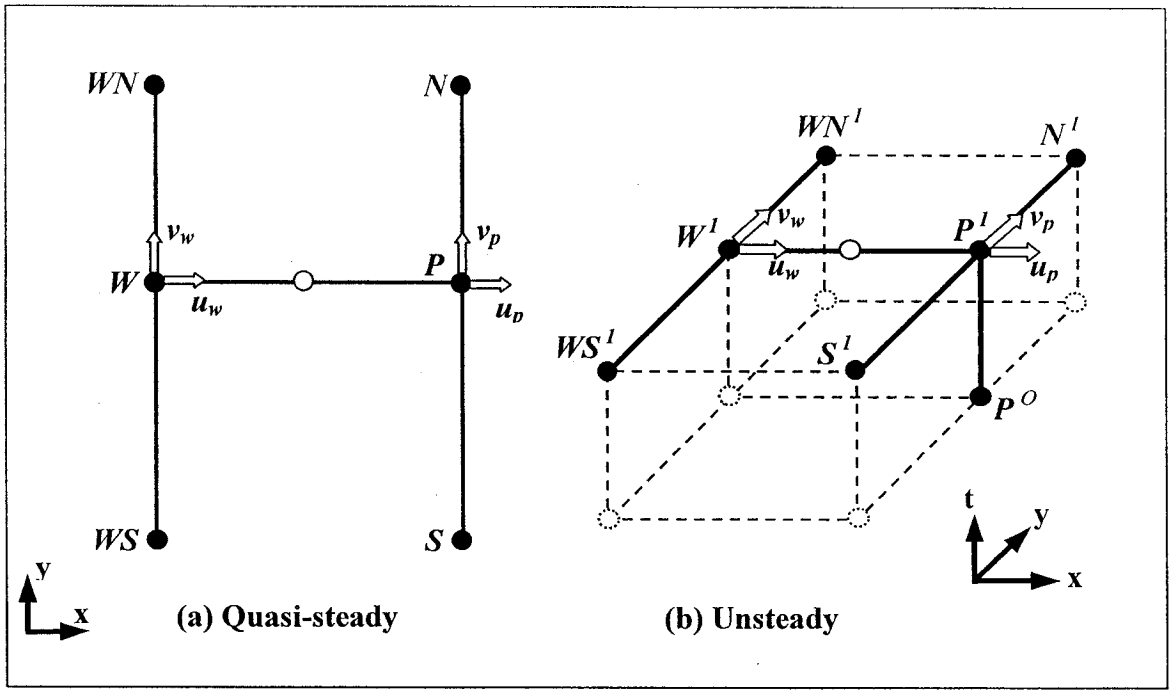

Figure 5-3 Finite difference stencil for convection mass transfer

- for the unsteady convective mass transfer

$$\frac{\theta_P^{\,1}-\theta_P^{\,0}}{\Delta t}\cdot\delta x_w\cdot\Delta y=$$
$$-\frac{1}{2}\cdot(u_W+u_P)\cdot\left(\theta_P^{\,1}-\theta_W^{\,1}\right)\cdot\Delta y-\frac{1}{2}\cdot\left[\frac{v_P}{\phi}\frac{\left(\theta_N^{\,1}-\theta_S^{\,1}\right)}{2}+\frac{v_W}{\phi}\frac{\left(\theta_{WN}^{\,1}-\theta_{WS}^{\,1}\right)}{2}\right]\cdot\delta x_w \quad (5\text{-}42)$$
$$+\frac{1}{2}\cdot\frac{\gamma}{\phi^2\,\mathrm{Re}_L\,Sc}\cdot\left[\left(\frac{\theta_N^{\,1}-\theta_P^{\,1}}{\delta y_n}-\frac{\theta_P^{\,1}-\theta_S^{\,1}}{\delta y_s}\right)+\left(\frac{\theta_{WN}^{\,1}-\theta_W^{\,1}}{\delta y_n}-\frac{\theta_W^{\,1}-\theta_{WS}^{\,1}}{\delta y_s}\right)\right]\cdot\delta x_w$$

where, $\gamma=D_a/D_a=1$ for the convection in the fluid.

Rearranging Eqs. (5-41) and (5-42) into the typical mode of discretization equations gives,

- for the quasi-steady convective mass transfer

$$a_P\cdot\theta_P=a_N\cdot\theta_N+a_S\cdot\theta_S+a_W\cdot\theta_W+a_{WN}\cdot\theta_{WN}+a_{WS}\cdot\theta_{WS} \quad (5\text{-}43)$$

where,
$$a_N=\frac{1}{2}(-F_P+\Gamma_n)\cdot\delta x_w=\frac{1}{2}\left(-\frac{v_P}{2\phi}+\frac{\gamma}{\phi^2\,\mathrm{Re}_L\,Sc\cdot\delta y_n}\right)\cdot\delta x_w;$$

$$a_S=\frac{1}{2}(F_P+\Gamma_s)\cdot\delta x_w=\frac{1}{2}\left(\frac{v_P}{2\phi}+\frac{\gamma}{\phi^2\,\mathrm{Re}_L\,Sc\cdot\delta y_s}\right)\cdot\delta x_w;$$

$$a_{WN}=\frac{1}{2}(-F_W+\Gamma_n)\cdot\delta x_w=\frac{1}{2}\left(-\frac{v_W}{2\phi}+\frac{\gamma}{\phi^2\,\mathrm{Re}_L\,Sc\cdot\delta y_n}\right)\cdot\delta x_w;$$

$$a_{WS}=\frac{1}{2}(F_W+\Gamma_s)\cdot\delta x_w=\frac{1}{2}\left(\frac{v_W}{2\phi}+\frac{\gamma}{\phi^2\,\mathrm{Re}_L\,Sc\cdot\delta y_s}\right)\cdot\delta x_w;$$

$$a_W=\frac{1}{2}\left[(u_P+u_W)\cdot\Delta y-(\Gamma_n+\Gamma_s)\cdot\delta x_w\right]$$

$$a_P=a_N+a_S+a_W+a_{WN}+a_{WS}=\frac{1}{2}\left[(u_P+u_W)\cdot\Delta y+(\Gamma_n+\Gamma_s)\cdot\delta x_w\right]$$

- for the unsteady convective mass transfer

$$a_P \cdot \theta_P{}^1 = a_N \cdot \theta_N{}^1 + a_S \cdot \theta_S{}^1 + a_W \cdot \theta_W{}^1 + a_{WN} \cdot \theta_{WN}{}^1 + a_{WS} \cdot \theta_{WS}{}^1 + a_P{}^0 \cdot \theta_P{}^0 \qquad (5\text{-}44)$$

where,

$$a_N = \frac{1}{2}\left(-F_P + \Gamma_n\right) \cdot \delta x_w;$$

$$a_S = \frac{1}{2}\left(F_P + \Gamma_s\right) \cdot \delta x_w;$$

$$a_{WN} = \frac{1}{2}\left(-F_W + \Gamma_n\right) \cdot \delta x_w;$$

$$a_{WS} = \frac{1}{2}\left(F_W + \Gamma_s\right) \cdot \delta x_w;$$

$$a_W = \frac{1}{2}\left[\left(u_P + u_W\right) \cdot \Delta y - \left(\Gamma_n + \Gamma_s\right) \cdot \delta x_w\right];$$

$$a_P{}^0 = \frac{\Delta y \cdot \delta x_w}{\Delta t};$$

$$a_P = a_P{}^0 + a_N + a_S + a_W + a_{WN} + a_{WS} = \frac{\Delta y \cdot \delta x_w}{\Delta t} + \frac{1}{2}\left[\left(u_P + u_W\right) \cdot \Delta y + \left(\Gamma_n + \Gamma_s\right) \cdot \delta x_w\right]$$

The computational domain for fluid was set as rectangular: from $x = 0$ to $x = L$, and from $y = 0$ to twice of the momentum boundary layer thickness at $x = L$. The momentum boundary layer thickness (δ) at $x = L$ [White, 1991] is

$$\frac{\delta}{L} = \frac{5.0}{\sqrt{\mathrm{Re}_L}} \qquad (5\text{-}45)$$

Applying Eq. (5-45), the upper boundary for the fluid computational domain becomes,

$$y_{\max}{}^+ = \frac{2 \times 5.0}{\phi \cdot \sqrt{\mathrm{Re}_L}} \qquad (5\text{-}46)$$

Since the Schmidt number is generally larger than 1.0 for VOCs, the boundary layer thickness for mass transfer is smaller than that of momentum; hence, the computational domain will be sufficiently larger than the boundary layer thickness.

The boundary conditions of no mass flux at the edges of solid (at $x = 0$, $x = L$) and the bottom of solid (at $y = -b$), can be easily implemented in the finite volume equations – Eq. (5-39) or (5-40) using the half control volume [Patankar, 1980]. The only procedure required is to set the coefficient of the non-existing neighboring point as zero: a_W , a_E, a_S is zero for no flux at $x = 0$, $x = L$, and $y = -b$, respectively.

At the solid-fluid interface, the concentration and the mass flux are continuous as given in Eqs. (5-26) and (5-27). The continuity of the concentration was implemented by locating the control volume face at the interface as shown in Fig. 5-4.

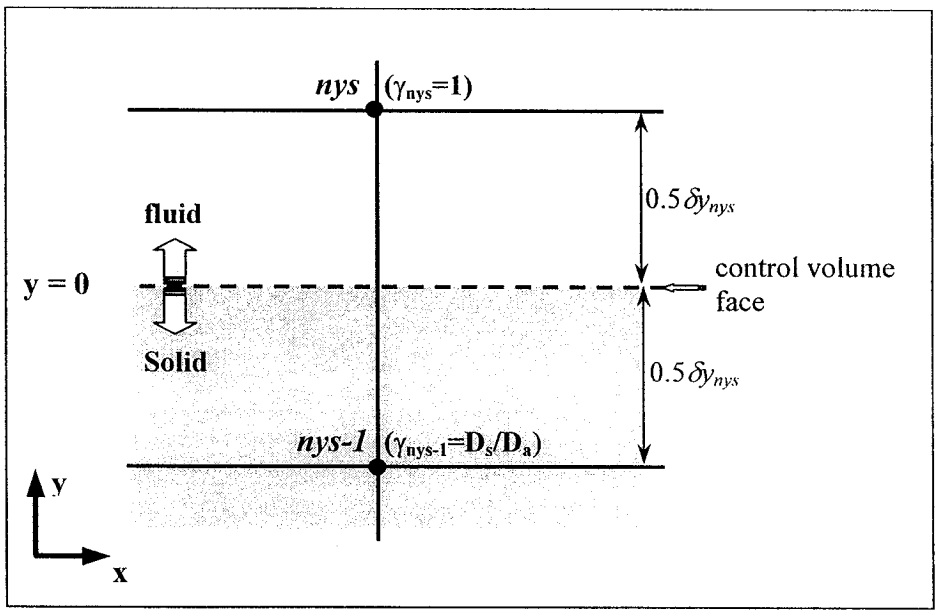

Figure 5-4 Control volume at the solid-air interface

The mass flux continuity was enforced by calculating the interface diffusivity ($\bar{\gamma}$) as the harmonic mean of solid diffusivity and fluid diffusivity [Patankar, 1980],

$$\bar{\gamma} = \frac{2 \cdot \gamma_{nys-1} \cdot \gamma_{nys}}{\gamma_{nys-1} + \gamma_{nys}} \tag{5-47}$$

where, γ_{nys-1} is γ for solid (i.e., D_s/D_a) and γ_{nys} is γ for fluid (i.e., D_a/D_a). Since Eq. (5-47) is derived based on the steady one-dimensional situation, this approach of implicit matching was examined by comparing its numerical results with those obtained from the explicit implementation of the interface conditions. The latter method calculates the separate solutions for the fluid and the solid regions involving an iterative procedure to match the concentration and the flux at the interface.

These two methods were applied in Model 2 – i.e., unsteady two-dimensional convection in fluid coupled with unsteady one-dimensional diffusion in solid with Henry (linear) sorption isotherm. Figure 5-5 presents the non-dimensioinal concentration at the interface, θ_w, in terms of Fourier number for both D_a/D_s =10 and 10^3. The other properties are constant as $Re_L = 10^4$, $Sc = 2.57$, $b/L = 10^{-3}$, and $(\varepsilon+K) = 10^2$. Figure 5-5 confirms that the predictions obtained from the implicit implementation of interface conditions using Eq. (5-47), are as accurate as those obtained from the explicit implementation of these interfacial conditions. The computation time was significantly longer in the explicit matching of the interfacial conditions due to the iterative procedure. The iterative procedure in the explicit matching was terminated when the sum (i.e., along x-direction) of residual in θ_w became less than 10^{-7}.

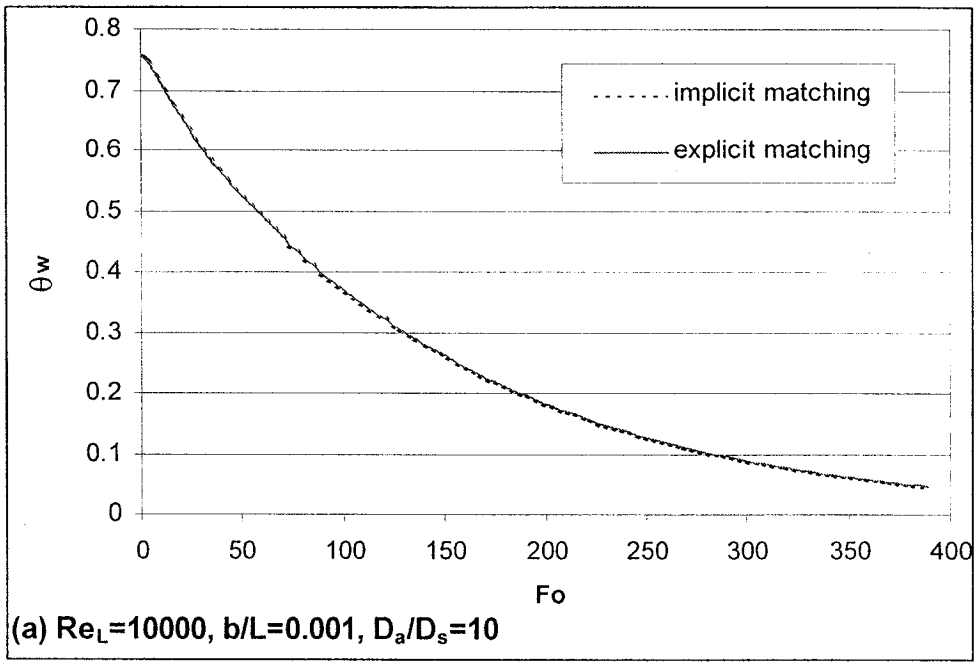

(a) Re_L=10000, b/L=0.001, D_a/D_s=10

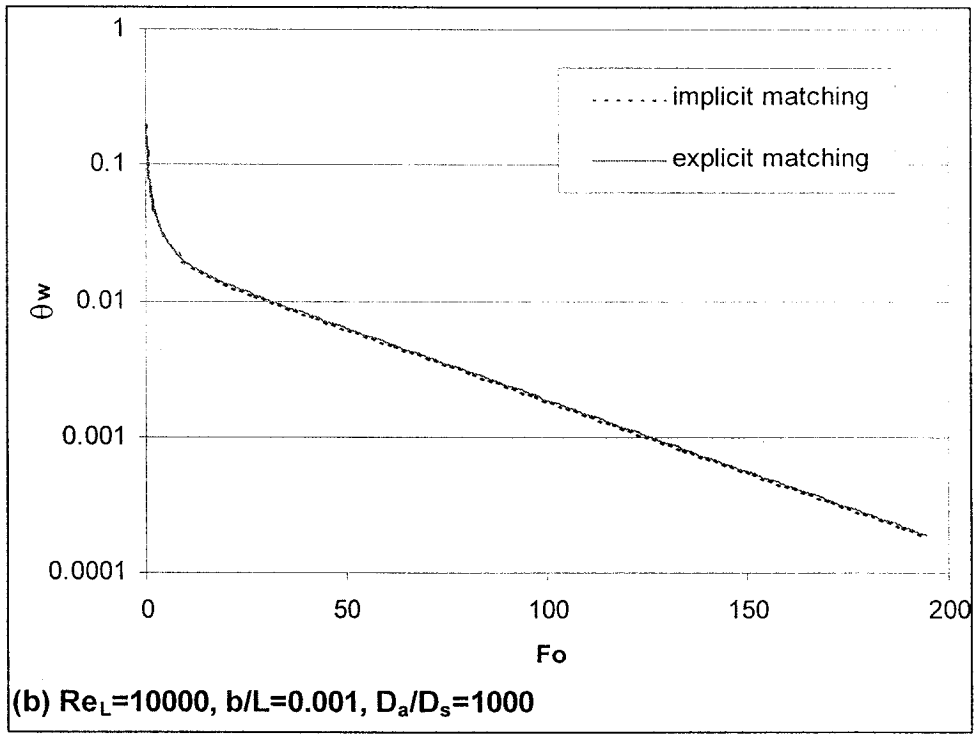

(b) Re_L=10000, b/L=0.001, D_a/D_s=1000

Figure 5-5 Validation of implicit implementation of interface conditions

The discretization equations for Models 1 and 2 can be generalized as

$$a_P \cdot \theta_P = a_N \cdot \theta_N + a_S \cdot \theta_S + a_W \cdot \theta_W + a_{WN} \cdot \theta_{WN} + a_{WS} \cdot \theta_{WS} + a_P^0 \cdot \theta_P^0 \quad (5\text{-}48)$$

The coefficients for convection and diffusion of each model are summarized in Table 5-3.

Table 5-3 Coefficients of discretization equations for Models 1 and 2

Discretization equation $a_P \cdot \theta_P = a_N \cdot \theta_N + a_S \cdot \theta_S + a_W \cdot \theta_W + a_{WN} \cdot \theta_{WN} + a_{WS} \cdot \theta_{WS} + a_P^0 \cdot \theta_P^0$ with $a_P = a_P^0 + a_N + a_S + a_W + a_{WN} + a_{WS}$			
Model no.	**Coefficient**	**Diffusion in solid** ($\gamma = D_s/D_a$)	**Convection in fluid** ($\gamma = D_a/D_a = 1$)
1	a_N	Γ_n	$0.5\delta x_w \cdot (-F_P + \Gamma_n)$
	a_S	Γ_s	$0.5\delta x_w \cdot (F_P + \Gamma_s)$
	a_W	0	$0.5 \cdot [(u_P + u_W) \cdot \Delta y - (\Gamma_n + \Gamma_s) \cdot \delta x_w]$
	a_{WN}	0	$0.5\delta x_w \cdot (-F_W + \Gamma_n)$
	a_{WS}	0	$0.5\delta x_w \cdot (F_W + \Gamma_s)$
	a_P^0	$(\varepsilon + K)\frac{\Delta y}{\Delta t}$	0
2	a_N	Γ_n	$0.5\delta x_w \cdot (-F_P + \Gamma_n)$
	a_S	Γ_s	$0.5\delta x_w \cdot (F_P + \Gamma_s)$
	a_W	0	$0.5 \cdot [(u_P + u_W) \cdot \Delta y - (\Gamma_n + \Gamma_s) \cdot \delta x_w]$
	a_{WN}	0	$0.5\delta x_w \cdot (-F_W + \Gamma_n)$
	a_{WS}	0	$0.5\delta x_w \cdot (F_W + \Gamma_s)$
	a_P^0	$(\varepsilon + K)\frac{\Delta y}{\Delta t}$	$\frac{\Delta y \cdot \delta x_w}{\Delta t}$

The general form of discretization equations for the Models 3 and 4 are,

$$a_P \cdot \theta_P = a_N \cdot \theta_N + a_S \cdot \theta_S + a_E \cdot \theta_E + a_W \cdot \theta_W + a_{WN} \cdot \theta_{WN} + a_{WS} \cdot \theta_{WS} + a_P^0 \cdot \theta_P^0 \quad (5\text{-}49)$$

with the coefficients presented in Table 5-4.

Table 5-4 Coefficients of discretization equations for Models 3 and 4

Discretization equation $a_P \cdot \theta_P = a_N \cdot \theta_N + a_S \cdot \theta_S + a_E \cdot \theta_E + a_W \cdot \theta_W + a_{WN} \cdot \theta_{WN} + a_{WS} \cdot \theta_{WS} + a_P^0 \cdot \theta_P^0$ with $a_P = a_P^0 + a_N + a_S + a_E + a_W + a_{WN} + a_{WS}$			
Model no.	**Coefficient**	**Diffusion in solid** ($\gamma = D_s/D_a$)	**Convection in fluid** ($\gamma = D_a/D_a$)
3	a_N	$\Gamma_n \cdot \Delta x$	$0.5\delta x_w \cdot (-F_P + \Gamma_n)$
	a_S	$\Gamma_s \cdot \Delta x$	$0.5\delta x_w \cdot (F_P + \Gamma_s)$
	a_E	$\Gamma_e \cdot \Delta y$	0
	a_W	$\Gamma_w \cdot \Delta y$	$0.5 \cdot [(u_P + u_W) \cdot \Delta y - (\Gamma_n + \Gamma_s) \cdot \delta x_w]$
	a_{WN}	0	$0.5\delta x_w \cdot (-F_W + \Gamma_n)$
	a_{WS}	0	$0.5\delta x_w \cdot (F_W + \Gamma_s)$
	a_P^0	$(\varepsilon + K)\dfrac{\Delta x \cdot \Delta y}{\Delta t}$	$\dfrac{\Delta y \cdot \delta x_w}{\Delta t}$
4	a_N	$\Gamma_n \cdot \Delta x$	$0.5\delta x_w \cdot (-F_P + \Gamma_n)$
	a_S	$\Gamma_s \cdot \Delta x$	$0.5\delta x_w \cdot (F_P + \Gamma_s)$
	a_E	$\Gamma_e \cdot \Delta y$	0
	a_W	$\Gamma_w \cdot \Delta y$	$0.5 \cdot [(u_P + u_W) \cdot \Delta y - (\Gamma_n + \Gamma_s) \cdot \delta x_w]$
	a_{WN}	0	$0.5\delta x_w \cdot (-F_W + \Gamma_n)$
	a_{WS}	0	$0.5\delta x_w \cdot (F_W + \Gamma_s)$
	a_P^0	$\left(\varepsilon + \alpha K_F \{C_\infty + (C_0 - C_\infty)\theta\}^{\alpha-1}\right) \times \dfrac{\Delta x \cdot \Delta y}{\Delta t}$	$\dfrac{\Delta y \cdot \delta x_w}{\Delta t}$

5.5 COMPUTATIONAL PROCEDURES FOR MASS TRANSFER

The major steps of the computation are:

1. Grid generation and calculation of geometric properties
2. Calculation of u^+ and v^+ at every node in the fluid field by applying the Blasius' solution presented in Section 5.3
3. Calculation of the constant coefficients in the discretization equations
4. Calculation of the variable coefficients – e.g., $(a_P^0 \cdot \theta_P^0)$ in all Models, and a_P in Model 4 - in the discretization equations from the previous time step results
5. Calculation of θ in both solid and fluid fields by solving the resulting matrix of the discretization equations
6. Numerical evaluation of other variables like local and average wall concentrations (θ_w and $(\theta_w)_{ave}$), local and average Sherwood numbers (Sh_x and Sh_L)

The procedures 4 to 6 are repeated until the time (t) reaches the desired termination time (t_{end}).

In this study, a finer grid was used where the concentration gradient is large, i.e., near the leading edge ($x = 0$) and near the interface in both fluid and solid fields ($y = 0^+$ and $y = 0^-$). Since the physical space is rectangular, three orthogonal one-dimensional algebraic transformations (i.e., x-direction in whole field, y-direction in fluid field, and y-direction in solid field) were applied using the following hyperbolic stretching function, which is described in the x-direction,

$$x_i = xl \cdot \frac{\sinh\left(c1 \cdot \frac{i}{N_i}\right)}{\sinh(c1)} \tag{5-50}$$

where, x_i is the x coordinate at the i^{th} node; xl is the total length in x-direction; N_t is the total number of nodes; and $c1$ is the hyperbolic stretching constant. As $c1$ is larger than 1.0, the nodes are more clustered near the leading edge (i.e., $x = 0$). In order to ensure that there is no abrupt change in grid spacing, the ratio between two neighboring grid spaces was limited to the range of 2/3 to 3/2.

In the discretization equation for Models 1 and 2, θ_P depends on θ_N, θ_S, θ_W, θ_{WN} and θ_{WS}, but not on θ_E. In other words, x-coordinate becomes a one-way coordinate and only y-coordinate is a two-way coordinate, which can be solved by a marching procedure along x-direction [Patanka, 1980]. The Thomas algorithm can directly solve a tridiagonal matrix formed in y-coordinates at each station along the x-direction, i.e., line-by-line method.

In Models 3 and 4, θ_P depends on θ_E only in solid field. Hence, x-coordinate in fluid field is a one-way coordinate, but x-coordinate in solid field and y-coordinate in whole field are two-way coordinates. ADI (Alternating-Direction Implicit) scheme was applied to solve the discretization equations of Models 3 and 4. The line-by-line iteration with the Thomas algorithm was used for the marching solution procedure. The x-sweep was applied in whole field since y-coordinate is two-way coordinates in whole domain. The y-sweep, however, was limited only to the solid domain because x-coordinate in fluid domain is one-way. The sweeping was repeated until the maximum residual in the computational domain becomes less than 10^{-15}.

From the solution of discretization equation, which is θ at every node in the computational domain, other variables like wall concentration and Sherwood number were numerically evaluated. The local wall concentration (θ_w) was calculated using the flux continuity at the interface, Eq. (5-27).

$$\theta_w = \frac{\theta_{nys} + \frac{D_s}{D_a}\theta_{nys-1}}{\left(1+\frac{D_s}{D_a}\right)} \tag{5-51}$$

The average wall concentration, $(\theta_w)_{ave}$ was obtained as

$$(\theta_w)_{ave} = \int_0^1 \theta_w \cdot dx^+ = \sum_{i=1}^{nx} (\theta_w)_i \cdot \Delta x_i \tag{5-52}$$

where, *nx* is the last node in *x*-direction.

The local mass flux (q_w) at the interface is,

$$q_w = h_D(C_w - C_\infty) = -D_a \frac{\partial C}{\partial y}\bigg)_{y=0^+} \tag{5-53}$$

Nondimensionalizing $\partial C/\partial y$ term in Eq. (5-53) with the same manner given in Eq. (5-19) results in

$$\frac{h_D}{D_a} = -\frac{\partial \theta}{\partial y^+}\bigg)_{y^+=0^+} \cdot \frac{1}{(\theta_w \cdot b)} \tag{5-54}$$

Hence, the local Sherwood number (Sh_x) can be computed as

$$Sh_x = \frac{h_D \cdot x}{D_a} = -\frac{\partial \theta}{\partial y^+}\bigg)_{y^+=0^+} \cdot \left(\frac{x^+}{\theta_w \cdot \phi}\right) = \left(\frac{\theta_w - \theta_{nys}}{0.5\delta y_{nys}}\right) \cdot \left(\frac{x^+}{\theta_w \cdot \phi}\right) \tag{5-55}$$

The average mass transfer coefficient, $(h_D)_{ave}$ was obtained in the following manner,

$$(h_D)_{ave} = \frac{(q_w)_{ave}}{(C_w - C_\infty)_{ave}} = \frac{\dfrac{\int_0^L \left(-D_a \dfrac{\partial C}{\partial y}\right)_{y=0^+} dx}{\int_0^L dx}}{\dfrac{\int_0^L (C_w - C_\infty) dx}{\int_0^L dx}} \tag{5-56}$$

where, the subscript '*ave*' refers the averaged value along the x-direction. Nondimesionalizing Eq. (5-56) gives,

$$(h_D)_{ave} = \frac{\dfrac{D_a}{b} \cdot \int_0^1 \left(-\dfrac{\partial \theta}{\partial y^+}\right)_{y^+=0^+} dx^+}{\int_0^1 \theta_w dx^+} \tag{5-57}$$

The averaged Sherwood number is then computed by substituting Eq. (5-57) as follows,

$$Sh_L = \frac{(h_D)_{ave} \cdot L}{D_a} = \frac{\sum_{i=1}^{nx} \left(\dfrac{(\theta_w - \theta_{nys})_i}{0.5\delta y_{nys}} \cdot \Delta x_i \right)}{\phi \cdot (\theta_w)_{ave}} \tag{5-58}$$

5.6 TESTING OF THE DEVELOPED CODES

The developed codes were tested at various levels. At first, the codes for diffusion in solid and for convection in fluid were tested separately. The numerical results of the code for the unsteady two-dimensional diffusion in solid were compared with the exact analytical solution obtained by the integral transform method [Özisik, 1980]. The considered initial and boundary conditions are at $t = 0$, θ=1.0 in whole solid; at $x = 0$ and L, $\theta = 0.5$; at upper surface of solid ($y = 0$), $\theta = 0$; and at lower surface ($y = -b$), there is

no mass flux. With a uniform grid of 201×41 nodes for b/L = 0.2 and $\Delta t_d^+ = 10^{-3}$, the average error is 1.81×10^{-3} at Fo = 0.05 and it decreases as time progresses, i.e., 9.98×10^{-4} at Fo = 5.0. The error was calculated as the absolute value of the difference between the numerical solution and analytical solution.

The Blasius solution for the steady laminar boundary layer flow that was presented in Section 5.3, can be applied for the steady convective mass transfer when the mass diffusivity is the same as the momentum diffusivity, i.e., the Schmidt number, Sc =1 [Welty et al., 1976]. The numerical solution of steady convection, Eq. (5-43) for the case of Sc = 1 and $Re_L = 10^4$ were compared with the Blasius solution and the average error was in the ranges of 10^{-3} to 10^{-5} depending on the selection of grid. For a given 1001×51 grids with the hyperbolic stretching function constant, $c1$ in Eq. (5-50), 1.0 for the x-direction and 2.15 for the y-direction, the maximum error is 2.86×10^{-2} and the average error is 7.27×10^{-4}. Also, the steady state results obtained from the unsteady convective mass transfer code also confirms the same errors compared with the Blasius solution.

The steady state solutions of unsteady conjugate mass transfer, where unsteady two-dimensional convection coupled with unsteady one-dimensional diffusion in solid, were compared with the steady conjugate heat transfer solution by Yu et al. (1991) through a heat-mass transfer analogy. Yu et al. (1991) presented expressions for the interfacial temperature and the local Nusselt number for steady conjugate heat transfer problems of forced convection in a laminar boundary layer coupled with one-dimensional heat conduction in solid whose temperature at the lower surface is kept as a constant. They

considered the Prandtl number from 10^{-3} to infinity for four cases of geometry: flat plate, wedge, stagnation flow, and rotating cone. Numerical solutions were obtained for the cases of flat plate and wedges using the Keller Box method, and exact solutions obtained for stagnation flow and rotating cone. They reported that the presented Nusselt number correlations for flat plate have less than 1.4% error.

Heat-mass transfer analogy was applied to the solutions by Yu et al. (1991) assuming that (1) the physical properties are constant; (2) there is no viscous dissipation; (3) the mass transfer does not affect the velocity profile [Welty et al., 1976]. This was carried out as a preliminary study to investigate the effect of air velocity (or Reynolds number) on VOC emissions from solid materials and the details are presented in Lee et al. (2000).

Figure 5-6 presents the comparisons of the results obtained from the unsteady conjugate mass transfer code with the steady state solution obtained through heat-mass analogy from the solution by Yu et al. (1991) for the case of $Re_L = 10^4$, $Sc = 1$, $b/L = 10^{-2}$, $D_a/D_s=10$, and $(\varepsilon+K) = 1$. Because the analogous solution from conjugate heat transfer cannot consider the sorption in solid, $(\varepsilon+K)$ was set as 1. With the zero initial concentration in solid and a constant concentration at the lower surface of solid (C_b), the dimensionless wall concentration, θ_w, which is defined as $(C_w-C_\infty)/(C_b-C_\infty)$, increases as time progresses. When the Fourier number is 7, it reaches the steady state and the maximum error compared with the analogous solution by Yu et al. (1991) is 4.79×10^{-3}.

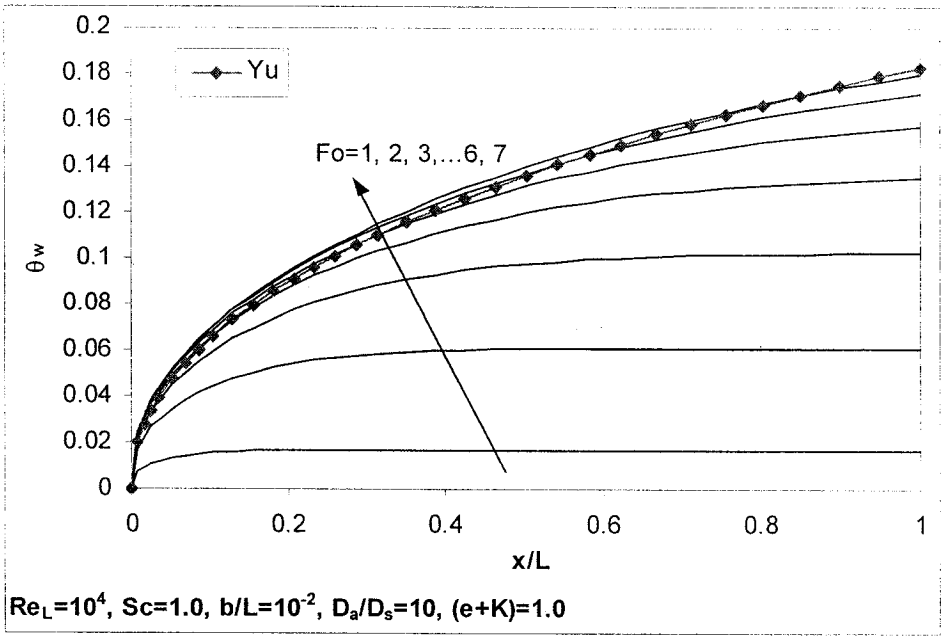

Figure 5-6 Unsteady conjugate mass transfer results vs. solution by Yu et al. (1991)

Table 5-5 Testing of unsteady conjugate mass transfer code

Re_L	b/L	Constant for hyperbolic stretching			Maximum error	Average error
		cI_x	cI_y in fluid	cI_y in solid		
10^4	10^{-3}	4.3	7.0	2.0	4.54×10^{-3}	3.23×10^{-3}
	10^{-2}	2.5	5.2	3.5	1.05×10^{-3}	6.00×10^{-4}
	10^{-1}	1.5	4.5	5.8	9.18×10^{-5}	6.33×10^{-5}
10^2	10^{-3}	6.9	9.2	1.5	1.65×10^{-2}	2.69×10^{-3}
	10^{-2}	4.3	7.0	2.0	4.54×10^{-3}	3.23×10^{-3}
	10^{-1}	2.5	5.2	3.5	1.05×10^{-3}	6.00×10^{-4}

The developed code was further tested for a wider range of independent parameters. Table 5-5 presents the comparison results with 501×150 (100 nodes in fluid and 50 nodes in solid) nodes for D_a/D_S=10 and Sc=2.57. Since the maximum and the average errors decrease as D_a/D_S increases, only the case of minimum D_a/D_S (i.e., 10) is presented in Table 5-5. The constants for the hyperbolic stretching functions were determined by trial-and-error and the combination that results in the minimum error was chosen.

5.7 SUMMARY

Four numerical conjugate mass transfer models were developed relaxing one or more assumptions made in developing the analytical model presented in Chapter 3. These assumptions are: constant wall concentration, quasi-steady convection mass transfer, one-dimensional diffusion in solid, and linear sorption isotherm. Since the momentum transfer and mass transfer are decoupled, the continuity and the momentum boundary layer equations were solved first using the Blasius' similarity solution. Inputting the obtained velocity distribution, the mass transfer of coupled convection-diffusion in the fluid and diffusion in the solid was solved by the control volume based finite difference method applying the Euler implicit scheme for time; the Crank-Nicholson method for the x-direction marching in fluid; and the central difference scheme for the y-direction in both fluid and solid, and the x-direction in solid. The discretization equations were solved by the line-by-line method for the models with one-dimensional diffusion in solid (Models 1 and 2), and by the ADI (Alternating-Direction Implicit) scheme for the models with two-dimensional diffusion in solid (Models 3 and 4). The developed numerical models were validated by comparing the predicted results with the exact analytical solutions and/or numerical solutions available in literature.

In the following chapter, the numerical models developed and validated in this chapter are used to solve the conjugate mass transfer problem and to assess the analytical model developed in the previous chapter.

Chapter 6

Numerical Simulation of the Conjugate Mass Transfer Problem

6.1 INTRODUCTION

The limits of the proposed analytical model presented in Chapter 3, will be assessed in this chapter using the four numerical models of conjugate mass transfer presented in Chapter 5. The numerical computations were carried out for various ranges of the independent variables: Re_L, D_a/D_s, and b/L. Since momentum and mass transfer are affected by convection in the fluid region, two values of Reynolds number, $Re_L = 10^2$ and 10^4, were considered and one value for the Schmidt number (Sc=2.57) was used since Sc varies very slightly from one VOC to another, as explained in Chapter 4.

Among the solid material properties, $(\varepsilon+K)$ for Models 1, 2, and 3 were set as constant since the parametric study results (see Chapter 4) show that the effect of $(\varepsilon+K)$ is linear. The parameters for Freundlich sorption isotherm that were used in Model 4, were obtained from the sorption experimental data by Tiffonnet et al. (2002), which are presented in Chapter 2. For the other material properties, a combination of three values were considered, i.e., D_a/D_s= 10, 10^2, and 10^3; and b/L=10^{-3}, 10^{-2}, and 10^{-1}.

In conjugate heat transfer, the Brun number is often used as a conjugation criterion [Luikov, 1974, Mosaad, 1999]. The local Brun number is defined for the flat plate:

$$Br_x = \frac{k_f}{k_s} \cdot \frac{b}{x} \cdot \mathrm{Re}_x^{1/2} \cdot \mathrm{Pr}^{1/3} \tag{6-1}$$

where, k_f and k_s are the thermal conductivity of fluid and solid, respectively [W/(m·K)], and Pr is the Prandtl number. Br_x is the ratio of the thermal resistance of the plate to that of laminar boundary layer over the length x. Luikov (1974) suggested that for Br_x less than 0.1, the problem can be solved by the traditional convective heat transfer problem without taking into account the thermal resistance of the plate, and he estimated the error to be less than 5%. The average Brun number for the flat plate is defined as follows

$$Br_L = \frac{k_f}{k_s} \cdot \frac{b}{L} \cdot \mathrm{Re}_L^{1/2} \cdot \mathrm{Pr}^{1/3} \tag{6-2}$$

The analogous forms for the local and the averaged Brun numbers for the conjugate mass transfer would be,

Local:
$$Br_x^* = \frac{D_a}{D_s} \cdot \frac{b}{x} \cdot \mathrm{Re}_x^{1/2} \cdot Sc^{1/3} \tag{6-3}$$

Average:
$$Br_L^* = \frac{D_a}{D_s} \cdot \frac{b}{L} \cdot \mathrm{Re}_L^{1/2} \cdot Sc^{1/3} \tag{6-4}$$

The averaged Brun number for conjugate mass transfer, Br_L^*, is similar to the Biot number (Bi), which is given in Eq. (4-3). The only difference is the constant, i.e., the constant is 1.0 for Br_L^* whilst 0.664 for Bi. For the combinations of considered independent variables, Bi varies from 9.1×10^{-2} to 9.1×10^{3}. To be consistent with the results presented in Chapter 4, the effects of independent variables will be presented in

terms of the Biot number. For local values, however, the local Brun number, Br_x^*, will be used.

In unsteady conjugate mass transfer problems, two different characteristic time scales are in effect: the convection characteristic time, t_c defined as L/u_∞ (Eq. (5-19)), and the diffusion characteristic time, t_d defined as b/D_s^2 (Eq. (3-15)). The ratio of these two values can be an important dimensionless parameter to describe the unsteadiness in conjugate mass transfer. In this study, the ratio of diffusion to convection characteristic time, τ, was adopted.

$$\tau = \frac{t_d}{t_c} = \frac{b^2/D_s}{L/u_\infty} = \mathrm{Re}_L\, Sc \cdot \left(\frac{D_a}{D_s}\right) \cdot \left(\frac{b}{L}\right)^2 \tag{6-5}$$

Table 6-1 presents all considered cases in numerical computation, and their Biot number and τ. When there are several cases of τ for the same Biot number, each case was denoted as *a, b, c* in ascending order for increasing values of τ.

The computational domain is affected by Re_L and b/L as shown in Eq. (5-45); hence, only these parameters (not D_a/D_s) can affect the grid generation. The same grid system that was used in testing the conjugate mass transfer as presented in Table 5-5, was applied in the present calculations. For each grid system, the grid spaces in the *y*-direction satisfy the local Peclet number limitation, i.e., $-2 \le Pe \le 2$, which is imposed by adopting the central difference scheme in *y*-direction in the fluid region. Figure 6-1 presents an example of the generated grids for both cases of $Re_L=10^4$ with $b/L=10^{-2}$ and $Re_L=10^2$ with

$b/L=10^{-1}$. It clearly shows the clustering of nodes near the leading edge and near the solid-air interface.

The time step Δt is set such that the time and space errors are of the same size. Note that, since the Euler implicit scheme is used in time discretization, there is no stability limitation on the size of time step Δt. For every case considered, several tests with different time steps were carried out.

Table 6-1 Considered ranges of parameters

Re_L	b/L	D_d/D_s	Bi	τ	Denote
10^2	10^{-3}	10	9.0952×10^{-2}	2.57×10^{-3}	$Bi = 0.091$
		10^2	9.0952×10^{-1}	2.57×10^{-2}	$Bi = 0.91a$
		10^3	9.0952	2.57×10^{-1}	Bi = 9.1a
	10^{-2}	10	9.0952×10^{-1}	2.57×10^{-1}	$Bi = 0.91b$
		10^2	9.0952	2.57	$Bi = 9.1b$
		10^3	9.0952×10	2.57×10	$Bi = 91a$
	10^{-1}	10	9.0952	2.57×10	$Bi = 9.1c$
		10^2	9.0952×10	2.57×10^2	$Bi = 91b$
		10^3	9.0952×10^2	2.57×10^3	$Bi = 910a$
10^4	10^{-3}	10	9.0952×10^{-1}	2.57×10^{-1}	$Bi = 0.91b$
		10^2	9.0952	2.57	$Bi = 9.1b$
		10^3	9.0952×10	2.57×10	$Bi = 91a$
	10^{-2}	10	9.0952	2.57×10	$Bi = 9.1c$
		10^2	9.0952×10	2.57×10^2	$Bi = 91b$
		10^3	9.0952×10^2	2.57×10^3	$Bi = 910a$
	10^{-1}	10	9.0952×10	2.57×10^3	$Bi = 91c$
		10^2	9.0952×10^2	2.57×10^4	$Bi = 910b$
		10^3	9.0952×10^3	2.57×10^5	Bi =9100

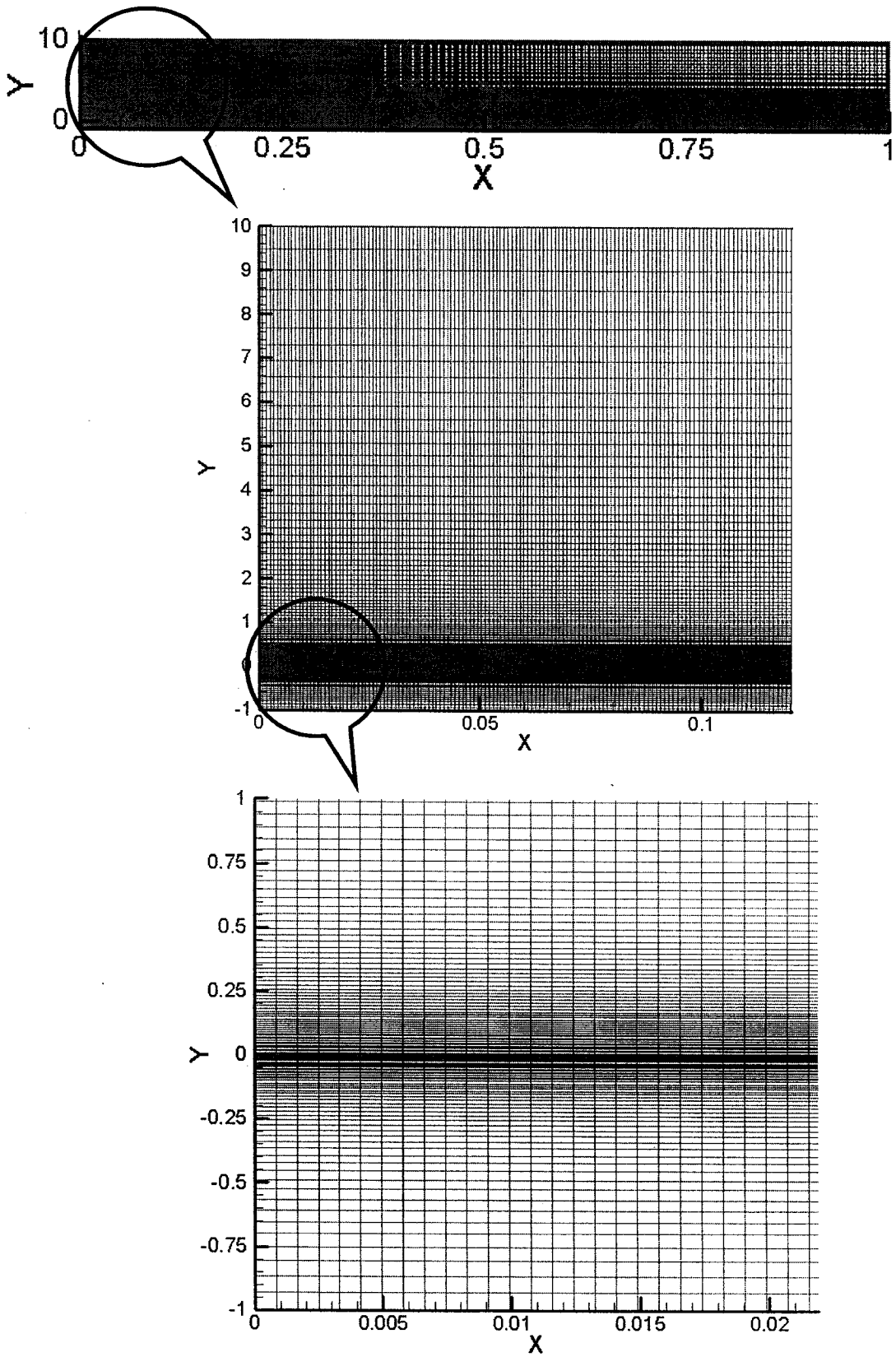

Figure 6-1 Grid for the case of $Re_L=10^4$, $b/L=0.01$ or $Re_L=10^2$, $b/L=0.1$

For instance, the convection time step sizes in the range of $0.01 \leq \Delta t_c^+ \leq 500$ were used for the case of $Re_L=10^4$, $b/L=10^{-2}$, and $D_\alpha/D_s=10$. Figure 6-2 presents the computation results of different Δt_c^+ for both quasi-steady and unsteady mass convection in the fluid coupled with unsteady one-dimensional diffusion in the solid, i.e., Models 1 and 2. The computation was carried out until the total mass transfer time, t_{total}. t_{total} of this case is 5735 in terms of t_c^+, which is equivalent to a Fourier number $Fo = 223$.

Figure 6-2 (a) presents results of the quasi-steady convection case (Model 1), which shows the average θ_w versus Fourier number profile for $\Delta t_c^+ =0.01$ matches that obtained by the analytical model presented in Chapter 3. As the time step increases, larger errors are observed. However, the errors even for large time steps are limited to the first several time steps, more explicitly the errors become less than 10^{-2} at the 8^{th} time step for all of the time steps. After that, the profiles obtained for all time step cases follow that of the analytical model or that corresponding to $\Delta t_c^+ =0.01$. Similar results are observed for the unsteady convection case (Model 2) as shown in Fig. 6-2 (b). Hence, larger time step can be used for long-term source/sink behavior without substantial sacrifice in accuracy. This result is somewhat similar to those when the Euler implicit method applied for the asymptotic solution of steady equilibrium problems and mixed equilibrium/propagation problems. The Euler implicit method is a recommended method for such problems since it can attain an asymptotic solution in a few steps [Hoffman, 1992]. Figure 6-3 presents the temporal variation of the error (defined as the absolute difference between profiles of the chosen time steps, $\Delta t_c^+=0.5$ and 0.01) for the case of $Re_L=10^4$, $b/L=10^{-2}$, and $D_\alpha/D_s=10$.

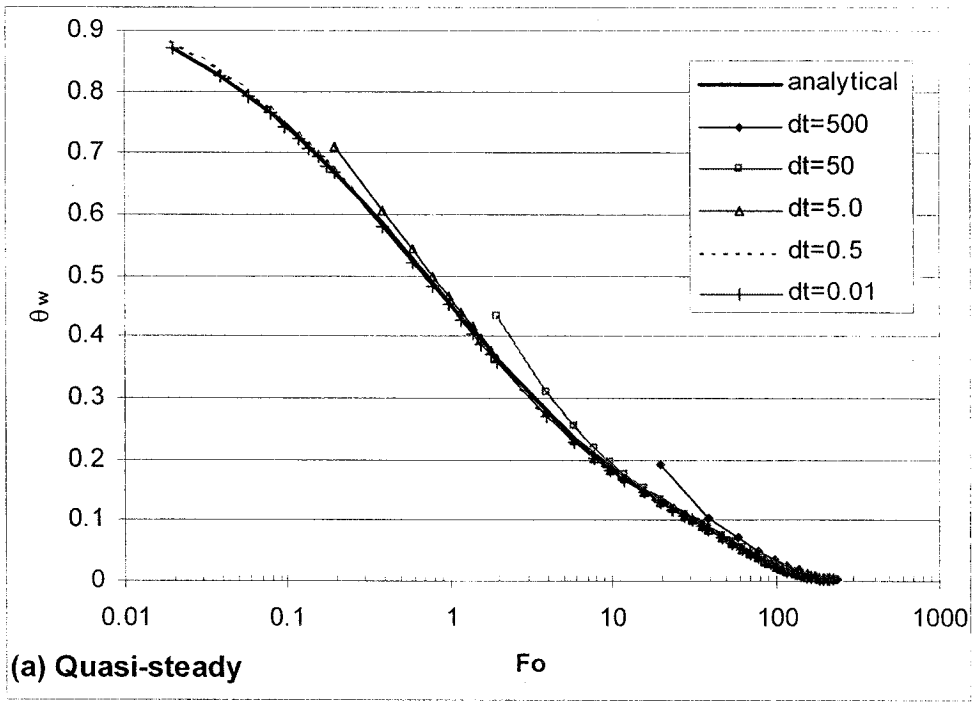

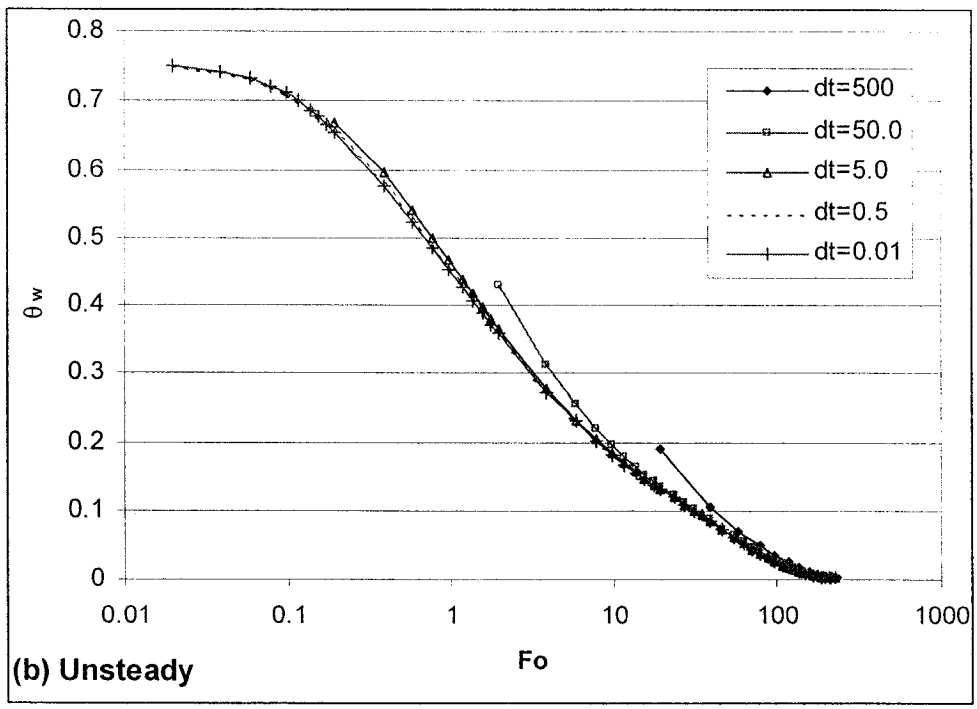

Figure 6-2 Testing of time steps

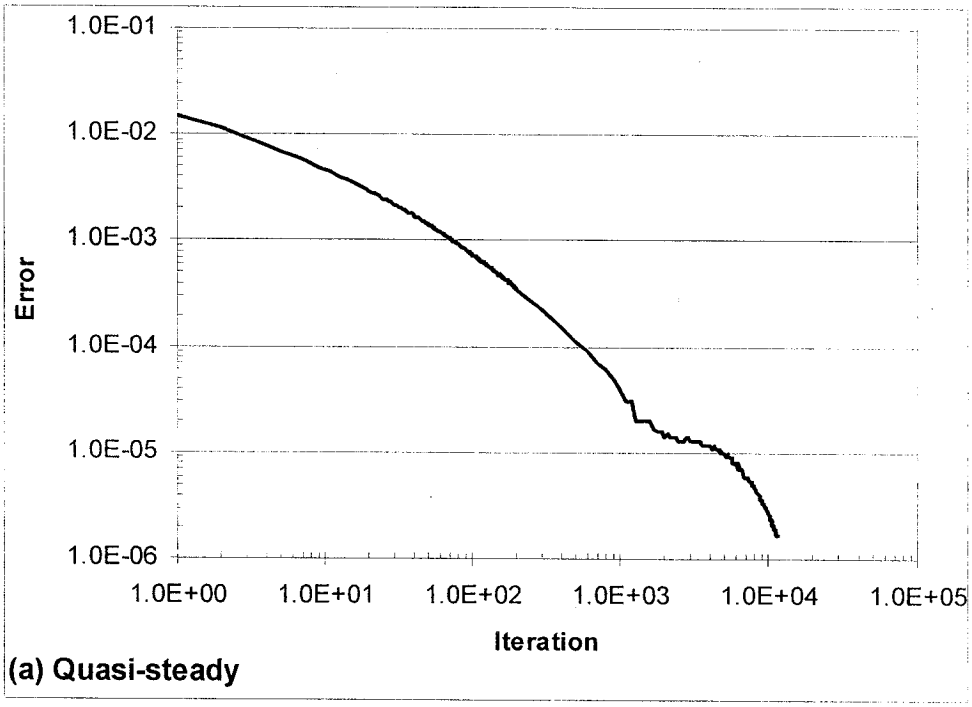

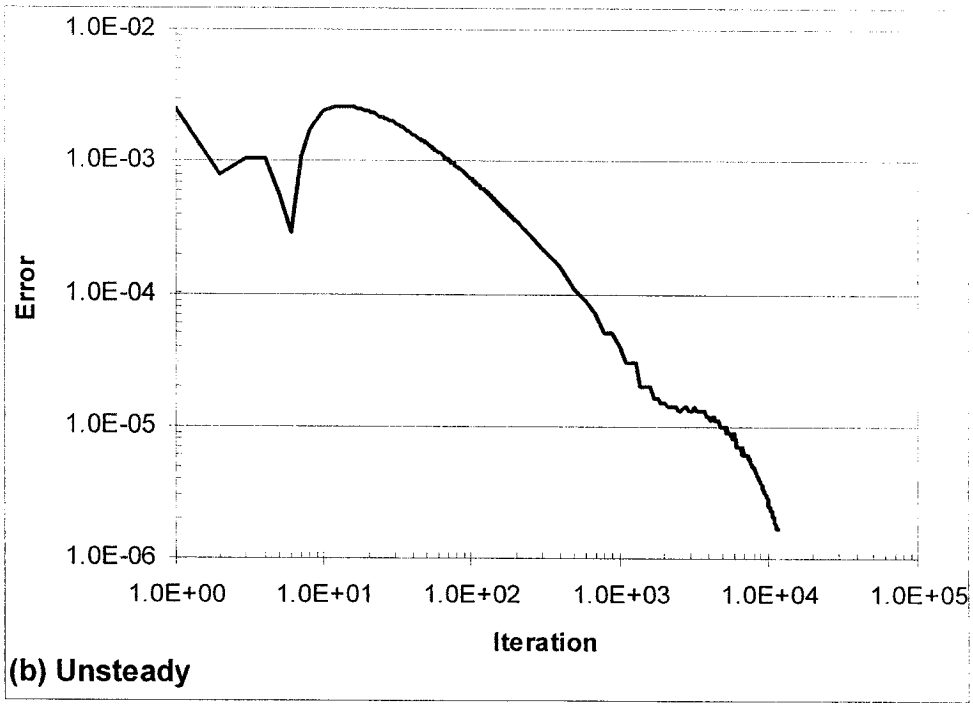

Figure 6-3 Error profiles of case Δt_c^+=0.5

The four major assumptions made in the analytical modeling, i.e., constant wall concentration, quasi-steady convective mass transfer, one-dimensional diffusion in solid, and linear sorption isotherm, will now be evaluated one by one in the given range assigned to independent variables. The numerical results will be presented in the following sections in terms of the dependant variables: the nondimensional concentration at the interface (θ_w), and the local and the averaged Sherwood numbers (Sh_x and Sh_L).

6.2 CONSTANT WALL CONCENTRATION

The proposed analytical model that was presented in Chapter 3, adopts the traditional convection mass transfer approach with an assumption of constant concentrations over the entire fluid-solid interface. In order to investigate the validity of the constant wall concentration assumption, a numerical model of conjugate mass transfer that couples the quasi-steady convective mass transfer in a two-dimensional laminar boundary layer with the unsteady one-dimensional diffusion in the solid with the linear sorption isotherm, was developed. The results obtained from the numerical model are compared with those obtained from the proposed analytical solution.

Figure 6-4 (a) shows the distribution of the nondimensional concentration at the solid-fluid interface, $\theta_w(x)$, along the plate when the Fourier number (Fo) is one. $\theta_w(x)$ increases in the downstream direction and more significant changes are observed near the leading edge, i.e., $x = 0$, because mass transfer takes place strongly near the leading edge and decreases downstream as the boundary layer thickens. $\theta_w(x)$ of all cases in Table 6-1 are presented in Fig. 6-4, and it shows that $\theta_w(x)$ profile along x-direction is identical

only if the Biot number (Bi) is the same regardless of τ. Since the quasi-steady convection mass transfer is considered in Model 1, the convection characteristic time does not affect the mass transfer process. Only diffusion characteristic time (t_d), hence Fo that is the time (t) normalized by t_d, is in effect. $\theta_w(x)$ decreases as Bi increases or in other words, the diffusion resistance gets larger than the convection resistance.

The local Sherwood number, Sh_x, which was obtained using Eq. (5-55), was normalized by that of laminar forced convection over a flat plate with constant wall concentration, whose Sherwood number ($Sh_{x,cw}$) correlation is as follows [Welty et al., 1976]:

$$Sh_{x,cw} = 0.332 \cdot \mathrm{Re}_x^{\frac{1}{2}} \cdot Sc^{\frac{1}{3}} \qquad (6\text{-}6)$$

In conjugate mass transfer problems, Sh_x can be affected by the boundary layer thickness and $\theta_w(x)$, while $Sh_{x,cw}$ in Eq. (6-6) is affected solely by the boundary layer thickness. The ratio of Sh_x to $Sh_{x,cw}$ (expressed as $\mathrm{Sh_x^+}$) is a good measure of the isolated effect of varying wall concentration on Sh_x. Figure 6-4 (b) shows the profiles of Sh_x^+ along the plate for various Bi at Fo =1, i.e. at a given instant of time. Sh_x^+ decreases in the downstream direction with an abrupt change near the leading edge, i.e., $x/L \leq 0.1$, because of the abrupt change of $\theta_w(x)$ in that region. Sh_x^+ is larger at larger Bi, since it is inversely proportional to $\theta_w(x)$ as given in Eq. (5-55). When Bi is larger than 91, Sh_x^+ profiles are almost identical: major changes are observed very near the leading edge and Sh_x^+ is almost constant after that. Sh_x^+ varies between 0.9 and 1.48 depending on Bi. This indicates that the local Sherwood number of conjugate mass transfer can be significantly different from that of conventional convection mass transfer with constant wall concentrations.

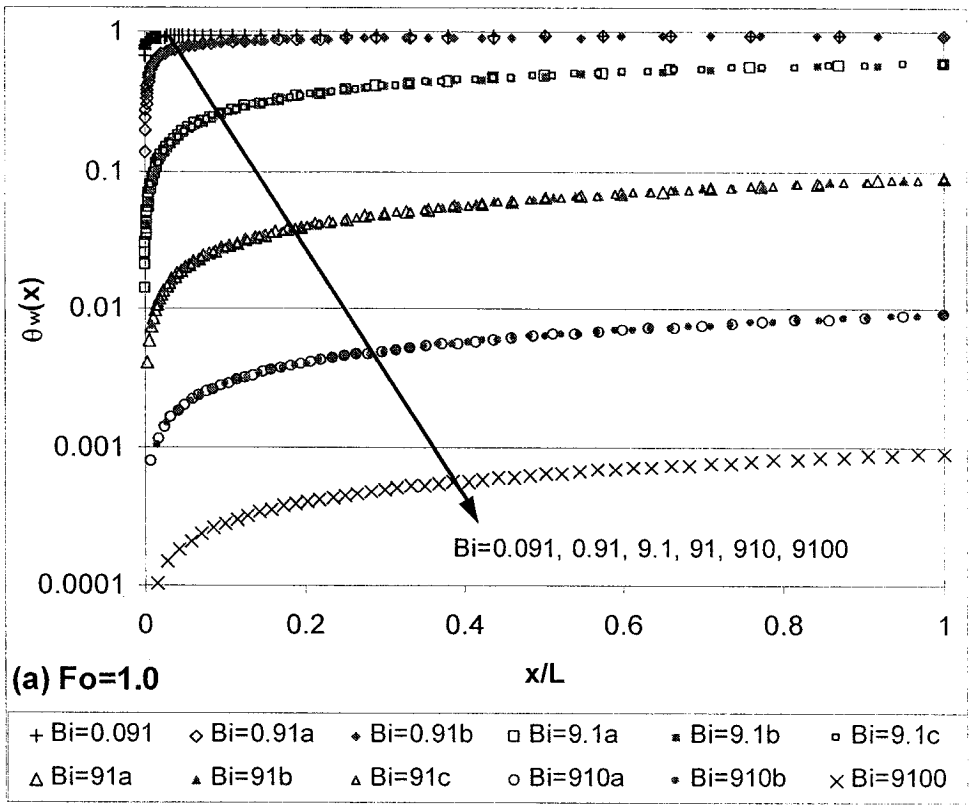

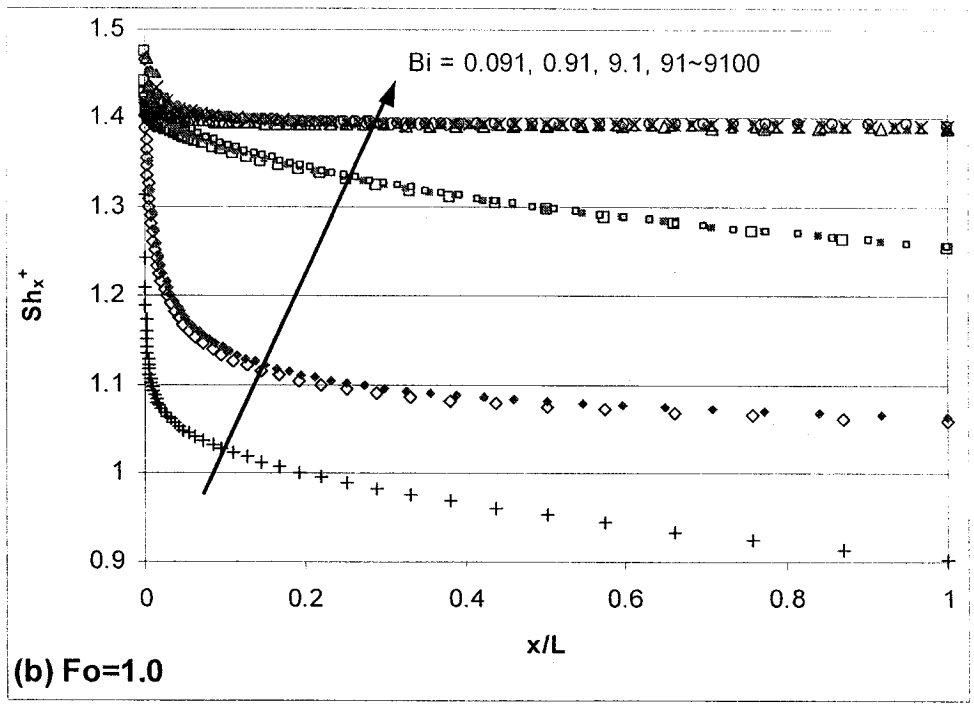

Figure 6-4 Model 1: $\theta_w(x)$ and Sh_x^+ distributions along the plate at Fo=1

Previous studies on the conjugate heat transfer problem [Luikov, 1974; Yu et al., 1991; Mosaad, 1999], i.e., forced convection in the steady laminar boundary layer coupled with steady one-dimensional conduction in solid of which temperature is kept constant at the bottom surface (T_b), indicated that conjugate heat transfer can be regarded as a hybrid system of the ordinary convection problem with the boundary condition of constant wall temperature and that of constant heat flux. When the conduction resistance of the plate is much smaller than convection resistance, i.e., Brun number is small, the temperature at the solid-fluid interface approaches T_b. This case is equivalent to the ordinary boundary condition of constant wall temperature. When the plate resistance is much greater than the fluid resistance, i.e., large Brun number, the temperature drop across the boundary layer is negligible compared with that across the plate; hence, it becomes comparable to the ordinary convection problem with the boundary condition of constant wall heat flux.

Similar behavior is observed in Fig. 6-4 (b). For small Biot number cases (diffusion resistance is smaller than that of convection), Sh_x^+ a little away from the leading edge is around 1.0. Hence, the conjugate mass transfer of those cases is close to the ordinary convection mass transfer of constant wall concentration of which Sherwood number correlation is given in Eq. (6-6). For larger Biot number cases i.e., Bi=91 or larger, Sh_x^+ a little away from the leading edge is almost constant as about less than 1.4. This indicates that large Bi cases approach the ordinary convection mass transfer with a constant wall mass flux of which Sherwood number ($Sh_{x,cf}$) correlation [Kays and Crawford, 1980] is,

$$Sh_{x,cf} = 0.453 \cdot \mathrm{Re}_x^{\frac{1}{2}} \cdot Sc^{\frac{1}{3}} \qquad (6\text{-}7)$$

The constant of Eq. (6-7) is 1.36 times larger than that of Eq. (6-6).

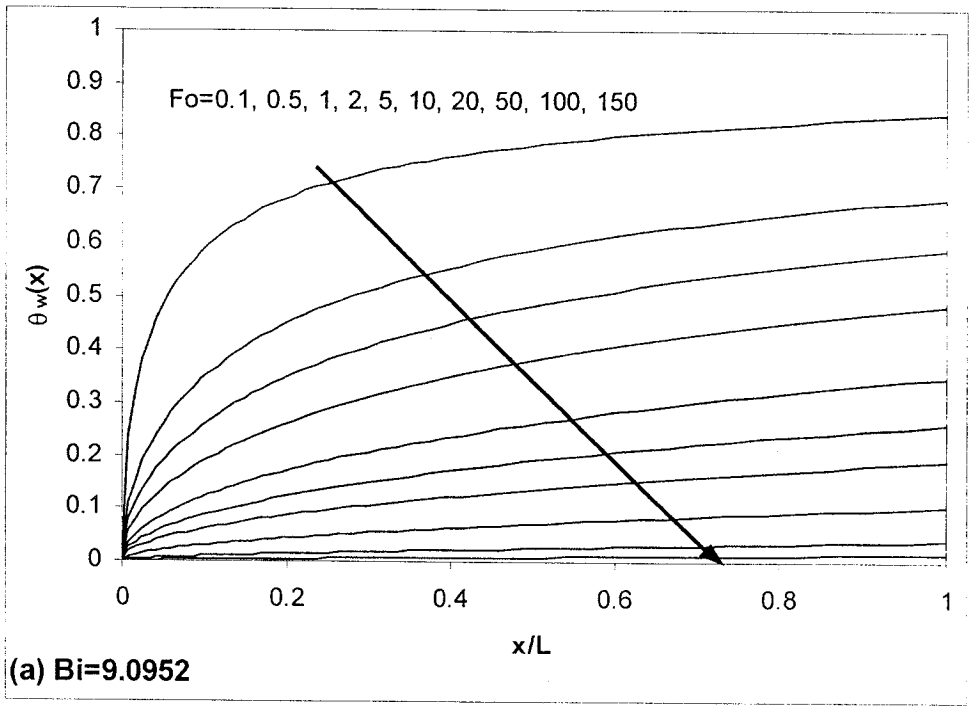

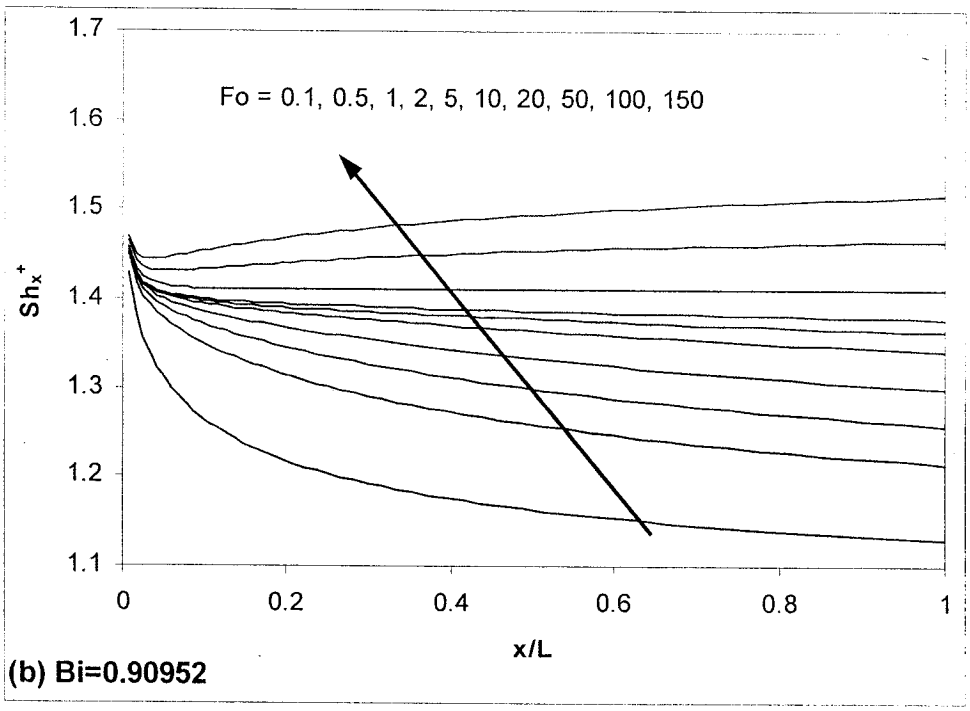

Figure 6-5 Model 1: Effect of Fourier number on $\theta_w(x)$ and Sh_x^+ for Bi=9.1

Figure 6-5 presents the effect of Fourier number on $\theta_w(x)$ and Sh_x^+ distributions over x for Bi = 9.1. As Fo increases or time progresses, $\theta_w(x)$ decreases since more and more mass is carried away (for source behavior). This results in the increase of Sh_x^+ with Fo. When Fo is larger than 50, Sh_x^+ decreases near the leading edge and then gradually increases along the down stream. When Fo=100, almost 90% of the initial total mass is already transferred, and the remaining mass to be transferred is least near the leading edge due to higher mass transfer rate there. This may cause more reduction in the concentration gradient in the y-direction relative to the increase of $\theta_w(x)$ in the downstream direction; hence, Sh_x^+ increases in the downstream direction at large Fo.

The dependence of $\theta_w(x)$ on the local Brun number (Br_x*) given by Eq. (6-3) in the range of Fo = 0.1 to 150, is presented in Fig. 6-6. As Br_x* goes to 0, $\theta_w(x)$ reaches to 1.0. Little

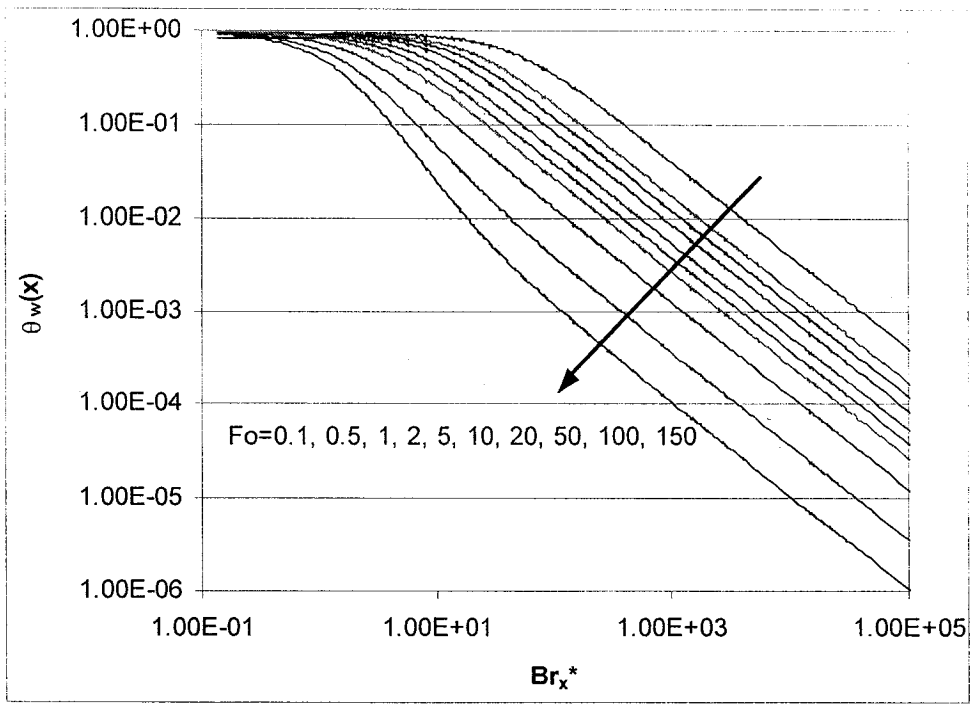

Figure 6-6 Model 1: Dependence of $\theta_w(x)$ on Br_x* for various Fo

decrease of $\theta_w(x)$ is observed till certain limit of Br_x^*. This limit decreases with increasing Fo, i.e., $Br_x^* \approx 20$ for Fo=0.1, $Br_x^* \approx 10$ for Fo=1, and $Br_x^* \approx 1$ for Fo=50. After these limits, $\theta_w(x)$ decreases significantly as Br_x^* increases.

Figure 6-7(a) presents the averaged dimensionless wall concentration of the plate, $(\theta_w)_{ave}$, as a function of Fo. $(\theta_w)_{ave}$ obtained by Model 1. This is compared with θ_w obtained by the analytical model in Chapter 3, and these two results agree very well for the considered range of Bi. Even though the proposed analytical model cannot account for the varying wall concentration along the plate, its prediction for θ_w can be regarded as the averaged wall concentration. In small Biot number, i.e., Bi = 0.091 or 0.91, $(\theta_w)_{ave}$ decreases gradually for Fo= 0 to 180, but for larger Bi cases, $(\theta_w)_{ave}$ decreases abruptly during Fo = 0 to 10.

The averaged Sherwood number (Sh_L) is normalized in the same manner as Sh_x^+. This averaged Sherwood number ratio, Sh_L^+ can be regarded as the averaged mass flux ratio. The dependence of Sh_L^+ on the Fourier number is presented in Fig. 6-7 (b) for different Biot numbers. Although Model 1 and the analytical model shows good agreement in $(\theta_w)_{ave}$, Sh_L of Model 1 is 0.6 to 7% larger than that of analytical model for Fo between 0.1 and 180. Considering the computation of Sh_L in Eq. (5-58), the difference may originate from the dependence of $(\theta_w)_{ave}$ on time unlike Sh_L given by Eq. (2-23), which assumes constant wall concentration regardless of time and space (x); and from the varying concentration gradient in the y-direction at the wall (y = 0) along the time and space (x) given by Model 1. The dependence of Sh_L^+ on Fo is significantly affected by Bi

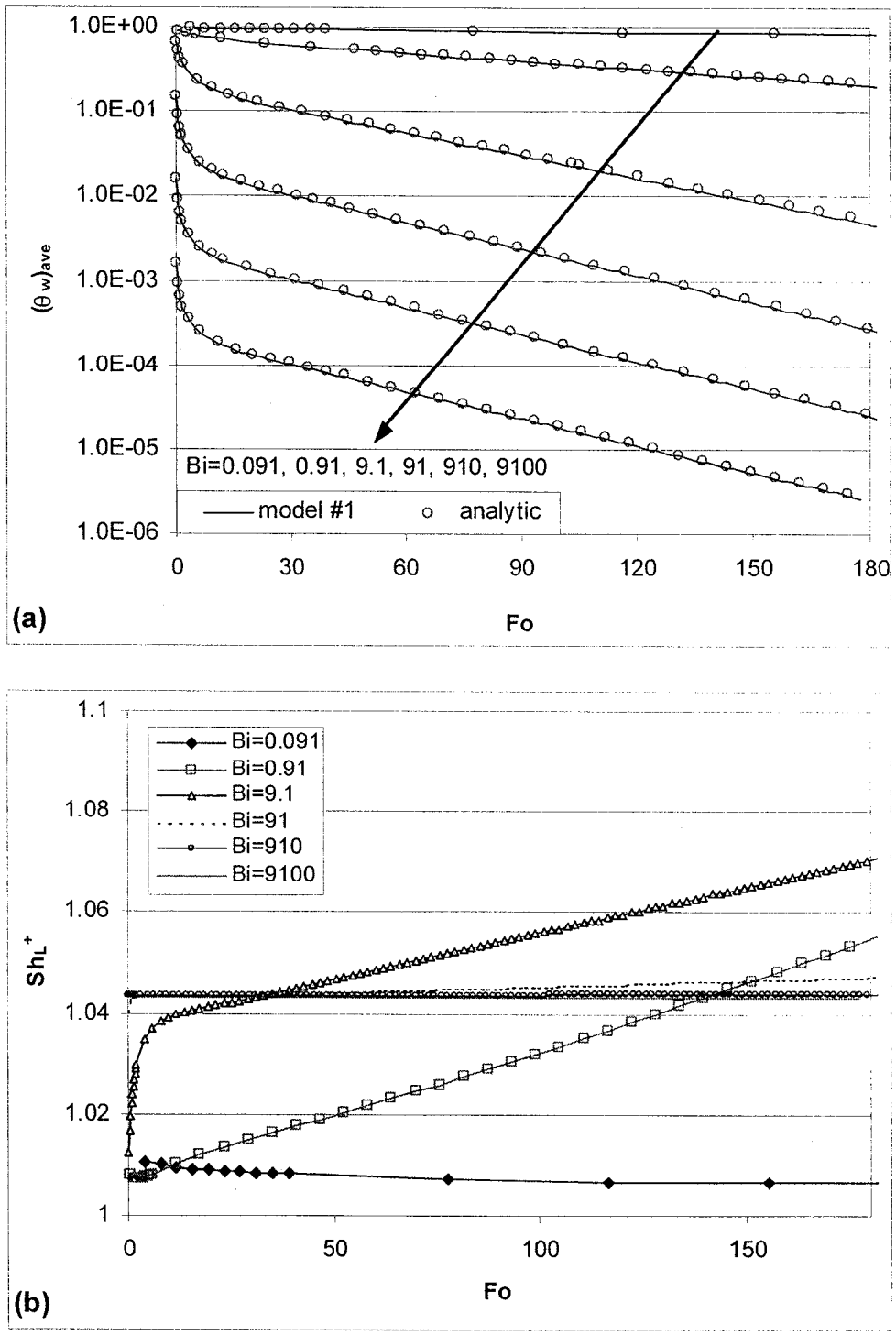

Figure 6-7 Model 1: Dependence of $(\theta_w)_{ave}$ and Sh_L^+ on Fo

and hardly exhibits any general trend. For Bi=91 or larger, Sh_L^+ shows minor dependence on Bi and Fo.

Luikov (1974) suggested that the local Nusselt number (Nu_x) correlation for steady conjugate heat transfer for laminar forced convection over a flat plate would take the following form,

$$Nu_x = 0.332 \cdot \mathrm{Re}_x^{\frac{1}{2}} \cdot \mathrm{Pr}^{\frac{1}{3}} \cdot f(Br_x) \tag{6-8}$$

Adopting this, the local Sherwood number, Sh_x, for conjugate mass transfer of laminar forced flow over a flat plate, will be proportional to $Re_x^{1/2}Sc^{1/3}$,

$$Sh_x \propto \mathrm{Re}_x^{\frac{1}{2}} \cdot Sc^{\frac{1}{3}} \tag{6-9}$$

Since unsteady diffusion in the solid was considered, the proportionality constant depends on Fourier number as well as Brun number for mass transfer or Biot number. Numerical results indicated that their effects are nonlinear and complex except for the cases of Bi = 91 or larger. For those cases, Sh_x correlation was obtained with R^2=0.9999 as follows (Fig. 6-8),

$$Sh_x = 0.4634 \cdot \mathrm{Re}_x^{\frac{1}{2}} \cdot Sc^{\frac{1}{3}} \tag{6-10}$$

The correlation constant is about 40% larger than that of constant wall concentration case in Eq. (6-6), i.e., 0.332. As previously explained, if the diffusion resistance is much greater than that of convection, the conjugate mass transfer approaches the ordinary convection problem with constant wall mass flux. The constant in Eq. (6-10), however, is slightly larger than that in Eq. (6-7), which may be caused by the truly unsteady nature of the considered conjugate mass transfer problem.

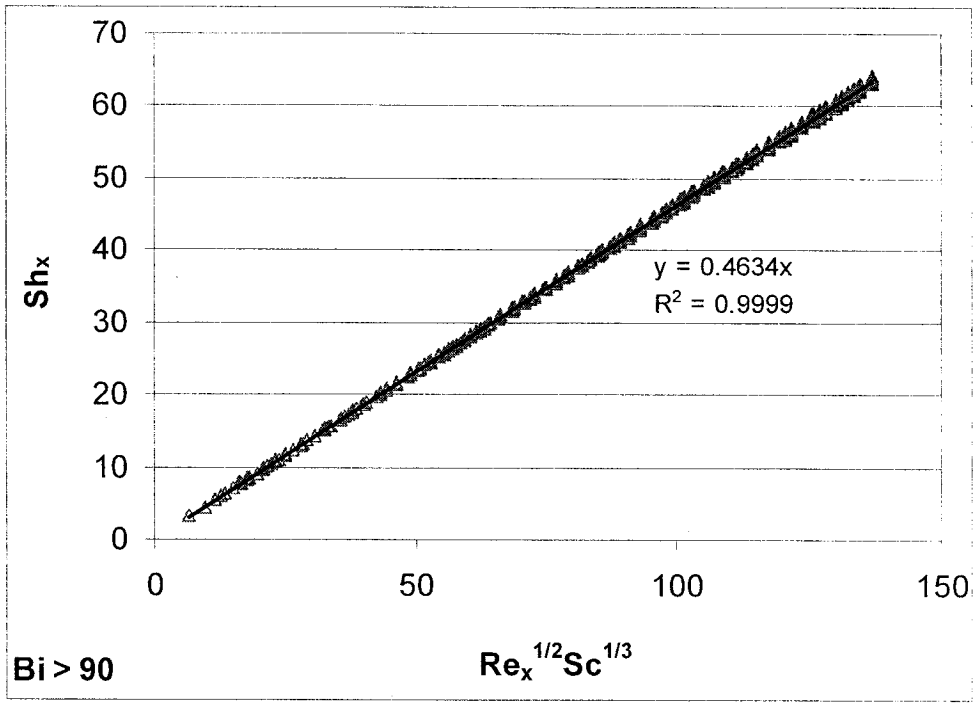

Figure 6-8 Model 1: Sh_x versus ($Re_x^{1/2} Sc^{1/3}$) for *Bi* larger than 90

In overall, the assumption of constant wall concentration, which simplifies predicting the interface concentration, θ_w, by the analytical model, corresponds to the averaged value of $\theta_w(x)$ obtained by the conjugate mass transfer given by Model 1. This assumption, however, results in 0.6 to 7% underestimation of the averaged Sherwood number, Sh_L, or the averaged mass flux for Bi = 0.091 to 9100 until Fo=180. For large Bi cases, the dependence of Sh_L on Fo or Bi becomes minor, and it approaches the ordinary convection problem with boundary condition of constant mass flux.

6.3 QUASI-STEADY CONVECTION MASS TRANSFER IN FLUID

The proposed analytical model in Chapter 3 as well as other mass transfer models with the third-kind boundary condition for convection [Huang and Haghighat, 2002, Blondeau

et al., 2000], assumes quasi-steady convection mass transfer noting that the time scale for the diffusion in solid is generally longer than that for convection. The validity of this assumption was numerically investigated by comparing the predictions of the conjugate mass transfer Model 2, which assumes unsteady mass convection mass transfer, with those by Model 1, which assumes quasi-steady one. The results of Model 1 were presented in the previous section (Section 6-2). Other than convection mass transfer, both models are the same, i.e., one-dimensional diffusion in the solid with linear sorption isotherm. Initially, $\theta = 0$ in the fluid field and $\theta = 1$ in the solid field.

Figure 6-9 presents $\theta_w(x)$ and Sh_x^+ profiles along the plate at $Fo=1$ for all considered cases given in Table 6-1. The results indicate that these profiles are not dependent solely on Bi unlike the results of Model 1 that are presented in Fig. 6-4. For the cases of $Bi = 91$ or larger, $\theta_w(x)$ and Sh_x^+ distributions are akin to those of Model 1. As presented in Table 6-1, τ values for $Bi=91$ or larger cases range from 25.7 to 2.57×10^5. In other words, the diffusion time scale is much longer than that of convection; hence, the quasi-steady assumption holds, and Models 1 and 2 give similar results. For smaller Bi cases, the convection time scale becomes compatible or smaller than that of diffusion, and the predictions of Models 1 and 2 become quite different. $\theta_w(x)$ of $Bi = 0.91$a and $Bi = 9.1$a, are relatively lower than other cases of the same Bi but larger τ.

Figure 6-9 (b) shows that for cases of $Bi = 9.1$ or less, Sh_x^+ profiles of the same Bi are different if τ is different. For cases with $\tau = 25.7$ or larger, Sh_x^+ always decreases downstream like the results of Model 1 in Fig. 6-4. For $\tau = 2.57$ or less, Sh_x^+ decreases

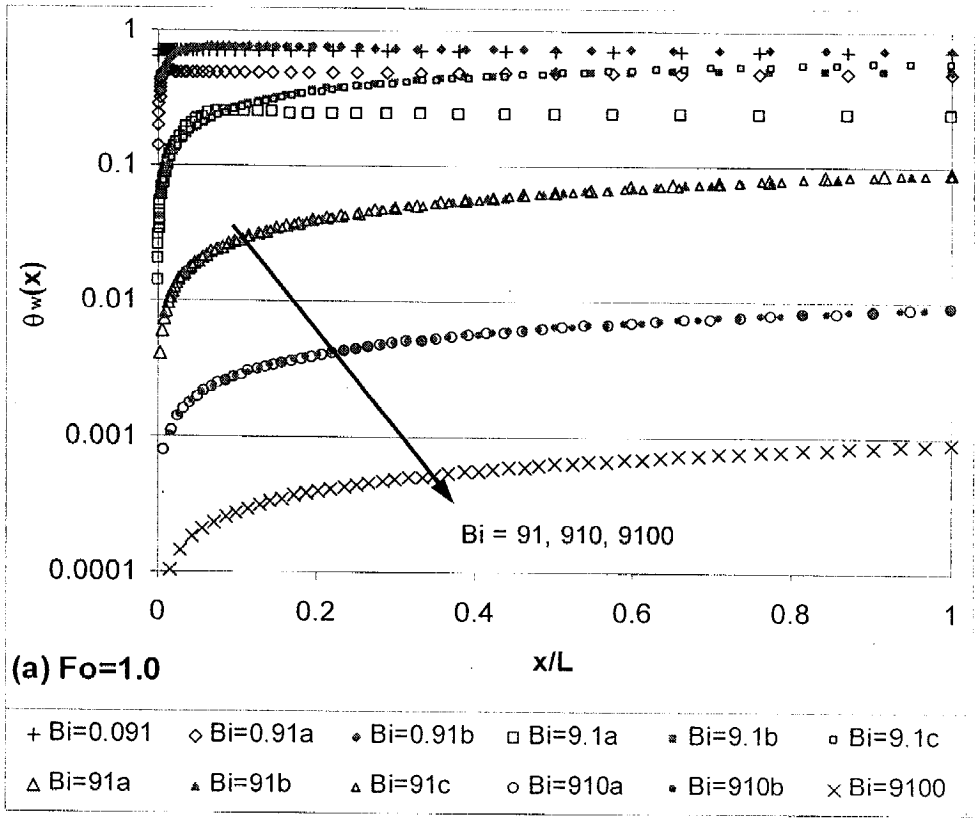

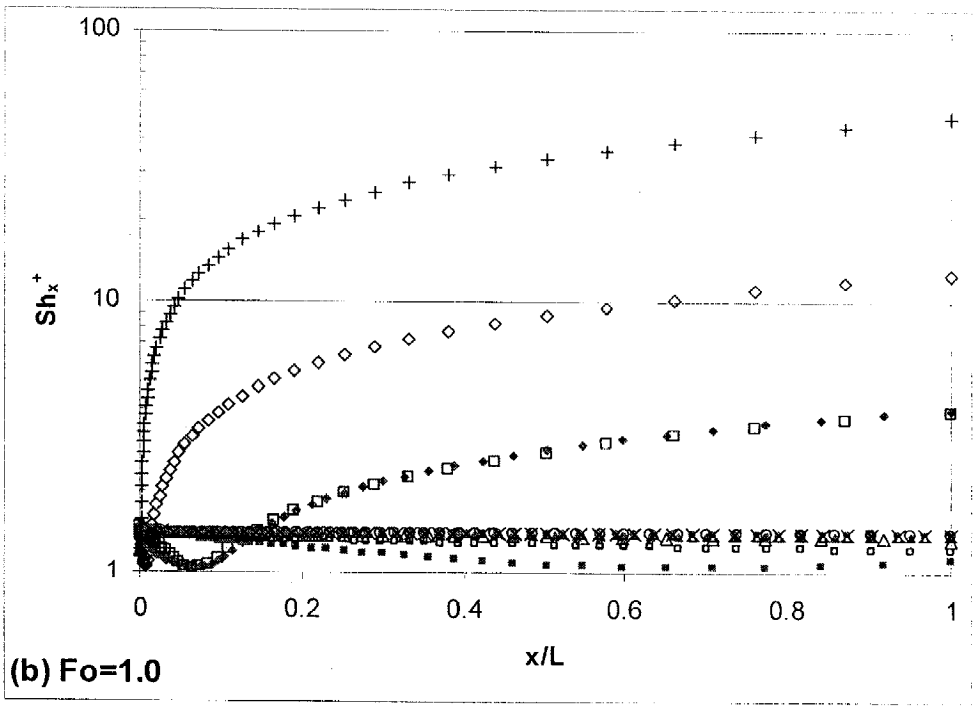

Figure 6-9 Model 2: $\theta_w(x)$ and Sh_x^+ along the plate for all cases

near the leading edge, but begin to increase downstream. The decreasing portion of Sh_x^+ is longer for larger τ. For $\tau = 2.57\times10^{-2}$ or less, Sh_x^+ begin to increase almost right at the leading edge; at about $x/L = 0.07$ for $\tau = 0.257$; and at about $x/L = 0.7$ for $\tau = 2.57$. Even though Fo is constant as 1 for all cases, the convection time (t_c^+), which corresponds to τ (since Fo equals to 1), varies significantly. If t_c^+ is less than 1, the air blowing from the leading edge, does not even reach the end of the plate, i.e., $x = L$. For example, when t_c^+ equals to 0.257, the air from leading edge travels only up to x/L=0.257 and the rest part is in direct contact without any resistance due to convection mass transfer. This would cause an increase in the mass transfer rate, or the Sherwood number.

$\theta_w(x)$ and Sh_x^+ distributions along the plate length for various Fo are presented in Fig. 6-10 for $Bi = 9.1$ and $\tau = 2.57$, and in Fig. 6-11 for $Bi = 9.1$ and $\tau = 25.7$. Those profiles corresponding to different τ values are clearly distinct. Also they are different from the profiles of the quasi-steady convection model (Model 1), which are shown in Fig. 6-5. For $\tau = 2.57$, $\theta_w(x)$ is smaller than that of Model 1 for $Fo = 1$ or less. Sh_x^+ profiles for $\tau = 2.57$ clearly shows the building up of boundary layer with time especially in the early transfer phase. When the boundary layer is not well developed, it shows high mass transfer rates due to the absence of boundary layer resistance. For $\tau = 25.7$, $\theta_w(x)$ and Sh_x^+ profiles become closer to those of Model 1: noticeable difference is observed only at $Fo = 0.1$. Although the same range of Fo is considered in both cases, t_c^+ differs by the factor of 10, implying that as far as mass convection is concerned, the case of $\tau = 25.7$ behaves more like a quasi-steady convection while the other is unsteady.

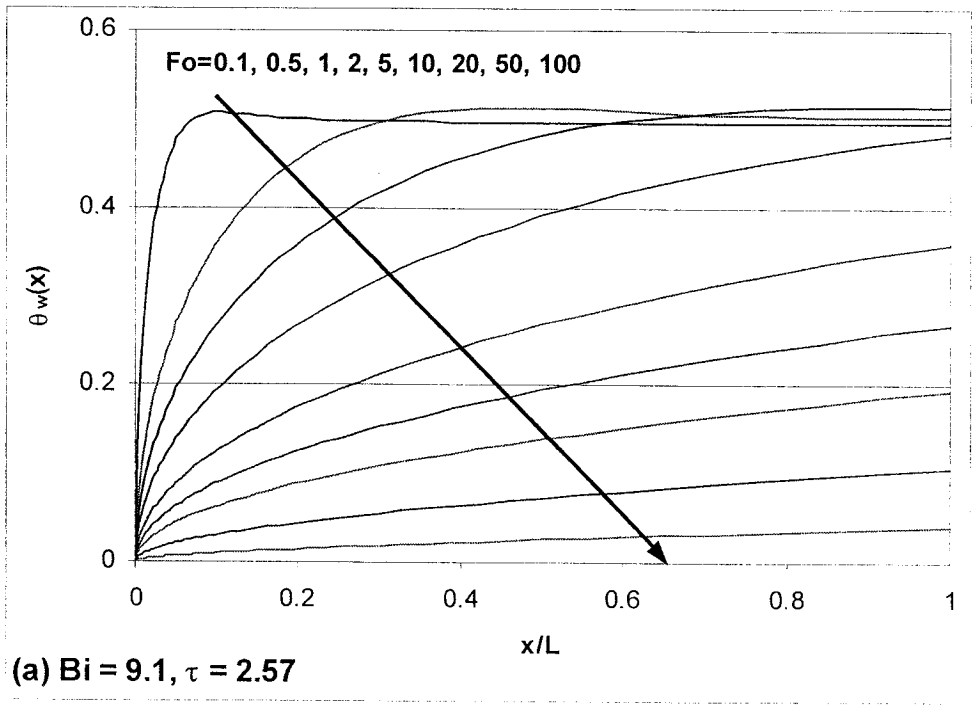

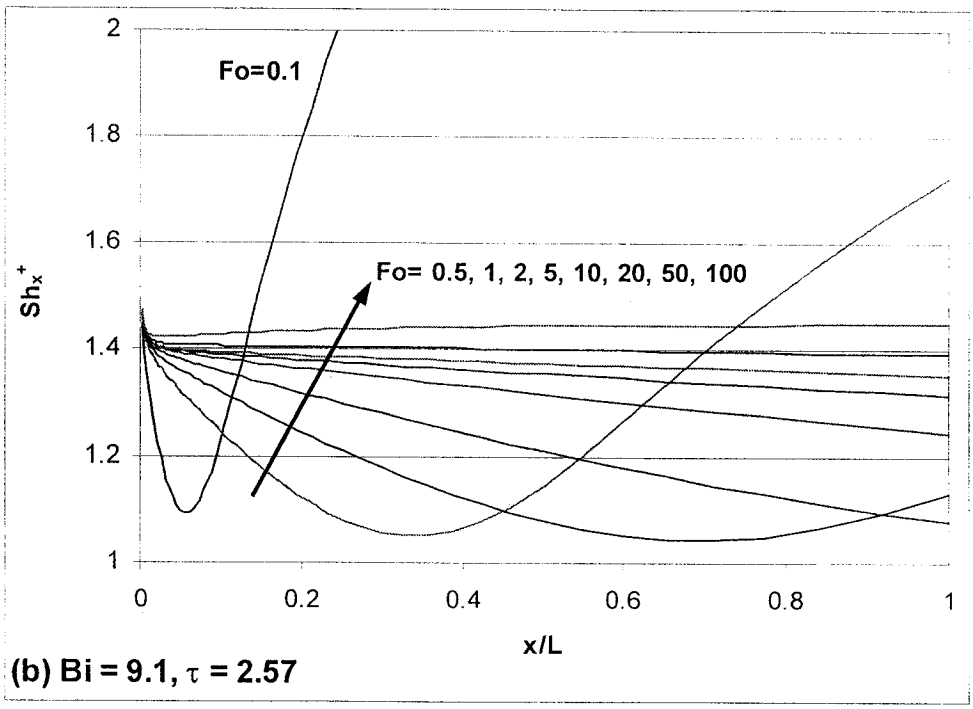

Figure 6-10 Model 2: $\theta_w(x)$ and Sh_x^+ along plate with different Fo for Bi=9.1, τ=2.57

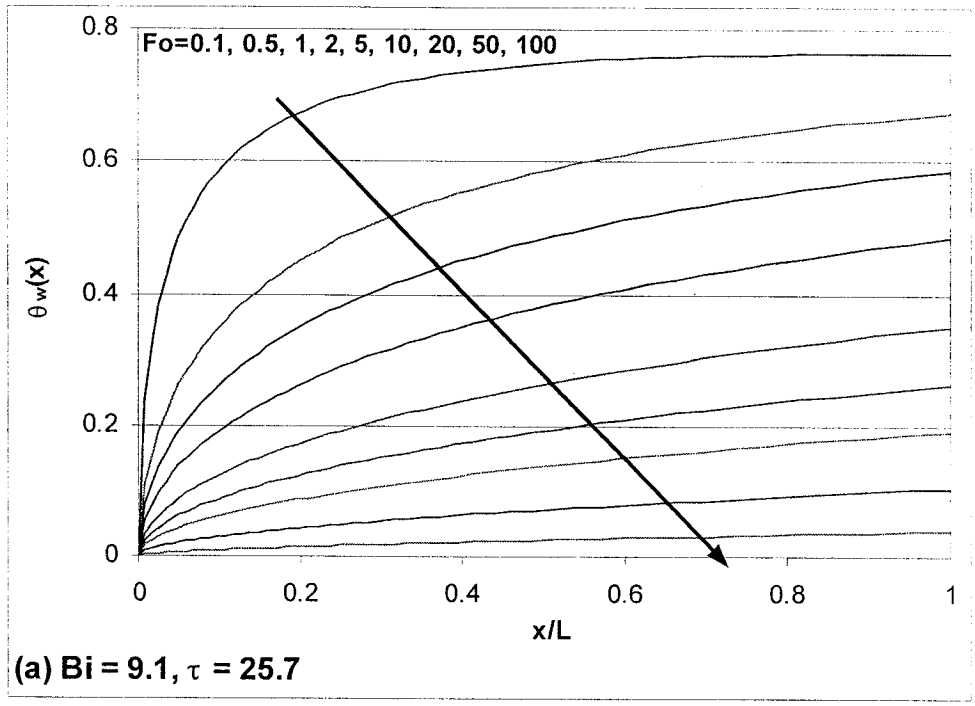

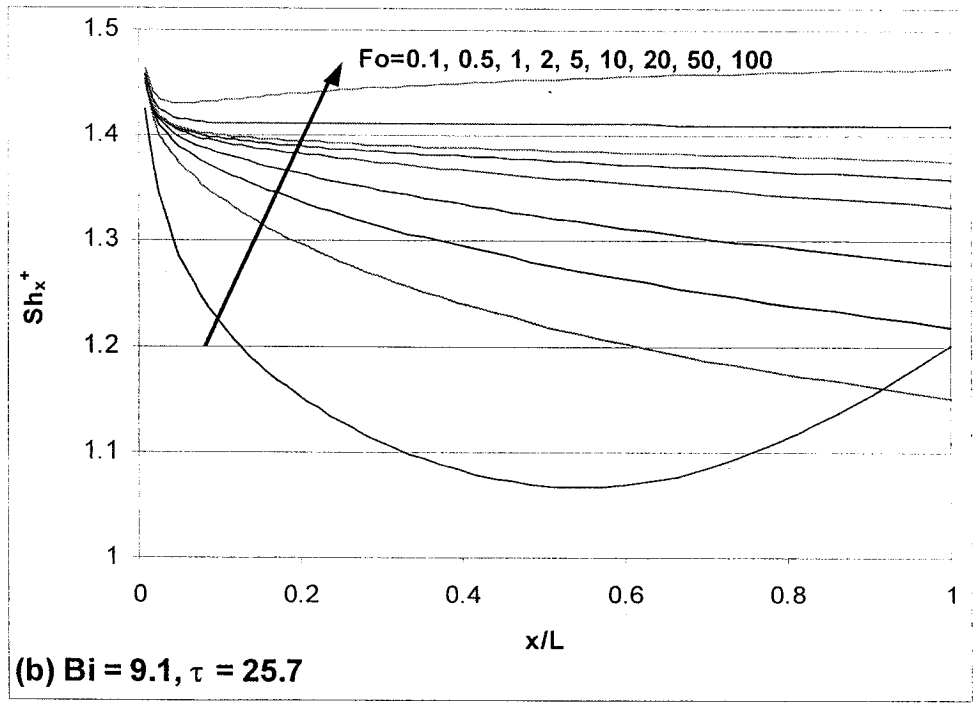

Figure 6-11 Model 2: $\theta_w(x)$ and Sh_x^+ along plate with different *Fo* for *Bi*=9.1, τ=25.7

Figure 6-12 compares the dependence of $(\theta_w)_{ave}$ and Sh_L^+ on Fo for three different cases of τ with $Bi = 9.1$ predicted by the unsteady convection model (Model 2), with that by the quasi-steady convection model (Model 1). At larger τ, the differences in $(\theta_w)_{ave}$ and Sh_L^+ between Models 1 and 2 get to be smaller. The difference decreases as time progresses or Fo increases. For $\tau = 25.7$, $(\theta_w)_{ave}$ and Sh_L^+ profiles are similar to those of Model 1. For $\tau = 2.57$, the error in $(\theta_w)_{ave}$ and Sh_L^+ are 0.18 and 0.54, respectively at $Fo = 0.2$. When Fo is larger than 1.0, the $(\theta_w)_{ave}$ profile follows that of quasi-steady convection model. The difference become significant for $\tau = 0.257$: at $Fo = 0.2$, $(\theta_w)_{ave}$ is about one third larger and Sh_L^+ is 4.6 times larger compared with the results of Model 1. For Fo larger than 30, the difference becomes negligible.

Figure 6-13 presents the dependence of $(\theta_w)_{ave}$ on Fo for all cases of Bi and τ. Fo ranged from about 0.2 to the total mass transfer time, t_{total}^+ given in Chapter 4. Due to the changes in modeling, t_{total}^+ obtained from the analytical model will not be the exact value for the numerical model as the time required to emit/sink 99% of the transferable mass from/into the material, but still it can provide a good measure as to how long the mass transfer will take place. When Bi is 9.1 or less, $(\theta_w)_{ave}$ obtained from the unsteady convection model are clearly different from those of the quasi-steady convection model, and the largest differences are observed at the smallest Fo. Significant impact of τ is observed especially for $\tau = 2.57$ or less. But for larger values of Bi, i.e., $Bi = 91$ or larger, little difference on $(\theta_w)_{ave}$ between Models 1 and 2, was observed in the given range of Fo regardless of τ.

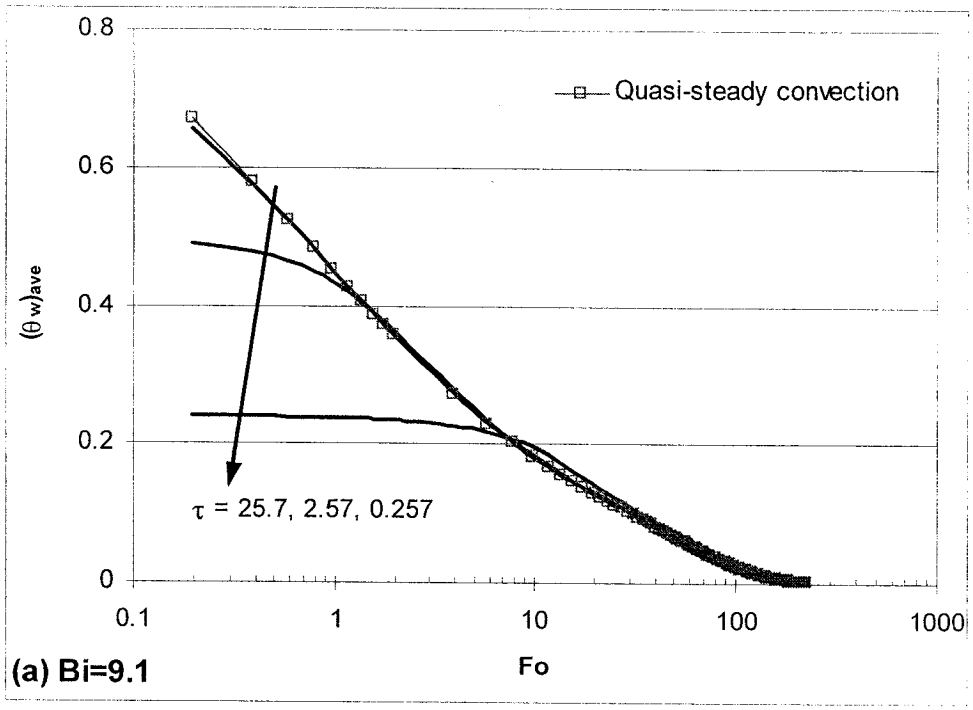

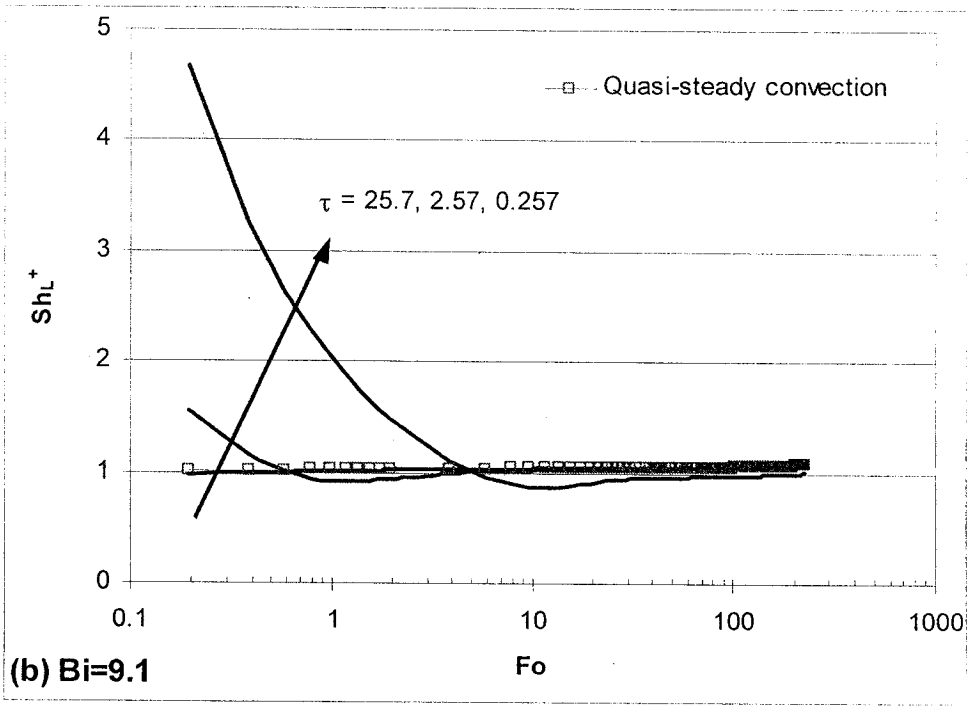

Figure 6-12 Model 2: Dependence of $(\theta_w)_{ave}$ and Sh_L^+ on Fo for different τ

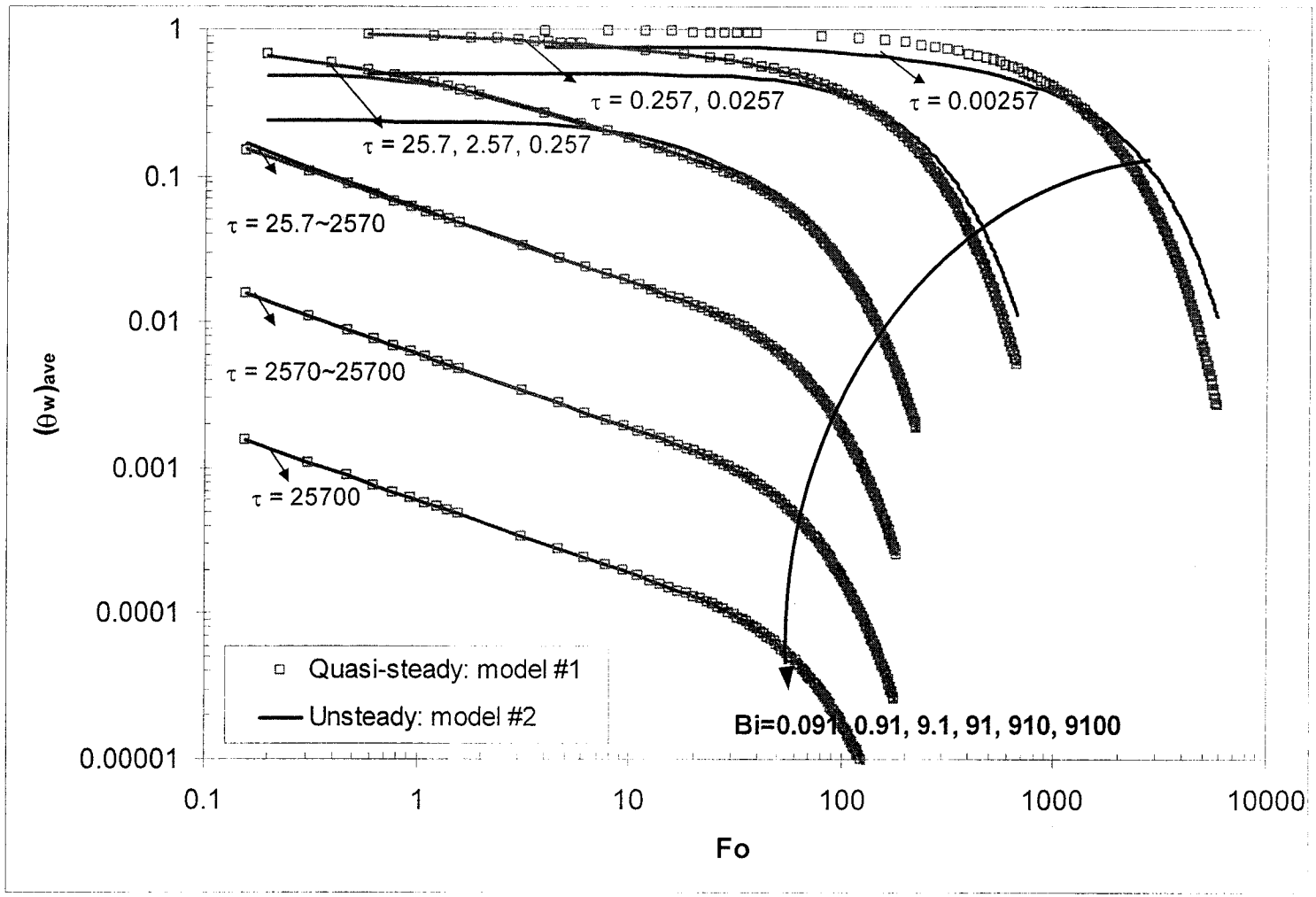

Figure 6-13 Model 2: Dependence of $(\theta_w)_{ave}$ on Fo for all cases of Bi and τ

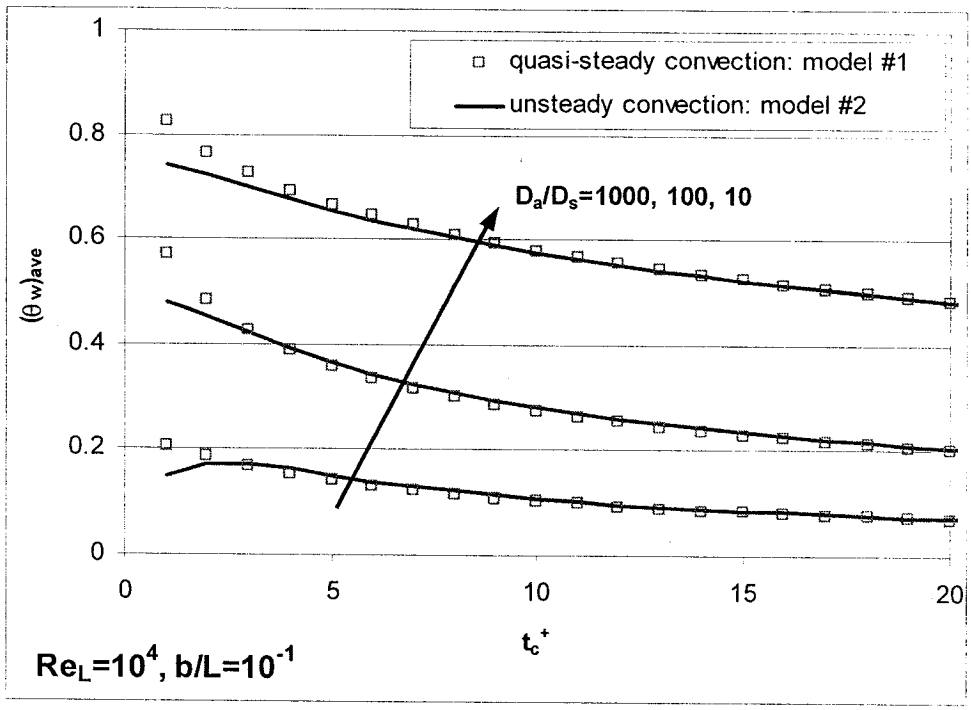

Figure 6-14 Model 2: Dependence of $(\theta_w)_{ave}$ on t_c^+ for the cases with $Re_L=10^4$ and $b/L=10^{-1}$

The variation of $(\theta_w)_{ave}$ as a function of t_c^+ is shown in Fig. 6-14 for three different cases of D_a/D_s (i.e., 10, 100, and 1000) with $Re_L = 10^4$ and $b/L = 0.1$. The Biot number of these three cases ranges from 91 to 9100. Fig. 6-14 shows the obvious differences between the predictions by Models 1 and 2 when t_c^+ is less than 3. This may indicate that the unsteadiness in convection will be always in effect in the early transfer phase regardless of Biot number. Table 6-2 presents the time (expressed in terms of both Fo and t_c^+, and denoted as $(Fo)_{5\%}$ and $(t_c^+)_{5\%}$) that is required to reach less than 5% of error on $(\theta_w)_{ave}$ between Models 1 and 2, for all considered cases of Bi and τ. The results show that the value of $(t_c^+)_{5\%}$ ranges from 0.98 to 2.31, while $(Fo)_{5\%}$ ranges from 4.4×10^{-6} to 897. In other words, quasi-steady convection assumption can be applied after less than two and half sweeps by the forced flow over the entire plate, but the proportion of this duration to

Fo depends on τ and varies widely. The ratio of $(Fo)_{5\%}$ to the total mass transfer time, t_{total}^{+} is also presented in Table 6-2. $(Fo)_{5\%}$ can be relatively long for cases of small τ - the maximum is 17.2% of t_{total}^{+} for $\tau = 2.57\times10^{-3}$. When the characteristic times for convection and diffusion are in the same order, the ratio, $(Fo)_{5\%}/t_{total}^{+}$ is in the order of 10^{-3}. When τ is larger than that, the ratio $(Fo)_{5\%}/t_{total}^{+}$ becomes infinitesimal. Figure 6-15 presents the general decrease in error of $(\theta_w)_{ave}$ between Models 1 and 2, as t_c^{+} increases. At $t_c^{+} = 10$, the error becomes 2.8% for $\tau = 2.57\times10^{-3}$; 2.3% for $\tau = 2.57\times10^{-2}$; and less than 0.7% for the rest of the cases.

Table 6-2 Time to reach less than 5% of error between $(\theta_w)_{ave}$ by Models 1 and 2

Denote	*Bi*	τ	time required to reach error < 5%		
			$(t_c^{+})_{5\%}$	$(Fo)_{5\%}$	$(Fo)_{5\%}/t_{total}^{+}$
Bi = 0.091	9.0952×10^{-2}	2.57×10^{-3}	2.31	8.97×10^{2}	1.72×10^{-1}
Bi = 0.91a	9.0952×10^{-1}	2.57×10^{-2}	1.71	6.65×10	1.00×10^{-1}
Bi = 0.91b	9.0952×10^{-1}	2.57×10^{-1}	1.76	6.83	1.03×10^{-2}
Bi = 9.1a	9.0952	2.57×10^{-1}	0.98	3.79	1.70×10^{-2}
Bi = 9.1b	9.0952	2.57	1.63	6.32×10^{-1}	2.83×10^{-3}
Bi = 9.1c	9.0952	2.57×10	1.75	6.81×10^{-2}	3.05×10^{-4}
Bi = 91a	9.0952×10	2.57×10	1.00	3.87×10^{-2}	2.12×10^{-4}
Bi = 91b	9.0952×10	2.57×10^{2}	1.62	6.28×10^{-3}	3.44×10^{-5}
Bi = 91c	9.0952×10	2.57×10^{3}	1.75	6.79×10^{-4}	3.72×10^{-6}
Bi = 910a	9.0952×10^{2}	2.57×10^{3}	1.14	4.42×10^{-4}	2.47×10^{-6}
Bi = 910b	9.0952×10^{2}	2.57×10^{4}	1.58	6.15×10^{-5}	3.44×10^{-7}
Bi =9100	9.0952×10^{3}	2.57×10^{5}	1.13	4.40×10^{-6}	2.47×10^{-8}

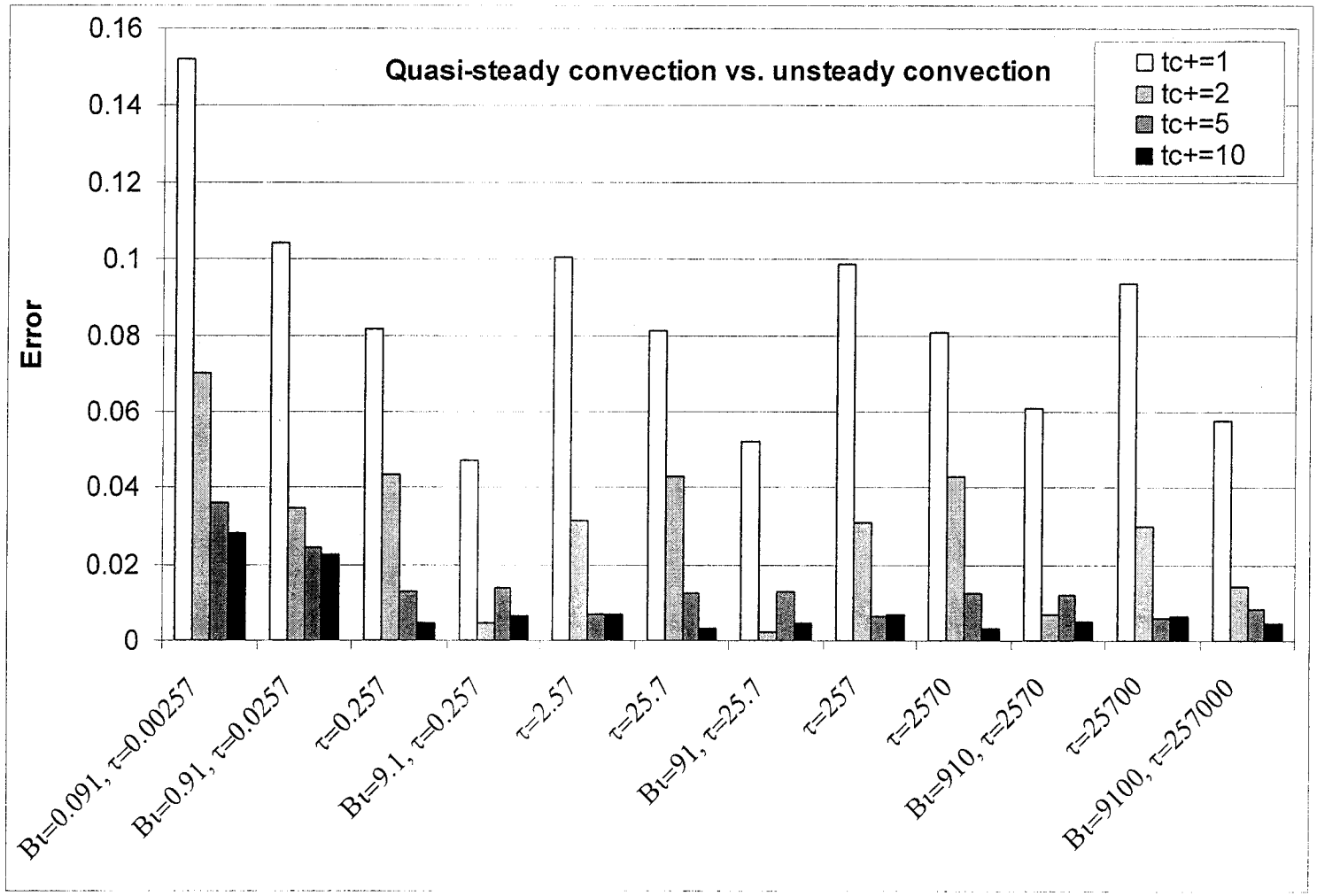

Figure 6-15: Error between $(\theta_w)_{ave}$ by Models 1 and 2 at different t_c^+ for all cases of *Bi* and τ

6.4 ONE-DIMENSIONAL DIFFUSION IN SOLID

One-dimensional diffusion is often adopted in modeling VOC source/sink behavior of solid building materials assuming the material is thin. The proposed analytical model in Chapter 3, as well as all other analytical models [Little et al., 1994, Yang et al, 1998, Huang and Haghighat, 2002] and some numerical models [Huang and Haghighat, 2002, Blondeau et al., 2000], use this assumption. The validity of this assumption was investigated by comparing the predictions of the conjugate mass transfer Model 3, i.e., unsteady two-dimensional convection coupled with unsteady two-dimensional diffusion (in x- and y-directions) in solid, to those of Model 2, i.e., unsteady two-dimensional convection coupled with unsteady one-dimensional diffusion (y-direction) in solid.

The difference between the two predictions increases with increasing thickness to length ratio of the solid, b/L, since the concentration gradient in x-direction, $\partial\theta/\partial x$ becomes relatively large if b/L increases. The difference generally increases as D_a/D_s decreases. Figure 6-16 presents the error between $\theta_w(x)$ obtained from Models 2 and 3 along the plate at various Fo for $Re_L = 10^4$, $b/L = 0.1$, and $D_a/D_s = 10$, which gives the largest error among all considered cases. Overall, the errors are insignificant ranging from the order of 10^{-5} to 10^{-7}. In other words, the one-dimensional diffusion in a solid is a proper assumption for the application on VOC source/sink behavior of porous materials. The error tends to decrease as time progresses or Fo increases. A larger error is observed at both edges of the plate, i.e., at $x = 0$ and $x = L$. Note that the no flux boundary condition, i.e., $\partial\theta/\partial x = 0$, implemented at $x = 0$ and $x = L$ for Model 3, was not required nor was it enforced for Model 2. This may cause larger errors at $x = 0$ and $x = L$.

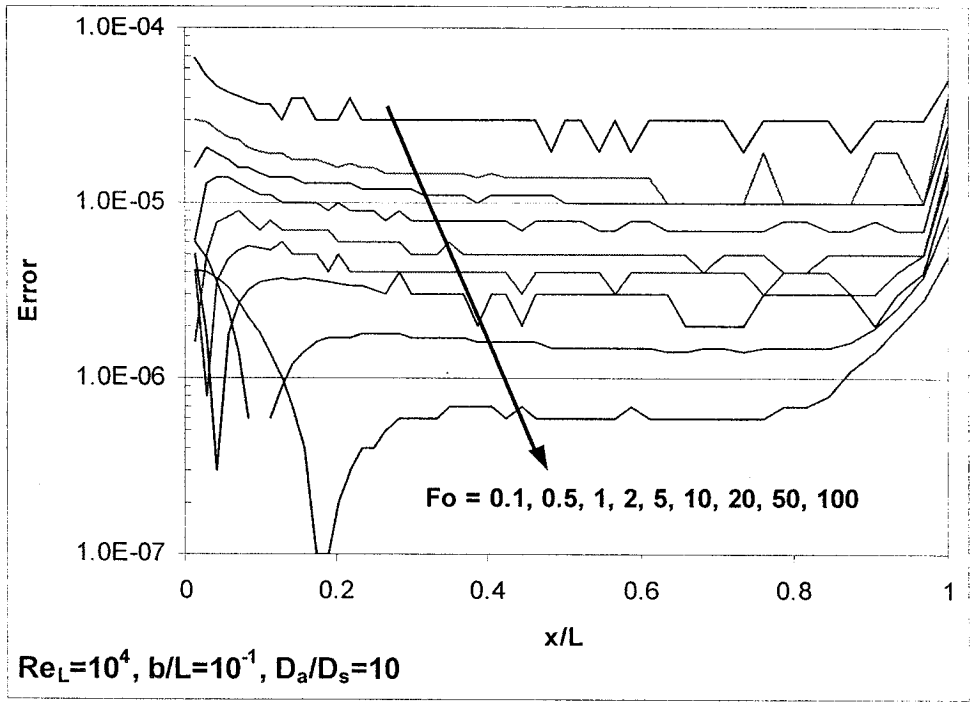

Figure 6-16 Error between $\theta_w(x)$ by Models 2 and 3 along the plate for various *Fo*

6.5 HENRY (LINEAR) SORPTION ISOTHERM

The analytical models for VOC source/sink behavior of solid building materials including the proposed analytical model in Chapter 3, are limited to linear problems. The proposed model adopts Henry (linear) isotherm for adsorption/desorption in porous material, assuming that the material is subjected to low VOC concentration levels. Sometimes, however, a building material can be exposed to high VOC concentrations, where the sorption isotherm becomes nonlinear. The effectiveness of the Henry isotherm was numerically investigated using conjugate mass transfer models (i.e., Model 3 for a linear isotherm and Model 4 for a nonlinear isotherm) with coupled unsteady two-dimensional convection and diffusion in the solid. The Freundlich isotherm in Eq. (2-3) was employed to represent a nonlinear isotherm.

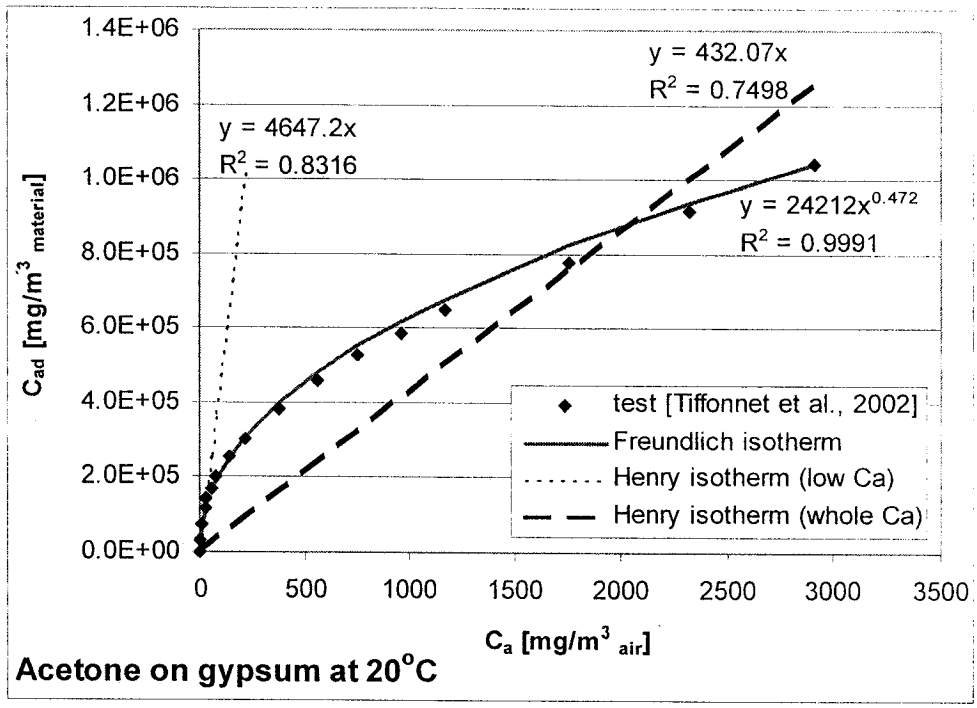

Figure 6-17 Determination of sorption parameters using the experimental data by Tiffonnet et al. (2002)

The parameters of both sorption isotherms were obtained from the sorption experimental data of gypsum board using acetone at 20°C as presented in Fig. 2-7 [Tiffonnet et al., 2002]. Since the data were reported in terms of mass-based concentration, these were converted to volume-based concentration using the reported density of gypsum board, (723.4 kg/m^3), and the density of air (1.205 kg/m^3) calculated from the ideal gas law. Tiffonnet et al. (2002) reported the parameters, i.e., K_F and α_F of the Freundlich isotherm for the same data, but the reported K_F cannot be used due to the conversion in units of concentrations. Hence, the best-fit value was chosen for K_F (K_F = 24212 with R^2 = 0.9991) using the reported α_F (α_F = *0.472*) as shown in Fig. 6-17. Two cases of Henry constants were obtained. One is from low concentration levels that exhibit linear profile (i.e., K = 4647.2 with R^2 = 0.8316 using data up to $C_a \approx 33$ mg/m^3), which is so called

Henry region. The other is obtained using the entire nonlinear data, i.e., K = 432.07 with R^2 = 0.7498. Some Henry constants available in the literature were obtained by curve fitting the nonlinear profiles with Henry isotherm [Meininghaus et al., 2000]. The porosity and diffusion coefficient of gypsum board (i.e., ε = 0.2953 and D_a/D_s = 6.83) were taken from another report prepared by the same researchers [Blondeau et al., 2000]. Two cases of Re_L (i.e., $Re_L = 10^4$ and 10^2) with b/L = 0.01 were considered.

Figure 6-18 presents $(\theta_w)_{ave}$ and Sh_L^+ as a function of Fo with $Re_L = 10^4$ for four different sorption cases: Freundlich isotherm for the material subjected to a low concentration range (i.e., C_o = 50 mg/m^3 and C_∞= 0), Freundlich isotherm for wide concentration range (i.e., C_o = 3000 mg/m^3 and C_∞ = 0); and both cases of Henry isotherm. Unlike Henry isotherm, the predictions by the model with a nonlinear sorption isotherm always vary by the concentration range that the material is exposed. $(\theta_w)_{ave}$ and Sh_L^+ profiles are quite different from one another. The results indicates that the error arises from the use of Henry isotherm can be reduced if the Henry constant is determined from the concentration levels similar to actual concentrations that the material is underwent. Compared to the Freundlich isotherm with C_o = 3000 mg/m^3 and C_∞ = 0, the maximum difference in $(\theta_w)_{ave}$ is 0.41 when a Henry constant obtained from different concentration levels, and it drops to 0.11 if a Henry constant is obtained from the same concentration levels. For $Re_L = 10^2$ (Fig. 6-19) smaller errors were observed in $(\theta_w)_{ave}$ and Sh_L^+, compared to $Re_L = 10^4$.

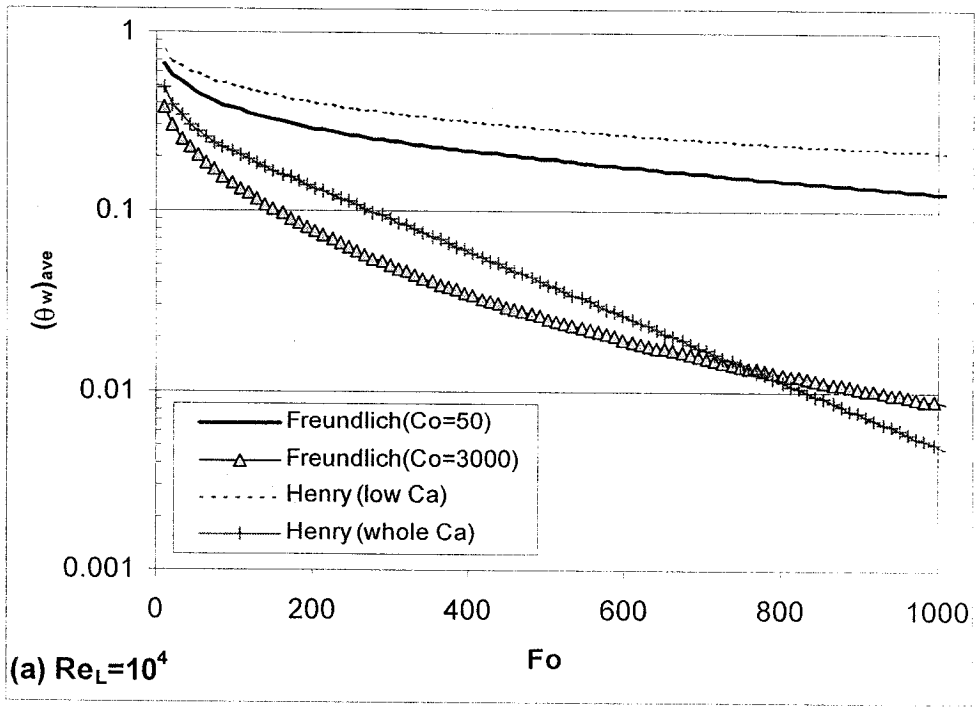

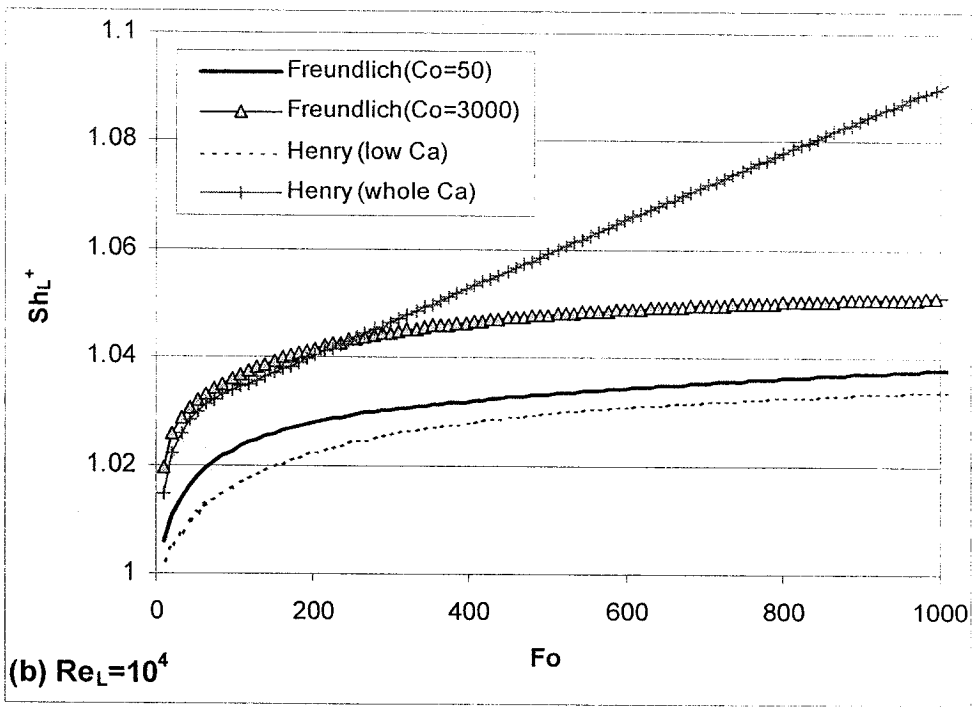

Figure 6-18 Henry versus Freundlich isotherm for $Re_L=10^4$

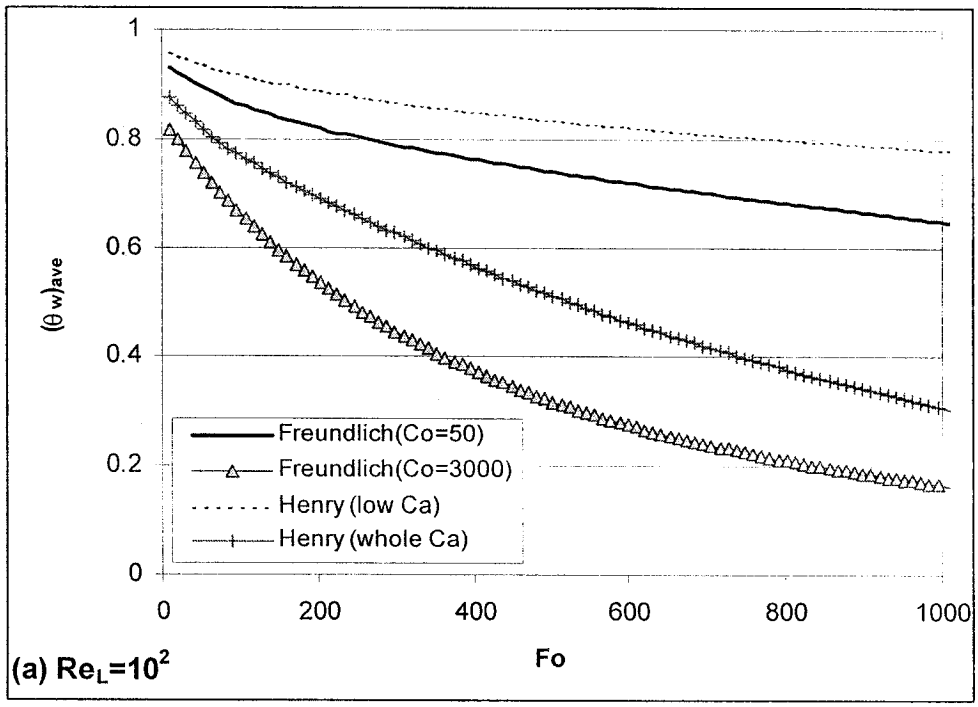

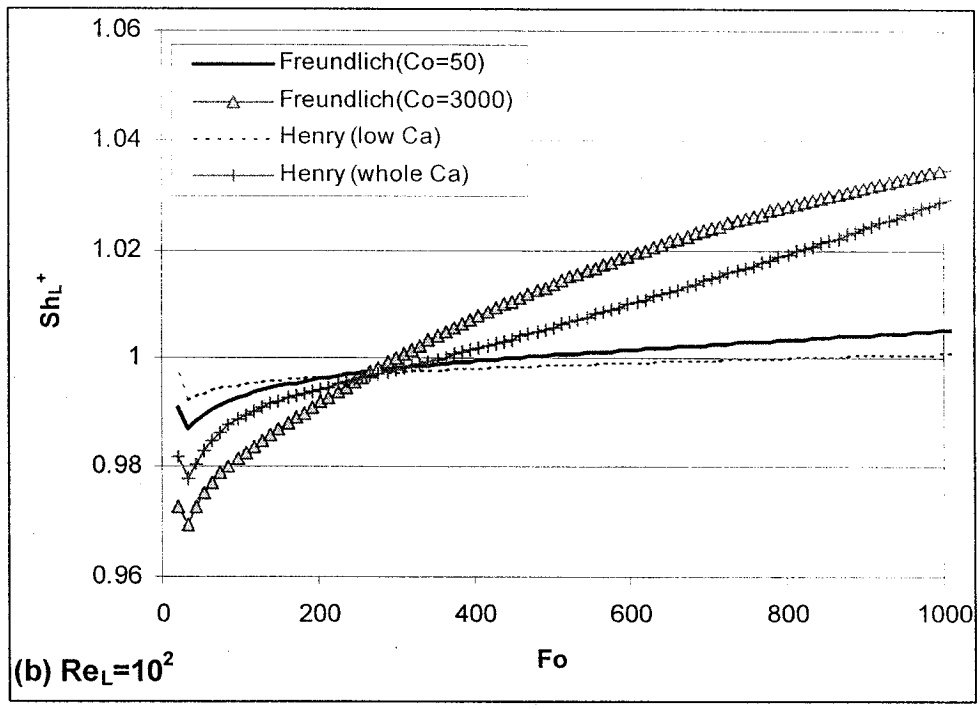

Figure 6-19 Henry versus Freundlich isotherm for $Re_L=10^2$

6.6 SUMMARY

In order to assess the validity limits of the analytical model proposed in Chapter 3, the assumptions made in deriving the analytical model were examined for several cases of material properties and Reynolds number, using the conjugate mass transfer models presented in Chapter 5. From the numerical computation results, the following conclusions are reached.

- Unlike the constant wall concentration assumption, the wall concentration varies along the plate (x-direction). The averaged wall concentration, however, corresponds to the wall concentration obtained by the analytical model The averaged Sherwood number is underestimated by about 0.6% to 7% for values of Bi varying between 0.091 and 9100 and Fo less than or equal 180.
- The quasi-steady assumption in convection mass transfer may result in significant overestimation of wall concentration or underestimation of Sherwood number in the early transfer phase; however, after less than 2.5 times of convection characteristic time, the quasi-steady assumption is a valid assumption. This duration is equivalent to at most 17.2% of total mass transfer time for cases with convection characteristic time longer than that of diffusion.
- The error caused by the assumption of one-dimensional diffusion in solid is negligible in typical VOC porous material cases; hence, this assumption is valid.
- Henry (linear) sorption isotherm may cause significant error. This error, however, can be minimized through selecting the Henry constant carefully using the actual concentration levels that the material will be subjected to.

Chapter 7

Conclusions and Recommendations

7.1 CONCLUSIONS

The objective of this study was to conduct a comprehensive theoretical investigation on the VOC source and sink behavior of porous building materials by developing a reliable mathematical model based on a critical review of mass transfer mechanisms in porous solids and an assessment of existing models. A novel analytical model was proposed and an exact solution for that model was obtained using the integral transform method. The proposed model considers the convection over the material, the gas-phase and/or adsorbed-phase diffusion within the porous material, the adsorption/desorption that takes place on the pore wall, and the generation or elimination of VOC within the material due to secondary source/sink behavior like chemical reactions. Compared to the currently available analytical models, the proposed analytical model can predict the secondary VOC source/sink behavior, which can be described by any function of space (y-direction) and time; it also considers the effect of air velocity or Reynolds number while Little's model (1994) neglected the convection boundary layer resistance; and can be applied for both source and sink behavior while Huang's analytical model (2002) can be applied only for the source behavior.

The predictions made by the proposed analytical model for the primary source and sink behavior, agree well with the carpet VOC emission test data and the wood chipboard

sorption test data. The prediction of the proposed model was compared with the prediction of Little's model (1994), which is the only existing analytical model that can be applied for both VOC source and sink behavior. Little's model tends to overestimate the emission/sorption rates in the early stage compared with the proposed model, and the difference is significant if the air velocity is low, i.e., when the convection resistance in the boundary layer is large.

A parametric study on the primary source/sink behavior of porous materials using the non-dimensionalized analytical model was carried out considering inclusive ranges of air velocity expressed as Reynolds number (Re_L); and material properties like the ratio of mass diffusion coefficient in the air to that in the solid (D_a/D_s), the thickness to length ratio of the solid (b/L), and the sum of porosity and sorption partition coefficient ($\varepsilon+K$). This investigation leads to the following conclusions:

- The primary source/sink behavior is a function of Fourier number (Fo), Biot number (Bi) and ($\varepsilon+K$).
- The linear effect of ($\varepsilon+K$) is observed for nondimensionalized wall concentration, θ_w, and the total transfer time, t_{total}, which is the time required to complete 99% of mass transfer. The effect of Bi, however, is nonlinear: as Bi increases, t_{total} decreases, but for Bi larger than 10, t_{total} becomes almost constant.
- When Bi is decomposed into Re_L and material properties, i.e., $(D_a/D_s)\times(b/L)$, the parametric study shows that the effect of Re_L decreases as $(D_a/D_s)\times(b/L)$ increases, and if $(D_a/D_s)\times(b/L)$ is larger than 1.0, there is little effect of Re_L on the VOC

emission/sorption rate. This limit can indicate the application limit of Little's model.

- For $(D_a/D_s)\times(b/L)$ larger than 1.0, (b/L) has the most significant impact on t_{total}: the effect of $(b/L)^2$ is obtained while the effects of both (D_a/D_s) and $(\varepsilon+K)$ are linear.
- The length scale (L) can affect the emission/sorption rates since Bi has dependence of $L^{-0.5}$ and air velocity, $u_\infty^{0.5}$ for laminar flow over flat plate (see Eq. (4-5)). Hence, for dynamic similarity between the small-scale chamber and the full-scale cases, the air velocity required in the small-scale chamber tests should be decreased such as to have the same Bi in both small-scale and full-scale cases, so as to obtain the same emission/sorption rate with full-scale cases. This applies only if the thickness of the material is not altered, which is common practice in material emission or sorption tests.

The case studies on the secondary source behavior using five hypothetical generation functions demonstrate that the proposed model can be suitable for describing various mechanisms involved in the secondary source/sink behavior due to little limitation imposed on the generation/elimination term; and can predict the effects of material properties and Re_L on the secondary emission/sorption rates. Case study results agree well with experimental findings on the secondary emissions available in literature.

The validity of the four main assumptions made in the proposed analytical model, was assessed using numerical conjugate mass transfer models where each model was obtained by relaxing one or more of the assumptions made in the analytical model. These

assumptions are constant wall concentration; quasi-steady convection mass transfer in fluid; one-dimensional diffusion in solid; and Henry or linear sorption isotherm. The computation results indicated that:

- The assumption of constant wall concentration did not affect the averaged wall concentration; however, it can lead to 0.6% to 7% of underestimation of the average Sherwood number, which is a measure of the emission/sorption rate.
- Quasi-steady convection mass transfer is valid after less than 2.5 times of the convection characteristic time t_c, which is the time taken by an air particle traveling at u_∞ to travel the length of the plate (L). For initial time intervals smaller than this time limit, the assumption can result in significant overestimation of wall concentration or underestimation of Sherwood number.
- One-dimensional diffusion in the solid is valid in the full range of material properties and Re_L that were considered in this study.
- Henry (linear) sorption isotherm may cause significant error; however, well-chosen Henry constant using the actual concentration levels that the material will be subjected to, can substantially reduce the error.

7.2 RECOMMENDATIONS FOR FUTURE WORK

The recommended future research work on the VOC source and sink behavior of building materials and its impact on indoor air quality (IAQ), follows from the advancement and the limitations of this study:

- The proposed analytical model needs further validation for the primary source and sink behavior through small-scale and/or full-scale emission/sorption experiments for various porous building materials.
- The investigation on the secondary source and sink behavior that was considered in this study was limited due to the lack of current knowledge. Since the secondary source/sink behavior may significantly affect IAQ, extensive experimental and theoretical studies for material characterization of the secondary source/sink behavior are necessary. The proposed analytical model can be applied to rule out the primary behavior from the secondary behavior in experimental data, and to obtain the generation/elimination functions.
- The proposed analytical model as well as other physical models, suffer from the lack of reliable input parameters including convection mass transfer coefficient and other material properties like mass diffusion coefficient, sorption properties, initial concentrations, etc.
  - Only limited cases of convection mass transfer coefficients or Sherwood number correlations are currently available. Efforts have to be made to characterize these convection properties for various flow conditions and geometries through experimental and/or numerical (CFD) studies.
  - Also limited data (in terms of considered VOC and/or building materials) are presently available for material properties like diffusion coefficient, sorption properties, initial concentration, and porosity. In addition, these properties were measured by various methods, which often results in significant differences. First, the standardization of material characterization methods has

to be established. And then an extensive database of material properties obtained from the standard procedures, has to be developed. At the same time efforts have to be made to develop models that can predict the material properties based on the chemical and physical properties of VOC and building materials.

- The assumption of constant temperature and humidity, which is made in the current models including the model proposed in this work, is mainly due to the lack of extensive experimental studies. Since building materials are generally subjected to thermal and/or moisture gradients in real conditions, the validity of these assumptions has to be investigated by experimental studies on the VOC source/sink behavior under these gradients and the sensitivity of material properties for temperature and humidity changes.
- Reliable models for building material assemblies have to be developed through careful examinations of the transfer mechanisms at the interface. The interface conditions adopted in the existing models are not well validated. Hence, more experimental studies are required.
- In order to diffuse the knowledge obtained from the numerous researches on VOC source/ sink behavior of building materials into the IAQ practice, it is necessary to develop proper simulation-based design tools that can allow designers and manufacturers to evaluate their designs or products for the course of the entire product life cycle, and assist designers in the selection of the most environmentally sensible building materials and furnishings.

- Several IAQ simulation programs have been developed. Since the existing programs are generally based on the early research work on material emissions, empirical and/or simple theoretical models were adopted and only the primary emission (source) was considered. Hence, there is a need for the development of a new program based on the up-to-date and advanced knowledge of VOC source/sink behavior of building materials.
- The current practice for a healthy building design considers only the primary emission; therefore, the building product with the lowest initial VOC content (or concentration) is regarded as the best choice. When we consider both the primary and the secondary source/sink behavior, selecting the optimum materials for IAQ is not a simple, straightforward task and may require applying an optimization technique.

References

Adamson, A.W., *Physical Chemistry of Surfaces*, John Wiley and Sons, Inc., 1990

American Society for Testing and Materials, *Standard Guide for Small-Scale Environmental Chamber Determinations of Organic Emissions from Indoor Materials/ Products*, ASTM Standard D-5116-90, Philadelphia, 1990

Anderson, D.A., Tannehill, J.C., and Pletcher, R.H., *Computational Fluid Dynamics and Heat Transfer*, McGraw-Hill, New York, 1984

Attard, G., and Barnes, C., *Surfaces*, Oxford University Press, 1998

Axley, J.W., "Adsorption modelling for building contaminant dispersal analysis", *Indoor Air*, vol. 1, pp. 147-171, 1991

Bejan, A, *Convection Heat Transfer*, 2nd edition, New York, John Wiley & Sons, Inc., 1995

Berglund, B., et al., "Assessment of discomfort and irritation from the indoor air", *Proceedings of IAQ-86*, Atlanta, GA, ASHRAE, pp. 138-149, 1986

Bjurman, J., "Release of MVOCs from microorganisms", *Organic Indoor Air Pollutants: Occurrence, Measurement, Evaluation*, Ed. Salthammer, T., pp.259-273, Wiley-VCH, 1999

Bjurman, J., Nordstrand, E., and Kristensson, J., "Growth-phase related production of potential volatile organic compounds by molds on wood", *Indoor Air*, vol.7, pp.2-7, 1997

Blondeau, P., Allard, F., and Tiffonnet, A.L., *Etude du role des parois dans la gestion de la qualité de l'air intérieur des bâtiments non industriels*, Convention n°A97-19 entre le PUCA et l'Université de La Rochell, 2000

Bodalal, A., Zhang, J.S. and Plett, E.G., "A method for measuring internal diffusion and equilibrium partition coefficients of volatile organic compounds for building materials", *Building and Environment*, vol. 35, pp. 101-110, 2000

Bolz, R.E. and Tuve, G.L. *Handbook of Tables for Applied Engineering Science*, 2nd edition, CRT press, Cleveland, Ohio, 1973

Brunauer, S., *The Adsorption of Gases and Vapors*, vol.1, Princeton University Press, Princeton, NJ, 1945.

Cebeci, T., and Bradshaw, P., *Momentum Transfer in Boundary Layers*, Hemisphere Publishing Corp., Washington D.C., 1977

Colombo, A. and De Bortoli, M., "Comparison of models used to estimate parameters of organic emissions from materials tested in small environmental chambers", *Indoor Air*, 2, pp.49-57, 1992

Cox, S.S., Little, J.C., and Hodgson, A.T., "Measuring concentrations of colatile organic compounds in vinyl flooring", *J. Air and Waste Management*, vol. 51, pp. 1195-1201, 2001a

Cox, S.S., Zhao, D., and Little, J.C., "Measuring partition and diffusion coefficients for volatile organic compounds in vinyl flooring", *Atmospheric Environment*, vol. 35, pp.3823-3830, 2001b

De Bellis, L., *Characterization of Pollutant Emissions from Paint and Varnish: Temperature and Relative Humidity Variations*, M.A.Sc. Thesis, Concordia University, Montreal, Canada, 1995

Derome, D, *Moisture Occurrence in Roof Assemblies Containing Moisture Storing Insulation and Its Impact on the Durability of Building Envelope*, Ph.D. thesis, Concordia University, 1999

Environmental Protection Agency, *Indoor Air Facts No. 4, Sick Building Syndrome*, revised 1991

Geankoplis, C.J., *Mass Transport Phenomena*, Ohio State University, Columbus, Ohio, 1972

Godish, T., *Indoor Environmental Quality*. Lewis Publishers, 2001

Gustafsson, H., *Building Materials Identified as Major Sources for Indoor Air Pollutants – A Critical Review of Case Studies s*, Swedish Council for Building Research, Stockholm, Sweden, 1992

Haghighat, F. and De Bellis, L., "Material emission rates: literature review and the impact of indoor air temperature and relative humidity", *Building and Environment*, vol. 33, no. 5, pp.261-277, 1998

Haghighat, F., and Huang, H., "Integrated IAQ model for prediction of VOC emissions from building material", *Building and Environment*, vol. 38, no. 8, pp. 1007-1018, 2003

Haghighat, F. and Zhang, Y., "Modelling of emission of volatile organic compounds from building materials- estimation of gas-phase mass transfer coefficient", *Building and Environment*, vol. 34, pp. 377-389, 1999

Haghighat, F., Lee, C.S., and Ghaly, W.S., "Measurement of diffusion coefficients of VOCs for building materials: review and development of a calculation procedure", *Indoor Air*, vol.12, pp. 81-91, 2002

Hansen, S.J., and Burroughs, H.E., *Managing Indoor Air Quality*, 2nd edition, Fairmont Press, 1999

Hansson, P. and Stymne, H., "VOC diffusion and absorption properties of indoor materials- consequences for indoor air quality", *Proceedings of Healthy Building 2000*, vol. 4, pp. 151-156, Espoo, Finland, August 6-10, 2000

Hoffman, J.D., *Numerical Methods for Engineers and Scientists*, McGraw-Hill, New York, 1992

Holman, J.P., *Heat Transfer*, 7th edition, McGraw-Hill, Inc., 1990

Huang, H., and Haghighat, F., "Modeling of volatile organic compounds emission from dry building materials", *Building and Environment*, vol. 37, no. 11, pp. 1127-1138, 2002a

Huang, H., and Haghighat, F., "Building material VOC emission – a systematic parametric study", *Proceedings of Indoor Air 2002*, 9th Int. Conf. on Indoor Air Quality and Climate, vol. 3, pp. 232-237, Monterey, USA, June 30- July 5, 2002b

Hutcheon, N.B. and Handegord, O.P., *Building Science for a Cold Climate*, National Research Council of Canada, 1995

Jensen, B., Wolkoff, P., and Wilkins, C.K., "Characterization of linoleum identification of oxidative emission processes", *Characterizing Sources of Indoor Air Pollution and Related Sink Effects*, ASTM STP 1287, pp.145-152, 1996

Jensen, B., Wolkoff, P., Wilkins, C.K., and Clausen, P.A., "Characterization of linoleum part 1: measurement of volatile organic compounds by use of the field and laboratory emission cell, FLEC", *Indoor Air*, vol. 5, pp.38-43, 1995

Jørgensen, R.B., Bjørseth, O., and Malvik, B., "Chamber testing of adsorption of volatile organic compounds (VOCs) on material surfaces", *Indoor Air*, vol.9, pp.2-9, 1999

Kärger, J., and Ruthven, D.M., *Diffusion in Zeolites and Other Microporous Solids*, John Wiley & Sons, Inc., 1992

Kays, W.M., and Crawford, M.E., *Convective Heat and Mass Transfer*, 2nd Edition, McGraw-Hill, New York, 1980

Kirchner, S., Badey, J.R., Knudsen, H.N., Meininghaus, R., Quenard, D., Sallee, H., and Saarinen, A., "Sorption capacities and diffusion coefficients of indoor surface materials exposed to VOCs: proposal of new test procedures", *Proceedings of Indoor Air '99*, 8th Int. Conf. on Indoor Air Quality and Climate, vol.1, pp.430-435, Edinburgh, Scotland, Aug. 8-13, 1999

Knudsen, H.N., Kjaer, U.D., Nielsen, P.A. and Wolkoff, P., "Sensory and chemical characterization of VOC emissions from building products: impact of concentration and air velocity", *Atmospheric Environment*, vol. 33, pp. 1217-1230, 1999

Kumar, D., and Little, J.C., "Barriers to reduce emission rates from diffusion controlled materials", *Proceedings of Indoor Air 2002*, 9th Int. Conf. on Indoor Air Quality and Climate, vol. 3, pp. 570-575, Monterey, USA, June 30- July 5, 2002

Lee, C.S., Ghaly, W., and Haghighat, F., "VOC emissions from diffusion-controlled building materials: analogy of conjugate heat transfer", *Proceedings of Healthy Building 2000*, vol. 4, pp. 163-168, Espoo, Finland, August 6-10, 2000

Little, J.C. and Hodgson, A.T., "A strategy for characterizing homogeneous, diffusion-controlled indoor sources and sinks", *Characterizing Sources of Indoor Air Pollution and Related Sink Effects*, ASTM STP 1287, B.A. Tichenor Ed., American Society for Testing and Materials, pp. 294-304, 1996

Little, J.C., Hodgson, A.T., and Gadgil, A.J., "Modeling emission of volatile organic compounds from new carpets", *Atmospheric Environment*, vol.28, pp. 227-234, 1994

Low, J.M., Zhang, J.S., Plett, E.G. and Shaw, C.Y., "Effects of air flow on emissions of volatile organic compounds from carpet-adhesive assemblies", *ASHRAE Transactions*: Symposia, TO-98-23-2, pp. 1281-1288, 1998

Luikov, A.V., "Conjugate convective heat transfer problems", *Int. J. of Heat Mass Transfer*, vol.17, pp.257-265, 1974

Lyman, W. J., Reehl, W. F. and Rosenblatt, D. H., *Handbook of Chemical Property Estimation Methods: Environmental Behavior of Organic Compounds*, Washington, DC, American Chemical Society, 1990

Maroni, M., Selfert, B., and Lindvall, T. (Eds.), *Indoor Air Quality*, Elsevier Science, 1995

McNeely, A., "Liability for sick building syndrome", *Construction Canada*, pp.33-34, November, 1999

Meininghaus, R., Gunnarsen, L., and Knudsen, H.N., "Diffusion and sorption of volatile organic compounds in building materials-impact on indoor air quality", *Environmental Science & Technology*, vol.34, pp.3101-3108, 2000a

Meininghaus, R., Kirchner, S., Maupetit, F., Sallée, H., and Quenard, D., "Gravimetric studies on VOC adsorption by indoor materials under near-ambient conditions", *Indoor Built Environment*, vol.9, pp.277-283, 2000b

Meininghaus, R., Knudsen, H.N. and Gunnarsen, L., "Diffusion and sorption of volatile organic compounds in indoor surface materials", *Proceedings of EPIC `98*, 2nd European Conf. on Energy Performance and Indoor Climate in Buildings and the 3rd Int. Conf. on Indoor Air Quality, Ventilation and Energy Conservation, vol. 1, pp. 33-38, Lyon, France, Nov. 19-21, 1998

Mosaad, M., "Laminar forced convection conjugate heat transfer over a flat plate", *Heat and Mass Transfer*, vol. 35, pp. 371-375, 1999

Murakami, S., Kato, S. and Ito, K., "Coupled analysis of TVOC emission and diffusion in a ventilated room by CFD", *Proceedings of EPIC `98*, 2nd European Conf. on Energy Performance and Indoor Climate in Buildings and the 3rd Int. Conf. on Indoor Air Quality, Ventilation and Energy Conservation, vol. 1, pp. 19-26, Lyon, France, Nov. 19-21, 1998

Murakami, S., Kato, S., Ito, K. and Yamamoto, A., "Analysis of chemical pollutants distribution based on coupled simulation of CFD and emission/sorption processes", *Proceedings of Indoor Air `99*, 8th Int. Conf. on Indoor Air Quality and Climate, vol. 4, pp. 725-730, Edinburgh, Scotland, Aug. 8-13, 1999

Ojanen, T., Salonvaara, M., Kohonen, R., and Nieminen, J., Moisture transfer in building structures: numerical methods (English translation)/ Kosteuden siirtyminen rakenteissa Laskentamenetelmat, Technical Research Center of Finland, Report no. 595, 1989. (referred in Derome, 1999)

Özisik, M.N., *Heat Conduction*, John Wiley & sons, Inc., 1980

Patankar, S.V., *Numerical Heat Transfer and Fluid Flow*, Hemisphere Publishing Corp., Washington D.C., 1980

Perry, R.H., and Chilton, C.H., *Chemical Engineers' Handbook*, 5th edition, McGraw-Hill, Inc., 1973

Popa, J., and Haghighat, F., "Characteriztion of the sink effect of VOCs on building materials, with specific emphasis on painted surfaces", *Proceedings of Indoor Air 2002*, 9th Int. Conf. on Indoor Air Quality and Climate, vol. 3, pp. 558-563, Monterey, USA, June 30- July 5, 2002

Popa, J.R., *Characterization of the Sink Effect of VOCs on Building Materials, with Specific Emphasis on Painted Surfaces*, M.A.Sc. Thesis, Concordia University, Montreal, Canada, 2002

Roodman, D.M., and Lenssen, N., "A building revolution: how ecology and health concerns are transforming construction", *World Watch Paper 124*, pp.23, World Watch Institute, Washington, D.C., March, 1995

Rothweiler, H., Mengon, W., Meier, G., Forss, A.-M., and Schlatter, C., "Emissions of degradation products of building materials in the indoor environment – case studies", *Indoor Air'93*, 6th Int. Conf. on Indoor Air Quality & Climate, vol. 2, pp. 465-470, Helsinki, Finland, 1993

Ruthven, D.M., *Principles of Adsorption and Adsorption Processes*, John Wiley & sons, Inc., 1984

Saarela, K., "Emission from floor coverings", *Organic Indoor Air Pollutants: Occurrence, Measurement, Evaluation*, Ed. Salthammer, T., pp. 185-202, Wiley-VCH, 1999

Salthammer, T. (Editor), *Organic Indoor Air Pollutants: Occurrence- Measurement-Evaluation*, Wiley-VCH, 1999

Satterfield, C.N., *Mass Transfer in Heterogeneous Catalysis*, MIT Press, 1970

Sereda, P.J., "Performance of building materials", *Canadian Building Digest*, CBD-115, National Research Council Canada, July, 1969

Sparks, L. E., Tichenor, B. A. and Guo, Z, "Gas-phase mass transfer model for predicting volatile organic compound (VOC) emission rates from indoor pollutant sources", *Indoor Air*, vol. 6, pp. 31-40, 1996b

Sparks, L.E., Mølhave, L., and Dueholm, S., "Source testing and data analysis for exposure and risk assessment of indoor pollutant sources", *Characterizing Sources of Indoor Air Pollution and Related Sink Effect*, ASTM STP 1287, pp., 367-375, American Society for Testing and Materials, 1996a

Ström, G., West, J., Wessén, B., and Palmgren, U., "Quantative analysis of microbial volatiles in damp Swedish houses", in Samson, R.A. et al. (ed.) *Air Quality Monographs, vol. 2, Health Implications of Fungi in Indoor Environments*, Amsterdam, Elsevier, pp.291-305, 1994

Tichenor, B.A., Guo, Z., and Sparks, L.E., "Fundamental mass transfer model for indoor air emissions from surface coatings", *Indoor Air*, vol. 3, pp.263-268, 1993

Tichenor, B.A., Guo, Z., and Sparks, L.E., "Fundamental mass transfer model for indoor air pollution sources", *Proceedings of Indoor Air '93*, 6th Int. Conf. on Indoor Air Quality and Climate, vol. 2, pp. 377-382, Helsinki, Finland, July 4-8, 1993

Tichenor, B.A., Guo, Z., Mason, M.A., and Dunn, J.E., "Evaluation of indoor air pollutant sinks for vapor phase organic compounds", Proceedings of Indoor Air '90, 5th International Conference on Indoor Air Quality and Climate, vol.3, pp.623-628, Toronto, Canada, 1990

Tiffonnet, A.-L., Blondeau, P., Allard, F., and Haghighat, F., "Sorption isotherms of acetone on various building materials", *Indoor Built Environment*, vol.11, pp.95-104, 2002

Tiffonnet, A.L., Blondeau, P., Amiri, O. and Allard, F., "Assessment of contaminant diffusivities in building materials from porosity tests", *Proceedings of Healthy Building 2000*, vol. 4, pp. 199-203, Espoo, Finland, August 6-10, 2000

Treybal, R.E., *Mass Transfer Operation*, McGraw-Hill, Inc., 1968

Versteeg, H.K., and Malalasekera, W., *An Introduction to Computational Fluid Dynamics: The Finite Volume Method*, Longman, Essex, England, 1995

Welty, J. R., Wicks, C. E., and Wilson, R. E., *Fundamentals of Momentum, Heat, and Mass Transfer*, 2nd Ed., John Wiley & Sons Inc., 1976

Weschler, C.J., "Ozone in indoor environments: concentration and chemistry", *Indoor Air*, vol.10, pp. 269-288, 2000

Weschler, C.J., Hodgson, A.T., and Wooley, J.D., "Indoor Chemistry: ozone, volatile organic compounds, and carpets", *Environmental Science and Technology*, vol.26, pp.2371-2377, 1992

White, F.M., *Viscous Fluid Flow*, 2nd edition, McGraw-Hill, New York, 1991

Wolkoff, P., "How to measure and evaluate volatile organic compound emissions from building products. A perspective", *The Science of the Total Environment*, vol. 227, pp.197-213, 1999

Wolkoff, P., "Impact of air velocity, temperature, humidity and air on long-term VOC emissions from building products", *Atmospheric Environment*, vol. 32, no. 14/15, pp. 2659-2668, 1998

Wolkoff, P., "Volatile Organic Compounds: Sources, Measurements, Emissions and the impact on Indoor Air Quality", *Indoor Air*, Suppl. 3, 1995

Wolkoff, P., and Nielsen, P.A., "A new approach for indoor climate labeling of building materials – emission testing, modeling, and comfort evaluation", *Atmospheric Environment*, vol. 30, pp. 2679-2689, 1996

Wolkoff, P., Clausen, P.A., and Nielsen, P.A., "Application of the Field and Laboratory Emission Cell (FLEC)- performance study, intercomparison study, and case study of damaged linoleum in an office", *Indoor Air,* vol. 5, no. 3, pp.196-203, 1995

Wolkoff, P., Clausen, P.A., Jensen, B., Nielsen, G.D., and Wilkins, C.K., "Are we measuring the relevant indoor pollutants?", *Indoor Air*, vol. 7, pp., 92-106, 1997

World Health Organization, *Indoor Air Pollutants: Exposure and Health Effects*, Copenhagen, WHO Regional Office for Europe, EURO Reports and Studies No. 78, 1983

World Health Organization, *Indoor Air Quality Research*, Copenhagen, WHO Regional Office for Europe, EURO Reports and Studies No. 103, 1986

World Health Organization, *Indoor Air Quality: Organic Pollutants*, Copenhagen, WHO Regional Office for Europe, EURO Reports and Studies No. 111, 1989

Yang, X., Chen, Q., and Bluyssen, P. M., "Prediction of short-term and long-term volatile organic compound emissions from SBR bitumen-backed carpet under different temperatures", *ASHRAE Transaction: Symposia*, TO-98-23-4, pp. 1297-1308, 1998

Yang, X., Chen, Q., Zeng, J., Zhang, J.S., Nong, G., and Shaw, C.Y., "Effects of air flow on VOC emissions from 'wet' coating materials: experimental measurements and numerical simulation", *ASHRAE Transaction*, 107 (1), 2001a

Yang, X., Chen, Q., Zeng, J., Zhang, J.S., and Shaw, C.Y., "A mass transfer model for simulating VOC sorption on building materials", *Atmospheric Environment*, vol. 35, no. 7, pp. 1291-1299, 2001b

Yang, X., Chen, Q., Zhang, J.S., Magee, R., Zeng, J., and Shaw, C.Y., "Numerical simulation of VOC emissions from dry materials", *Building and Environment*, vol. 36, no. 10, pp. 1099-1108, 2001c

Young, D.M. and Crowell, A.D., *Physical Adsorption of Gases*, Butterworth & Co. Limited, 1962

Yu, W.-S., Lin, H.-T. and Hwang, T.-Y., "Conjugate heat transfer of conduction and forced convection along wedges and a rotating cone", *Int. J. of Heat Mass Transfer*, vol. 34, no. 10, pp.2497-2507, 1991

Zhang, J.S., Chen, Q., and Zhang, J., *Modeling VOC Sorption of Building Materials and Its Impact on Indoor Air Quality*, ASHRAE RP-1097, 2001

Zhang, J.S., Shaw, C.Y., Kanabus-Kaminska, J.M., MacDonald, R.A., Magee, R.J., Lusztyk, E. and Weichert, H.J., "Study of air velocity and turbulence effects on organic compound emissions from building materials/furnishings using a new small test chamber", *Characterizing Sources of Indoor Air Pollution and Related Sink Effects*, ASTM STP 1287, B.A. Tichenor Ed., American Society for Testing and Materials, pp. 184-199, 1996

Zhou, W., and Warner, S.B., "Pore sizes in carpet", *Textile Research Journal*, vol. 69, no. 6, pp. 423-430, 1999

Appendix A.

Analytical Solution by the Integral Transform Method

The governing equation,

$$\frac{\partial C}{\partial t} = \frac{D_s}{(\varepsilon + K)} \frac{\partial^2 C}{\partial y^2} + \frac{g(y,t)}{(\varepsilon + K)} \tag{a-1}$$

with the boundary conditions,

$$\text{at } y = -b, \qquad \frac{\partial C}{\partial y} = 0 \tag{a-2}$$

$$\text{at } y = 0, \qquad D_s \frac{\partial C}{\partial y} + h_D \cdot C = h_D \cdot C_\infty(t) \tag{a-3}$$

and the initial condition,

$$\text{at } t = 0, \qquad C = C_O \tag{a-4}$$

is solved using the integral transform technique. The eigenvalues and the kernal for the integral transform can be easily obtained by solving the equivalent homogeneous problem [Özisik, 1980].

Eigenvalues β_m are the positive roots of

$$\beta \cdot \tan(\beta \cdot b) = \frac{h_D}{D_s} = H \tag{a-5}$$

and the kernal is

$$\phi(\beta_m, y) = \sqrt{2}\left[\frac{\beta_m{}^2 + H^2}{b(\beta_m{}^2 + H^2) + H}\right]^{\frac{1}{2}} \cdot \cos[\beta_m \cdot (y + b)] \tag{a-6}$$

The integral transform pairs are as follows,

- Integral transform

$$\overline{C}(\beta_m,t)=\int_{y=-b}^{0}\phi(\beta_m,y)\cdot C(y',t)dy' \tag{a-7}$$

- Inversion formula

$$C(y,t)=\sum_{m=1}^{\infty}\phi(\beta_m,y)\cdot\overline{C}(\beta_m,t) \tag{a-8}$$

Applying the transform Eq. (a-7) of the differential equation (a-1),

$$\int_{-b}^{0}\phi(\beta_m,y)\frac{\partial C(y,t)}{\partial t}dy = \frac{D_s}{(\varepsilon+K)}\int_{-b}^{0}\phi(\beta_m,y)\frac{\partial^2 C(y,t)}{\partial y^2}dy+\frac{1}{(\varepsilon+K)}\int_{-b}^{0}\phi(\beta_m,y)\cdot g(y,t)dy \tag{a-9}$$

The equation (a-9) can be expresses as follows,

$$\frac{d\overline{C}(\beta_m,t)}{dt}=\frac{D_s}{(\varepsilon+K)}\int_{-b}^{0}\phi(\beta_m,y)\frac{\partial^2 C(y,t)}{\partial y^2}dy+\frac{1}{(\varepsilon+K)}\overline{g}(\beta_m,t) \tag{a-10}$$

The first term in the right-side of Eq. (a-10) is evaluated as,

$$\begin{aligned}\int_{-b}^{0}\phi(\beta_m,y)\frac{\partial^2 C(y,t)}{\partial y^2}dy &= \left[\phi_m\frac{\partial C}{\partial y}\right]_{-b}^{0}-\int_{-b}^{0}\frac{\partial\phi_m}{\partial y}\cdot\frac{\partial C}{\partial y}dy\\ &=\left[\phi_m\frac{\partial C}{\partial y}\right]_{-b}^{0}-\left\{\left[C\frac{\partial\phi_m}{\partial y}\right]_{-b}^{0}-\int_{-b}^{0}C\frac{\partial^2\phi_m}{\partial y^2}dy\right\}\\ &=\left[\phi_m\frac{\partial C}{\partial y}-C\frac{\partial\phi_m}{\partial y}\right]_{-b}^{0}+\int_{-b}^{0}C\frac{\partial^2\phi_m}{\partial y^2}dy\end{aligned} \tag{a-11}$$

Since, $\frac{d^2\phi_m}{dy^2}+\beta_m{}^2\cdot\phi_m=0$,

$$\int_{-b}^{0}C\cdot\frac{d^2\phi_m}{dy^2}dy=-\beta_m{}^2\int_{-b}^{0}\phi_m\cdot Cdy \tag{a-12}$$

Applying the boundary conditions,

$$\phi_m \frac{\partial C}{\partial y} - C\frac{\partial \phi_m}{\partial y}\bigg|_{y=0} = \phi_m \cdot \left(\frac{h_D \cdot C_\infty(t) - h_D \cdot C}{D_s}\right) - C\left(-\frac{h_D \cdot \phi_m}{D_s}\right)\bigg|_{y=0}$$
$$= \frac{\phi_m}{D_s} \cdot h_D \cdot C_\infty(t)\bigg|_{y=0} \tag{a-13}$$

$$\phi_m \frac{\partial C}{\partial y} - C\frac{\partial \phi_m}{\partial y}\bigg|_{y=-b} = \phi_m \cdot 0 - C \cdot 0 = 0 \tag{a-14}$$

Substitute Eqs. (a-11 to 14) into Eq.(10) then it becomes ordinary differential equation (ODE) as follows,

$$\frac{d\overline{C}(\beta_m,t)}{dt} + \frac{D_s}{(\varepsilon+K)} \cdot \beta_m{}^2 \cdot \overline{C}(\beta_m,t) = A(\beta_m,t) \tag{a-15}$$

where,

$$A(\beta_m,t) = \frac{1}{(\varepsilon+K)} \cdot \left\{\phi_m \cdot h_D \cdot C_\infty(t)\big|_{y=0} + \overline{g}(\beta_m,t)\right\}$$

Taking the integral transform of the initial condition,

$$\int_b^0 K(\beta_m, y') \cdot C_o dy' = \overline{C}_o(\beta_m) \tag{a-16}$$

Solving the ODE in Eq. (a-15) with the initial condition Eq. (a-16),

$$\overline{C}(\beta_m,t) = e^{-D\cdot\beta_m{}^2\cdot t} \cdot \left[\int_{t=0} e^{D\cdot\beta_m{}^2\cdot t} \cdot A(\beta_m,t)dt + \overline{C}_o(\beta_m)\right] \tag{a-17}$$

Using the inversion formula Eq. (a-8),

$$C(y,t) = \sum_{m=1}^{\infty} \phi(\beta_m, y) \cdot e^{-D\cdot\beta_m{}^2\cdot t} \cdot \left[\int_{t=0} e^{D\cdot\beta_m{}^2\cdot t} \cdot A(\beta_m,t)dt + \overline{C}_o(\beta_m)\right] \tag{a-18}$$

where,

$$A(\beta_m,t)=\frac{1}{(\varepsilon+K)}\cdot\left\{\phi_m\cdot h_D\cdot C_\infty(t)\Big|_{y=0}+\bar{g}(\beta_m,t)\right\}$$

$$\bar{C}_o(\beta_m)=\int_{-b}^{0}\phi(\beta_m,y')\cdot C_o dy'$$

$$\bar{g}(\beta_m,t)=\int_{-b}^{0}\phi(\beta_m,y')\cdot g(y',t)dy'$$

Substituting the kernal Eq. (a-6) into the Eq. (a-18), the analytical solution is obtained.

$$\begin{aligned}C(y,t)=2\sum_{m=1}^{\infty}&\left[\frac{\beta_m{}^2+H^2}{b\cdot(\beta_m{}^2+H^2)+H}\right]\cdot\cos\{\beta_m\cdot(y+b)\}\cdot e^{-D\cdot\beta_m{}^2\cdot t}\\&\times\left[\frac{C_o}{\beta_m}\cdot\sin(\beta_m\cdot b)+\frac{h_D}{(\varepsilon+K)}\cdot\cos(\beta_m\cdot b)\cdot\int_{t'=0}e^{D\cdot\beta_m{}^2\cdot t'}\cdot C_\infty(t')\,dt'\right.\\&\left.+\frac{1}{(\varepsilon+K)}\int_{t'=0}\int_{-b}^{0}e^{D\cdot\beta_m{}^2\cdot t'}\cdot\cos\{\beta_m\cdot(y+b)\}\cdot g(y,t')\,dy\,dt'\right]\end{aligned}\qquad\text{(a-19)}$$

Appendix B.

Analytical Solutions for 5 Cases of Secondary VOC Source Behaviors

The solution of each secondary emission case in Chapter 4, is presented.

- ***Case 1-a: Continuous constant generation throughout the entire thickness***

$$C(y,t) = 2 \cdot \sum_{m=1}^{\infty} \left[\frac{\beta_m{}^2 + H^2}{b \cdot \left(\beta_m{}^2 + H^2\right) + H} \right] \cdot \cos\left\{\beta_m \cdot (y+b)\right\} \cdot e^{-D \cdot \beta_m{}^2 \cdot t} \times \left[\frac{C_o}{\beta_m} \cdot \sin(\beta_m \cdot b) + \left(e^{D \cdot \beta_m{}^2 \cdot t} - 1\right) \left(\frac{h_D \cdot C_\infty}{D_s \cdot \beta_m{}^2} \cdot \cos(\beta_m \cdot b) + \frac{A_g}{D_s \cdot \beta_m{}^3} \cdot \sin(\beta_m \cdot b) \right) \right] \quad \text{(b-1)}$$

- ***Case 1-b: Continuous constant generation at the solid-air interface***

$$C(y,t) = 2 \cdot \sum_{m=1}^{\infty} \left[\frac{\beta_m{}^2 + H^2}{b \cdot \left(\beta_m{}^2 + H^2\right) + H} \right] \cdot \cos\left\{\beta_m \cdot (y+b)\right\} \cdot e^{-D \cdot \beta_m{}^2 \cdot t} \times \left[\frac{C_o}{\beta_m} \cdot \sin(\beta_m \cdot b) + \left(e^{D \cdot \beta_m{}^2 \cdot t} - 1\right) \cdot \frac{\cos(\beta_m \cdot b)}{D_s \cdot \beta_m{}^2} \cdot \left(h_D \cdot C_\infty + B_g\right) \right] \quad \text{(b-2)}$$

- ***Case 1-c: Continuous constant generation at the bottom surface of solid***

$$C(y,t) = 2 \cdot \sum_{m=1}^{\infty} \left[\frac{\beta_m{}^2 + H^2}{b \cdot \left(\beta_m{}^2 + H^2\right) + H} \right] \cdot \cos\left\{\beta_m \cdot (y+b)\right\} \cdot e^{-D \cdot \beta_m{}^2 \cdot t} \times \left[\frac{C_o}{\beta_m} \cdot \sin(\beta_m \cdot b) + \left(e^{D \cdot \beta_m{}^2 \cdot t} - 1\right) \cdot \frac{1}{D_s \cdot \beta_m{}^2} \cdot \left(h_D \cdot C_\infty \cdot \cos(\beta_m \cdot b) + B_g\right) \right] \quad \text{(b-3)}$$

- ***Case 2: Constant generation for a limited time throughout the entire thickness***

$$C(y,t) = 2\cdot\sum_{m=1}^{\infty}\left[\frac{{\beta_m}^2 + H^2}{b\cdot\left({\beta_m}^2 + H^2\right)+H}\right]\cdot\cos\left\{\beta_m\cdot(y+b)\right\}\cdot e^{-D\cdot{\beta_m}^2\cdot t}$$
$$\times\left[\frac{C_o}{\beta_m}\cdot\sin(\beta_m\cdot b)+\frac{h_D\cdot C_\infty}{D_s\cdot{\beta_m}^2}\cdot\cos(\beta_m\cdot b)\cdot\left(e^{D\cdot{\beta_m}^2\cdot t}-1\right)\right. \qquad \text{(b-4)}$$
$$\left.+\frac{A_g}{D_s\cdot{\beta_m}^3}\cdot\sin(\beta_m\cdot b)\cdot\left(e^{D\cdot{\beta_m}^2\cdot t_g}-1\right)\right]$$

- ***Case 3: Seasonal variation using sinusoidal function***

$$C(y,t) = 2\sum_{m=1}^{\infty}\left[\frac{{\beta_m}^2 + H^2}{b\cdot\left({\beta_m}^2 + H^2\right)+H}\right]\cdot\cos\left\{\beta_m\cdot(y+b)\right\}\cdot e^{-D\cdot{\beta_m}^2\cdot t}$$
$$\times\left[\frac{C_o}{\beta_m}\cdot\sin(\beta_m\cdot b)+\frac{h_D\cdot C_\infty}{D_s\cdot{\beta_m}^2}\cdot\cos(\beta_m\cdot b)\cdot\left(e^{D\cdot{\beta_m}^2\cdot t}-1\right)+G(t)\right] \qquad \text{(b-5)}$$

where,

$$G(t) = \frac{A_g}{2\cdot(\varepsilon+K)}\cdot\frac{\sin(\beta_m\cdot b)}{\beta_m}\cdot\left[\frac{1}{D\cdot{\beta_m}^2}\cdot\left(e^{D\cdot{\beta_m}^2\cdot t}-1\right)+\frac{\frac{2\cdot\pi}{t_g}}{\left(D^2\cdot{\beta_m}^4+\frac{4\cdot\pi^2}{{t_g}^2}\right)}\right.$$
$$\left.+\frac{e^{D\cdot{\beta_m}^2\cdot t}}{\left(D^2\cdot{\beta_m}^4+\frac{4\cdot\pi^2}{{t_g}^2}\right)}\cdot\left\{D\cdot{\beta_m}^2\cdot\sin\left(\frac{2\cdot\pi}{t_g}\cdot t\right)-\frac{2\cdot\pi}{t_g}\cdot\cos\left(\frac{2\cdot\pi}{t_g}\cdot t\right)\right\}\right]$$